



MONASH University

Renal Oxygenation and its Determinants in Chronic Kidney Disease

Md Mahbub Ullah

Bachelor of Science (Honours) in Biochemistry and Biotechnology

Masters of Science in Biotechnology

A thesis submitted for the degree of *Doctor of Philosophy* at

Monash University in 2018

Department of Physiology

Faculty of Medicine, Nursing and Health Sciences

COPYRIGHT NOTICE

© Md Mahbub Ullah (2018).

I certify that I have made all reasonable efforts to secure copyright permissions for third-party content included in this thesis and have not knowingly added copyright content to my work without the owner's permission.

ABSTRACT

The precise roles of renal hypoxia in the initiation and progression of chronic kidney disease (CKD) remain a matter of controversy. In the experiments described in this thesis I investigated this issue by deploying a suite of methods for assessing renal oxygenation and its determinants. For example, in adenine-induced CKD (Ad-CKD), radiotelemetry was used to assess renal tissue oxygen tension (PO_2) in unanesthetized rats (Chapter 4). Furthermore, in anesthetized rats, renal tissue PO_2 was measured by Clark electrode while renal oxygen delivery and renal oxygen consumption were determined through measurement of total renal blood flow and arterial and renal venous blood oxygen content (Chapter 4). Cellular hypoxia in Ad-CKD was assessed with pimonidazole adduct immunohistochemistry (Chapters 2 & 3) and analysis of the tissue expression of hypoxia inducible factors (Chapter 4). To investigate the potential role of glomerular hyperfiltration in the development of renal hypoxia in the early stages of diabetes, I used the transcutaneous measurement of fluorescein isothiocyanate (FITC)-sinistrin clearance to measure glomerular filtration rate (GFR) in conscious rats (Chapter 5). Finally, I performed pilot studies in an attempt to generate a method for quantification of the spatial relationships between peritubular capillaries and renal tubules, so as to improve the structural basis of computational models of renal oxygen transport.

In Chapter 1 of this thesis I provide the rationale for my choice of experimental models of CKD and of methods for assessing renal oxygenation and its determinants. All of these methods have strengths and limitations. However, their use in combination overcomes many of these limitations. I also provide the specific rationale for each of the experimental studies described in Chapters 2-6.

In the experiments described in Chapter 2 of this thesis I used pimonidazole adduct immunohistochemistry to demonstrate the presence of cellular hypoxia in the kidneys of rats fed adenine by gavage for a two-week period. Adenine-feeding induced CKD which was already well advanced after the two-week treatment period. In the course of these studies I identified the presence of false positive staining for pimonidazole in damaged renal tissue with the use of the standard monoclonal mouse anti-pimonidazole antibody. In the experiments described in Chapter 3 of this thesis I showed that this false-positive staining could be avoided by use of an anti-pimonidazole antibody raised in rabbits. These studies confirmed the presence of renal cellular hypoxia after two weeks of adenine feeding. To determine whether renal tissue hypoxia is an early

event in Ad-CKD, in the experiments described in Chapter 4, I assessed renal tissue PO₂, either by using Clark electrode or radio-telemetry technique, during the first 7 days of adenine treatment. Cortical tissue PO₂ was comparable, between adenine-treated and vehicle-treated rats, as assessed either by Clark electrode in anesthetized rats at the end of a 7 day treatment period or by radiotelemetry in unanesthetized rats across the course of the 7 day treatment period. I found relatively stable medullary tissue PO₂ measured by radio-telemetry across a 7 day treatment period in unanesthetized adenine-treated rats. In contrast, under anesthesia medullary tissue PO₂ was 44% less in adenine-treated rats than in vehicle-treated rats. Our observations in rats instrumented with radio-telemeters indicate that the apparent medullary hypoxia in anesthetized adenine-treated rats could be an artefact due to differential effects of anesthesia and laparotomy in adenine-treated compared with vehicle-treated rats. This conclusion was also supported by measurement of hypoxia inducible factor-1 α protein expression, which was downregulated throughout the kidney in adenine-treated rats. The relative preservation of renal tissue PO₂ within the first 7 days of adenine treatment may be due to the fact that the deficit in renal oxygen consumption (65%) matched the deficit in renal oxygen delivery (51%). Renal dysfunction and damage was already present by day 7 of adenine treatment, as shown by decreased GFR (65%) and the presence of interstitial fibrosis in the kidneys of adenine-treated rats. Thus, I conclude that renal tissue hypoxia might not be an early characteristic of Ad-CKD so may not be a primary driver of pathology in this model.

In diabetes, glomerular hyperfiltration has been proposed as an important mechanism driving the development of renal tissue hypoxia. Therefore, in the experiments described in Chapter 5 of this thesis I measured GFR, by measuring the clearance of FITC-sinistrin using a transcutaneous-based technique, across the first 4 weeks of streptozotocin (STZ)-induced diabetes in rats. There were statistically significant positive relationships between blood glucose concentration and GFR on day 14 and day 28 after induction of diabetes, as well as a strong tendency for a relationship 3 days after induction of diabetes. Importantly, I could not detect significant albuminuria or interstitial fibrosis 4 weeks after induction of diabetes. Thus, I conclude that hyperfiltration is an early and persistent characteristic of STZ-induced diabetes in rats that may contribute to the development of renal tissue hypoxia.

Computational models have helped us understand the factors that render the kidney susceptible to hypoxia. Currently available models of oxygen transport in the kidney do not adequately capture the transport of oxygen between peritubular capillaries and tubules. Therefore, in the studies

described in Chapter 6 of this thesis I performed a preliminary experiment to develop a method for characterizing the spatial relationships between renal peritubular capillaries and tubules. I was able to visualize peritubular capillaries by filling the renal vasculature with a gelatin solution in which FITC-labeled albumin was suspended. The tissue was then optically cleared and imaged by confocal microscopy, with z-stacked being used to generate a 3-dimensional reconstruction of the renal cortical vascular network. I also attempted to label tubules with a pan cytokeratin antibody conjugated with Alexa Fluor 647[®], but this was not successful. However, I was able to visualize tubules to some extent simply through their autofluorescence. Nevertheless, considerable further development is required before we can reconstruct the 3-dimensional relationships between peritubular capillaries and renal tubules.

Finally, in Chapter 7 of this thesis I provide an overview of the major findings and the conclusions I draw from them, and identify the remaining critical questions that merit investigation.

DECLARATION

This thesis contains no material which has been accepted for the award of any other degree or diploma at any university or equivalent institution and that, to the best of my knowledge and belief, this thesis contains no material previously published or written by another person, except where due reference is made in the text of the thesis.

Chapters 3, 4, 5 and 6 are unpublished manuscripts, and have not been submitted nor accepted for publication in any form.

Chapter 3: An improved method for pimonidazole-adduct immunohistochemistry using a primary antibody raised in the rabbit: Application to adenine-induced CKD

My contribution: 80%

Co-authors: Connie Ow, Lucinda Hilliard and Roger G. Evans.

Chapter 4: Renal oxygenation during the early stages of adenine-induced chronic kidney disease

My contribution: 80%

Co-authors: Connie Ow, Lucinda M. Hilliard and Roger G. Evans.

Chapter 5: Transcutaneous measurement of glomerular filtration rate in conscious rats during the progression of streptozotocin-induced type 1 diabetes

My contribution: 80%

Co-authors: Lucinda M. Hilliard and Roger G. Evans.

Chapter 6: Assessment of the spatial relationships between peritubular capillaries and renal tubules in the rat kidney: A pilot study

My contribution: 75%

Co-authors: Jennifer P. Ngo, Lucinda M. Hilliard and Roger G. Evans.

Signature: 

Print Name: **MD MAHBUB ULLAH**

Date:21.11.2018.....

PUBLICATIONS DURING ENROLMENT

1. Fong D, **Ullah MM**, Lal JG, Abdelkader A, Ow CP, Hilliard LM, Ricardo SD, Kelly DJ, and Evans RG. Renal cellular hypoxia in adenine-induced chronic kidney disease. *Clin Exp Pharmacol Physiol* 43: 896-905, 2016.
2. Ow CPC, Ngo JP, **Ullah MM**, Hilliard LM, and Evans RG. Renal hypoxia in kidney disease: Cause or consequence? *Acta Physiol* 222: e12999, 2018.
3. Ow CPC, Ngo JP, **Ullah MM**, Barsha G, Meex RCR, Watt MJ, Hilliard LM, Koeners MP, and Evans RG. Absence of renal hypoxia in the subacute phase of severe renal ischemia reperfusion injury. *Am J Physiol Renal Physiol* 315: F1358–F1369, 2018.

PRESENTATION

Poster presentation at ISN Frontiers Meetings:

Md Mahbub Ullah, Connie P.C. Ow, Lucinda M. Hilliard, Roger G. Evans. Renal oxygenation in the early stage of adenine-induced chronic kidney disease, The International Society of Nephrology (ISN) Frontiers Meetings, Tokyo, Japan (2018).

				<p>research, edited and revised manuscript</p> <p>7. Darren J. Kelly (3%) Provided design of the research, edited and revised manuscript</p> <p>8. Roger G. Evans (10%) Provided design of the research, analysed data, and interpreted results, edited and revised manuscript.</p>	N
Appendix 1	Renal hypoxia in kidney disease: Cause or consequence	Published	5% Edited and revised manuscript	<p>1. Ow CPC (70%) Concept, prepared the figures, writing and editing draft</p> <p>2. Ngo JP (5%) edited and revised the draft</p> <p>3. Hilliard LM (5%) edited and revised the draft</p> <p>4. Evans RG (15%) provided desing of the paper, editing and revised draft</p>	Y Y N N
Appendix 2	Absence of renal hypoxia in the subacute phase of severe renal ischemia reperfusion injury	Published	5% Contributed to data analysis, edited and revised manuscript	<p>1. Ow CPC (60%) provided design of research, performed experiment, collecting data, data analysis, prepared the figures, writing and editing draft</p> <p>2. Ngo JP (5%) interpreted results, edited and revised manuscript</p> <p>3. Barsha G (5%) interpreted results, edited and revised manuscript</p> <p>4. Meex RCR (5%) edited and revised manuscript</p> <p>5. Watt MJ (5%) edited and revised manuscript</p> <p>6. Hilliard LM (5%) edited and revised manuscript</p> <p>7. Koeners MP (5%) edited and revised manuscript</p>	Y Y Y N N N N N

				5. Evans RG (10%) provided desing of research, interpreted results, editing and revised draft	

**If no co-authors, leave fields blank*

I have not renumbered sections of submitted or published papers in order to generate a consistent presentation within the thesis.

Student signature:



Date: 21.11.18

The undersigned hereby certify that the above declaration correctly reflects the nature and extent of the student's and co-authors' contributions to this work. In instances where I am not the responsible author I have consulted with the responsible author to agree on the respective contributions of the authors.

Main Supervisor signature:



Date: 21.11.2018

ACKNOWLEDGEMENTS

The work presented in this thesis would not be possible to complete without the constant support and motivation of the following people.

First and foremost, I would like to thank and express my deepest gratitude to my primary supervisor Professor Roger Evans, who has been an incredible mentor throughout my PhD journey. Thank you, Roger, for your guidance, encouragement and invaluable suggestions regarding my experiments. I would like to thank you for providing enough resources and care towards the completion of my PhD project. Your constructive feedback on scientific writing has significantly improved my dissertation. The way you encouraged and nurtured scientific thinking in me has elevated my professional attitude toward handling research.

Thank you to Dr. Lucinda Hilliard, my co-supervisor, for all the support and encouragement you have given to me during my candidature. Thank you for all of your help with experiments, particularly the GFR study as well as thesis proofreading and editing.

To Connie, I offer innumerable thanks for teaching me the surgical skills and construction of radio-telemeters. All the animal work would not have been possible without your unconditional support. Thank you for your unwavering willingness to read my thesis chapters. Thank you, Jennifer, for all of your help, especially for showing me how to perfusion fix. Finally, I wish to extend my gratitude to all the members of the Cardiovascular and Renal Research Group.

I would like to thank Professor John Bertram for sharing your expertise in imaging of renal vasculatures and tubules and for giving me the privilege to work in your lab for my pilot experiment of this thesis. Thank you, Sarah, for teaching me the optical clearing process and aiding me with confocal microscopy.

Farzana, I cannot express my gratitude enough for everything you did for me and supporting me to complete the thesis. Thank you for being positive and adaptable especially when I have been less than social throughout my work on thesis. Thanks for your incredible love and care.

Thank you Bappy, you are always a great younger brother. I owe you a lot for taking care of our parents while I am not at home.

I would like to offer thanks to my father, mother and close friends for their unwavering support and motivation. A special thank you to Ammu, for your continuous support, counselling and for daily phone conversations all the way from Bangladesh. I do not know whether I would be in this position without your support.

Last, but not the least, a very special thanks and gratitude to my in-laws for their prayers and belief in me.

The research was supported by the Australian Government Research Training Program (RTP) Scholarship.

TABLE OF CONTENTS

COPYRIGHT NOTICE.....	2
ABSTRACT.....	3
DECLARATION.....	6
PUBLICATIONS DURING ENROLMENT.....	7
THESIS INCLUDING PUBLISHED WORKS DECLARATION.....	8
ACKNOWLEDGEMENTS.....	11
LIST OF FIGURES.....	15
LIST OF TABLES.....	18
SYMBOLS.....	19
ABBREVIATIONS.....	20

CHAPTER 1: INTRODUCTION

1.1. CHRONIC KIDNEY DISEASE.....	22
1.2. THE CHRONIC HYPOXIA HYPOTHESIS.....	23
1.3. ADENINE-INDUCED CKD.....	30
1.4. METHODS FOR ASSESSING RENAL OXYGENATION.....	31
1.5. DIABETIC NEPHROPATHY.....	34
1.5.1 Diabetic nephropathy and renal hypoxia.....	34
1.5.2 Glomerular hyperfiltration.....	35
1.5.3 Experimental model of diabetes.....	39
1.5.4 Transcutaneous measurement of glomerular filtration rate using FITC–sinistrin....	40
1.6.ASSESSMENT OF SPATIAL ARRANGEMENT BETWEEN PERITUBULAR CAPILLARIES AND RENAL TUBULES IN THE RAT KIDNEY.....	47
1.7.AIMS.....	51
1.8.REFERENCES.....	52

CHAPTER 2: RENAL CELLULAR HYPOXIA IN ADENINE-INDUCED CHRONIC KIDNEY DISEASE..... 64

CHAPTER 3: AN IMPROVED METHOD FOR PIMONIDAZOLE-ADDUCT IMMUNOHISTOCHEMISTRY USING A PRIMARY ANTIBODY RAISED IN THE RABBIT: APPLICATION TO ADENINE-INDUCED CKD

3.1 ABSTRACT.....	76
3.2 INTRODUCTION.....	77
3.3 METHODS.....	78
3.3.1. Tissue preparation.....	78
3.3.2. Pimonidazole adduct immunohistochemistry.....	78
3.3.3. Co-localization of fibrosis and hypoxia in the kidneys of adenine-treated rats.....	80
3.3.4. Hypoxia and patency of renal tubules in the kidneys of adenine-treated rats.....	80
3.3.5. Statistical analysis.....	80
3.4 RESULTS.....	80
3.4.1. Cellular staining for pimonidazole adducts.....	80
3.4.2. Staining in renal tissue not exposed to pimonidazole chloride.....	84
3.4.3. Co-localization of fibrosis and hypoxia.....	87
3.4.4. Hypoxia and the patency of renal tubules in adenine-induced CKD.....	87

3.5 DISCUSSION	89
3.6 REFERENCES	94

CHAPTER 4: RENAL OXYGENATION DURING THE EARLY STAGES OF ADENINE-INDUCED CHRONIC KIDNEY DISEASE

4.1 ABSTRACT	97
4.2 INTRODUCTION	98
4.3 METHODS	99
4.3.1. Animals	99
4.3.2. Induction of Ad-CKD	100
4.3.3. Protocol 1: Renal tissue oxygenation and its determinants in anesthetized rats ...	100
4.3.4. Protocol 2: Temporal changes in renal tissue PO₂ during the first 7 days of treatment with adenine or its vehicle	103
4.3.5. Statistical analyses	109
4.4 RESULTS	110
4.4.1. Protocol 1: Renal tissue oxygenation and its determinants in anesthetized rats ...	110
4.4.2. Protocol 2: Temporal changes in renal tissue PO₂ during the first 7 days of treatment with adenine or its vehicle	115
4.5 DISCUSSION	126
4.6 REFERENCES	132

CHAPTER 5: TRANSCUTANEOUS MEASUREMENT OF GLOMERULAR FILTRATION RATE IN CONSCIOUS RATS DURING THE PROGRESSION OF STREPTOZOTOCIN-INDUCED TYPE 1 DIABETES

5.1. ABSTRACT	137
5.2. INTRODUCTION	138
5.3. METHODS	140
5.3.1. Animals	140
5.3.2. Induction of diabetes	140
5.3.3. Experimental protocol	141
5.3.4. Measurement of glomerular filtration rate	142
5.3.5. Experimental procedure	142
5.3.6. Data analyses	143
5.3.7. Metabolic cage studies	143
5.3.8. Analysis of urine and plasma samples	144
5.3.9. Histological assessment of tissue damage and collagen deposition	144
5.3.10. Statistical analyses	144
5.4. RESULTS	145
5.4.1. Body weight and blood glucose concentrations	145
5.4.2. Glomerular filtration rate	145
5.4.3. Blood and urine chemistry	151
5.4.4. Kidney and heart weight	152
5.4.5. Histological assessment of tissue damage and collagen deposition	153
5.5. DISCUSSION	156
5.6. REFERENCES	161

CHAPTER 6: ASSESSMENT OF THE SPATIAL RELATIONSHIPS BETWEEN PERITUBULAR CAPILLARIES AND RENAL TUBULES IN THE RAT KIDNEY: A PILOT STUDY

6.1. ABSTRACT..... 165
6.2. INTRODUCTION..... 166
6.3. METHODS..... 168
 6.3.1. Animals..... 168
 6.3.2. Protocol: Staining of renal vasculature and renal tubules..... 168
6.4. RESULTS..... 172
 6.4.1. Visualization of kidney slices after perfusion with gelatin or gelatin-FITC..... 172
 6.4.2. Labeling of renal blood vessels and tubules..... 172
 6.4.3. Three-dimensional visualization of renal vasculature and tubules..... 173
6.5. DISCUSSION..... 176
6.6. REFERENCES..... 179

CHAPTER 7: PERSPECTIVES AND FUTURE DIRECTIONS

7.1. IS RENAL TISSUE HYPOXIA ASSOCIATED WITH ADENINE-INDUCED CHRONIC KIDNEY DISEASE?..... 184
7.2. ARE RENAL TUBULAR HYPOXIA AND INTERSTITIAL FIBROSIS SPATIALLY ASSOCIATED IN ADENINE-INDUCED CHRONIC KIDNEY DISEASE?..... 185
7.3. DOES HYPOXIA PRECEDE RENAL DYSFUNCTION IN ADENINE-INDUCED CHRONIC KIDNEY DISEASE?..... 186
7.4. IS GLOMERULAR HYPERFILTRATION, WHICH WOULD BE EXPECTED TO DRIVE RENAL HYPOXIA, AN EARLY EVENT IN TYPE 1 DIABETES?..... 189
7.5. SPATIAL ARRANGEMENT OF PERITUBULAR CAPILLARIES AND RENAL TUBULES..... 190
7.6. REFERENCES..... 193

APPENDIX 1: RENAL HYPOXIA IN KIDNEY DISEASE: CAUSE OR CONSEQUENCE? 198

APPENDIX 2: ABSENCE OF RENAL HYPOXIA IN THE SUBACUTE PHASE OF SEVERE RENAL ISCHEMIA-REPERFUSION INJURY..... 217

LIST OF FIGURES

CHAPTER 1

- Figure 1.1** The Chronic hypoxia hypothesis..... 24
- Figure 1.2** Schematic representation of a one-compartment kinetic model and an example of the excretion kinetics of a GFR marker after intravenous injection..... 44
- Figure 1.3** Schematic representation of a two-compartment kinetic model and an example of the excretion kinetics of a GFR marker after intravenous injection..... 45
- Figure 1.4** Schematic representation of a three-compartment kinetic model and an example of the excretion kinetics of a GFR marker after intravenous injection..... 46

CHAPTER 2

- Figure 1** Micrographs of kidney sections from rats treated with vehicle (a–d) or adenine (e–h), stained with haematoxylin and eosin..... 68 (P 899)
- Figure 2** Micrograph of a kidney section from a rat treated with adenine, stained with haematoxylin and eosin..... 68 (P 899)
- Figure 3** Micrographs of kidney sections from rats treated with vehicle (a–d) or adenine (e–h), stained with picosirius red..... 69 (P 900)
- Figure 4** Micrograph of kidney sections from rats treated with vehicle (a–d) or adenine (e–h) stained with Masson’s trichrome..... 69 (P 900)
- Figure 5** Quantification of fibrosis in the cortex and medulla..... 70 (P 901)
- Figure 6** Micrographs of kidney sections from rats treated with vehicle (a–d) or adenine (e–h), showing immunohistochemical localisation of pimonidazole adducts..... 70 (P 901)
- Figure 7** Relationship between hypoxia and the patency of tubules in kidneys of adenine-treated rats..... 70 (P 901)
- Figure 8** Co-localisation of fibrosis and hypoxia..... 71 (P 902)

CHAPTER 3

- Figure 3.1** Schematic representation of the protocol for pimonidazole adduct immunohistochemistry..... 79
- Figure 3.2** Pimonidazole adduct immunohistochemistry of kidney sections after 14 days of vehicle treatment..... 82
- Figure 3.3** Pimonidazole adduct immunohistochemistry of kidney sections after 14 days of adenine treatment..... 83
- Figure 3.4** Pimonidazole adduct immunohistochemistry of kidney sections from rats, not exposed to pimonidazole chloride, after 14 days of vehicle treatment..... 85
- Figure 3.5** Pimonidazole adduct immunohistochemistry of kidney sections of rats, not exposed to pimonidazole chloride, after 14 days of adenine treatment..... 86
- Figure 3.6** Co-localization of fibrosis and hypoxia in kidneys of adenine treated rats..... 88
- Figure 3.7** Relationship between pimonidazole staining and the patency of tubules in kidneys of adenine-treated rats..... 89

CHAPTER 4

Figure 4.1	Schematic of the protocol for measurement of renal tissue PO ₂ in anesthetized rats.	101
Figure 4.2	Schematic representation of the protocol for measurement of renal tissue PO ₂ in unanesthetized rats.	103
Figure 4.3	An example of a typical trace during the calibration procedure.	105
Figure 4.4	Whole kidney oxygenation in vehicle-treated and adenine-treated rats.	113
Figure 4.5	Assessment of renal tissue PO ₂ in vehicle-treated rats (n = 7) and adenine-treated rats (n = 7) under anesthesia.	114
Figure 4.6	Body weight and water intake in vehicle-treated and adenine-treated rats during the 7 day treatment period.	115
Figure 4.7	Temporal changes of cortical and medullary tissue PO ₂ in vehicle-treated and adenine-treated rats.	116
Figure 4.8	Responsiveness of radio-telemeters to changes in inspired oxygen content in unanesthetized rats.	117
Figure 4.9	Effects of anesthesia and laparotomy on renal tissue PO ₂ in vehicle-treated and adenine-treated rats.	118
Figure 4.10	Micrographs of kidney sections from rats treated with vehicle (a–d) or adenine (e–h), stained with hematoxylin and eosin.	121
Figure 4.11	Figure 4.11 Micrographs of kidney sections from rats treated with vehicle (a–d) or adenine (e–h), stained with picrosirius red.	122
Figure 4.12	Figure 4.12 Quantification of collagen deposition in the cortex and medulla.	123
Figure 4.13	Levels of HIF-1 α protein in vehicle-treated and adenine-treated rats after the 7 day treatment period.	124
Figure 4.14	Levels of HIF-2 α protein in vehicle-treated and adenine-treated rats after the 7 day treatment period.	125

CHAPTER 5

Figure 5.1	Time line of the experimental protocol.	141
Figure 5.2	Body weight (A) and blood glucose (B) in vehicle-treated and diabetic rats during the 4 week experimental protocol.	147
Figure 5.3	Renal clearance of FITC-sinistrin at baseline.	148
Figure 5.4	Temporal profile of renal clearance of FITC-sinistrin in vehicle-treated and diabetic rats during the 4 week experimental protocol.	149
Figure 5.5	Relationships between concentrations of blood glucose and excretion half-life (t _{1/2}), rate constant, and glomerular filtration rate in diabetic rats.	151
Figure 5.6	Logarithmic transformed urinary albumin to creatinine ratio in vehicle-treated rats and diabetic rats during the four week experimental protocol.	152
Figure 5.7	Micrographs of kidney sections, stained with hematoxylin and eosin, taken from vehicle-treated rats (a–d) and diabetic rats (e–h) at the end of the four week experimental protocol.	154
Figure 5.8	Micrographs of kidney sections, stained with picrosirius red, taken from vehicle-treated rats (a–d) and diabetic rats (e–h) at the end of the four week experimental protocol.	155

Figure 5.9	Quantification of collagen deposition in the cortex and medulla at the end of the 4 week experimental protocol.....	156
-------------------	---	-----

CHAPTER 6

Figure 6.1	Schematic of a benchtop experiment for determination of outflow temperature of the gelatin-FITC at specific flow rates.....	169
Figure 6.2	Schematic diagram for processing of kidney sections.....	171
Figure 6.3	Micrographs of kidney slices after perfusion with gelatin or gelatin-FITC.....	173
Figure 6.4	Visualization of vascular and tubular elements in kidney slices after optical clearing.....	174
Figure 6.5	Visualization of vascular and tubular architecture of the rat kidney.....	175

APPENDIX 1

Figure 1	Evidence of renal hypoxia in various forms of chronic kidney disease (CKD)...	201
	(3)	
Figure 2	Evidence of renal hypoxia in various forms of acute kidney injury.....	203 (5)
Figure 3	Evidence that renal tissue hypoxia per se leads to kidney disease.....	207 (9)
Figure 4	Evidence that renal tissue hypoxia precedes renal dysfunction in diabetic nephropathy and sepsis.....	208 (10)
Figure 5	Evidence of colocalization of tissue hypoxia and pathology.....	209 (11)

APPENDIX 2

Figure 1	Temporal changes of inner medullary tissue PO ₂ following renal ischemia or sham ischemia.....	221 (F1361)
Figure 2	Assessment of tissue PO ₂ by Clark electrode.....	222 (F1362)
Figure 3	Pimonidazole adduct immunohistochemistry of renal sections 24 h following recovery from bilateral renal ischemia or sham ischemia.....	224 (F1364)
Figure 4	Pimonidazole adduct immunohistochemistry of renal sections 5 days following recovery from bilateral renal ischemia or sham surgery.....	225 (F1365)
Figure 5	Expression of hypoxia-inducible factor (HIF) proteins after bilateral renal ischemia or sham ischemia.....	226 (F1366)
Figure 6	mRNA expression of HIF-1 α , HIF-2 α , VEGF- α , and heme oxygenase 1 (HO-1).....	227 (F1367)
Figure 7	Collagen deposition in kidneys of rats.....	227 (F1367)
Figure 8	Indicators of renal dysfunction.....	227 (F1367)

LIST OF TABLES

CHAPTER 1

Table 1.1	Classification of CKD as proposed by the Kidney Disease Outcomes Quality Initiative Guidelines.....	23
------------------	---	----

CHAPTER 2

Table 1	Characteristics of adenine-treated and vehicle-treated rats across the course of the first 14 days of the experiment.....	67 (898)
Table 2	Characteristics of rats on day 15 of adenine or vehicle treatment.....	67 (898)

CHAPTER 4

Table 4.1	Characteristics of vehicle-treated and adenine-treated rats under anesthesia.....	110
Table 4.2	Systemic and renal hemodynamic and functional parameters in anesthetized vehicle-treated and adenine-treated rats.....	111
Table 4.3	Blood oxygenation in anesthetized vehicle-treated and adenine-treated rats.....	112
Table 4.4	Characteristics of vehicle-treated and adenine-treated rats after the 7 day treatment period.....	119

CHAPTER 5

Table 5.1	Insulin regimen according to the concentration of blood glucose.....	141
Table 5.2	Outcomes of repeated-measures ANOVA for the data shown in Figure 5.4.....	150
Table 5.3	Characteristics of rats four weeks after injection of vehicle or streptozotocin.....	153

APPENDIX 1

Table 1	The adaptive and maladaptive responses to downstream transcription of various hypoxia-responsive genes induced by the activation of hypoxia-inducible factors (HIF).....	205 (7)
----------------	--	------------

APPENDIX 2

Table 1	Systemic and blood oxygen parameters of rats 24 h or 5 days after ischemia or sham ischemia.....	221 (F1361)
Table 2	Renal hemodynamic parameters of rats 24 h or 5 days after ischemia or sham ischemia.....	223 (F1363)

SYMBOLS

±	plus-minus
~	Approximately
mmHg	Millimeters mercury
nCi	Nanocurie
λ	Lambda
°C	Degree Celsius
v/v	Volume per volume
w/v	Weight per volume
α	Alpha
β	Beta
g	Gram
mg	Milligram
kg	Kilogram
M	Molar
Mm	Micromolar
mM	Millimolar
%	Percentage
μm	Micrometer
mm	Millimeter
ml	Milliliter
dl	Deciliter
min	Minute
s	Second
h	Hour
nA	Nanoamperes
mV	Millivolt
Hz	Hertz
®	Registered

ABBREVIATIONS

Adenine-induced CKD (Ad-CKD)
Adenine phosphoribosyl transferase (APRT)
Angiotensin converting enzyme (ACE)
Angiotensin receptor antagonist (ARB)
Carbon-paste electrode (CPE)
Chronic kidney disease (CKD)
Diabetic nephropathy (DN)
Elimination rate constant (λ)
Excretion half-life ($t_{1/2}$)
Fluorescein isothiocyanate–sinistrin (FITC-sinistrin)
Hypoxia inducible factors (HIFs)
Insulin-dependent diabetes mellitus (IDDM)
Mean arterial pressure (MAP)
Micro-computed tomography (CT)
Non-invasive clearance Kidney device (NIC-Kidney device)
One-compartment kinetic model (1-COM)
Oxygen gas (O₂)
Partial pressure of oxygen (PO₂)
Peritubular capillaries (PTC)
Phosphate buffered saline (PBS)
Renal blood flow (RBF)
Renal oxygen consumption (VO₂)
Renal oxygen delivery (DO₂)
Renin-angiotensin system (RAS)
Standard error of the mean (SEM)
Streptozotocin (STZ)
Three-compartment kinetic model (3-COM)
Three-compartment kinetic model with baseline correction (3-COMB)
Three-dimensions (3D)
Two-compartment kinetic model (2-COM)

CHAPTER 1

INTRODUCTION

1.1 CHRONIC KIDNEY DISEASE

Chronic kidney disease (CKD) has emerged as a major global challenge and economic burden to public health care (69, 165). Current estimates indicate that approximately 11% to 13% of the total population worldwide is affected by CKD (69). In 2002, an operational definition of CKD was proposed by the Kidney Disease Outcomes Quality Initiative (KDOQI) (110). According to their definition, CKD is characterized by the presence of kidney damage for at least 3 months. Specifically, either: (i) the presence of pathological abnormalities in the kidney such as the presence of cysts in polycystic kidney disease, (ii) the presence of markers of kidney damage such as proteinuria or abnormalities identified through imaging procedures, or (iii) decreased renal function as indicated by glomerular filtration rate (GFR) less than 60 ml/min/1.73 m² with or without any sign of other kidney damage (110, 165).

Based on estimated GFR (eGFR) the KDOQI guidelines also proposed a 5-stage system for classification of CKD (Table 1) (110). The eGFR cut-off progressively decreases across CKD stages 1 to 5 (Table 1.1). Individuals with either CKD stages 1 or 2 exhibit the presence of markers of kidney damage but differ in absence (stage 1) or presence (stage 2) of mildly reduced GFR. Stages 3 to 5 are characterized based on the level of eGFR.

Several risk factors are associated with the initiation and progression of CKD (102). Among them, diabetes mellitus is a major risk factor for the development and progression of CKD (171). Other factors that appear to contribute to the initiation and progression of CKD include: glomerular, vascular and tubulointerstitial damage (79, 146, 150), polycystic kidney disease, hypertension, lupus erythematosus and renal obstruction from stones (33, 167).

Table 1.1 Classification of CKD as proposed by the Kidney Disease Outcomes Quality Initiative Guidelines (110).

CKD stage	eGFR (ml/min/1.73 m ²)	Description
1	≥90	Kidney damage with normal or increased GFR
2	60 - 89	Kidney damage with mild decrease in GFR
3	30 - 59	Moderate decrease in GFR
4	15 – 29	Severe decrease in GFR
5	<15	Kidney failure

CKD, chronic kidney disease; eGFR, estimated glomerular filtration rate

The pathophysiology of CKD is complex and differs according to the primary cause of CKD. After acute or chronic insults to the kidney many signaling pathways are activated, which initiate either glomerular or tubulointerstitial injury (23, 24, 31, 98). However, in 1998 Fine and colleagues proposed a unifying hypothesis, ‘the chronic hypoxia hypothesis’ (49), as a common final pathogenic pathway that leads to progression of CKD.

1.2 THE CHRONIC HYPOXIA HYPOTHESIS

According to the chronic hypoxia hypothesis proposed by Fine *et al*, initial glomerular injury causes decreased renal blood flow and oxygen delivery (DO₂) from peritubular capillaries (PTCs) thereby resulting in decreased renal tissue oxygen tension (PO₂) (49). This regional hypoxia activates various signaling pathways that promote tubulointerstitial fibrosis. Simultaneously, the remaining glomeruli maintain normal whole kidney GFR through increased single nephron GFR, in part through increased glomerular capillary pressure, which in turn increases damage to the glomerulus and capillary networks and promotes further development of fibrosis. Rarefaction of PTC can lead to tubulointerstitial hypoxia and accelerates the progression of CKD (Figure 1.1) (48, 49).

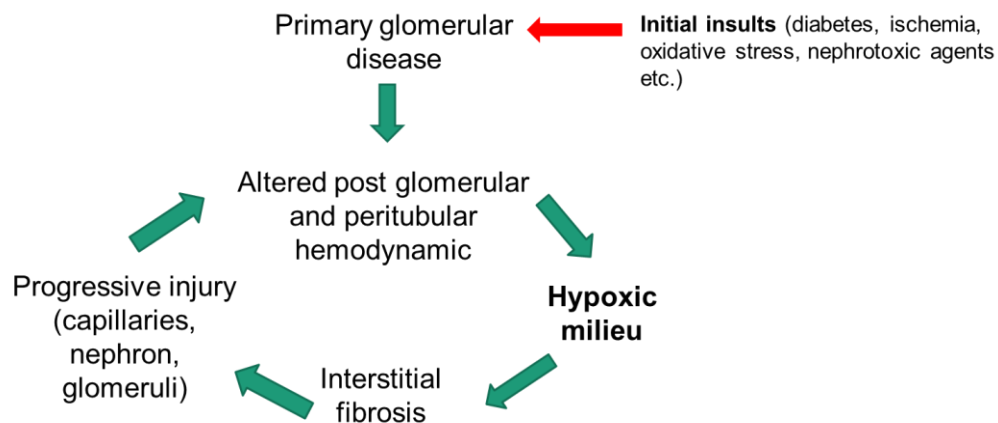


Figure 1.1 The chronic hypoxia hypothesis. Primary glomerular injury alters post-glomerular hemodynamics and restricts peritubular blood flow. Reduced peritubular blood flow leads to a hypoxic state. This hypoxic milieu further activates various downstream signaling pathways, which subsequently induces the development of interstitial fibrosis. This increased interstitial fibrosis, in turn, further exacerbates and accelerates renal injury and initiates a vicious cycle of hypoxia and injury, ultimately leading to organ failure.

A number of lines of evidence demonstrate the association of glomerular injury with obliteration of PTCs in experimental models of CKD (13, 21, 120). For example, Ohashi *et al* characterized the features of disruption of PTCs in anti-glomerular basement membrane-induced glomerulonephritis in rats. In their model, primary glomerular injury was associated with obliteration of glomerular capillaries and thus the downstream peritubular microcirculation (120). Similar observations were reported by Basile and colleagues in a rat model of ischemia/reperfusion injury (13). They utilized Microfil® infusion into rat kidneys 4, 8 and 40 weeks after ischemia/reperfusion injury. They found depletion of PTC density by 30 to 50% in the outer medulla. This study also provided evidence that tubulointerstitial fibrosis gradually exacerbates and induces the loss of PTCs and subsequently promotes renal dysfunction (13). Furthermore, in a study by Manotham and colleagues, inappropriate activation of the intrarenal renin-angiotensin system (RAS) was reported to contribute to reduced microcirculation in PTCs of the early phase of the rat remnant kidney model of CKD (98). This decreased downstream microcirculation may further contribute to the development of hypoxia.

There are multiple lines of experimental evidence in support of the chronic hypoxia hypothesis (49, 59, 98, 100, 197). But none of this experimental evidence demonstrates a direct causal relationship

between hypoxia and nephropathy (45). As we have recently reviewed in detail (127), at least six lines of evidence are required to confirm or reject this chronic hypoxia hypothesis (46, 127). These are:

- 1) CKD should always be associated with renal tissue hypoxia.
- 2) Renal tissue hypoxia should stimulate signaling cascades like inflammation, fibrosis, and capillary rarefaction to accelerate disease progression.
- 3) Hypoxia *per se* should be able to induce renal tissue injury in the absence of other contributing factors.
- 4) The initiation and progression of CKD should be prevented by preventing renal hypoxia.
- 5) Hypoxia should occur before the development of renal dysfunction.
- 6) Both renal tissue hypoxia and injury should be found in close vicinity.

A brief discussion on the current status of these lines of evidence is provided below. A more detailed analysis of these issues is provided in our recent review of this topic (127), which is reproduced in Appendix 1.

1) CKD should always be associated with renal tissue hypoxia

Experimental evidence demonstrates the presence of renal tissue hypoxia in multiple forms of CKD, including diabetic nephropathy (DN) (54, 131, 148, 149), the remnant kidney model (98), polycystic kidney disease (PKD) (33, 125) and CKD after recovery from ischemia/reperfusion injury (132). Rosenberger and colleagues reported development of regional hypoxia (outer medulla) in early stage of experimental type 1 diabetes (149). Renal tissue PO₂ was found to be decreased throughout the renal parenchyma, and most profoundly in the medullary region 4 weeks after induction of type 1 diabetes by streptozotocin (STZ) in rats (130). Pimonidazole adduct immunohistochemistry demonstrated the presence of cellular hypoxia in a rat model of PKD, in association with progressive renal injury (33). A clinical study by Manotham *et al* demonstrated significant lower intra-renal oxygenation in patients with diabetic CKD compared to the kidneys of healthy controls (96). The above studies clearly implicate hypoxia as a potential pathogenic factor in the progression of CKD. How might this hypoxia contribute to the progression of CKD?

2) Renal tissue hypoxia should stimulate signaling cascades like inflammation, fibrosis and capillary rarefaction to accelerate disease progression.

Chronic tissue hypoxia stabilizes hypoxic inducible factors (HIFs), transcription factors through which hypoxia stimulates downstream signaling pathways, which could potentially promote or retard progression of CKD (64). For example, under hypoxic conditions the stabilization of HIFs induce angiogenesis (64), erythropoiesis and iron metabolism (64), epithelial-to-mesenchymal transition and fibrogenesis (65, 97), increased apoptosis of proximal tubular cells (174), increased inflammatory responses via immature dendritic cell differentiation (143), and generation of reactive oxygen species (157).

A study by Manotham and colleagues demonstrated that hypoxia induces epithelial-to-mesenchymal trans-differentiation of tubular cells *in vitro* (97). Similar phenotypic changes in renal tubular cells have been found in many experimental models of CKD (1, 111). These phenotypic changes in the tubulointerstitium might disturb the homeostasis of extracellular matrix (ECM) production and subsequently increase the formation of interstitial fibrosis. Furthermore, this increased fibrosis may impede tissue oxygen diffusion and augment hypoxia.

Proximal tubular cells of the kidney are particularly susceptible to hypoxia due to their considerable demand for oxygen to drive sodium reabsorption (85). In turn, hypoxia increases apoptotic cell death of proximal epithelial cells (174). Thus, development of hypoxia may play a crucial role in the progression of interstitial injury.

3) Hypoxia per se should be able to induce renal tissue injury in the absence of other contributing factors.

Recent experimental evidence reported by Friedrich-Persson and colleagues supports the hypothesis that hypoxia itself leads to development of nephropathy, even in the absence of other insults like hyperglycemia, hypertension or oxidative stress (59). In their landmark study, 2,4-dinitrophenol, a mitochondrial uncoupler, was administered for 30 consecutive days to normoglycemic rats. This treatment increased mitochondrial oxygen consumption resulting in renal tissue hypoxia followed by nephropathy. Renal tissue hypoxia in these rats was associated with increased urinary protein excretion, increased renal vimentin expression and infiltration of inflammatory cells. On the other hand, arterial blood pressure, renal blood flow, renal markers of oxidative stress and GFR remained

unaffected in 2,4-dinitrophenol-treated rats (59). A similar observation was also reported when triiodothyronine, a thyroid hormone, was administered to normoglycemic rats for 10 days (58). These studies demonstrate that renal tissue hypoxia itself can act as an important pathogenic mediator of development of nephropathy.

4) *The initiation and progression of CKD should be prevented by preventing renal hypoxia.*

Experimental evidence (98, 116) indicate that activation of the RAS in the early stages of kidney disease also contributes to development of renal tissue hypoxia and thereby contributes to the progression of CKD. An angiotensin receptor antagonist (ARB) attenuated hypoxia in tubular cells and preserved PTCs network structure in the remnant kidney model of CKD (98). The findings of this study also demonstrate this therapeutic approach decreased hypoxia-responsive gene expression in the treated animals, suggesting a role of activation of the RAS in tubulointerstitial hypoxia (98). Both an ARB and an angiotensin converting enzyme (ACE) inhibitor were reported to raise tissue PO₂ in the interstitial microvascular compartment of the rat kidney (116). These agents have also been shown to slow the progression of CKD (91, 151). Taken together, these results suggest that activation of the RAS alters the tubulointerstitial microvascular circulation and consequently drives the development of hypoxia.

Administration of drugs targeting oxidative stress could not alleviate hypoxia completely in experimental models of CKD (130, 132). Hyperglycemia induces formation of reactive oxygen species, which directly affect mitochondrial oxygen utilization (59, 129). Palm *et al* treated diabetic rats with α -tocopherol across a 4-week period. The treatment was shown to prevent diabetes-induced oxidative stress and the associated decrease in tissue PO₂ in the renal medulla, but could not prevent decreased cortical PO₂ completely (130). Papazova and colleagues (132) found that renal transplantation in rats was accompanied by increased renal oxygen consumption (VO₂), decreased renal tissue PO₂ and increased renal oxidative stress. However, treatment with an antioxidant (mito-TEMPO) targeting mitochondrial superoxide production after renal transplantation, normalized oxidative stress but did not improve whole kidney oxygen consumption or renal tissue PO₂. These findings indicate that currently available treatments with antioxidants are not able to prevent renal hypoxia and thereby progression of CKD completely. Thus, there is an urgent need to better understand the causal relationship between hypoxia and nephropathy, through development of new therapies to alleviate renal hypoxia.

5) *Hypoxia should occur before the development of renal dysfunction*

An experimental study by Manotham and colleagues (98) demonstrated renal tubular hypoxia in the early stage of the remnant kidney model of CKD, before any histological tubulointerstitial damage could be observed. This was evinced by the presence of positive staining for pimonidazole adducts and expression of HIF-1 α , and by increased transcription of hypoxia responsive genes (98). Similarly, Matsumoto *et al* provided evidence of tubular hypoxia in the early stage of a model of a rat glomerulonephritis (100). The overall structure of the renal tubules remained normal during the evolution of renal hypoxia. However, this study could not demonstrate the precise time-point of the initiation of hypoxia or a causal relationship between hypoxia and disease progression in these experimental models of CKD. Recently, Franzen *et al* demonstrated cortical tissue hypoxia 3 days after induction of type 1 diabetes in mice (54). They implanted an oxygen-sensing probe in the renal cortex for repeated measurement of tissue PO₂ using electron paramagnetic resonance oximetry. In this study, intrarenal tissue hypoxia developed before the onset of DN and was sustained until the end of the study, 2 weeks after administration of STZ (54). However, the tissue PO₂ was measured in anesthetized mice in this study (54), so a potentially confounding effect of anesthesia could not be excluded. To address this gap in our knowledge, in the experiments described in Chapter 4 of this thesis, I used a newly developed telemetric method for measurement of renal tissue oxygenation in unanesthetized rats, to characterize the time-course of changes in renal oxygenation in adenine-induced CKD (Ad-CKD).

Diabetes is associated with glomerular hyperfiltration (18, 181, 189). Approximately 80% of VO₂ is utilized to drive tubular sodium reabsorption (43). Thus, hyperfiltration would be expected to promote renal hypoxia by increasing the filtered load of sodium. Most evidence suggests that hyperfiltration is an early and sustained event in diabetes. However, much of this evidence comes from studies of anesthetized animals (73, 162, 189). In those studies in which GFR has been measured in conscious rats, using the newly developed method of transcutaneous measurement of clearance of fluorescein isothiocyanate (FITC)-sinistrin (57, 161, 170), a variety of mathematically derived models have been applied to analysis of the data. In the studies described in Chapter 5 of this thesis I attempted to clarify the potential for hyperfiltration to contribute to the early appearance of renal hypoxia in diabetes. To achieve this aim I measured GFR, using FITC-sinistrin, during the first four weeks of STZ-induced

diabetes in rats. I compared available mathematical models for analysis of these data to determine whether the choice of model could influence the conclusions drawn.

6) *Both renal tissue hypoxia and injury should be found in close vicinity*

This important question has received remarkably little attention. Therefore, in the experimental studies described in Chapters 2 and 3 of this thesis, I investigated the spatial relationships between hypoxia and tissue fibrosis in Ad-CKD using a combination of pimonidazole adduct immunohistochemistry and histochemical analysis of fibrosis.

One of the barriers to understanding the roles of fibrosis and microvascular rarefaction in the development of renal hypoxia in CKD is our relatively poor understanding of the biophysical basis of oxygen delivery to renal tissue in CKD. In an attempt to better understand this issue, our research group has recently developed a series of mathematical models of oxygen transport in the kidney (61, 62, 81, 88-90, 113). The major missing factor in these models is precise information about the geometry of vascular-tubular interactions within the cortex and medulla. Therefore, in the experiments described in Chapter 6 of this thesis, I performed preliminary studies aimed towards development of high resolution imaging of the spatial relationships between capillaries and tubules in renal tissue.

Summary: The balance of available evidence supports the presence of hypoxia in CKD and its association with the progression of disease. However, whether hypoxia is a cause or consequence of renal injury has still not been determined. None of the studies discussed above precisely demonstrate the time-course of development of hypoxia (temporal) and its association (spatial) with progression of CKD (45, 127). There is, therefore, a need for more definitive evidence to allow us to accept or refute the chronic hypoxia hypothesis.

In the studies described in this thesis, I investigated the temporal relationships between hypoxia and its causes and the progression of CKD (Chapters 2-5). I also investigated the spatial relationship between tissue hypoxia and fibrosis (Chapters 2-3). Finally, I performed preliminary studies with the aim of developing a new approach to characterizing the spatial relationships between PTCs and tubules, which could be applied to generation of structural information for computational models of oxygen delivery to renal tissue. I employed two models of CKD; Ad-CKD and DN. Below, I provide a brief description of the pathophysiology of these experimental models and their relevance to the

overall aims of my project. I also outline the methods I have used to assess renal oxygenation and its determinants.

1.3 ADENINE-INDUCED CKD

Adenine: Adenine is a purine that is incorporated into nucleic acids (DNA and RNA). In DNA it binds to thymine by two hydrogen bonds that stabilize the structure of DNA (196). In addition, its derivatives have a variety of roles to modulate energy metabolism, in signal transduction, and as structural components of some co-enzymes (*i.e.* nicotinamide adenine dinucleotide and flavin adenine dinucleotide (95)).

Adenine metabolism: In mammalian tissue, adenine is synthesized by purine metabolism. Under normal physiological conditions, adenine is converted to adenylyate monophosphate by adenine phosphoribosyl transferase (APRT), thus resulting in low concentrations of adenine in blood and urine (36, 39). However, deficiency of APRT can occur in the human population as an autosomal recessive trait, which is characterized by the presence of kidney stones, crystalluria, dysuria and urinary tract infections (80, 109, 152). Besides this, if adenine is present in excess in mammalian tissue due to deficiency of APRT or consumption of purine-rich foods, it becomes a significant substrate for xanthine dehydrogenase, which further oxidizes adenine to 2,8-dihydroxyadenine (DHA) via the intermediate 8-hydroxyadenine (200). Both adenine and DHA are excreted in urine. But due to very low solubility, the DHA can precipitate and obstruct renal tubules, resulting in kidney disease (22, 36).

Prevalence of adenine-induced chronic kidney disease: The prevalence of Ad-CKD is largely unknown. The majority of patients with Ad-CKD remain undiagnosed due to a lack of knowledge related to the pathogenesis of the disease and inadequate evaluation of kidney stones from patients (37). However, the calculated heterozygote frequency in various populations ranges from 0.4 to 1.2% (68, 153) with the majority of cases reported from Japan, France and Iceland (37, 152).

Characteristics of Ad-CKD: Both clinical and experimental evidence demonstrate the presence of increased plasma urea (101) and creatinine concentration (154) as well as proteinuria (53, 154) in Ad-CKD due to altered kidney function. Furthermore, hematoxylin and eosin-stained histological kidney sections exhibit deposition of DHA crystals in tubular and interstitial regions of both human and animal kidneys (53, 80, 154). Ad-CKD is also characterized by the presence of interstitial fibrosis (53,

80, 101, 109), extensive tubular dilatation (39), degeneration of the proximal tubular epithelium with loss of the brush border (80, 154) and inflammatory cell infiltration (154).

Ad-CKD is categorized as a tubular crystal nephropathy (106). Deficiency of the APRT enzyme results in an insoluble crystal (DHA) precipitate in the renal tubules that obstructs tubular flow and initiates injury (80, 109, 200). Santana *et al* demonstrated that glomeruli remain intact in kidneys of mice after 6 weeks of adenine treatment (154), whereas tubular deposition of crystals in these mice is accompanied by tubular dilatation and marked renal interstitial fibrosis (34, 101, 154). Thus, like most other forms of CKD, Ad-CKD exhibits tubulointerstitial fibrosis (53, 101, 154). In the case of Ad-CKD, tubulointerstitial fibrosis develops in the early stages of disease progression (53, 101, 121, 154).

Renal interstitial fibrosis and renal hypoxia: The early presence of tubulointerstitial fibrosis in Ad-CKD makes this an excellent model to assess the temporal relationships between renal tissue hypoxia and the progression of CKD. Therefore, in the studies described in Chapters 2, 3 and 4 of this thesis, I applied multiple methods for assessing renal tissue oxygenation and its determinants (*e.g.* DO₂ and VO₂) in this model. Below, I provide brief descriptions of these methods with commentary on their strengths and limitations.

1.4. METHODS FOR ASSESSING RENAL OXYGENATION

Experimental evidence demonstrates an association between renal hypoxia and the pathogenesis of multiple forms of CKD (58, 115, 125). However, due in part to limitations in available methods for characterizing renal oxygenation with high temporal and spatial resolution, the chronic hypoxia hypothesis has still not been fully tested. The combination of multiple techniques, each with varying spatial and temporal resolution, could potentially overcome these limitations and allow better characterization of renal tissue oxygenation in experimental models of CKD. These techniques are briefly described below and are described in more detail in Chapters 2- 4 of this thesis.

1) Pimonidazole adduct immunohistochemistry

Pimonidazole adduct immunohistochemistry (98) has been used to characterize the cellular localization of hypoxia in multiple forms of CKD (53, 149). Pimonidazole is irreversibly reduced to a hydroxylamine intermediate (6, 7) in cells with oxygen tension less than 10 mmHg. The hydroxylamine intermediate binds to thiol containing compounds such as glutathione and proteins and

forms pimonidazole adducts in tissues. These adducts can be detected by immunohistochemistry (149). Thus, it is a marker of cellular hypoxia (6), providing excellent spatial resolution. However, it does not provide direct quantification of renal tissue hypoxia. The chromogen 3-diaminobenzidine, used to visualize pimonidazole adducts, does not follow the Beer-Lambert law (191). As a result, the concentration of pimonidazole adducts is not directly proportional to the intensity of staining. In addition, the method can only be used at discrete single time points. I used pimonidazole adduct immunohistochemistry for cellular localization of hypoxia (spatial distribution) in Ad-CKD (Chapters 2 and 3).

2) *The Clark electrode and blood oximetry:*

Clark electrode: The Clark electrode measures PO₂ in tissues based on an oxidation-reduction reaction (14, 71, 194). It consists of two units: i) three electrodes, namely an O₂-sensitive cathode (platinum), a reference electrode (silver anode), and a guard cathode (silver), and ii) a voltage source (93). At the anode, silver is oxidized to silver chloride ($4\text{Cl}^- + 4\text{Ag} \rightarrow 4\text{AgCl} + 4\text{e}^-$) and at the cathode an oxygen molecule is reduced to water ($\text{O}_2 + 4\text{e}^- + 4\text{H}^+ \rightarrow 2\text{H}_2\text{O}$). The more oxygen available for the reaction, the greater the flow of electrons in the system (*i.e.* a higher current) (71). Thus, the Clark electrode uses amperometry to determine PO₂. The electrode compartment is insulated from the reaction compartment (solution, tissue) by an oxygen-permeable but liquid impermeable membrane (93, 194).

The Clark electrode can be used to determine renal tissue PO₂ at various depths below the kidney surface, so can provide some degree of spatial resolution of renal tissue PO₂ (14). In 1960, Aukland and Krogh determined renal tissue PO₂ in anesthetized dogs by stepwise insertion of micro electrodes from the renal surface to a depth of 7 mm below the renal capsule (8). For the first time, they demonstrated that medullary tissue PO₂ is less than cortical tissue PO₂. This observation has since been confirmed in the kidneys of dogs (14) and rats (93). In 1997, Liss and colleagues introduced a modified Clark electrode with an outer tip diameter of $5.5 \pm 1.9 \mu\text{m}$ and measured renal tissue PO₂ in the cortex (average 45 ± 2 mmHg), outer medulla (32 ± 2 mmHg) and in the inner medulla (average 25 ± 2 mmHg) of rats (93). The important observation from the above studies is that Clark-type micro electrodes could provide quantitative information about renal tissue PO₂ and some level of spatial resolution. However, this method provides no information about the determinants of renal oxygenation, especially the balance between DO₂ and VO₂.

Blood oximetry: Renal DO_2 is the product of renal blood flow and arterial blood oxygen concentration (2). Renal VO_2 is the product of renal blood flow and the difference in oxygen concentration between arterial and renal venous blood (2). This information can thus be obtained through measurement of the oxygen content of arterial and renal venous blood combined with measurement of total renal blood flow. Furthermore, the major determinant of renal VO_2 , tubular sodium reabsorption, can be determined by quantification of the renal clearance of inulin (a measure of GFR) and sodium.

The application of the Clark electrode for measurement of renal tissue PO_2 has several limitations: i) It is highly invasive and requires removal of a portion of the renal capsule for electrode insertion. This prevents its application in humans as well as for repeated within-animal measurements (limited temporal resolution). ii) Renal tissue PO_2 is measured under anesthesia. Thus the observations made by Clark electrode may be confounded by the effect of anesthesia, and iii) the electrodes are fragile and subject to some baseline drift. Consequently, technical skill is required to handle the electrode during experiments and for accurate measurement of tissue PO_2 . Despite these disadvantages, the Clark electrode can provide a quantitative profile of tissue PO_2 at multiple sites (*i.e.* with some spatial resolution) throughout the kidney at multiple time-points. Therefore, I applied the Clark electrode in combination with blood oximetry to characterize renal oxygenation in Ad-CKD (Chapter 4).

3) *The oxygen telemeter*

Recently, Koeners *et al* developed a radio-telemeter based oxygen sensor for continuous monitoring of renal tissue PO_2 in freely moving rats (83). After implantation of the telemeter in the rat kidney they were able to record stable levels of medullary tissue PO_2 over a 3 week experimental protocol (83). Emans and colleagues implanted radio-telemeters in the renal cortex of rats and reported stable recording of cortical tissue PO_2 for 3 weeks under conscious state (38). They were also able to detect renal tissue hypoxia during acute infusion of angiotensin II and activation of the endogenous RAS. More recently, Ow and colleagues used this technique to demonstrate the absence of renal tissue hypoxia during the sub-acute phase of recovery from ischemia/reperfusion injury (126). Adamovich *et al* were able to use this technique to demonstrate circadian rhythms in renal cortical oxygenation in freely moving rats (3). Thus, this technique provides an opportunity for continuous measurement of renal tissue PO_2 , with high temporal resolution, for periods of weeks in animals in their natural condition. However, this technique is also not without limitations. Most importantly, renal tissue PO_2 can be measured only in relative terms and at only one site of the kidney.

The functional radio-telemeter consists of two separate units: i) a three electrode system and ii) the probe body (84). The three electrodes required for measurement of tissue PO₂ are an oxygen sensing carbon paste electrode, a reference electrode, and an auxiliary electrode. The probe body contains a battery unit and a potentiostat circuit which maintains a -650 mV potential on the carbon paste electrode to the reference electrode (83). The potential difference resulting from reduction of oxygen in the tip of the carbon paste is measured and transmitted wirelessly to a remote receiving station (83). In the studies described in Chapter 4 of this thesis, I utilized this method to characterize renal tissue oxygenation during the first week of Ad-CKD. Details regarding the construction and implantation of the telemeter are provided in Chapter 4.

1.5 DIABETIC NEPHROPATHY

DN is the most common cause of CKD and end-stage renal disease (ESRD) globally (92). It is characterized by persistent albuminuria (ratio of albumin to creatinine excretion ≥ 30 mg/g), the presence of glomerular lesions, and impaired GFR (< 60 ml/min/1.73 m²) (92, 144). The prevalence of diabetes and DN is increasing at an alarming rate (63). Globally, the prevalence of diabetes is expected to grow from 382 million people in 2013 to 592 million by 2035 (63). It has been estimated that approximately 20% to 40% of diabetic patients developed DN (133).

1.5.1 Diabetic nephropathy and renal hypoxia

Numerous studies have been carried out to determine the time-course and causes of renal hypoxia in diabetes and its role in the pathogenesis of DN (115, 130, 148, 149). Palm *et al* and Nordquist *et al* showed the development of renal hypoxia throughout the renal parenchyma of diabetic rats as early as 4 weeks after induction of diabetes (115, 130). Renal VO₂ was markedly increased in diabetic rats (115, 130). More recently, Franzen and colleagues observed renal tissue hypoxia as early as 3 days after induction of diabetes in mice, well before the onset of albuminuria (54). Thus, renal tissue hypoxia appears to be an early and persistent event in DN.

The causes of renal tissue hypoxia remain a matter of considerable interest in the field of diabetic nephropathy. Renal hypoxia in diabetic rats has been found to be associated with glomerular hyperfiltration, proteinuria and interstitial damage. Of note, acute administration of cobalt chloride, a hypoxia mimetic agent, prevented diabetes-induced renal hypoxia in rats with STZ-induced diabetes

(115). Potential mechanisms underlying this effect include normalization of GFR, prevention of mitochondrial leak respiration and improvement of tubular transport efficiency (115). Consistent with a role for hyperfiltration, Körner *et al* reported that glomerular hyperfiltration and proteinuria are associated with elevated VO_2 in the proximal tubules of diabetic rats (85). Approximately 80% of the oxygen consumed by the kidney under normal physiological conditions is used to drive sodium reabsorption (43). Thus, anything that increases the filtered load of sodium would be expected to increase VO_2 and thus promote renal tissue hypoxia. This led us to consider the potential role of hyperfiltration as an early driver of renal hypoxia in diabetes.

1.5.2 Glomerular hyperfiltration

Glomerular hyperfiltration, a sustained absolute increase in GFR, is a characteristic finding in experimental animal models of type 1 diabetes (10, 179) and patients with insulin-dependent diabetes mellitus (IDDM) (66, 103). The mechanisms involved in development of glomerular hyperfiltration in diabetes mellitus are not yet fully understood. Vallon and colleagues proposed a tubulo-centric hypothesis for development of glomerular hyperfiltration in the early stages of type 1 diabetes (185). This proposition centres on the important role of the sodium-glucose co-transporter in tubular reabsorption of glucose and sodium.

Under normoglycemic conditions approximately 99% of the filtered load of glucose is reabsorbed by the sodium dependent glucose co-transporter-2 (SGLT-2), expressed in the brush-border membrane of the proximal tubules (184, 188). Reabsorption of glucose in the proximal tubule is dependent on the reabsorption of sodium, which is in turn dependent on the transcellular concentration gradient of sodium generated by the $\text{Na}^+\text{-K}^+$ ATPase pump on the basolateral side of the cell (12, 86, 164). Approximately 80% of the oxygen consumption of the kidney under physiological conditions is used to drive $\text{Na}^+\text{-K}^+$ ATPase (43). Thus, glucose reabsorption indirectly depends on an energy consuming process dependent upon oxygen-dependent ATP production. The increased reabsorption of glucose by the proximal tubule in diabetes thus has the potential to greatly influence sodium transport in the proximal tubule, and through the mechanisms of tubuloglomerular feedback (TGF) (183), afferent arteriolar tone and single nephron GFR.

Tubulo-centric hypothesis of diabetic hyperfiltration: A growing body of evidence indicates that hyperglycemia is associated with an increase in proximal tubular reabsorption of sodium and fluid in

experimental models of diabetes mellitus (137, 186, 189) and patients with IDDM (25, 66, 119, 198). Micropuncture experiments in Munich-Wistar rats (a strain with superficial glomeruli accessible for direct measurement of glomerular capillary pressure) have shown that fractional tubular reabsorption of electrolytes (Na^+ , Cl^- , and K^+) is increased upstream to the early distal tubule in STZ-diabetic rats compared to control rats (189). In patients with type 1 diabetes, observations using lithium clearance as a marker of distal sodium delivery indicate that both fractional and absolute proximal sodium reabsorption is increased significantly compared to proximal tubular reabsorption observed in healthy subjects (66). Bróchner-Mortensen *et al* reported increased rates of both fractional and absolute reabsorption of fluid in proximal tubules in patients with IDDM compared to controls (25). In this study the absolute reabsorption rate in proximal tubule in patients with IDDM was 107.4 ± 10.1 ml/min and in control group was 79.9 ± 13.6 ml/min.

The high concentration of glucose in glomerular filtrate appears to increase the reabsorption of sodium in the proximal tubule under a diabetic milieu (12). A microperfusion study by Bank and Aynedjian showed that stepwise increases in luminal glucose concentration markedly stimulates sodium and water reabsorption in the proximal tubules of both STZ-diabetic rats and control rats (12). This sodium reabsorption coupled with glucose is mediated by SGLT (12, 138, 188), located on the luminal aspects of the proximal tubule (11, 188). The broad-spectrum SGLT (subtype 1 and 2) inhibitor, phlorizin, inhibited sodium reabsorption in the early proximal tubule of diabetic rats (189). In this micropuncture study, phlorizin was directly applied into the free flowing early proximal tubule of diabetic rats. This SGLT inhibitor markedly reduced the fractional and absolute reabsorption of sodium and glucose in the early proximal tubule and abolished hyper-reabsorption in diabetic rats (189).

The increased fractional reabsorption of electrolytes in the proximal tubule in diabetes is associated with reduced (20-28%) concentrations of electrolytes (Na^+ , Cl^- , and K^+) in the early distal tubular fluid in STZ-diabetic rats compared to non-diabetic rats (189). This reduction of distal delivery was associated with increased single nephron glomerular filtration rate (SNGFR) in STZ-diabetic rats (189). Conversely, inhibition of proximal tubular sodium reabsorption in STZ-diabetic rats increased electrolyte concentrations in the early distal tubule leading to a marked reduction in SNGFR (189). Microperfusion experiments have shown that alterations in the rate of either proximal tubular reabsorption or electrolyte delivery to the distal tubule influence SNGFR within the same nephron by modulating vascular tone in the afferent arteriole (20, 73, 182, 189, 199). This mechanism, which

maintains the fluid and electrolytes delivery in the distal nephron within certain ranges through control of SNGFR, is called TGF (183).

Adenosine is a major mediator of TGF-mediated vasoconstriction in pre-glomerular arterioles (123). The macula densa, a collection of specialized epithelial cells in the distal convoluted tubule, releases ATP at the basolateral membrane in response to increased luminal NaCl concentration (16). This ATP is converted to adenosine, a purine nucleoside, by a series of enzymatic process (145). Adenosine can mediate vasoconstriction in afferent arterioles through activation of purinergic A₁ receptors (A₁ARs) (26). Osswald *et al* found that continuous intrarenal infusion of adenosine preferentially constricts the afferent arterioles of the superficial cortex (123), which consequently reduces renal blood flow. This afferent arteriolar constriction was associated with decreased superficial SNGFR as well as whole kidney GFR in dogs. Local pharmacological blockade of adenosine activity, by inhibition of the ecto-5'-nucleotidase (an enzyme that catalyzes extracellular conversion of adenine nucleotides to adenosine) (145, 178), or by blockade of the A₁AR) by 8-cyclopentyl-1,3-dipropylxanthine (158), attenuated the TGF response in anesthetized rats. Micropuncture studies in the kidneys of mice lacking ecto-5'-nucleotidase demonstrated diminished TGF responses. That is, in the knockout mice smaller fractional changes in SNGFR were observed in response to given changes in distal tubule flow compared to their wild-type littermate controls (74). Thus, TGF regulation of SNGFR appears to be mainly mediated by adenosine, which is released in response to high distal nephron fluid and electrolyte flow (145). In STZ-diabetic rats, decreased electrolyte flux across the macula densa due to increased proximal tubular reabsorption (189) could diminish the TGF signal, resulting in an increased SNGFR (186).

In diabetes mellitus, glomerular hyperfiltration occurs at the single nephron level and is associated with an absolute increase in GFR at the whole kidney level (73). Much of the evidence to support this statement comes from assessment of renal function by micropuncture of superficial nephrons in the intact kidney (73, 77, 78, 162, 203). Scholey and Meyer reported that STZ-diabetic rats with moderate hyperglycemia exhibit increased SNGFR as well as whole kidney GFR compare to non-diabetic rats (162).

Hyperfiltration could also promote the development of tubulointerstitial damage by promoting hypoxia. As discussed in detail earlier (section 1.5.1) hypoxia appears to be an early and persistent

feature in diabetes. Therefore, if hyperfiltration is an important contributor to tubulointerstitial hypoxia in diabetes, we should expect it to also be an early and persistent characteristic of diabetes. Indeed, by understanding the time-course of hyperfiltration in diabetes we should be able to generate a better understanding of its role in promoting renal tissue hypoxia.

The precise time-course of development of glomerular hyperfiltration in conscious animals after the onset of diabetes is still controversial (10, 50, 117, 181). Bak and co-workers measured GFR, using the steady state constant infusion technique, across the first 7 days after induction of diabetes in unanesthetized female Sprague-Dawley rats (10). GFR was 16% greater in STZ-diabetic rats at day 7 compared with the respective control group (10). In a different study Tucker *et al* showed that GFR was significantly greater 24 hours after induction of diabetes, in an rats not receiving insulin replacement, compared to their pre-diabetic state (181). Furthermore, in that study GFR remained increased during the 15 day experimental protocol (181). In contrast, there was a modest increase of GFR in insulin treated STZ-diabetic rats, when the concentration of blood glucose was tightly maintained, only at day 15 compared to their baseline measurements (181). Bell *et al* detected elevated GFR in STZ- diabetic rats compared to the respective control group, when GFR was assessed at day 4 and day 12 after induction of diabetes (17, 18). In two separate studies, glomerular hyperfiltration could not be detected in unanesthetized STZ-diabetic rats across 3-4 week experimental protocols, where GFR was measured by using either the steady state constant infusion technique or a noninvasive single injection technique (50, 117). However, a significant elevation of GFR was detected at 1 and 4 week after induction of diabetes, when GFR was indexed to body weight (117). Thus, there remains considerable controversy regarding the time-course of development of hyperfiltration in STZ-induced diabetes in rats.

Why does the time-course of development of glomerular hyperfiltration differ among these studies of conscious diabetic rats? One possible reason is the use of different methods to measure GFR as well as the use of differing mathematical formulas, with differing underlying assumptions, to calculate GFR in conscious rats (117, 181). The constant intravenous infusion based method is commonly used to measure GFR in experimental and clinical settings (10, 35, 50, 181). This method requires a constant intravenous infusion of an exogenous marker (e.g. inulin) to maintain steady-state plasma concentrations. After an equilibration period, urine and blood samples are collected at multiple time points (10). These urine and blood samples are then analyzed for determination of the plasma and

urinary concentrations of the marker, thus allowing measurement of its renal clearance. An alternative approach for measurement of GFR requires injection of a radioactive marker by tail vein and then timed collection of blood samples from the tail vein. The levels of the radioactive marker can then be determined and GFR can be estimated using a specific formula (28, 117). The major disadvantage of this technique is that a separate group of rats is required for determination of the volume of distribution of the marker (117). There are limitations of these techniques, associated with the need for surgical preparation for catheter implantation, collection of multiple blood and/or urine samples and laboratory analysis of the samples (10, 35). Overall these techniques are invasive, cumbersome and time consuming.

To address the limitations in standard methods for estimation of GFR in experimental animals, a new technique has recently become available that relies on transcutaneous measurement of the concentration of FITC-sinistrin, and thus its clearance (57, 160, 161). This new method overcomes many of the limitations of the more established techniques described above. However, it does require the application of a specific mathematical model of the clearance of FITC-sinistrin, and thus assumptions about the nature of the compartments from which it is cleared (57, 161). Therefore, in the experiments described in Chapter 5 of this thesis, I deployed this technique to assess the time-course of development of glomerular hyperfiltration in STZ-induced diabetes in rats. Importantly, I compared available models for calculating the clearance of FITC-sinistrin, to determine whether the choice of model could influence the interpretation of our findings. Below, I describe the nature of the experimental model used and the theoretical and practical considerations underlying the use of transcutaneous FITC-sinistrin clearance for estimation of GFR.

1.5.3 Streptozotocin-induced type 1 diabetes

STZ-induced type 1 diabetes in rats is a commonly used experimental model (50, 135, 175, 190). Animals are rendered diabetic by a single intravenous injection of STZ (50, 77, 175), which causes rapid destruction of pancreatic β -cells resulting in overt hyperglycemia (72). The great advantage of this model of diabetes is that it can be induced with a single injection of STZ, so the time of onset of hyperglycemia is known, providing a precise reference point for characterization of the development of glomerular hyperfiltration in experimental animals.

In the studies described in Chapter 5 of this thesis I chose to provide diabetic animals with insulin therapy so that they exhibited only moderate hyperglycemia. This experimental model of moderate hyperglycemia recapitulates many aspects of type 1 diabetes in humans, including the presence of glomerular hyperfiltration (118, 192). STZ-diabetic rats develop characteristics of DN including renal hypertrophy, glomerular hyperfiltration (52, 135, 187, 190) and albuminuria (52, 190). In addition, histological examinations of renal specimens of diabetic rats, treated with low doses of insulin to maintain moderate blood glucose, exhibit glomerular lesions including glomerular basement membrane thickening (124, 190), focal glomerular sclerosis, and diffuse mesangial expansion (190) .

1.5.4 Transcutaneous measurement of glomerular filtration rate using FITC–sinistrin

Sinistrin, a sugar polymer, chemically labeled with FITC, can be used as an exogenous marker for the transcutaneous measurement of GFR (57, 136). It is readily soluble in water at room temperature (136). Sinistrin is freely filtered at the glomerular capillary membrane but is not secreted, reabsorbed or metabolized in the renal tubules (29, 41, 176). These characteristics make sinistrin an ideal marker for measurement of GFR.

The fluorescence-based transcutaneous measurement of GFR involves injection of an exogenous fluorescent marker (FITC-sinistrin) and detection of the clearance of this marker by a device (non-invasive clearance (NIC)-kidney device; Mannheim Pharma and Diagnostics GmbH, Mannheim, Germany) that measures fluorescence generated by the FITC-sinistrin within the skin (i.e. transcutaneously) (57, 67, 159, 161). After intravenous administration of the fluorescent marker, it equilibrates within the extracellular (plasma and interstitial) space and is excreted by the kidneys. The clearance of this marker in the interstitial space is measured by a NIC-kidney device placed on the animal's skin (161). The device comprises a light-emitting diode, a photodiode and an internal memory (161). The light-emitting diode repeatedly excites the fluorescence marker within the interstitial space at a 480 nm wavelength and the light emitted by the marker (wavelength 520 nm) is detected by the photodiode (161). The device converts the emitted light into a digital signal, which can be opened and analyzed by the MPD Studio software package (Mannheim Pharma and Diagnostics GmbH) (57). The software generates the elimination kinetics of FITC-sinistrin from which the excretion half-life ($t_{1/2}$) of the marker measured in the interstitial space can be estimated using one or more mathematical models that are based on consideration of the compartments that the FITC-sinistrin is present in (57,

160, 161). This $t_{1/2}$ can then be used to generate an elimination rate constant (λ) (57) and thus, an estimate of GFR (57, 161). Advantages of this technique over more traditional clearance-based techniques include the fact that no blood or urine samples are required, no time-consuming laboratory analysis is required, and that an estimate of GFR can be generated immediately after completion of the procedure (105, 160).

A mathematically derived model is applied to the exponential phase of the excretion kinetics to calculate the $t_{1/2}$ and λ . The $t_{1/2}$ is calculated by using equation 1 (57, 108).

$$t_{1/2} = \frac{\ln(2)}{\lambda} \quad (1)$$

Here, $t_{1/2}$ is defined as the time over which half of any given amount of an exogenous marker is cleared (108). The elimination rate constant is denoted by λ , which is defined as the elimination of a constant fraction of the marker per unit time. The term $\ln(2)$ is the natural logarithm of 2, which is approximately 0.693. The λ can be derived from equation (1)

$$\lambda = t_{1/2} \times \ln(2) \quad (2)$$

In the single injection technique, GFR is calculated from the elimination rate constant multiplied by the extracellular fluid volume (108).

$$GFR \text{ (ml/min)} = \text{Extracellular fluid volume (ml)} \times \lambda \quad (3)$$

To calculate GFR after a single injection of an exogenous marker, knowledge of the volume of the distribution of the GFR marker and elimination rate constant of that marker are needed. However, the elimination rate constant is an expression of GFR, which is indexed to extracellular fluid volume (equation 4) (134, 142). Therefore, the elimination rate constant in the form $t_{1/2}$ is required for estimation of GFR. Variables such as the injected dose of the marker or variables related to body composition are not required, including height and weight (134) and volume of extracellular fluid (161). Rabito *et al* demonstrated a very close correlation ($r^2=0.97$) between the rate constant measured by clearance of ^{99m}Tc -diethylenetriaminepentaacetic acid from extracellular space and the GFR values determined by the standard ^{125}I -iothalamate clearance technique (142).

$$\lambda = \frac{GFR (ml/min)}{\text{Extracellular fluid volume (ml)}} \quad (4)$$

The $t_{1/2}$ can be used for calculation of GFR according to the following formula (57):

$$GFR (ml/min)/100 g \text{ body weight} = \frac{21.33 (ml/100 g \text{ body weight})}{t_{1/2}} \quad (5)$$

Where, the numerator 21.33 (ml/100g body weight) is an empirically derived conversion factor for GFR calculation for rats (57) and $t_{1/2}$ is the excretion half-life of the GFR marker.

The transcutaneous technique for measurement of GFR can be used to measure GFR in unanesthetized, freely moving animals (57, 161, 163) and thus avoids the confounding effects of anesthesia. In contrast, in rats, infusion based methods for measurement of GFR often require anesthesia (125, 126), or when they are used in conscious rats it is often only several hours after surgery for implantation of intravascular catheters (193). There is strong evidence that anesthesia can reduce GFR in rats. For example, GFR, measured by enzymatic analysis of sugar moiety of FITC-sinistrin, was 37% less in rats anesthetized with a combination of ketamine and xylazine (0.90 ± 0.16 mL/min/100 g body weight) than in conscious rats (1.41 ± 0.14 mL/min/100 g body weight) (160). Transcutaneous methods for measurement of GFR using FITC-sinistrin have been validated in unanesthetized, freely moving laboratory animals, including rats (57, 161), mice (159), cats and dogs (170) . For example, Schock-Kusch *et al* found that, in healthy conscious rats, the mean GFR determined by the transcutaneous method was comparable to that obtained by plasma-based measurement of FITC-sinistrin concentration (161).

The transcutaneous technique for measurement of GFR has been deployed in studies of multiple experimental forms of kidney disease, including type 2 diabetes (60), oxalate-induced CKD (107), adriamycin-induced nephropathy (156), and placental ischemia-induced hypertension (169). For example, Mulay *et al* observed a gradual reduction in GFR, using the transcutaneous technique, across a three week experimental protocol in a mouse model of oxalate-induced CKD (107). This progressive reduction of renal function was determined by repeated measurements of GFR (107). The transcutaneous technique has been directly compared with the plasma clearance technique for estimation of GFR in unilaterally nephrectomized mice and in a mouse model of nephronophthisis

(163). The mean GFR determined by the two techniques were comparable in both experimental models (163). Similar observations have been reported by Schock-Kusch *et al* in a study of unilateral nephrectomy in rats and in a rat model of polycystic kidney disease (161). Thus the transcutaneous method for measurement of GFR appears to be a promising technique for investigation of the progression of kidney disease in experimental models of CKD. However, there remains some dispute regarding the most appropriate way to model the elimination kinetics of FITC-sinistrin to estimate GFR.

Models for determination of the elimination kinetics of FITC-sinistrin: The $t_{1/2}$ of FITC-sinistrin is calculated from the elimination kinetics of the marker using mathematically derived models that differ based on assumptions made about the compartments amongst which the FITC-sinistrin is distributed (57, 161, 166). Such mathematical models are used to describe the distribution of a substance inside the body after intravenous injection and its elimination from the body (55, 160, 161, 204). A brief description of the various models that can be applied to the clearance GFR marker are described below.

One-compartment kinetic model: This model is based on the assumption that the body is a single and kinetically homogeneous unit. After intravenous injection of the GFR marker, the marker is distributed into a single compartment (plasma) and is excreted from only that compartment without distributing in other spaces (Figure 1.2). The concentration of the GFR marker at time t is modeled by the exponential function (55):

$$c(t) = C_0 \times e^{-\lambda t}$$

Here, $c(t)$ is the plasma concentration of the GFR marker at time t , C_0 is the initial plasma concentration of the GFR marker, and λ is the elimination rate constant of the marker from the compartment.

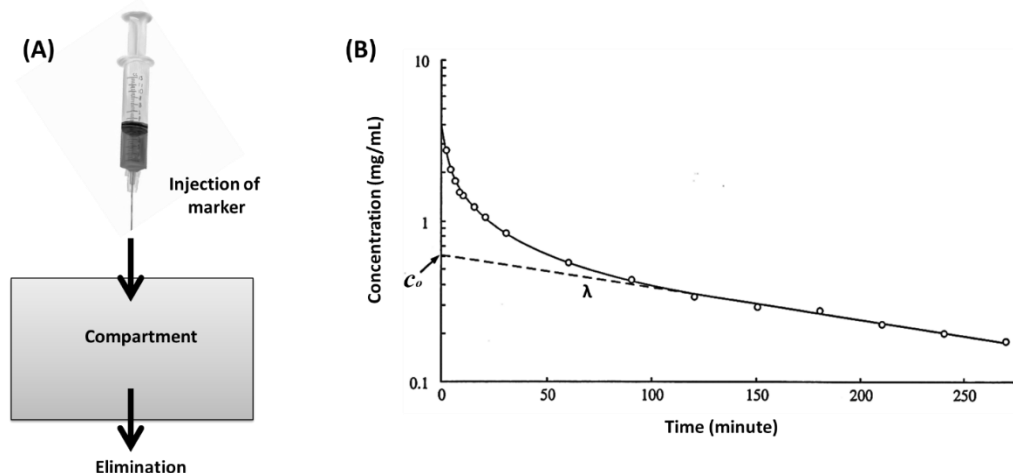


Figure 1.2 Schematic representation of a one-compartment kinetic model and an example of the excretion kinetics of a GFR marker after intravenous injection. (A) After a single bolus injection, the GFR marker is distributed into a single compartment (plasma) and then eliminated from that compartment. (B) The Log_{10} concentration-time curve of a marker shows a mono exponential form, where λ is the elimination rate constant of the marker and C_0 is the corresponding intercept on the ordinate. Images were modified from Frennby and Sterner (55).

In the one-compartment model, which has been used extensively (70, 160), the whole body is considered as a single compartment (55). Clearly, this may not be the case because the marker could also distribute to the interstitial or intracellular spaces (155). This has led to the development of kinetic models that incorporate more complexity.

Two-compartment kinetic model: The two-compartment model is based on the assumption that the GFR marker is distributed between a central compartment (plasma) and a peripheral compartment (the interstitial space) after intravenous injection (Figure 1.3). The marker can transfer between one compartment to the other but elimination of the marker takes place from plasma (55). The concentration of the GFR marker at time t is modeled by the exponential function (55):

$$c(t) = C_1 \times e^{-\lambda_1 t} + C_2 \times e^{-\lambda_2 t}$$

Here, $c(t)$ is the plasma concentration of the marker at time t , $C_1 \times e^{-\lambda_1 t}$ is the distribution phase of the marker and $C_2 \times e^{-\lambda_2 t}$ is the elimination phase. The elimination rate constants of the two compartments

are λ_1 and λ_2 and the corresponding intercepts on the y-axis are C_1 and C_2 respectively. C_1 and C_2 have units of concentration.

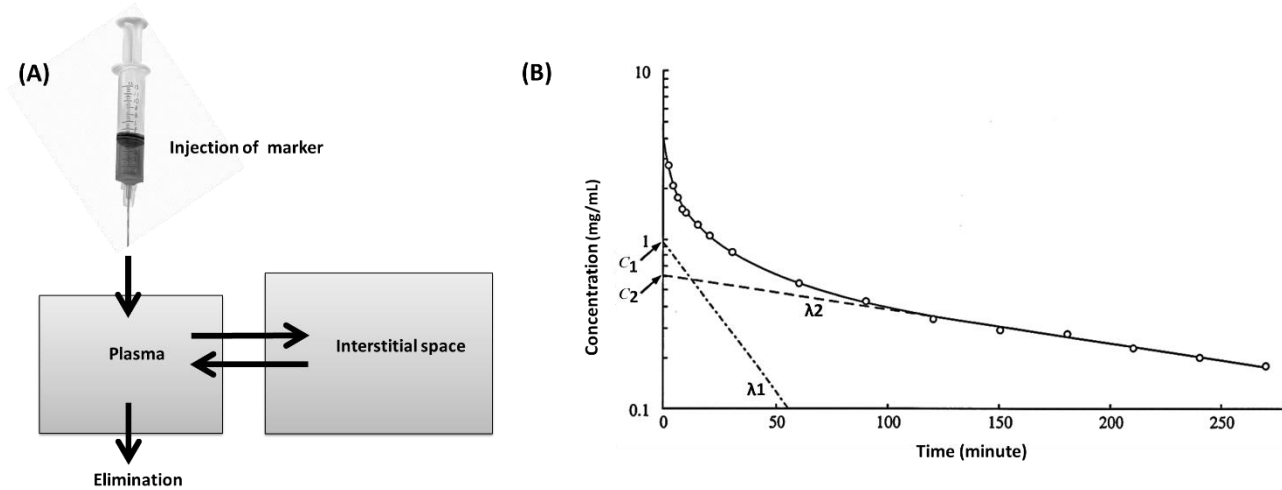


Figure 1.3 Schematic representation of a two-compartment kinetic model and an example of the excretion kinetics of a GFR marker after intravenous injection. (A) After a single bolus injection, an exogenous marker is distributed into a central compartment (plasma) and then transferred to the peripheral compartment (interstitial space) and vice versa. Finally the marker is eliminated from the central compartment. (B) The Log_{10} concentration-time curve of a marker represents the sum of two exponential functions, C_1 and C_2 are the zero time intercepts of the distribution and elimination phase respectively, and λ_1 and λ_2 are the corresponding elimination rate constants. Images were modified from Frennby and Sterner (55).

Three-compartment kinetic model: After intravenous injection, the GFR marker is assumed to distribute from a central compartment to an interstitial space and from the interstitial space to a ‘deeper compartment’ such as the intracellular compartment (Figure 1.4). During the elimination phase, the GFR marker is eliminated from the intracellular compartment to the extracellular compartment and back to the plasma. Finally, the elimination of the marker from the body takes place from plasma (55). The concentration of the GFR marker at time t is modeled by the exponential function (55):

$$c(t) = C_1 \times e^{-\lambda_1 t} + C_2 \times e^{-\lambda_2 t} + C_3 \times e^{-\lambda_3 t}$$

Here, $c(t)$ is the plasma concentration of the marker at time t , and the elimination rate constants of the three compartments are λ_1 , λ_2 and λ_3 and the corresponding intercepts on the y-ordinates are C_1, C_2 and C_3 , respectively. C_1, C_2 and C_3 have units of concentrations.

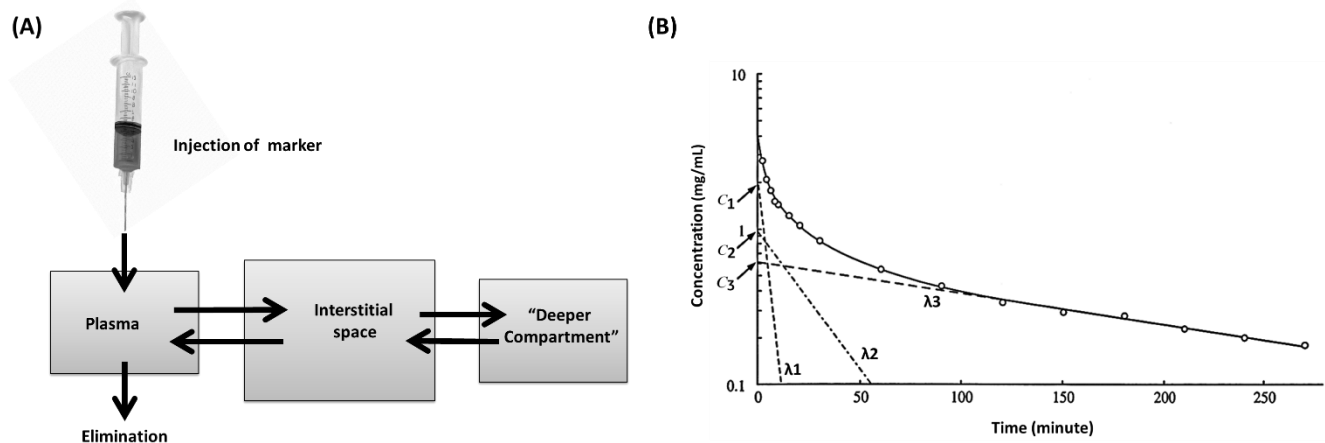


Figure 1.4 Schematic representation of a three-compartment kinetic model and an example of the excretion kinetics of a GFR marker after intravenous injection. (A) After a single bolus injection, the GFR marker is distributed into the central compartment (plasma) followed by a peripheral compartment (interstitial space). From the peripheral compartment, the marker is distributed into the intracellular compartment (deeper compartment) and vice versa. Finally the GFR marker is eliminated from the central compartment. (B) The Log_{10} concentration-time curve of the marker is represented as the sum of three exponential functions, where λ_1 , λ_2 and λ_3 are elimination rate constants of the three-compartments and C_1 , C_2 and C_3 are the corresponding intercepts on the y-axis. Images were modified from Frennby and Sterner (55).

For transcutaneous-based GFR measurements, an optical signal is measured (160, 161). The concentration of the fluorescent-labeled GFR marker in the extracellular space is proportional to the fluorescence intensity of the marker (161). The intensity of the signal may be influenced by the optical nature of the skin, including the presence of auto-fluorescence (47) and effects produced by changes in skin perfusion (99) during attachment of transcutaneous device. These factors might affect the baseline signal generated by the transcutaneous device and thus influence the actual estimate of GFR (57).

Recently, Friedemann and co-workers developed a three-compartment model with baseline correction (57). This mathematical algorithm describes the complete course of clearance kinetics for FITC-sinistrin from the point of injection with automated correction for drifts of the baseline signal. The $t_{1/2}$ of FITC-sinistrin derived by this three-compartment model with baseline correction was found to be comparable to the $t_{1/2}$ values determined by the ‘gold standard’ constant intravenous infusion technique (57). A detailed description of the mathematical algorithm incorporated in this three-compartment model with baseline correction has been described previously (56, 57). From a theoretical perspective, a model that corrects for changes in baseline signal, and incorporates a more realistic set of assumptions about the nature of the compartments that FITC-sinistrin is distributed in, should be superior to simpler one-, two- and three-compartment models. However, I am not aware of any previous systematic comparisons, of GFR generated using these various models, during the early stage of type 1 diabetes. Therefore, in the studies described in Chapter 5 of this thesis I compared the results generated by the four models described above in rats before and during three time points (3 days, 2 weeks and 4 weeks) after administration of STZ.

1.6 ASSESSMENT OF SPATIAL ARRANGEMENT BETWEEN PERITUBULAR CAPILLARIES AND RENAL TUBULES IN THE RAT KIDNEY

In the kidney, PTCs supply oxygen and nutrients to nearby interstitial cells and tubules and thus maintain the functional activities of nephrons (104). Most of the supplied oxygen is utilized by Na^+ - K^+ -ATPase pumps in the basolateral membrane of the renal tubules to drive reabsorption of filtered sodium (Na^+) (87). The high level of oxygen consumption by the tubules is one of the reasons the kidney is susceptible to the development of tissue hypoxia if any reduction of oxygen supply occurs from the microvasculature to renal tubules (44).

There is strong evidence of a correlation between a decline in PTC density and the development of renal hypoxia in experimental models of CKD (100, 120). In an experimental model of glomerulonephritis, Matsumoto and coworkers showed that renal tubular hypoxia occurs at an early stage (by 2 weeks) of disease, in association with loss of PTCs (structural rarefaction) and reduced blood flow (functional rarefaction) in remaining PTCs (100). Similarly, Sun *et al* reported loss of PTCs density in a rat model of aristolochic acid nephropathy by 8 weeks after induction of disease (173). In this model of CKD, the PTCs density was progressively reduced about 2-fold by week 8, 3-fold by

week 12 and 5-fold by week 16 (173). There was a significant increase in nuclear expression of HIF-1 α , a mediator of cellular adaptive responses to hypoxia, in the renal cortex at weeks 12 and 16. However, at week 8 renal expression of HIF did not differ between rats with CKD and control rats (173). In a model of ischemia/reperfusion injury that progresses to CKD there was depletion of PTC density (by 30 to 40% in the renal outer medulla) 4–40 weeks after reperfusion (13). There is also recent evidence that structural and functional abnormalities in PTCs are common to all forms of CKD, regardless of etiology (9). Thus, loss of PTCs, which should result in impaired delivery of oxygen to renal tissue, appears to be a critical factor initiating and/or exacerbating renal hypoxia in CKD (100).

Despite the evidence that structural abnormalities in PTCs are common to all forms of CKD, our understanding of the impact of these abnormalities on renal oxygenation is rudimentary. One of the barriers to improving our understanding of this issue is the complexity of the physiology of renal oxygenation (42). To tackle this problem, our research team has generated a series of computational models of oxygen transport in the kidney, based on realistic data regarding the three-dimensional geometry of the renal vasculature and its relationship with renal tissue (61, 62, 81, 88-90, 113). These models are multi-scale, in the sense that individual components of kidney oxygen physiology (e.g. the diffusion of oxygen from a glomerulus) are modeled in isolation and then incorporated into a larger-scale model that incorporates as many individual processes as possible. Currently, the major limitation of these models is their relatively simple representation of oxygen diffusion between PTCs and the renal tubules (88-90). In the experiments described in Chapter 6 of this thesis I have made some initial steps towards generating the information required to model this ‘scale’ of renal oxygen transport.

The spatial relationships between the microvasculature and tubules in the kidney have not been well-defined. In part, this is due to the difficulties in identifying these structures at high resolution. Immunohistochemical and immunofluorescent labeling of the endothelium of the blood vessels is a common approach to identify the vasculature involved (4, 76, 141, 201). These techniques have proven successful when applied to organs other than the kidney. The autofluorescence properties of the renal tissues hinders visualization of blood vessels and thus limits the use of immunofluorescence technique in labelling renal vasculature (112). Previous studies in our laboratory indicate that histochemical and immunohistochemical techniques have limited utility for identification of capillaries and veins in the rat kidney (112). An alternative approach to identifying the renal vasculature is synchrotron-based micro-computed tomography (CT) (81, 114). Following filling the renal circulation with a radio-

opaque substance such as Microfil®, synchrotron-based micro-CT allows visualization of the renal vasculature in three-dimensions (3D) (112, 114). However, this approach has limited resolution. Additionally, tubules cannot be visualized in 3D micro-CT images as the radio-opaque substance only fills the vasculature.

Given the limitations of available techniques, I reasoned that a combination of (i) filling the renal circulation with fluorescent gel, and (ii) labeling tubules by immunofluorescence, might allow the identification of not only the renal vasculature, but also its association with tubules at high resolution. Therefore, in the studies described in Chapter 6 of this thesis I performed preliminary experiments to assess the feasibility of this approach. I reasoned that a successful method would combine labeling of both blood vessels and renal tubules followed by optical clearing of the tissue for visualization of labeled structures using confocal microscopy. Below, I review some of the relevant literature to identify the rationale for the approach I took.

Staining of the blood vessel lumen: Tasi *et al* used fluorescent gel to stain blood vessels in the brain of the mouse (180). The fluorescent gel they used was composed of FITC-conjugated albumin dissolved in gelatin (94, 180). The gelatin containing FITC-albumin was retained in the vascular lumen during and after the optical clearing processes (32, 94). Thus, at least in brain tissue, this method allows the blood vessels to be clearly distinguished from surrounding tissues under confocal microscopy. This is the method I chose to employ in the experiments described in Chapter 6, to visualize the microvasculature of the kidney.

Tubular labeling by immunohistochemistry: Cytokeratins are the largest subgroup of intermediate filament proteins of epithelial cells. Renal tubular epithelial cells expressed a wide variety of cytokeratins (5, 51). Thus the abundance of cytokeratins in tubular epithelial cells make them excellent markers for diagnostic pathology (5, 122). In Chapter 6 of this thesis, I used a monoclonal pan-cytokeratin antibody conjugated with a fluorescent dye (Alexa Fluor 647) for labeling of tubular epithelial cells. The pan-cytokeratin antibody contains a combination of monoclonal antibodies which react with multiple cytokeratins present in epithelial tissues (30, 128). After incubation with antibodies, kidney tissues were processed by optical clearing in order to reduce the heterogeneity in the scattering of light within tissue during imaging.

Optical clearing: Visualization of large pieces of tissue or entire organs using standard confocal or multiphoton microscopy is rendered difficult by the opaque or at best translucent nature of the tissues (147). This translucent appearance is due to absorption and scattering of incident light within the thick tissues (172). Tissues from biological sources contain heterogeneous materials such as cell membranes, cytoplasm and organelles, each with varying refractive indices (19, 27). For example, the mean refractive index (RI) of cytoplasm is 1.36-1.375, of mitochondria is 1.40, and of lipids is 1.48 (19, 27). RI is defined as the ratio of the speed of the light in the vacuum to the speed of the light in the medium (147). Scattering of the light is induced by heterogeneity of the RI of the tissue substances (147). Light rays that should travel in straight lines are instead deflected by the tissue substances (147). This scattering of the light is problematic during imaging of thick tissue (several hundred microns), as the intensity of the unscattered light reaching the focal plane reduces exponentially with depth, thus resulting in poor resolution of the structure (177).

Spalteholz first described a clearing technique using a mixture of organic solvents (benzyl alcohol and methyl salicylate) that could be applied to an entire organ such as the heart (147, 168). The purpose of this optical clearing is to make the tissue transparent by matching the refractive index of the tissue substances throughout the sample to the clearing solvent (147). This clearing process reduces the heterogeneity in the scattering of light (147). There are now multiple solvent-based clearing techniques that can be used for clearing of tissues (139, 147). The clearing process is performed in two steps: (i) dehydration of the tissues and (ii) additional lipid removal and clearing of the dehydrated tissues by RI matching.

In the first step of the tissue clearing process, samples are dehydrated by using either ethanol (82), peroxide free tetrahydrofuran (THF) (15), or methanol (140). These agents remove water and lipids from the tissues resulting in a protein dense sample. Next, this dehydrated tissue is immersed in an optical clearing agent with high RI, which removes the additional lipid from the tissue and clears the tissue by equilibrating the refractive index throughout the sample to reduce light scattering.

Solvent-based clearing agents such as benzyl alcohol/benzyl benzoate (BABB) (15, 140), dibenzylether (DBE) (15, 40) and THF (15, 40) are commonly used for clearing tissues. There are a few limitations of these clearing agents that limit their widespread applications in the optical clearing process. For example, BABB is a toxic and corrosive agent (75) and DBE and THF can form explosive

peroxides when stored in air (40). BABB can also quench the signal from fluorescent proteins during the optical clearing process (202). More recently, Klingberg *et al* used ethyl cinnamate (82), RI > 1.5, as an optical clearing agent (195). Ethyl cinnamate is a nontoxic organic solvent used as a food flavor and as an additive for cosmetic products (195). They used ethyl cinnamate for clearing both soft tissue such as kidney and heart and hard tissue like bone (82). They found that the signals from fluorescent proteins within the cell of the tissue remain stable after 14 days of constant exposure to the ethyl cinnamate. Most importantly, in the context of our current aim, immunolabeling of the renal vascular endothelium by an antibody directed against CD 31 (conjugated with Alexa Fluor-647) remained stable and confined to blood vessels after clearing of the kidney tissues (82). Thus, I reasoned that this method could be useful for our proposed application; characterization of the spatial relationships between peritubular capillaries and tubules.

1.7 AIMS

The specific aims of the studies described in the subsequent 5 chapters of this thesis were:

- Chapter 2:** To determine whether renal cellular hypoxia is present in Ad-CKD and whether hypoxia and tissue fibrosis are spatially associated.
- Chapter 3:** To refine methods for detecting cellular hypoxia in Ad-CKD to better understand its cellular localization in Ad-CKD.
- Chapter 4:** To determine whether tissue hypoxia precedes renal dysfunction in Ad-CKD.
- Chapter 5:** To determine whether glomerular hyperfiltration, which would be expected to drive renal hypoxia, precedes renal dysfunction in experimental type 1 diabetes.
- Chapter 6:** To develop a new method to assess the spatial relationship between capillaries and tubules in the kidney.

1.8 REFERENCES

1. **Abbate M, Zoja C, Rottoli D, Corna D, Tomasoni S, and Remuzzi G.** Proximal tubular cells promote fibrogenesis by TGF-beta1-mediated induction of peritubular myofibroblasts. *Kidney Int* 61: 2066-2077, 2002.
2. **Abdelkader A, Ho J, Ow CP, Eppel GA, Rajapakse NW, Schlaich MP, and Evans RG.** Renal oxygenation in acute renal ischemia-reperfusion injury. *Am J Physiol Renal Physiol* 306: F1026-1038, 2014.
3. **Adamovich Y, Ladeux B, Golik M, Koeners MP, and Asher G.** Rhythmic oxygen levels reset circadian clocks through HIF1alpha. *Cell Metab* 25: 93-101, 2017.
4. **Advani A, Kelly DJ, Advani SL, Cox AJ, Thai K, Zhang Y, White KE, Gow RM, Marshall SM, Steer BM, Marsden PA, Rakoczy PE, and Gilbert RE.** Role of VEGF in maintaining renal structure and function under normotensive and hypertensive conditions. *Proc Natl Acad Sci* 104: 14448-14453, 2007.
5. **Alexa A, Baderca F, Lighezan R, Izvernariu D, and Raica M.** The diagnostic value of cytokeratins expression in the renal parenchyma tumors. *Rom J Morphol Embryol* 51: 27-35, 2010.
6. **Arteel GE, Thurman RG, and Raleigh JA.** Reductive metabolism of the hypoxia marker pimonidazole is regulated by oxygen tension independent of the pyridine nucleotide redox state. *Eur J Biochem* 253: 743-750, 1998.
7. **Arteel GE, Thurman RG, Yates JM, and Raleigh JA.** Evidence that hypoxia markers detect oxygen gradients in liver: pimonidazole and retrograde perfusion of rat liver. *Br J Cancer* 72: 889-895, 1995.
8. **Aukland K, and Krog J.** Renal Oxygen Tension. *Nature* 188: 671, 1960.
9. **Babickova J, Klinkhammer BM, Buhl EM, Djudjaj S, Hoss M, Heymann F, Tacke F, Floege J, Becker JU, and Boor P.** Regardless of etiology, progressive renal disease causes ultrastructural and functional alterations of peritubular capillaries. *Kidney Int* 91: 70-85, 2017.
10. **Bak M, Thomsen K, Christiansen T, and Flyvbjerg A.** Renal enlargement precedes renal hyperfiltration in early experimental diabetes in rats. *J Am Soc Nephrol* 11: 1287-1292, 2000.
11. **Balen D, Ljubojevic M, Breljak D, Brzica H, Zlender V, Koepsell H, and Sabolic I.** Revised immunolocalization of the Na⁺-D-glucose cotransporter SGLT1 in rat organs with an improved antibody. *Am J Physiol Cell Physiol* 295: C475-489, 2008.
12. **Bank N, and Aynedjian HS.** Progressive increases in luminal glucose stimulate proximal sodium absorption in normal and diabetic rats. *J Clin Invest* 86: 309-316, 1990.
13. **Basile DP, Donohoe D, Roethe K, and Osborn JL.** Renal ischemic injury results in permanent damage to peritubular capillaries and influences long-term function. *Am J Physiol Renal Physiol* 281: F887-899, 2001.
14. **Baumgartl H, Leichtweiss HP, Lubbers DW, Weiss C, and Huland H.** The oxygen supply of the dog kidney: measurements of intrarenal pO₂. *Microvasc Res* 4: 247-257, 1972.
15. **Becker K, Jahrling N, Saghafi S, Weiler R, and Dodt HU.** Chemical clearing and dehydration of GFP expressing mouse brains. *PLoS One* 7: e33916, 2012.
16. **Bell PD, Lapointe JY, Sabirov R, Hayashi S, Peti-Peterdi J, Manabe K, Kovacs G, and Okada Y.** Macula densa cell signaling involves ATP release through a maxi anion channel. *Proc Natl Acad Sci* 100: 4322-4327, 2003.
17. **Bell TD, DiBona GF, Biemiller R, and Brands MW.** Continuously measured renal blood flow does not increase in diabetes if nitric oxide synthesis is blocked. *Am J Physiol Renal Physiol* 295: F1449-1456, 2008.

18. **Bell TD, DiBona GF, Wang Y, and Brands MW.** Mechanisms for renal blood flow control early in diabetes as revealed by chronic flow measurement and transfer function analysis. *J Am Soc Nephrol* 17: 2184, 2006.
19. **Beuthan J, Minet O, Helfmann J, Herrig M, and Muller G.** The spatial variation of the refractive index in biological cells. *Phys Med Biol* 41: 369-382, 1996.
20. **Blantz RC, and Konnen KS.** Relation of distal tubular delivery and reabsorptive rate to nephron filtration. *Am J Physiol* 233: F315-324, 1977.
21. **Bohle A, von Gise H, Mackensen-Haen S, and Stark-Jakob B.** The obliteration of the postglomerular capillaries and its influence upon the function of both glomeruli and tubuli. Functional interpretation of morphologic findings. *Klin Wochenschr* 59: 1043-1051, 1981.
22. **Bollee G, Dollinger C, Boutaud L, Guillemot D, Bensman A, Harambat J, Deteix P, Daudon M, Knebelmann B, and Ceballos-Picot I.** Phenotype and genotype characterization of adenine phosphoribosyltransferase deficiency. *J Am Soc Nephrol* 21: 679-688, 2010.
23. **Brenner BM.** Nephron adaptation to renal injury or ablation. *Am J Physiol* 249: F324-337, 1985.
24. **Brenner BM, Lawler EV, and Mackenzie HS.** The hyperfiltration theory: a paradigm shift in nephrology. *Kidney Int* 49: 1774-1777, 1996.
25. **Brochner-Mortensen J, Stockel M, Sorensen PJ, Nielsen AH, and Ditzel J.** Proximal glomerulo-tubular balance in patients with type 1 (insulin-dependent) diabetes mellitus. *Diabetologia* 27: 189-192, 1984.
26. **Brown R, Ollerstam A, Johansson B, Skott O, Gebre-Medhin S, Fredholm B, and Persson AE.** Abolished tubuloglomerular feedback and increased plasma renin in adenosine A1 receptor-deficient mice. *Am J Physiol Regul Integr Comp Physiol* 281: R1362-1367, 2001.
27. **Brunsting A, and Mullaney PF.** Differential light scattering from spherical mammalian cells. *Biophys J* 14: 439-453, 1974.
28. **Bryan CW, Jarchow RC, and Maher JF.** Measurement of glomerular filtration rate in small animals without urine collection. *J Lab Clin Med* 80: 845-856, 1972.
29. **Buclin T, Sechaud R, Bertsch AP, Decosterd LA, Belaz N, Appenzeller M, Burnier M, and Biollaz J.** Estimation of glomerular filtration rate by sinistrin clearance using various approaches. *Ren Fail* 20: 267-276, 1998.
30. **Chu PG, and Weiss LM.** Keratin expression in human tissues and neoplasms. *Histopathology* 40: 403-439, 2002.
31. **Deen WM, Robertson CR, and Brenner BM.** A model of glomerular ultrafiltration in the rat. *Am J Physiol* 223: 1178-1183, 1972.
32. **Di Giovanna AP, Tibo A, Silvestri L, Mullenbroich MC, Costantini I, Allegra Mascaro AL, Sacconi L, Frasconi P, and Pavone FS.** Whole-brain vasculature reconstruction at the single capillary level. *Sci Rep* 8: 12573, 2018.
33. **Ding A, Kalaighanasundaram P, Ricardo SD, Abdelkader A, Witting PK, Broughton BR, Kim HB, Wyse BF, Phillips JK, and Evans RG.** Chronic treatment with tempol does not significantly ameliorate renal tissue hypoxia or disease progression in a rodent model of polycystic kidney disease. *Clin Exp Pharmacol Physiol* 39: 917-929, 2012.
34. **Diwan V, Gobe G, and Brown L.** Glibenclamide improves kidney and heart structure and function in the adenine-diet model of chronic kidney disease. *Pharmacol Res* 79: 104-110, 2014.
35. **Dixon JJ, Lane K, Dalton RN, Turner C, Grounds RM, MacPhee IA, and Philips BJ.** Validation of a continuous infusion of low dose iohexol to measure glomerular filtration rate: randomised clinical trial. *J Transl Med* 13: 58, 2015.

36. **Edvardsson V, Palsson R, Olafsson I, Hjaltadottir G, and Laxdal T.** Clinical features and genotype of adenine phosphoribosyltransferase deficiency in iceland. *Am J Kidney Dis* 38: 473-480, 2001.
37. **Edvardsson VO, Goldfarb DS, Lieske JC, Beara-Lasic L, Anglani F, Milliner DS, and Palsson R.** Hereditary causes of kidney stones and chronic kidney disease. *Pediatr Nephrol* 28: 1923-1942, 2013.
38. **Emans TW, Janssen BJ, Pinkham MI, Ow CP, Evans RG, Joles JA, Malpas SC, Krediet CT, and Koeners MP.** Exogenous and endogenous angiotensin-II decrease renal cortical oxygen tension in conscious rats by limiting renal blood flow. *J Physiol* 594: 6287-6300, 2016.
39. **Engle SJ, Stockelman MG, Chen J, Boivin G, Yum MN, Davies PM, Ying MY, Sahota A, Simmonds HA, Stambrook PJ, and Tischfield JA.** Adenine phosphoribosyltransferase-deficient mice develop 2,8-dihydroxyadenine nephrolithiasis. *Proc Natl Acad Sci* 93: 5307-5312, 1996.
40. **Erturk A, Becker K, Jahrling N, Mauch CP, Hojer CD, Egen JG, Hellal F, Bradke F, Sheng M, and Dodt HU.** Three-dimensional imaging of solvent-cleared organs using 3DISCO. *Nat Protoc* 7: 1983-1995, 2012.
41. **Estelberger W, Petek W, Zitta S, Mauric A, Horn S, Holzer H, and Pogglichsch H.** Determination of the glomerular filtration rate by identification of sinistrin kinetics. *Eur J Clin Chem Clin Biochem* 33: 201-209, 1995.
42. **Evans RG, Gardiner BS, Smith DW, and O'Connor PM.** Intrarenal oxygenation: unique challenges and the biophysical basis of homeostasis. *Am J Physiol Renal Physiol* 295: F1259-1270, 2008.
43. **Evans RG, Harrop GK, Ngo JP, Ow CP, and O'Connor PM.** Basal renal O₂ consumption and the efficiency of O₂ utilization for Na⁺ reabsorption. *Am J Physiol Renal Physiol* 306: F551-560, 2014.
44. **Evans RG, Ince C, Joles JA, Smith DW, May CN, O'Connor PM, and Gardiner BS.** Haemodynamic influences on kidney oxygenation: clinical implications of integrative physiology. *Clin Exp Pharmacol Physiol* 40: 106-122, 2013.
45. **Evans RG, and O'Connor PM.** Initiation and progression of chronic kidney disease: can we definitively test the chronic hypoxia hypothesis? *Hypertension* 62: 827-828, 2013.
46. **Evans RG, Ow CP, and Bie P.** The chronic hypoxia hypothesis: the search for the smoking gun goes on. *Am J Physiol Renal Physiol* 308: F101-102, 2015.
47. **Ferulova I, Lihachev A, and Spigulis J.** Photobleaching effects on in vivo skin autofluorescence lifetime. *J Biomed Opt* 20: 051031, 2015.
48. **Fine LG, Bandyopadhyay D, and Norman JT.** Is there a common mechanism for the progression of different types of renal diseases other than proteinuria? Towards the unifying theme of chronic hypoxia. *Kidney Int Suppl* 75: S22-26, 2000.
49. **Fine LG, Orphanides C, and Norman JT.** Progressive renal disease: the chronic hypoxia hypothesis. *Kidney Int Suppl* 65: S74-78, 1998.
50. **Fitzgerald SM, and Brands MW.** Nitric oxide may be required to prevent hypertension at the onset of diabetes. *Am J Physiol Endocrinol Metab* 279: E762-768, 2000.
51. **Fleming S, and Symes CE.** The distribution of cytokeratin antigens in the kidney and in renal tumours. *Histopathology* 11: 157-170, 1987.
52. **Flynn ER, Marbury DC, Sawyer RT, Lee J, Teutsch C, Kauser K, and Maric-Bilkan C.** Amlodipine reduces inflammation despite promoting albuminuria in the streptozotocin-induced diabetic rat. *Nephron Extra* 2: 205-218, 2012.

53. **Fong D, Ullah MM, Lal JG, Abdelkader A, Ow CP, Hilliard LM, Ricardo SD, Kelly DJ, and Evans RG.** Renal cellular hypoxia in adenine-induced chronic kidney disease. *Clin Exp Pharmacol Physiol* 43: 896-905, 2016.
54. **Franzen S, Pihl L, Khan N, Gustafsson H, and Palm F.** Pronounced kidney hypoxia precedes albuminuria in type 1 diabetic mice. *Am J Physiol Renal Physiol* 310: F807-809, 2016.
55. **Frennby B, and Sterner G.** Contrast media as markers of GFR. *Eur Radiol* 12: 475-484, 2002.
56. **Friedemann J.** Development of a pharmacokinetic model to describe the distribution and excretion kinetics of a renal function marker using transcutaneously obtained data in rats (Doctoral dissertation). In: *Medizinische Fakultät Mannheim* Germany: University of Heidelberg, 2015, p. 117.
57. **Friedemann J, Heinrich R, Shulhevich Y, Raedle M, William-Olsson L, Pill J, and Schock-Kusch D.** Improved kinetic model for the transcutaneous measurement of glomerular filtration rate in experimental animals. *Kidney Int* 90: 1377-1385, 2016.
58. **Friederich-Persson M, Persson P, Fasching A, Hansell P, Nordquist L, and Palm F.** Increased kidney metabolism as a pathway to kidney tissue hypoxia and damage: effects of triiodothyronine and dinitrophenol in normoglycemic rats. *Adv Exp Med Biol* 789: 9-14, 2013.
59. **Friederich-Persson M, Thorn E, Hansell P, Nangaku M, Levin M, and Palm F.** Kidney hypoxia, attributable to increased oxygen consumption, induces nephropathy independently of hyperglycemia and oxidative stress. *Hypertension* 62: 914-919, 2013.
60. **Gallo LA, Ward MS, Fotheringham AK, Zhuang A, Borg DJ, Flemming NB, Harvie BM, Kinneally TL, Yeh SM, McCarthy DA, Koepsell H, Vallon V, Pollock C, Panchapakesan U, and Forbes JM.** Once daily administration of the SGLT2 inhibitor, empagliflozin, attenuates markers of renal fibrosis without improving albuminuria in diabetic db/db mice. *Sci Rep* 6: 26428, 2016.
61. **Gardiner BS, Smith DW, O'Connor PM, and Evans RG.** A mathematical model of diffusional shunting of oxygen from arteries to veins in the kidney. *Am J Physiol Renal Physiol* 300: F1339-1352, 2011.
62. **Gardiner BS, Thompson SL, Ngo JP, Smith DW, Abdelkader A, Broughton BR, Bertram JF, and Evans RG.** Diffusive oxygen shunting between vessels in the preglomerular renal vasculature: anatomic observations and computational modeling. *Am J Physiol Renal Physiol* 303: F605-618, 2012.
63. **Guariguata L, Whiting DR, Hambleton I, Beagley J, Linnenkamp U, and Shaw JE.** Global estimates of diabetes prevalence for 2013 and projections for 2035. *Diabetes Res Clin Pract* 103: 137-149, 2014.
64. **Haase VH.** Hypoxia-inducible factors in the kidney. *Am J Physiol Renal Physiol* 291: F271-281, 2006.
65. **Haase VH.** Oxygen regulates epithelial-to-mesenchymal transition: insights into molecular mechanisms and relevance to disease. *Kidney Int* 76: 492-499, 2009.
66. **Hannedouche TP, Delgado AG, Gnionsahe DA, Boitard C, Lacour B, and Grunfeld JP.** Renal hemodynamics and segmental tubular reabsorption in early type 1 diabetes. *Kidney Int* 37: 1126-1133, 1990.
67. **Herrera Perez Z, Weinfurter S, and Gretz N.** Transcutaneous assessment of renal function in conscious rodents. *J Vis Exp* e53767, 2016.
68. **Hidaka Y, Tarle SA, O'Toole TE, Kelley WN, and Palella TD.** Nucleotide sequence of the human APRT gene. *Nucleic Acids Res* 15: 9086, 1987.

69. **Hill NR, Fatoba ST, Oke JL, Hirst JA, O'Callaghan CA, Lasserson DS, and Hobbs FD.** Global prevalence of chronic kidney disease - A systematic review and meta-analysis. *PLoS One* 11: e0158765, 2016.
70. **Hilliard LM, and Denton KM.** Transcutaneous assessment of glomerular filtration rate in unanesthetized rats using a small animal imager: impact on arterial pressure, heart rate, and activity. *Physiological Reports* 4: e12723, 2016.
71. **Hirakawa Y, Tanaka T, and Nangaku M.** Renal hypoxia in CKD; pathophysiology and detecting methods. *Front Physiol* 8: 99, 2017.
72. **Hirose K, Osterby R, Nozawa M, and Gundersen HJ.** Development of glomerular lesions in experimental long-term diabetes in the rat. *Kidney Int* 21: 689-695, 1982.
73. **Hostetter TH, Troy JL, and Brenner BM.** Glomerular hemodynamics in experimental diabetes mellitus. *Kidney Int* 19: 410-415, 1981.
74. **Huang DY, Vallon V, Zimmermann H, Kozalka P, Schrader J, and Osswald H.** Ecto-5'-nucleotidase (cd73)-dependent and -independent generation of adenosine participates in the mediation of tubuloglomerular feedback in vivo. *Am J Physiol Renal Physiol* 291: F282-288, 2006.
75. **Ivins S, Roberts C, Vernay B, and Scambler PJ.** Analysis of coronary vessels in cleared embryonic hearts. *J Vis Exp* 54800, 2016.
76. **Jen KY, Nguyen TB, Vincenti FG, and Laszik ZG.** C4d/CD34 double-immunofluorescence staining of renal allograft biopsies for assessing peritubular capillary C4d positivity. *Mod Pathol* 25: 434-438, 2012.
77. **Jensen PK, Christiansen JS, Steven K, and Parving HH.** Renal function in streptozotocin-diabetic rats. *Diabetologia* 21: 409-414, 1981.
78. **Jensen PK, Christiansen JS, Steven K, and Parving HH.** Strict metabolic control and renal function in the streptozotocin diabetic rat. *Kidney Int* 31: 47-51, 1987.
79. **Johnson CA, Levey AS, Coresh J, Levin A, Lau J, and Eknoyan G.** Clinical practice guidelines for chronic kidney disease in adults: Part I. Definition, disease stages, evaluation, treatment, and risk factors. *Am Fam Physician* 70: 869-876, 2004.
80. **Kaartinen K, Hemmila U, Salmela K, Raisanen-Sokolowski A, Kouri T, and Makela S.** Adenine phosphoribosyltransferase deficiency as a rare cause of renal allograft dysfunction. *J Am Soc Nephrol* 25: 671-674, 2014.
81. **Khan Z, Ngo JP, Le B, Evans RG, Pearson JT, Gardiner BS, and Smith DW.** Three-dimensional morphometric analysis of the renal vasculature. *Am J Physiol Renal Physiol* 314: F715-F725, 2018.
82. **Klingberg A, Hasenberg A, Ludwig-Portugall I, Medyukhina A, Mann L, Brenzel A, Engel DR, Figge MT, Kurts C, and Gunzer M.** Fully automated evaluation of total glomerular number and capillary tuft size in nephritic kidneys using lightsheet microscopy. *J Am Soc Nephrol* 28: 452-459, 2017.
83. **Koeners MP, Ow CP, Russell DM, Abdelkader A, Eppel GA, Ludbrook J, Malpas SC, and Evans RG.** Telemetry-based oxygen sensor for continuous monitoring of kidney oxygenation in conscious rats. *Am J Physiol Renal Physiol* 304: F1471-1480, 2013.
84. **Koeners MP, Ow CPC, Russell DM, Evans RG, and Malpas SC.** Prolonged and continuous measurement of kidney oxygenation in conscious rats. *Methods Mol Biol* 1397: 93-111, 2016.
85. **Korner A, Eklof AC, Celsi G, and Aperia A.** Increased renal metabolism in diabetes. Mechanism and functional implications. *Diabetes* 43: 629-633, 1994.
86. **Kumar AM, Gupta RK, and Spitzer A.** Intracellular sodium in proximal tubules of diabetic rats. Role of glucose. *Kidney Int* 33: 792-797, 1988.

87. **Lassen NA, Munck O, and Thaysen JH.** Oxygen consumption and sodium reabsorption in the kidney. *Acta Physiol Scand* 51: 371-384, 1961.
88. **Lee CJ, Gardiner BS, Evans RG, and Smith DW.** A model of oxygen transport in the rat renal medulla. *Am J Physiol Renal Physiol* 2018.
89. **Lee CJ, Gardiner BS, Ngo JP, Kar S, Evans RG, and Smith DW.** Accounting for oxygen in the renal cortex: a computational study of factors that predispose the cortex to hypoxia. *Am J Physiol Renal Physiol* 313: F218-F236, 2017.
90. **Lee CJ, Ngo JP, Kar S, Gardiner BS, Evans RG, and Smith DW.** A pseudo-three-dimensional model for quantification of oxygen diffusion from preglomerular arteries to renal tissue and renal venous blood. *Am J Physiol Renal Physiol* 313: F237-F253, 2017.
91. **Lewis EJ, Hunsicker LG, Clarke WR, Berl T, Pohl MA, Lewis JB, Ritz E, Atkins RC, Rohde R, Raz I, and Collaborative Study G.** Renoprotective effect of the angiotensin-receptor antagonist irbesartan in patients with nephropathy due to type 2 diabetes. *N Engl J Med* 345: 851-860, 2001.
92. **Lim A.** Diabetic nephropathy - complications and treatment. *Int J Nephrol Renovasc Dis* 7: 361-381, 2014.
93. **Liss P, Nygren A, Revsbech NP, and Ulfendahl HR.** Intrarenal oxygen tension measured by a modified clark electrode at normal and low blood pressure and after injection of x-ray contrast media. *Pflugers Arch* 434: 705-711, 1997.
94. **Lugo-Hernandez E, Squire A, Hagemann N, Brenzel A, Sardari M, Schlechter J, Sanchez-Mendoza EH, Gunzer M, Faissner A, and Hermann DM.** 3D visualization and quantification of microvessels in the whole ischemic mouse brain using solvent-based clearing and light sheet microscopy. *J Cereb Blood Flow Metab* 37: 3355-3367, 2017.
95. **Maiuolo J, Oppedisano F, Gratteri S, Muscoli C, and Mollace V.** Regulation of uric acid metabolism and excretion. *Int J Cardiol* 213: 8-14, 2016.
96. **Manotham K, Ongvilawan B, Urusopone P, Chetsurakarn S, Tanamai J, Limkuansuwan P, Tungsanga K, and Eiam-Ong S.** Angiotensin II receptor blocker partially ameliorated intrarenal hypoxia in chronic kidney disease patients: a pre-/post-study. *Intern Med J* 42: e33-37, 2012.
97. **Manotham K, Tanaka T, Matsumoto M, Ohse T, Inagi R, Miyata T, Kurokawa K, Fujita T, Ingelfinger JR, and Nangaku M.** Transdifferentiation of cultured tubular cells induced by hypoxia. *Kidney Int* 65: 871-880, 2004.
98. **Manotham K, Tanaka T, Matsumoto M, Ohse T, Miyata T, Inagi R, Kurokawa K, Fujita T, and Nangaku M.** Evidence of tubular hypoxia in the early phase in the remnant kidney model. *J Am Soc Nephrol* 15: 1277-1288, 2004.
99. **Martin P, Debreczenya, Rebecca Batesb, Rick M. Fitchb, Karen P. Galenb, Jiajia Geb, B. R, and Dorshow.** Human skin auto-fluorescence decay as a function of irradiance and skin type. *Proc of SPIE* 7897-78971T-2: 2011.
100. **Matsumoto M, Tanaka T, Yamamoto T, Noiri E, Miyata T, Inagi R, Fujita T, and Nangaku M.** Hypoperfusion of peritubular capillaries induces chronic hypoxia before progression of tubulointerstitial injury in a progressive model of rat glomerulonephritis. *J Am Soc Nephrol* 15: 1574-1581, 2004.
101. **Milman Z, Axelrod JH, Heyman SN, Nachmansson N, and Abramovitch R.** Assessment with unenhanced MRI techniques of renal morphology and hemodynamic changes during acute kidney injury and chronic kidney disease in mice. *Am J Nephrol* 39: 268-278, 2014.
102. **Mobley AM.** Slowing the progression of chronic kidney disease. *J Nurse Pract* 5: 188-194, 2009.

103. **Mogensen CE, and Christensen CK.** Predicting diabetic nephropathy in insulin-dependent patients. *N Engl J Med* 311: 89-93, 1984.
104. **Molema G, and Aird WC.** Vascular heterogeneity in the kidney. *Semin Nephrol* 32: 145-155, 2012.
105. **Mondritzki T, Steinbach SML, Boehme P, Hoffmann J, Kullmann M, Schock-Kusch D, Vogel J, Kolkhof P, Sandner P, Bischoff E, Huser J, Dinh W, and Truebel H.** Transcutaneous glomerular filtration rate measurement in a canine animal model of chronic kidney disease. *J Pharmacol Toxicol Methods* 90: 7-12, 2018.
106. **Mulay SR, and Anders HJ.** Crystal nephropathies: mechanisms of crystal-induced kidney injury. *Nat Rev Nephrol* 13: 226-240, 2017.
107. **Mulay SR, Eberhard JN, Pfann V, Marschner JA, Darisipudi MN, Daniel C, Romoli S, Desai J, Grigorescu M, Kumar SV, Rathkolb B, Wolf E, Hrabe de Angelis M, Bauerle T, Dietel B, Wagner CA, Amann K, Eckardt KU, Aronson PS, Anders HJ, and Knauf F.** Oxalate-induced chronic kidney disease with its uremic and cardiovascular complications in C57BL/6 mice. *Am J Physiol Renal Physiol* 310: F785-F795, 2016.
108. **Murray AW, Barnfield MC, Waller ML, Telford T, and Peters AM.** Assessment of glomerular filtration rate measurement with plasma sampling: a technical review. *J Nucl Med Technol* 41: 67-75, 2013.
109. **Nasr SH, Sethi S, Cornell LD, Milliner DS, Boelkins M, Broviac J, and Fidler ME.** Crystalline nephropathy due to 2,8-dihydroxyadeninuria: an under-recognized cause of irreversible renal failure. *Nephrol Dial Transplant* 25: 1909-1915, 2010.
110. **National Kidney F.** K/DOQI clinical practice guidelines for chronic kidney disease: evaluation, classification, and stratification. *Am J Kidney Dis* 39: S1-266, 2002.
111. **Ng YY, Huang TP, Yang WC, Chen ZP, Yang AH, Mu W, Nikolic-Paterson DJ, Atkins RC, and Lan HY.** Tubular epithelial-myofibroblast transdifferentiation in progressive tubulointerstitial fibrosis in 5/6 nephrectomized rats. *Kidney Int* 54: 864-876, 1998.
112. **Ngo JP.** The structural basis of kidney oxygenation (Doctoral dissertation). In: *Department of Physiology*. Australia: Monash University, 2016.
113. **Ngo JP, Kar S, Kett MM, Gardiner BS, Pearson JT, Smith DW, Ludbrook J, Bertram JF, and Evans RG.** Vascular geometry and oxygen diffusion in the vicinity of artery-vein pairs in the kidney. *Am J Physiol Renal Physiol* 307: F1111-1122, 2014.
114. **Ngo JP, Le B, Khan Z, Kett MM, Gardiner BS, Smith DW, Melhem MM, Maksimenko A, Pearson JT, and Evans RG.** Micro-computed tomographic analysis of the radial geometry of intrarenal artery-vein pairs in rats and rabbits: Comparison with light microscopy. *Clin Exp Pharmacol Physiol* 44: 1241-1253, 2017.
115. **Nordquist L, Friederich-Persson M, Fasching A, Liss P, Shoji K, Nangaku M, Hansell P, and Palm F.** Activation of hypoxia-inducible factors prevents diabetic nephropathy. *J Am Soc Nephrol* 26: 328-338, 2015.
116. **Norman JT, Stidwill R, Singer M, and Fine LG.** Angiotensin II blockade augments renal cortical microvascular pO₂ indicating a novel, potentially renoprotective action. *Nephron Physiol* 94: p39-46, 2003.
117. **O'Brien RC, Allen TJ, Cooper ME, Bach L, and Jerums G.** Glomerular filtration rate in early experimental diabetes. *J Diabet Complications* 2: 8-11, 1988.
118. **O'Donnell MP, Kasiske BL, and Keane WF.** Glomerular hemodynamic and structural alterations in experimental diabetes mellitus. *FASEB J* 2: 2339-2347, 1988.

119. **O'Hagan M, Howey J, and Greene SA.** Increased proximal tubular reabsorption of sodium in childhood diabetes mellitus. *Diabet Med* 8: 44-48, 1991.
120. **Ohashi R, Kitamura H, and Yamanaka N.** Peritubular capillary injury during the progression of experimental glomerulonephritis in rats. *J Am Soc Nephrol* 11: 47-56, 2000.
121. **Okada H, Kaneko Y, Yawata T, Uyama H, Ozono S, Motomiya Y, and Hirao Y.** Reversibility of adenine-induced renal failure in rats. *Clin Exp Nephrol* 3: 82-88, 1999.
122. **Oosterwijk E, Van Muijen GN, Oosterwijk-Wakka JC, and Warnaar SO.** Expression of intermediate-sized filaments in developing and adult human kidney and in renal cell carcinoma. *J Histochem Cytochem* 38: 385-392, 1990.
123. **Osswald H, Spielman WS, and Knox FG.** Mechanism of adenosine-mediated decreases in glomerular filtration rate in dogs. *Circ Res* 43: 465-469, 1978.
124. **Osterby R, and Gundersen HJ.** Glomerular basement membrane thickening in streptozotocin diabetic rats despite treatment with an aldose reductase inhibitor. *J Diabet Complications* 3: 149-153, 1989.
125. **Ow CP, Abdelkader A, Hilliard LM, Phillips JK, and Evans RG.** Determinants of renal tissue hypoxia in a rat model of polycystic kidney disease. *Am J Physiol Regul Integr Comp Physiol* 307: R1207-1215, 2014.
126. **Ow CPC, Ngo JP, Ullah MM, Barsha G, Meex RCR, Watt MJ, Hilliard LM, Koeners MP, and Evans RG.** Absence of renal hypoxia in the subacute phase of severe renal ischemia reperfusion injury. *Am J Physiol Renal Physiol* 315: F1358-F1369, 2018.
127. **Ow CPC, Ngo JP, Ullah MM, Hilliard LM, and Evans RG.** Renal hypoxia in kidney disease: Cause or consequence? *Acta Physiol* 222: e12999, 2018.
128. **Painter JT, Clayton NP, and Herbert RA.** Useful immunohistochemical markers of tumor differentiation. *Toxicol Pathol* 38: 131-141, 2010.
129. **Palm F.** Intrarenal oxygen in diabetes and a possible link to diabetic nephropathy. *Clin Exp Pharmacol Physiol* 33: 997-1001, 2006.
130. **Palm F, Cederberg J, Hansell P, Liss P, and Carlsson PO.** Reactive oxygen species cause diabetes-induced decrease in renal oxygen tension. *Diabetologia* 46: 1153-1160, 2003.
131. **Palm F, Ortsater H, Hansell P, Liss P, and Carlsson PO.** Differentiating between effects of streptozotocin per se and subsequent hyperglycemia on renal function and metabolism in the streptozotocin-diabetic rat model. *Diabetes Metab Res Rev* 20: 452-459, 2004.
132. **Papazova DA, Friederich-Persson M, Joles JA, and Verhaar MC.** Renal transplantation induces mitochondrial uncoupling, increased kidney oxygen consumption, and decreased kidney oxygen tension. *Am J Physiol Renal Physiol* 308: F22-28, 2015.
133. **Persson F, and Rossing P.** Diagnosis of diabetic kidney disease: state of the art and future perspective. *Kidney Int Suppl* 8: 2-7, 2018.
134. **Peters AM.** Expressing glomerular filtration rate in terms of extracellular fluid volume. *Nephrol Dial Transplant* 7: 205-210, 1992.
135. **Pihl L, Persson P, Fasching A, Hansell P, DiBona GF, and Palm F.** Insulin induces the correlation between renal blood flow and glomerular filtration rate in diabetes: implications for mechanisms causing hyperfiltration. *Am J Physiol Regul Integr Comp Physiol* 303: R39-47, 2012.
136. **Pill J, Kraenzlin B, Jander J, Sattelkau T, Sadick M, Kloetzer HM, Deus C, Kraemer U, and Gretz N.** Fluorescein-labeled sinistrin as marker of glomerular filtration rate. *European journal of medicinal chemistry* 40: 1056-1061, 2005.
137. **Pollock CA, Lawrence JR, and Field MJ.** Tubular sodium handling and tubuloglomerular feedback in experimental diabetes mellitus. *Am J Physiol* 260: F946-952, 1991.

138. **Poulsen SB, Fenton RA, and Rieg T.** Sodium-glucose cotransport. *Curr Opin Nephrol Hypertens* 24: 463-469, 2015.
139. **Puelles VG, Moeller MJ, and Bertram JF.** We can see clearly now: optical clearing and kidney morphometrics. *Curr Opin Nephrol Hypertens* 26: 179-186, 2017.
140. **Puelles VG, van der Wolde JW, Schulze KE, Short KM, Wong MN, Bensley JG, Cullen-McEwen LA, Caruana G, Hokke SN, Li J, Firth SD, Harper IS, Nikolic-Paterson DJ, and Bertram JF.** Validation of a three-dimensional method for counting and sizing podocytes in whole glomeruli. *J Am Soc Nephrol* 27: 3093-3104, 2016.
141. **Pusztaszeri MP, Seelentag W, and Bosman FT.** Immunohistochemical expression of endothelial markers CD31, CD34, von Willebrand factor, and Fli-1 in normal human tissues. *J Histochem Cytochem* 54: 385-395, 2006.
142. **Rabito CA, Moore RH, Bougas C, and Dragotakes SC.** Noninvasive, real-time monitoring of renal function: the ambulatory renal monitor. *J Nucl Med* 34: 199-207, 1993.
143. **Rama I, Bruene B, Torras J, Koehl R, Cruzado JM, Bestard O, Franquesa M, Lloberas N, Weigert A, Herrero-Fresneda I, Gulias O, and Grinyo JM.** Hypoxia stimulus: An adaptive immune response during dendritic cell maturation. *Kidney Int* 73: 816-825, 2008.
144. **Reidy K, Kang HM, Hostetter T, and Susztak K.** Molecular mechanisms of diabetic kidney disease. *J Clin Invest* 124: 2333-2340, 2014.
145. **Ren Y, Garvin JL, Liu R, and Carretero OA.** Role of macula densa adenosine triphosphate (ATP) in tubuloglomerular feedback. *Kidney Int* 66: 1479-1485, 2004.
146. **Richards N, Harris K, Whitfield M, O'Donoghue D, Lewis R, Mansell M, Thomas S, Townend J, Eames M, and Marcelli D.** Primary care-based disease management of chronic kidney disease (CKD), based on estimated glomerular filtration rate (eGFR) reporting, improves patient outcomes. *Nephrol Dial Transplant* 23: 549-555, 2008.
147. **Richardson DS, and Lichtman JW.** Clarifying Tissue Clearing. *Cell* 162: 246-257, 2015.
148. **Ries M, Basseau F, Tyndal B, Jones R, Deminiere C, Catargi B, Combe C, Moonen CW, and Grenier N.** Renal diffusion and BOLD MRI in experimental diabetic nephropathy. Blood oxygen level-dependent. *J Magn Reson Imaging* 17: 104-113, 2003.
149. **Rosenberger C, Khamaisi M, Abassi Z, Shilo V, Weksler-Zangen S, Goldfarb M, Shina A, Zibertrest F, Eckardt KU, Rosen S, and Heyman SN.** Adaptation to hypoxia in the diabetic rat kidney. *Kidney Int* 73: 34-42, 2008.
150. **Rossert J, Levin A, Roger SD, Horl WH, Fouqueray B, Gassmann-Mayer C, Frei D, and McClellan WM.** Effect of early correction of anemia on the progression of CKD. *Am J Kidney Dis* 47: 738-750, 2006.
151. **Ruggenenti P, Fassi A, Ilieva AP, Bruno S, Iliev IP, Brusegan V, Rubis N, Gherardi G, Arnoldi F, Ganeva M, Ene-Iordache B, Gaspari F, Perna A, Bossi A, Trevisan R, Dodesini AR, Remuzzi G, and Bergamo Nephrologic Diabetes Complications Trial I.** Preventing microalbuminuria in type 2 diabetes. *N Engl J Med* 351: 1941-1951, 2004.
152. **Sahota A, Chen J, Behzadian MA, Ravindra R, Takeuchi H, Stambrook PJ, and Tischfield JA.** 2,8-Dihydroxyadenine lithiasis in a Japanese patient heterozygous at the adenine phosphoribosyltransferase locus. *Am J Hum Genet* 48: 983-989, 1991.
153. **Sahota A, Chen J, Boyadjiev SA, Gault MH, and Tischfield JA.** Missense mutation in the adenine phosphoribosyltransferase gene causing 2,8-dihydroxyadenine urolithiasis. *Hum Mol Genet* 3: 817-818, 1994.

154. **Santana AC, Degaspari S, Catanozi S, Delle H, de Sa Lima L, Silva C, Blanco P, Solez K, Scavone C, and Noronha IL.** Thalidomide suppresses inflammation in adenine-induced CKD with uraemia in mice. *Nephrol Dial Transplant* 28: 1140-1149, 2013.
155. **Sapirstein LA, Vidt DG, Mandel MJ, and Hanusek G.** Volumes of distribution and clearances of intravenously injected creatinine in the dog. *Am J Physiol* 181: 330-336, 1955.
156. **Scarfe L, Rak-Raszewska A, Geraci S, Darssan D, Sharkey J, Huang J, Burton NC, Mason D, Ranjzad P, Kenny S, Gretz N, Levy R, Kevin Park B, Garcia-Finana M, Woolf AS, Murray P, and Wilm B.** Measures of kidney function by minimally invasive techniques correlate with histological glomerular damage in SCID mice with adriamycin-induced nephropathy. *Sci Rep* 5: 13601, 2015.
157. **Schafer M, Schafer C, Ewald N, Piper HM, and Noll T.** Role of redox signaling in the autonomous proliferative response of endothelial cells to hypoxia. *Circ Res* 92: 1010-1015, 2003.
158. **Schnermann J, Weihprecht H, and Briggs JP.** Inhibition of tubuloglomerular feedback during adenosine1 receptor blockade. *Am J Physiol* 258: F553-561, 1990.
159. **Schock-Kusch D, Geraci S, Ermeling E, Shulhevich Y, Sticht C, Hesser J, Stsepankou D, Neudecker S, Pill J, Schmitt R, and Melk A.** Reliability of transcutaneous measurement of renal function in various strains of conscious mice. *PLoS One* 8: e71519, 2013.
160. **Schock-Kusch D, Sadick M, Henninger N, Kraenzlin B, Claus G, Kloetzer HM, Weiss C, Pill J, and Gretz N.** Transcutaneous measurement of glomerular filtration rate using FITC-sinistrin in rats. *Nephrol Dial Transplant* 24: 2997-3001, 2009.
161. **Schock-Kusch D, Xie Q, Shulhevich Y, Hesser J, Stsepankou D, Sadick M, Koenig S, Hoecklin F, Pill J, and Gretz N.** Transcutaneous assessment of renal function in conscious rats with a device for measuring FITC-sinistrin disappearance curves. *Kidney Int* 79: 1254-1258, 2011.
162. **Scholey JW, and Meyer TW.** Control of glomerular hypertension by insulin administration in diabetic rats. *J Clin Invest* 83: 1384-1389, 1989.
163. **Schreiber A, Shulhevich Y, Geraci S, Hesser J, Stsepankou D, Neudecker S, Koenig S, Heinrich R, Hoecklin F, Pill J, Friedemann J, Schweda F, Gretz N, and Schock-Kusch D.** Transcutaneous measurement of renal function in conscious mice. *Am J Physiol Renal Physiol* 303: F783-788, 2012.
164. **Schultz SG, and Curran PF.** Coupled transport of sodium and organic solutes. *Physiol Rev* 50: 637-718, 1970.
165. **Shafi T, and Coresh J.** Chronic Kidney Disease. In: *Chronic Kidney Disease, Dialysis, and Transplantation*, edited by Sayegh JHH. Philadelphia: W.B. Saunders, 2010, p. 3-21.
166. **Shmarlouski A, Schock-Kusch D, Shulhevich Y, Buschmann V, Rohlicke T, Herdt D, Radle M, Hesser J, and Stsepankou D.** A novel analysis technique for transcutaneous measurement of glomerular filtration rate with ultralow dose marker concentrations. *IEEE Trans Biomed Eng* 63: 1742-1750, 2016.
167. **Snively CS, and Gutierrez C.** Chronic kidney disease: prevention and treatment of common complications. *Am Fam Physician* 70: 1921-1928, 2004.
168. **Spalteholz W.** *Über das Durchsichtigmachen von menschlichen und tierischen Präparaten.* Leipzig: S. Hierzel, 1914.
169. **Spradley FT, Tan AY, Joo WS, Daniels G, Kussie P, Karumanchi SA, and Granger JP.** Placental growth factor administration abolishes placental ischemia-induced hypertension. *Hypertension* 67: 740-747, 2016.

170. **Steinbach S, Krolop N, Strommer S, Herrera-Perez Z, Geraci S, Friedemann J, Gretz N, and Neiger R.** A pilot study to assess the feasibility of transcutaneous glomerular filtration rate measurement using fluorescence-labelled sinistrin in dogs and cats. *PLoS One* 9: e111734, 2014.
171. **Stengel B, and Couchoud C.** Chronic kidney disease prevalence and treated end-stage renal disease incidence: A complex relationship. *J Am Soc Nephrol* 17: 2094-2096, 2006.
172. **Steven LJ.** Optical properties of biological tissues: a review. *Physics in Medicine & Biology* 58: R37, 2013.
173. **Sun D, Feng J, Dai C, Sun L, Jin T, Ma J, and Wang L.** Role of peritubular capillary loss and hypoxia in progressive tubulointerstitial fibrosis in a rat model of aristolochic acid nephropathy. *Am J Nephrol* 26: 363-371, 2006.
174. **Tanaka T, Hanafusa N, Ingelfinger JR, Ohse T, Fujita T, and Nangaku M.** Hypoxia induces apoptosis in SV40-immortalized rat proximal tubular cells through the mitochondrial pathways, devoid of HIF1-mediated upregulation of Bax. *Biochem Biophys Res Commun* 309: 222-231, 2003.
175. **Taskiran E, Erbas O, Yigitturk G, Meral A, Akar H, and Taskiran D.** Exogenously administered adenosine attenuates renal damage in streptozotocin-induced diabetic rats. *Ren Fail* 38: 1276-1282, 2016.
176. **Tett SE, Kirkpatrick CM, Gross AS, and McLachlan AJ.** Principles and clinical application of assessing alterations in renal elimination pathways. *Clin Pharmacokinet* 42: 1193-1211, 2003.
177. **Theer P, and Denk W.** On the fundamental imaging-depth limit in two-photon microscopy. *J Opt Soc Am A Opt Image Sci Vis* 23: 3139-3149, 2006.
178. **Thomson S, Bao D, Deng A, and Vallon V.** Adenosine formed by 5'-nucleotidase mediates tubuloglomerular feedback. *J Clin Invest* 106: 289-298, 2000.
179. **Thomson SC, Deng A, Bao D, Satriano J, Blantz RC, and Vallon V.** Ornithine decarboxylase, kidney size, and the tubular hypothesis of glomerular hyperfiltration in experimental diabetes. *J Clin Invest* 107: 217-224, 2001.
180. **Tsai PS, Kaufhold JP, Blinder P, Friedman B, Drew PJ, Karten HJ, Lyden PD, and Kleinfeld D.** Correlations of neuronal and microvascular densities in murine cortex revealed by direct counting and colocalization of nuclei and vessels. *J Neurosci* 29: 14553-14570, 2009.
181. **Tucker BJ, Collins RC, Ziegler MG, and Blantz RC.** Disassociation between glomerular hyperfiltration and extracellular volume in diabetic rats. *Kidney Int* 39: 1176-1183, 1991.
182. **Tucker BJ, Steiner RW, Gushwa LC, and Blantz RC.** Studies on the tubulo-glomerular feedback system in the rat. The mechanism of reduction in filtration rate with benzolamide. *J Clin Invest* 62: 993-1004, 1978.
183. **Vallon V.** Tubuloglomerular feedback and the control of glomerular filtration rate. *News Physiol Sci* 18: 169-174, 2003.
184. **Vallon V, Rieg T, Cunard R, and H. K.** Impaired proximal tubular and kidney glucose reabsorption in gene-targeted mice lacking SGLT1. *Am Soc Nephrol* 21: 262A: 2010.
185. **Vallon V, Blantz RC, and Thomson S.** Glomerular hyperfiltration and the salt paradox in early type 1 diabetes mellitus: a tubulo-centric view. *J Am Soc Nephrol* 14: 530-537, 2003.
186. **Vallon V, Blantz RC, and Thomson S.** Homeostatic efficiency of tubuloglomerular feedback is reduced in established diabetes mellitus in rats. *Am J Physiol* 269: F876-883, 1995.
187. **Vallon V, Huang DY, Deng A, Richter K, Blantz RC, and Thomson S.** Salt-sensitivity of proximal reabsorption alters macula densa salt and explains the paradoxical effect of dietary salt on glomerular filtration rate in diabetes mellitus. *J Am Soc Nephrol* 13: 1865-1871, 2002.

188. **Vallon V, Platt KA, Cunard R, Schroth J, Whaley J, Thomson SC, Koepsell H, and Rieg T.** SGLT2 mediates glucose reabsorption in the early proximal tubule. *J Am Soc Nephrol* 22: 104-112, 2011.
189. **Vallon V, Richter K, Blantz RC, Thomson S, and Osswald H.** Glomerular hyperfiltration in experimental diabetes mellitus: potential role of tubular reabsorption. *J Am Soc Nephrol* 10: 2569-2576, 1999.
190. **van den Born J, van Kraats AA, Bakker MA, Assmann KJ, van den Heuvel LP, Veerkamp JH, and Berden JH.** Selective proteinuria in diabetic nephropathy in the rat is associated with a relative decrease in glomerular basement membrane heparan sulphate. *Diabetologia* 38: 161-172, 1995.
191. **van der Loos CM.** Multiple immunoenzyme staining: methods and visualizations for the observation with spectral imaging. *J Histochem Cytochem* 56: 313-328, 2008.
192. **Vervoort G, Veldman B, Berden JH, Smits P, and Wetzels JF.** Glomerular hyperfiltration in type 1 diabetes mellitus results from primary changes in proximal tubular sodium handling without changes in volume expansion. *Eur J Clin Invest* 35: 330-336, 2005.
193. **Walker LA, Gellai M, and Valtin H.** Renal response to pentobarbital anesthesia in rats: effect of interrupting the renin-angiotensin system. *J Pharmacol Exp Ther* 236: 721-728, 1986.
194. **Wang W, and Vadgama P.** O₂ microsensors for minimally invasive tissue monitoring. *J R Soc Interface* 1: 109-117, 2004.
195. **Wang Y, Zhang DH, Zhang JY, Chen N, and Zhi GY.** High-yield synthesis of bioactive ethyl cinnamate by enzymatic esterification of cinnamic acid. *Food Chem* 190: 629-633, 2016.
196. **Watson JD, and Crick FH.** Molecular structure of nucleic acids; a structure for deoxyribose nucleic acid. *Nature* 171: 737-738, 1953.
197. **Welch WJ, Baumgartl H, Lubbers D, and Wilcox CS.** Renal oxygenation defects in the spontaneously hypertensive rat: role of AT1 receptors. *Kidney Int* 63: 202-208, 2003.
198. **Wiseman MJ, Mangili R, Alberetto M, Keen H, and Viberti G.** Glomerular response mechanisms to glycemic changes in insulin-dependent diabetics. *Kidney Int* 31: 1012-1018, 1987.
199. **Wright FS, and Schnermann J.** Interference with feedback control of glomerular filtration rate by furosemide, triflocin, and cyanide. *J Clin Invest* 53: 1695-1708, 1974.
200. **Wyngaarden JB, and Dunn JT.** 8-Hydroxyadenine as the intermediate in the oxidation of adenine to 2, 8-dihydroxyadenine by xanthine oxidase. *Arch Biochem Biophys* 70: 150-156, 1957.
201. **Xu C, Chang A, Hack BK, Eadon MT, Alper SL, and Cunningham PN.** TNF-mediated damage to glomerular endothelium is an important determinant of acute kidney injury in sepsis. *Kidney Int* 85: 72-81, 2014.
202. **Yushchenko DA, and Schultz C.** Tissue clearing for optical anatomy. *Angew Chem Int Ed Engl* 52: 10949-10951, 2013.
203. **Zatz R, Dunn BR, Meyer TW, Anderson S, Rennke HG, and Brenner BM.** Prevention of diabetic glomerulopathy by pharmacological amelioration of glomerular capillary hypertension. *J Clin Invest* 77: 1925-1930, 1986.
204. **Zollner FG, Schock-Kusch D, Backer S, Neudecker S, Gretz N, and Schad LR.** Simultaneous measurement of kidney function by dynamic contrast enhanced MRI and FITC-sinistrin clearance in rats at 3 tesla: initial results. *PLoS One* 8: e79992, 2013.

CHAPTER 2

Renal cellular hypoxia in adenine-induced chronic kidney disease

Debra Fong¹ | Md Mahbub Ullah¹ | Jaswini G. Lal¹ | Amany Abdelkader¹ |
Connie P.C. Ow¹ | Lucinda M. Hilliard¹ | Sharon D. Ricardo² | Darren J. Kelly³ |
Roger G. Evans¹

¹Biomedicine Discovery Institute and Department of Physiology, Monash University, Clayton, Melbourne, Vic., Australia

²Biomedicine Discovery Institute and Department of Anatomy and Developmental Biology, Monash University, Clayton, Melbourne, Vic., Australia

³Department of Medicine, University of Melbourne, St Vincent's Hospital, Fitzroy, Melbourne, Vic., Australia

Correspondence

Dr Roger Evans, Department of Physiology, Monash University, Melbourne, Vic., Australia.

Email: roger.evans@monash.edu

Summary

We determined whether adenine-induced chronic kidney disease (CKD) in rats is associated with renal tissue hypoxia. Adenine (100 mg) or its vehicle was administered to male Sprague-Dawley rats, daily by oral gavage, over a 15-day period. Renal function was assessed before, and 7 and 14 days after, adenine treatment commenced, by collection of a 24-hour urine sample and a blood sample from the tail vein. On day 15, arterial pressure was measured in conscious rats via the tail artery. Renal tissue hypoxia was then assessed by pimonidazole adduct immunohistochemistry and fibrosis was assessed by staining tissue with picosirius red and Masson's trichrome. CKD was evident within 7 days of commencing adenine treatment, as demonstrated by increased urinary albumin to creatinine ratio (30 ± 12 -fold). By day 14 of adenine treatment plasma creatinine concentration was more than 7-fold greater, and plasma urea more than 5-fold greater, than their baseline levels. On day 15, adenine-treated rats had slightly elevated mean arterial pressure (8 mmHg), anaemia and renomegaly. Kidneys of adenine-treated rats were characterised by the presence of tubular casts, dilated tubules, expansion of the interstitial space, accumulation of collagen, and tubulointerstitial hypoxia. Pimonidazole staining (hypoxia) co-localised with fibrosis and was present in both patent and occluded tubules. We conclude that renal tissue hypoxia develops rapidly in adenine-induced CKD. This model, therefore, should prove useful for examination of the temporal and spatial relationships between tubulointerstitial hypoxia and the development of CKD, and thus the testing of the 'chronic hypoxia hypothesis'.

KEYWORDS

fibrosis, hypoxia, pimonidazole

1 | INTRODUCTION

Renal tissue hypoxia has been demonstrated in multiple forms of chronic kidney disease (CKD), including polycystic kidney disease,¹⁻³ diabetic nephropathy,⁴ the remnant kidney model,⁵ and CKD following ischaemia-reperfusion injury.^{6,7} This has led to the proposition that hypoxia represents a final common pathway for the development of

multiple forms of CKD;⁸ the so-called 'chronic hypoxia hypothesis'.⁹ More recent observations have even provided evidence that renal hypoxia per se might be sufficient to initiate the development of CKD.¹⁰

The relatively slow development of injury and/or diminished glomerular filtration rate (GFR) in most rodent models of CKD has made it difficult to tease out the causal relationships between tubulointerstitial

hypoxia and the pathogenesis of nephropathy. For example, after recovery from acute ischaemia-reperfusion injury, there is little evidence of renal functional abnormalities or abnormal tubular morphology 8 weeks after the initial insult and only mild proteinuria is observed after 16 weeks.¹¹ In most rodent models of polycystic kidney disease, there is some evidence of abnormalities in renal tissue structure at birth, but then many weeks or months are required for the condition to progress to frank CKD.^{12,13} Furthermore, in type 1 diabetes, induced by streptozotocin in rats, only relatively mild tissue damage is observed in the first month after the induction of diabetes.¹⁴ Even in the remnant kidney model, which has been extensively used in studies of the pathogenesis of CKD, nephropathy develops over weeks rather than days.⁵

In order for us to test the chronic hypoxia hypothesis in a definitive manner, it is vital that we are able to precisely define the temporal and spatial relationships between hypoxia and the progression of disease.¹⁵ That is, we must determine whether hypoxia occurs *before*, and *in the same place* as, tissue damage. Consequently, we require experimental models of CKD in which pathological changes in renal tissue develop rapidly in response to a defined stimulus. Administration of adenine, either in food^{16–25} or by oral gavage,²⁶ has been shown to result in reproducible renal dysfunction. Adenine is metabolised to 2,8-dihydroxy-adenine which forms crystalline casts within the renal tubules. The formation of these casts is thought to initiate renal dysfunction.²¹ CKD in adenine-treated rats is associated with hypertension and vascular calcification, renal interstitial fibrosis, proteinuria, increased water intake and urine flow, uraemia, and hyperkalaemia.²⁵ Only modest increases in serum creatinine are observed after 2 weeks of adenine treatment, while more prolonged treatment results in marked renal pathology and markedly increased serum creatinine.^{17,18,20–22} In the current study, we tested the hypothesis that the early phase of adenine-induced CKD (i.e. after 2-weeks of treatment) is accompanied by renal tissue hypoxia, in order to evaluate the potential for this model to be used for testing the chronic hypoxia hypothesis.

2 | RESULTS

2.1 | Progression of chronic kidney disease

Across the 2 weeks during which rats were treated with the vehicle for adenine, body weight increased $27 \pm 11\%$, while food intake and faecal output slightly decreased (Table 1). Food intake and faecal output were consistently less in adenine-treated rats than vehicle-treated rats. There were tendencies for adenine-treated rats to gain less weight than the vehicle-treated rats, although this apparent effect was not statistically significant (time \times treatment interaction; $P=.14$). In vehicle-treated rats, water intake and urine output gradually increased across the 14 days of the study, to be $28 \pm 18\%$ and $116 \pm 57\%$ greater than their baseline level at day 14, respectively. In contrast to vehicle-treated rats, much greater increases in water intake and urine output were observed in adenine-treated rats. Water intake had increased by $154 \pm 38\%$ at day 7 and by $150 \pm 46\%$ at day 14. Urine output had increased by $346 \pm 83\%$ at day 7 and by $372 \pm 96\%$ at day 14.

The rates of excretion of sodium, chloride and osmolytes were indistinguishable in adenine-treated compared with vehicle-treated rats (Table 1). However, potassium excretion tended to increase in rats treated with adenine. This apparent effect was particularly evident on day 7, when potassium excretion was 67% greater in adenine-treated rats than vehicle-treated rats. By day 7 of adenine-treatment urine osmolality was reduced by approximately $69 \pm 5\%$ of its pre-treatment level. Proteinuria was also present at day 7 of adenine treatment. Urinary protein excretion had increased by $287 \pm 58\%$ from its pre-treatment level and remained similarly increased at day 14 of adenine treatment. In contrast, the vehicle treated rats excreted little protein throughout the 2 week treatment period. In adenine-treated rats, urinary albumin excretion had increased 29 ± 9 -fold and the urinary albumin to creatinine ratio had increased 30 ± 12 fold by day 7 of adenine treatment. Plasma creatinine, measured in three rats on day 0, was below the level of detection (i.e. ≤ 0.20 mg/dL). By day 14 of adenine treatment it was more than 7-fold greater (1.50 ± 0.13 mg/dL, $n=4$). Plasma urea averaged 4.8 ± 0.5 mmol/L ($n=3$) on day 0 and 25.5 ± 0.9 mmol/L ($n=3$) on day 14 of adenine treatment.

On the 15th day of treatment, the body weight of adenine-treated rats was 16% less than that of vehicle treated rats (Table 2). Mean arterial pressure of adenine-treated rats averaged 8 mmHg higher than that of vehicle treated rats but heart rate did not differ significantly between the two groups. The kidneys of adenine-treated rats were 86% heavier than those of vehicle-treated rats. Haematocrit was less in adenine-treated rats ($31.9 \pm 3.2\%$) than in vehicle-treated rats ($38.2 \pm 1.4\%$).

2.2 | Histology and immunohistochemistry

To visualise the tubular and vascular elements of the rat kidney, haematoxylin and eosin staining was performed. Kidneys of rats treated with vehicle (Fig. 1a) were considerably smaller than the kidneys of adenine-treated rats (Fig. 1e). Tissue architecture of the cortex and medulla in the kidneys of the rats treated with vehicle appeared normal (Fig. 1a–d). The tubules were closely spaced and the interstitial space and blood vessels were not prominent. The glomeruli appeared regular with normal thickness of the basement membrane (Fig. 1b). In contrast, the tissue architecture of the kidneys of rats treated with adenine was very different. There was considerable expansion of the interstitial space in the cortex and medulla (Fig. 1e–h). The tubules appeared abnormal with irregular lumen space. The glomeruli were intact in their basement membrane but dilation of Bowman's space was seen (Fig. 1f). The blood vessels appeared unaffected and similar to those of vehicle-treated rats. Characteristic tubular casts, presumably containing 2,8-dihydroxyadenine, were also observed (Fig. 2).

Tissues were stained with picosirius red (Fig. 3) and Masson's trichrome (Fig. 4) to examine fibrosis. Masson's trichrome stains type I collagen as well as variety of matrix elements.²⁷ In contrast, picosirius red is highly specific for type I and type III collagen.²⁸ Sections of kidneys of vehicle-treated rats stained with picosirius red appeared yellow and lacked red collagen positive stain (Fig. 3a). The only staining observed was in the perivascular adventitia and

TABLE 1 Characteristics of adenine-treated and vehicle-treated rats across the course of the first 14 days of the experiment

Variable	Treat	n	Day 0	Day 7	Day 14	<i>P</i> _{Treat}	<i>P</i> _{Time}	<i>P</i> _{Interaction}
Fluid/energy balance								
Body weight (g)	Vehicle	6	215 ± 13	256 ± 9	269 ± 13	.43	.003	.14
	Adenine	6	221 ± 10	248 ± 15	236 ± 13			
Food intake (g/day)	Vehicle	6	20.1 ± 0.6	15.4 ± 2.3	18.4 ± 1.3	.04	.003	.08
	Adenine	6	19.7 ± 0.5	12.8 ± 2.0	11.2 ± 1.4			
Faeces output (g/day)	Vehicle	6	10.0 ± 0.4	6.9 ± 1.3	7.1 ± 1.0	.03	.004	.99
	Adenine	6	8.2 ± 0.5	5.1 ± 0.6	5.3 ± 1.1			
Water intake (mL/day)	Vehicle	6	23.3 ± 2.1	23.3 ± 4.0	29.2 ± 3.7	.001	.002	.009
	Adenine	6	23.3 ± 3.3	54.2 ± 5.2	54.2 ± 7.8			
Urine output (mL/day)	Vehicle	6	8.0 ± 0.8	11.3 ± 1.9	15.1 ± 2.8	<.001	<.001	.003
	Adenine	6	11.1 ± 2.7	40.1 ± 4.3	43.0 ± 6.0			
Electrolyte excretion								
Sodium (μmol/min)	Vehicle	6	0.80 ± 0.14	0.75 ± 0.10	0.77 ± 0.09	.93	.54	.73
	Adenine	6	0.89 ± 0.07	0.75 ± 0.11	0.71 ± 0.12			
Chloride (μmol/min)	Vehicle	6	1.38 ± 0.21	1.24 ± 0.14	1.57 ± 0.10	.38	.64	.30
	Adenine	6	1.44 ± 0.08	1.60 ± 0.13	1.47 ± 0.16			
Potassium (μmol/min)	Vehicle	6	1.25 ± 0.13	1.07 ± 0.13	1.54 ± 0.11	.03	.09	.15
	Adenine	6	1.29 ± 0.13	1.79 ± 0.19	1.78 ± 0.26			
Osmolar (μOsm/min)	Vehicle	6	11.9 ± 0.8	11.2 ± 1.1	13.6 ± 1.0	.97	.41	.28
	Adenine	6	11.2 ± 0.9	13.2 ± 2.3	12.4 ± 1.2			
Renal dysfunction								
Urine osmolality (mOsm/kg)	Vehicle	6	2304 ± 340	1521 ± 143	1509 ± 248	<.001	<.001	.45
	Adenine	6	1704 ± 240	495 ± 96	433 ± 42			
Urinary protein excretion (mg/day)	Vehicle	6	7.48 ± 2.21	8.25 ± 0.55	8.65 ± 1.22	.001	.001	.002
	Adenine	6	5.64 ± 0.19	21.84 ± 3.76	24.17 ± 1.39			
Urinary albumin excretion (μg/day)	Vehicle	6	129 ± 33	141 ± 48	63 ± 10	<.001	<.001	<.001
	Adenine	6	197 ± 51	3852 ± 967	5274 ± 1112			
Urinary albumin/creatinine ratio (mg/g)	Vehicle	6	14.6 ± 4.8	15.6 ± 5.9	6.0 ± 0.9	.05	.07	.07
	Adenine	6	23.4 ± 7.0	542 ± 304	593 ± 213			

P values represent the outcomes of repeated measures analysis of variance. The Greenhouse-Geisser correction was applied to within-subject *P* values to correct for compound asymmetry.⁴⁹ Treat = Treatment. Bolded *P* values are ≤.05.

TABLE 2 Characteristics of rats on day 15 of adenine or vehicle treatment

Variable	Vehicle-treated rats		Adenine-treated rats		<i>P</i>
	n	Day 15	N	Day 15	
Body weight (g)	6	276 ± 14	6	233 ± 12	.04
Mean arterial pressure (mmHg)	5	112 ± 2	3	120 ± 1	.01
Heart rate (beats/min)	5	368 ± 25	3	317 ± 11	.14
Left kidney weight (g)	5	1.32 ± 0.11	5	2.38 ± 0.12	<.001
Right kidney weight (g)	5	1.23 ± 0.06	5	2.37 ± 0.16	.001

P values are the outcomes of Student's unpaired *t*-test.

around the glomeruli (Fig. 3b). In contrast, there was extensive picrorisurid red staining in the kidney of the adenine-treated rats (Fig. 3e). Considerable staining, denoting collagen deposition, was observed in the expanded interstitial space (Fig. 3f–h). Regarding Masson's trichrome staining, there was little blue staining (reflecting fibrosis) in sections from vehicle-treated rats (Fig. 4b,c), except for the expected perivascular staining around intrarenal arteries. In contrast, there was considerable positive staining in the cortex, outer medulla and inner medulla of adenine-treated rats (Fig. 4f–h). Quantification of Masson's trichrome staining revealed more than 3-fold greater staining in the cortex and medulla of adenine-treated rats compared to vehicle-treated rats (Fig. 5).

Pimonidazole immunohistochemistry was performed to detect the presence of hypoxia. In the kidneys of all vehicle-treated rats, positive staining, denoting hypoxia, was mainly seen in the thick ascending

limb and collecting ducts in the outer and inner medulla respectively (Fig. 6a–d). Very little apparent staining was seen in the cortex of all of the vehicle-treated rats (Fig. 6b). In contrast, considerable staining was observed throughout the entire kidney of all rats that were treated with adenine (Fig. 6e). The degree of pimonidazole staining was markedly greater in the cortex of adenine-treated rats, particularly in the epithelial lining of tubules, when compared to vehicle-treated rats. There was also considerable staining seen in the outer and inner medulla (Fig. 6g–h).

It was noted that some tubules in the cortex of adenine-treated rats were patent or even dilated, while others had a closed lumen. This phenomenon likely arises from the formation of tubular casts (Fig. 2). We reasoned that tubules with an open lumen may consume more oxygen, for reabsorption of sodium, than tubules with a closed lumen. We hypothesised that the resultant heterogeneity of tubular oxygen consumption might lead to heterogeneity in renal hypoxia. However, the proportion of open tubules that stained positive for pimonidazole adducts was similar to the proportion of positive stained closed tubules (Fig. 7).

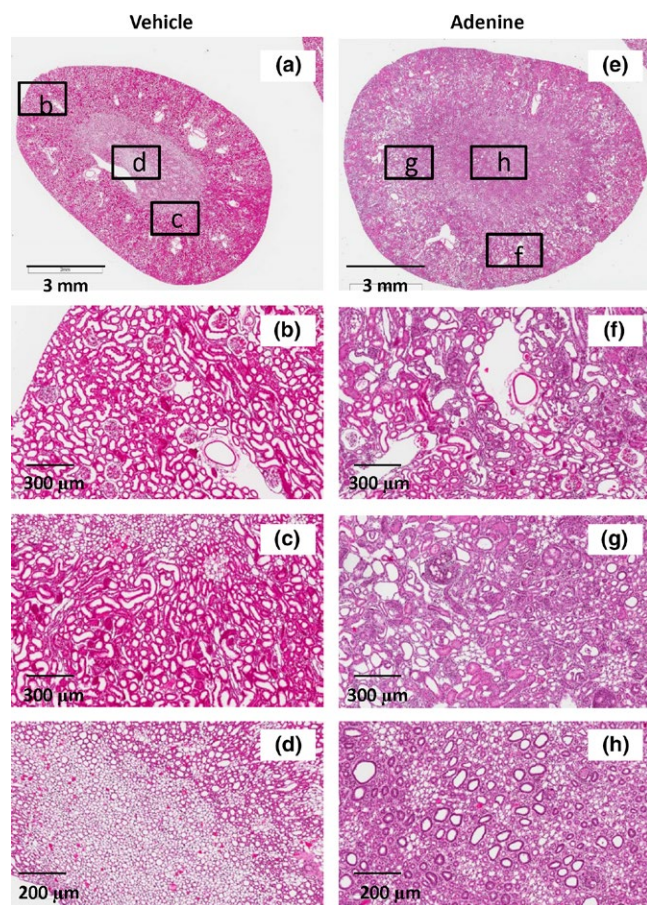


FIGURE 1 Micrographs of kidney sections from rats treated with vehicle (a–d) or adenine (e–h), stained with haematoxylin and eosin. Cortical (b, f), outer medullary (c, g) and inner medullary (d, h) regions are shown. Boxes in (a) and (e) show regions presented in (b–d) and (f–h). Note hypertrophy of the kidney of adenine-treated rats, interstitial expansion and irregular lumen of tubules. Images are typical of two sections taken from each kidney

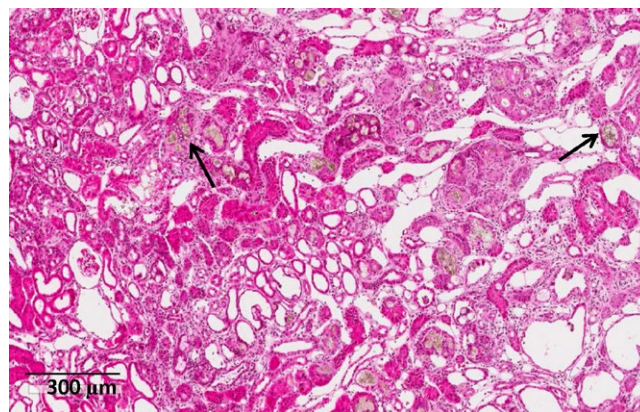


FIGURE 2 Micrograph of a kidney section from a rat treated with adenine, stained with haematoxylin and eosin. Note the presence of tubular casts (arrows) formed from precipitation of 2,8-dihydroxyadenine

The co-localisation of hypoxia and fibrosis was examined in serial sections stained for pimonidazole adducts and with Masson's trichrome (Fig. 8). Hypoxia and fibrosis were ubiquitously distributed in kidneys of adenine-treated rats. It was not possible to identify areas of the kidney that were hypoxic but not fibrotic, or fibrotic but not hypoxic.

3 | DISCUSSION

We found that 15 days of administration of adenine resulted in marked tubulointerstitial hypoxia associated with fibrosis, along with profound renal dysfunction. Thus, this experimental model may be useful for teasing out the temporal and spatial relationships between tubulointerstitial hypoxia, fibrogenesis, and the initiation and progression of CKD.

Chronic kidney disease is usually defined as a gradual loss of renal function, as quantified by measurement of GFR or plasma or serum concentrations of creatinine. According to this definition, the rats we studied had severe CKD by day 14 of adenine-treatment, as reflected by a more than 7-fold increase in plasma creatinine and 5-fold increase in plasma urea. Our findings are consistent with those of previous studies in which adenine has been administered for longer periods (i.e. 4 or more weeks).^{17,18,20–22} It is well established that creatinine clearance overestimates glomerular filtration rate in rats, principally due to tubular secretion of creatinine.²⁹ Nevertheless, between-subject and within-subject differences in plasma creatinine concentration usually reflect differences in GFR.³

Pathological changes were detectable at the tissue level after 2-weeks of adenine treatment, particularly in the form of interstitial fibrosis and tubular casts. There were also marked increases in urinary albumin and total protein excretion. There was a marked increase in urine flow and reduced urinary osmolarity. Reduced urinary concentrating ability is a hallmark of CKD in humans³⁰ and animal models (e.g. polycystic kidney disease²). However, we cannot discount the possibility that the effect of adenine-treatment on urinary osmolarity was

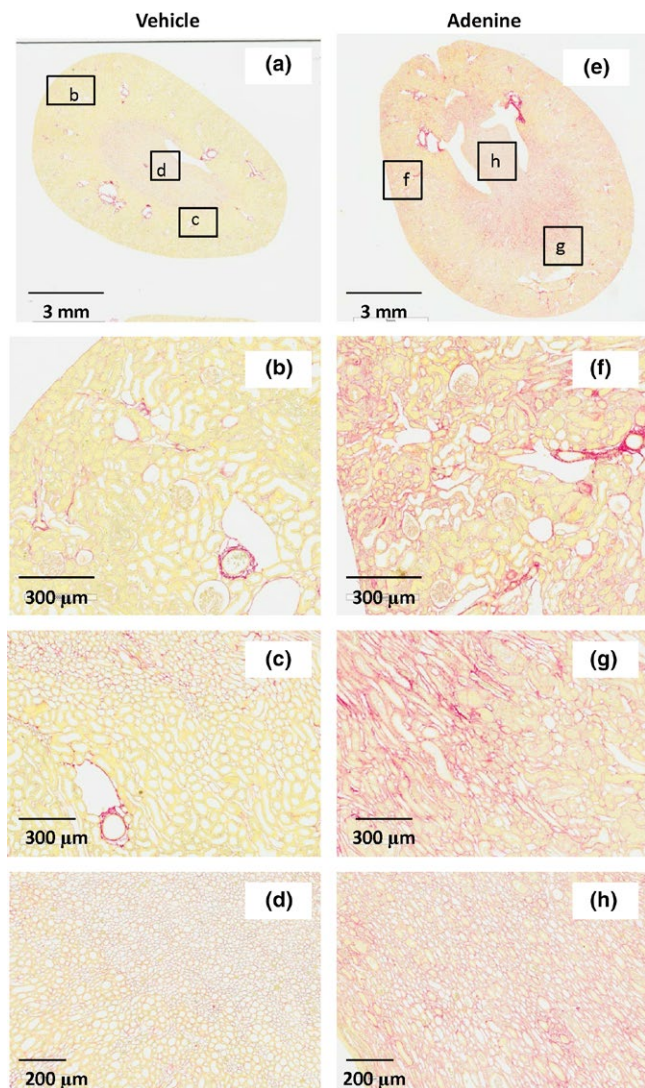


FIGURE 3 Micrographs of kidney sections from rats treated with vehicle (a–d) or adenine (e–h), stained with picosirius red. Cortical (b, f), outer medullary (c, g) and inner medullary (d, h) regions are shown. Boxes in (a) and (e) show regions presented in (b–d) and (f–h). Note the intense red staining in the kidneys of adenine-treated rats, showing collagen accumulation in the expanded interstitial space. In contrast, vehicle treated rats show faint staining around the glomerulus and considerable staining around arteries and some veins. Images are typical of two sections taken from each kidney

caused by increased thirst as opposed to reduced urinary concentrating ability.

Multiple mechanisms likely contribute to the development of renal tissue hypoxia during adenine-treatment. Our current findings indicate development of renal fibrosis in this model that is co-localized with hypoxia. Indeed, in serial sections, we were unable to identify regions of the kidneys of adenine-treated rats that stained positive for pimonidazole but not the blue stain of Masson's trichrome, or vice versa. Tubulointerstitial fibrosis increases the barriers to diffusion of oxygen from the vascular to the tubulointerstitial compartment.^{9,31} Thus, fibrosis likely makes some direct contribution to the development of hypoxia in adenine-treated rats. There is also strong evidence that, in

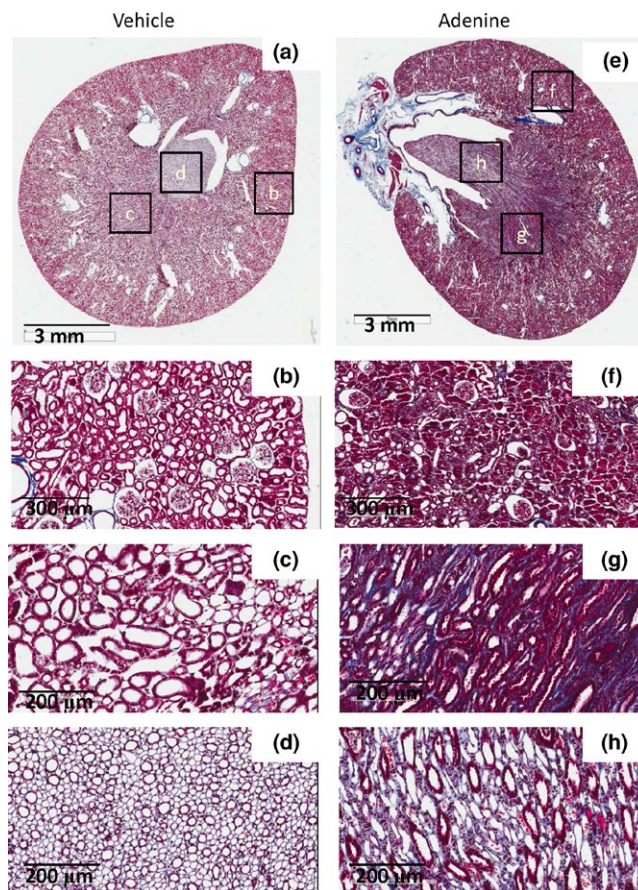


FIGURE 4 Micrograph of kidney sections from rats treated with vehicle (a–d) or adenine (e–h) stained with Masson's trichrome. Cortical (b, f), outer medullary (c, g) and inner medullary (d, h) regions are shown. Boxes in (a) and (e) show regions presented in (b–d) and (f–h). Note blue staining, representing fibrosis, is ubiquitous in the interstitium of adenine treated rats, but not vehicle-treated rats. Images are typical of two sections taken from each kidney

other models of CKD such as renovascular disease, fibrosis drives rarefaction of capillaries which in turn would be expected to reduce oxygen delivery to tissue.³² We are not aware of any published reports of renal vascular structure in adenine-induced CKD. However, Milman and colleagues recently provided evidence of blunted perfusion and renal vascular reactivity in anaesthetised mice with adenine-induced CKD, using a magnetic resonance imaging technique for assessing the renal vascular response to hyperoxia.²⁴ Consistent with these observations, renal blood flow measured directly by transit-time ultrasound flowmetry³³ or electromagnetic flowmetry³⁴ under anaesthesia, and by the clearance of para-aminohippurate in the conscious state,³⁵ has been observed to be less in rats with adenine-induced CKD compared to control animals. Thus, it is likely that abnormalities in both renal vascular structure and function contribute to the development of tissue hypoxia in adenine-treated rats. It is also likely that anaemia contributes to the development of renal hypoxia, since haematocrit was considerably less after 15 days of adenine-treatment than after vehicle treatment. This observation is also consistent with those arising from previous studies using this model.³³

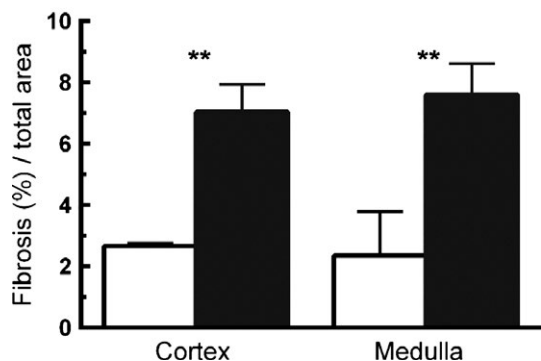


FIGURE 5 Quantification of fibrosis in the cortex and medulla. Two sections were analysed from each kidney. Values are between-rat mean \pm SEM for adenine- (n=6; filled bars) and vehicle- (n=4; opened bars) treated rats. ** $P < .01$ for adenine vs control (Student's unpaired *t*-test). (□) Control; (■) adenine

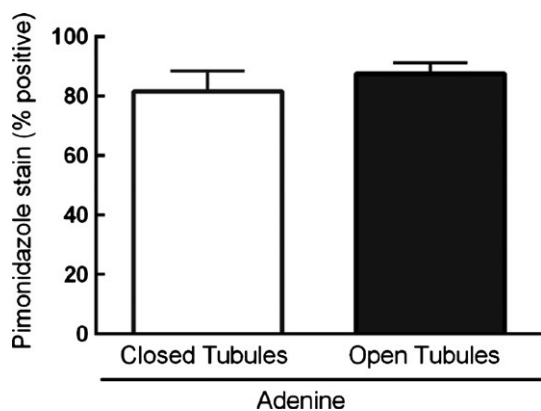


FIGURE 7 Relationship between hypoxia and the patency of tubules in kidneys of adenine-treated rats. Twenty non-dilated tubules with a visible lumen (open tubules) and twenty tubules with no visible lumen (closed tubules) were selected from each of the kidney sections stained with Masson's trichrome. These tubules were then identified in serial sections processed for pimonidazole adduct histochemistry. Each tubule was then classified as hypoxic (by the presence of pimonidazole stain) or not hypoxic (by the absence of pimonidazole stain). Columns and error bars are between-rat mean \pm SEM of n=6. $P = .39$ for comparison between open and closed tubules (Student's paired *t*-test)

According to the chronic hypoxia hypothesis developed by Fine and colleagues, one of the major drivers of tubulointerstitial hypoxia in CKD is hyperfiltration in remnant functional nephrons.³⁶ This is thought to be a consequence of increased tubular sodium reabsorption, the major source of oxygen consumption in the kidney.³⁷ We reasoned that this might lead to localisation of hypoxia selectively within patent tubules in the kidneys of adenine-treated rats and the presence of less severe hypoxia in those tubules that are occluded due to the presence of upstream tubular casts. Our use of perfusion fixation in the current study allowed us to examine this proposition, since we could clearly distinguish between patent and occluded tubules. We could not detect differences in the proportion of tubular

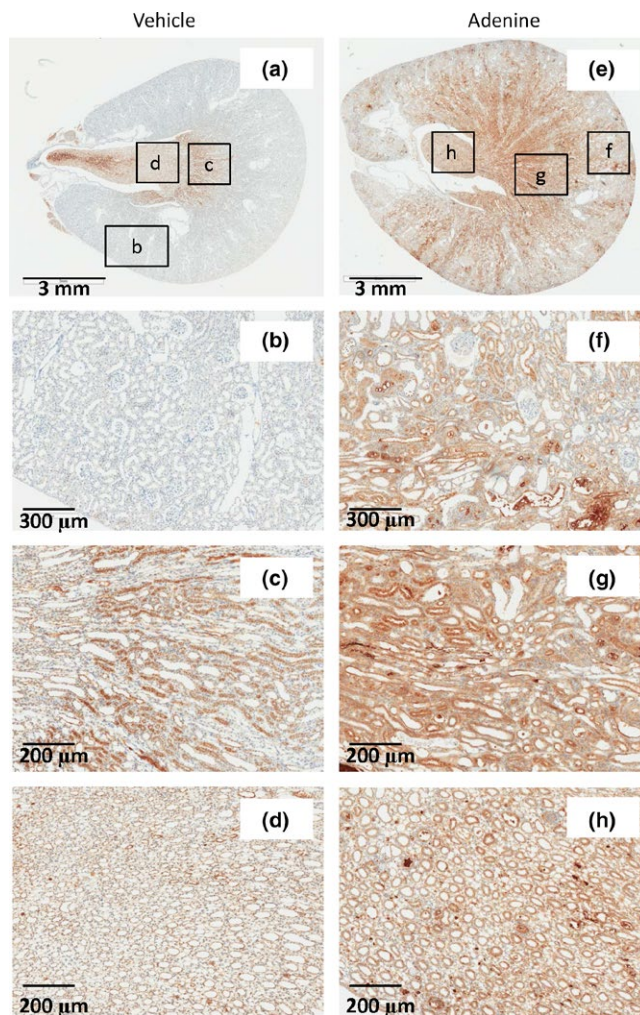


FIGURE 6 Micrographs of kidney sections from rats treated with vehicle (a–d) or adenine (e–h), showing immunohistochemical localisation of pimonidazole adducts. Cortical (b, f), outer medullary (c, g) and inner medullary (d, h) regions are shown. Note the intense staining in the cortex and medulla of adenine-treated rats. In contrast, vehicle treated rats show minimal staining in the cortex but some staining in the medulla. Images are typical of two sections taken from each kidney

profiles that stained positive for pimonidazole, according to whether the tubules were occluded or patent. Thus, our current findings do not provide support for this aspect of the chronic hypoxia hypothesis. However, we must acknowledge an important limitation of pimonidazole adduct immunohistochemistry using 3,3'-diaminobenzidine (DAB). DAB cannot be quantified because it does not obey the Beer-Lambert law.³⁸ Thus, future studies should examine the impact of tubular patency on renal tissue oxygenation in greater detail through use of quantitative methods for analysis of hypoxia at the cellular level.

Renal fibrosis in adenine-treated rats is also likely to be driven by multiple factors. The role of epithelial-to-mesenchymal transition in the development of fibrosis in CKD remains controversial.³⁹ Nevertheless, there are a number of pieces of evidence that support a role for this mechanism in adenine-treated rodents. For example,

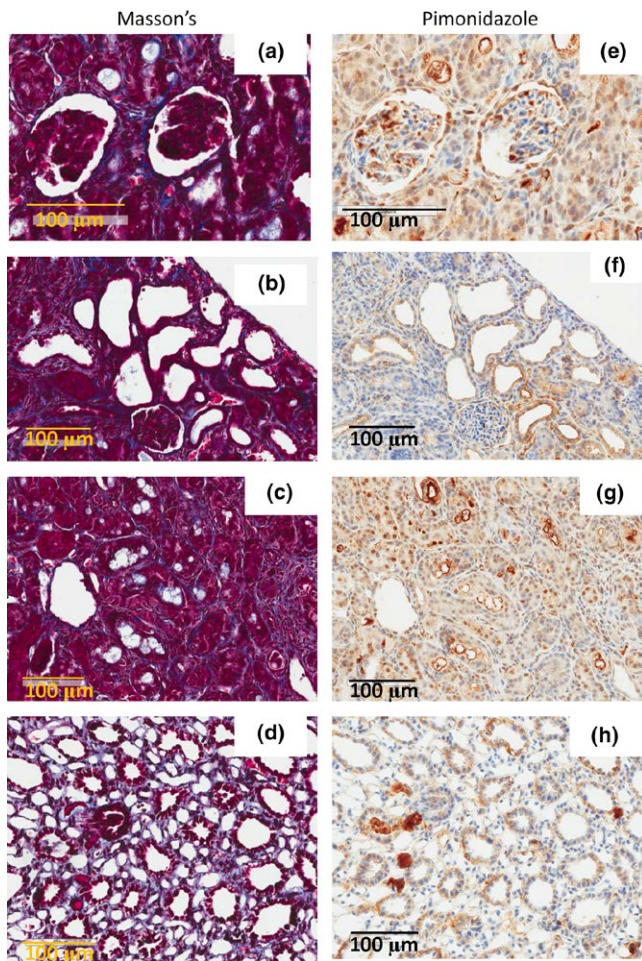


FIGURE 8 Co-localisation of fibrosis and hypoxia. The micrographs show serial sections from the kidney of a typical adenine-treated rat, stained with Masson's trichrome (a–d), and for pimonidazole adducts (e–h). Cortical (a, e, b, f, c, g) and medullary (d, h) regions are shown

Wang et al. demonstrated up-regulation of the pro-fibrogenic factors transforming growth factor (TGF)- β 1 and TGF- β 2, together with down-regulation of the (anti-fibrotic) translational repressors of TGF- β 2, micro-RNA (miR) miR200a and miR-141, in mice with adenine-induced CKD.²⁶ The authors provided evidence from cell-culture studies that TGF- β 1 and TGF- β 2 can drive epithelial-to-mesenchymal transition and so fibrogenesis. On the other hand, Wu et al. recently provided evidence for a role of endothelial-to-mesenchymal transition, driven by elevated circulating levels of parathyroid hormone, in fibrogenesis in adenine-induced CKD.²³ Interestingly, they were able to inhibit both endothelial-to-mesenchymal transition and the development of fibrosis with the calcimetic cinacalcet.

Hypoxia, through increased signalling via hypoxia-inducible factors (HIFs), may also play an important role in the development of fibrosis in CKD.⁴⁰ For example, renal fibrosis in rats with two-kidney-one-clip hypertension can be blunted by silencing HIF-1 α .⁴¹ Indeed, HIF activation and TGF β signalling may be able to induce fibrosis even in the absence of hypoxia.⁴² The role of hypoxia and HIFs in driving fibrosis in adenine-induced CKD has not, to our knowledge, been directly

assessed. Nevertheless, it remains possible that a vicious cycle may develop whereby hypoxia drives fibrosis and fibrosis drives hypoxia, as has been postulated to occur in other forms of CKD.^{15,36}

Our current finding of marked proteinuria in adenine-treated rats, as early as 1 week after commencing treatment, together with the documentation of both fibrosis and cellular hypoxia after 2 weeks, provides the basis for examination of the role of hypoxia in the development of nephropathy in this model. In particular, it should be possible to use radiotelemetry, in conscious rats, to precisely define the time-course of the development of renal tissue hypoxia.⁴³ It should also be possible to define the relative contributions of anaemia, renal ischemia, and altered renal oxygen consumption in the development of this hypoxia.^{3,7} A major challenge will be to find ways to ameliorate hypoxia in adenine-induced CKD to determine whether such treatments can blunt the development of renal dysfunction. Exposure of adenine-treated rats to hyperoxia is one possibility. However, the efficacy of such treatments will be limited both by the potential for oxygen toxicity⁴⁴ and by loss of oxygen in the pre-glomerular circulation.^{45,46} Anti-fibrotic therapy might also be a useful approach to break the putative vicious cycle of hypoxia and fibrosis.⁴⁷

In conclusion, our current findings indicate that severe renal dysfunction, accompanied by hypoxia and fibrosis, develops within 2-weeks of adenine-treatment. Therefore, in the future, this model should prove useful for testing the chronic hypoxia hypothesis for the development of CKD.

4 | METHODS

4.1 | Animals

Eighteen male Sprague-Dawley rats (Monash Animal Research Platform, Monash University, Melbourne, VIC, Australia), weighing on average 214 ± 5 g, were used in this study. At the commencement of treatment, the rats were 7 weeks of age. The rats were housed under standard laboratory conditions; $22 \pm 1^\circ\text{C}$, $40 \pm 1\%$ humidity and with a 12-hour light/dark cycle (06.00–18.00 hours). Tap water and standard rat chow were available ad libitum. All experimental procedures were approved by the Animal Ethics Committee of the School of Biomedical Sciences, Monash University, and were in accordance with the Australian Code of Practice for the Care and Use of Animals for Scientific Purposes. Rats were housed individually and allowed 1 week to acclimatise to these conditions before entering the study protocol.

4.2 | Experimental protocol

4.2.1 | Adenine-induced chronic kidney disease

All rats were treated daily with either adenine (100 mg; Sigma-Aldrich, Castle Hill, NSW, Australia) or its vehicle (1 mL of 0.5% w/v methylcellulose; Sigma-Aldrich) by oral gavage for a period of 15 days. The experiments were performed in two series. In the first series, six adenine-treated rats and six vehicle-treated rats were studied as

described below (165–252 g). For technical reasons, we were unable to obtain sufficient blood from most of these animals for measurement of plasma creatinine concentration. Therefore, an additional cohort of rats (192–212 g) were included in a supplementary study ($n=3$ per group). The rats were treated identically to those in the first series, but the only analysis performed was measurement of plasma creatinine concentration.

4.2.2 | Metabolic studies

Rats were housed individually in metabolic cages for 24 hours before, and 7 and 14 days after, commencement of the treatments (metabolic studies). Consumption of food and water and production of faeces and urine were measured over the 24-hour period. A day prior to the first metabolic study, the rats underwent a 6-hour training period for acclimatisation. Urine samples were transferred into several 1-mL aliquots and stored at -20°C for later analysis. At the completion of the 24-hour period in the metabolic cage a 0.5–1 mL blood sample was collected from the tail vein from the conscious rat. Blood was centrifuged at 3000 g at 4°C for 10 minutes and the plasma stored in 50 μL aliquots at -20°C for later analysis.

4.2.3 | Measurement of arterial pressure and tissue processing

On day 15 of the experimental protocol, arterial pressure was measured via the tail artery. The tail artery was catheterised under anaesthesia with isoflurane (1–4% v/v in 100% O_2 , Isoflo, Baxter Healthcare, Old Toongabbie, NSW, Australia). Following a 60-minute recovery period, with the rats fully conscious, the catheter was connected to a pressure transducer (Cobe, Arvada, CO, USA) and bridge amplifier (QA1, Scientific Concepts, Mount Waverley, VIC, Australia) interfaced with a computer running a LabView-based data acquisition program (Universal Acquisition, University of Auckland, New Zealand). After a 5–10 minute equilibration period, mean arterial pressure and heart rate were recorded for 30 minutes in the conscious rat.

After measurement of arterial pressure, the hypoxic marker 2-pimonidazole (60 mg/kg pimonidazole hydrochloride, Hypoxyprobe Inc, Burlington, MA, USA) was administered intraperitoneally. Sixty minutes later, each rat was anaesthetised with pentobarbitone sodium (60 mg/kg, i.p.; Sigma-Aldrich). Once a surgical level of anaesthesia was reached, a midline incision was made to expose the abdominal aorta and inferior vena cava. The left kidney was then perfusion fixed with 50–100 mL 4% w/v paraformaldehyde (PFA; Sigma-Aldrich), weighed and decapsulated, and post-fixed in a 4% PFA solution at 4°C overnight.

4.3 | Analytical methods

4.3.1 | Analysis of urine and plasma samples

Urinary electrolyte (Na^+ , K^+ and Cl^-) concentration was measured using an ion analyser (Rapidchem, Siemens Healthcare Diagnostics,

Bayswater, Vic., Australia). Urine osmolarity was measured by freezing point estimation (Model 2020, Advanced Instruments; John Morris Scientific, Chatswood, NSW, Australia). Urinary albumin concentration was determined using an enzyme-linked immunosorbent assay (Rat Albumin ELISA Kit; Bethyl Laboratories, Montgomery, TX, USA). Urinary creatinine concentration was measured using a creatinine assay kit (Cayman Chemical Company, Ann Arbor, MI, USA). Urinary protein concentration was measured by the Bradford method (Bio-Rad Laboratories, Hercules, CA, USA).⁴⁸ Plasma creatinine and urea were measured using a point-of-care device (iSTAT, Chem8+ Cartridge; Abbot Laboratories, Abbott Park, IL, USA).

4.3.2 | Histology and immunohistochemistry

Two sections from each kidney were stained with haematoxylin and eosin,⁷ Masson's trichrome,⁴³ or picosirius red,² or processed for pimonidazole adduct immunohistochemistry⁷ as previously described. Masson's trichrome stains type I collagen as well as variety of matrix elements,²⁷ whereas picosirius red is highly specific for type I and type III collagen.²⁸

Additionally, two sets of serial sections from each kidney were processed so that adjacent sections could be stained with Masson's trichrome⁴³ and for pimonidazole adducts.⁷ All sections were scanned using Scan Scope (Aperio, Vista, CA, USA). Quantification of fibrosis in sections processed for Masson's trichrome staining was performed using the Image Scope Positive Pixel Count Algorithm (Version 9; Aperio). An additional analysis was performed to determine whether hypoxia was associated with the state of patency of individual tubules. For this analysis, 20 open (patent) tubules and 20 closed (occluded) tubules were identified in the cortex of each kidney section stained with Masson's trichrome from six adenine-treated rats. These tubules were then identified in the adjacent sections stained for pimonidazole adducts and scored for either the presence or absence of pimonidazole staining.

4.4 | Statistical analysis

All data are expressed as mean \pm standard error of the mean (SEM). Hypothesis testing was performed using the software package SYSTAT (Version 13; Systat Software, Chicago, IL, USA). Measurements obtained before and 7 and 14 days after commencing treatment with adenine or its vehicle were subjected to repeated measures analysis of variance. *P* values derived from the within-subjects factor 'time' were conservatively adjusted using the Greenhouse-Geisser correction.⁴⁹ Measurements obtained on day 15 of treatment with adenine or its vehicle were subjected to Student's unpaired *t*-test. Two sided $P \leq .05$ was considered statistically significant.

ACKNOWLEDGEMENTS

This work was supported by grants from the National Health and Medical Research Council of Australia (606601 & 1024575).

DISCLOSURE

None.

REFERENCES

- Bernhardt WM, Wiesener MS, Weidemann A, et al. Involvement of hypoxia-inducible transcription factors in polycystic kidney disease. *Am J Pathol.* 2007;170:830–842.
- Ding A, Kalaiganasundaram P, Ricardo SD, et al. Chronic treatment with tempol does not significantly ameliorate renal tissue hypoxia or disease progression in a rodent model of polycystic kidney disease. *Clin Exp Pharmacol Physiol.* 2012;39:917–929.
- Ow CP, Abdelkader A, Hilliard LM, Phillips JK, Evans RG. Determinants of renal tissue hypoxia in a rat model of polycystic kidney disease. *Am J Physiol Regul Integr Comp Physiol.* 2014;307:R1207–R1215.
- Palm F, Cederberg J, Hansell P, Liss P, Carlsson PO. Reactive oxygen species cause diabetes-induced decrease in renal oxygen tension. *Diabetologia.* 2003;46:1153–1160.
- Manotham K, Tanaka T, Matsumoto M, et al. Evidence of tubular hypoxia in the early phase in the remnant kidney model. *J Am Soc Nephrol.* 2004;15:1277–1288.
- Basile DP, Donohoe DL, Roethe K, Mattson DL. Chronic renal hypoxia after acute ischemic injury: effects of L-arginine on hypoxia and secondary damage. *Am J Physiol Renal Physiol.* 2003;284:F338–F348.
- Abdelkader A, Ho J, Ow CP, et al. Renal oxygenation in acute renal ischemia-reperfusion injury. *Am J Physiol Renal Physiol.* 2014;306:F1026–F1038.
- Mimura I, Nangaku M. The suffocating kidney: tubulointerstitial hypoxia in end-stage renal disease. *Nat Rev Nephrol.* 2010;6:667–678.
- Fine LG, Norman JT. Chronic hypoxia as a mechanism of progression of chronic kidney diseases: from hypothesis to novel therapeutics. *Kidney Int.* 2008;74:867–872.
- Friederich-Persson M, Thorn E, Hansell P, Nangaku M, Levin M, Palm F. Kidney hypoxia, attributable to increased oxygen consumption, induces nephropathy independently of hyperglycemia and oxidative stress. *Hypertension.* 2013;62:914–919.
- Basile DP, Donohoe D, Roethe K, Osborn JL. Renal ischemic injury results in permanent damage to peritubular capillaries and influences long-term function. *Am J Physiol Renal Physiol.* 2001;281:F887–F899.
- Guay-Woodford LM. Murine models of polycystic kidney disease: molecular and therapeutic insights. *Am J Physiol Renal Physiol.* 2003;285:F1034–F1049.
- Phillips JK, Hopwood D, Loxley RA, et al. Temporal relationship between renal cyst development, hypertension and cardiac hypertrophy in a new rat model of autosomal recessive polycystic kidney disease. *Kidney Blood Press Res.* 2007;30:129–144.
- Kiran G, Nandini CD, Ramesh HP, Salimath PV. Progression of early phase diabetic nephropathy in streptozotocin-induced diabetic rats: evaluation of various kidney-related parameters. *Indian J Exp Biol.* 2012;50:133–140.
- Evans RG, O'Connor PM. Initiation and progression of chronic kidney disease: can we definitively test the chronic hypoxia hypothesis? *Hypertension.* 2013;62:827–828.
- Katsumata K, Kusano K, Hirata M, et al. Sevelamer hydrochloride prevents ectopic calcification and renal osteodystrophy in chronic renal failure rats. *Kidney Int.* 2003;64:441–450.
- Nagano N, Miyata S, Abe M, et al. Effect of manipulating serum phosphorus with phosphate binder on circulating PTH and FGF23 in renal failure rats. *Kidney Int.* 2006;69:531–537.
- Neven E, Dauwe S, De Broe ME, D'Haese PC, Persy V. Endochondral bone formation is involved in media calcification in rats and in men. *Kidney Int.* 2007;72:574–581.
- Terai K, Mizukami K, Okada M. Comparison of chronic renal failure rats and modification of the preparation protocol as a hyperphosphataemia model. *Nephrology.* 2008;13:139–146.
- Matsui I, Hamano T, Mikami S, et al. Fully phosphorylated fetuin-A forms a mineral complex in the serum of rats with adenine-induced renal failure. *Kidney Int.* 2009;75:915–928.
- Ikeda R, Imai Y, Maruyama W, Mizoguchi K. Systemic disorders of calcium dynamics in rats with adenine-induced renal failure: implication for chronic kidney disease-related complications. *Nephrology.* 2010;15:54–62.
- Nguy L, Nilsson H, Lundgren J, et al. Vascular function in rats with adenine-induced chronic renal failure. *Am J Physiol Regul Integr Comp Physiol.* 2012;302:R1426–R1435.
- Wu M, Tang RN, Liu H, Xu M, Pan MM, Liu BC. Cinacalcet attenuates the renal endothelial-to-mesenchymal transition in rats with adenine-induced renal failure. *Am J Physiol Renal Physiol.* 2014;306:F138–F146.
- Milman Z, Axelrod JH, Heyman SN, Nachmansson N, Abramovitch R. Assessment with unenhanced MRI techniques of renal morphology and hemodynamic changes during acute kidney injury and chronic kidney disease in mice. *Am J Nephrol.* 2014;39:268–278.
- Diwan V, Small D, Kauter K, Gobe GC, Brown L. Gender differences in adenine-induced chronic kidney disease and cardiovascular complications in rats. *Am J Physiol Renal Physiol.* 2014;307:F1169–F1178.
- Wang B, Koh P, Winbanks C, et al. miR-200a Prevents renal fibrogenesis through repression of TGF-beta2 expression. *Diabetes.* 2011;60:280–287.
- Lillie RD. Further experiments with the Masson trichrome modification of Mallory's connective tissue stain. *Stain Technol.* 1940;15:17–22.
- Junqueira LC, Cossermelli W, Brentani R. Differential staining of collagens type I, II and III by Sirius Red and polarization microscopy. *Archivum histologicum Japonicum = Nihon soshikigaku kiroku* 1978;41:267–274.
- Darling IM, Morris ME. Evaluation of "true" creatinine clearance in rats reveals extensive renal secretion. *Pharm Res.* 1991;8:1318–1322.
- Perucca J, Bouby N, Valeix P, Bankir L. Sex difference in urine concentration across differing ages, sodium intake, and level of kidney disease. *Am J Physiol Regul Integr Comp Physiol.* 2007;292:R700–R705.
- Nangaku M. Chronic hypoxia and tubulointerstitial injury: a final common pathway to end-stage renal failure. *J Am Soc Nephrol.* 2006;17:17–25.
- Chade AR. Renal vascular structure and rarefaction. *Compr Physiol.* 2013;3:817–831.
- Saeed A, Dibona GF, Grimberg E, et al. High-NaCl diet impairs dynamic renal blood flow autoregulation in rats with adenine-induced chronic renal failure. *Am J Physiol Regul Integr Comp Physiol.* 2014;306:R411–R419.
- Johns EJ, Rutkowski B. The action of atriopeptin III on renal function in two models of chronic renal failure in the rat. *Br J Pharmacol.* 1990;99:317–322.
- Ienaga K, Yokozawa T. Treatment with NZ-419 (5-Hydroxy-1-methyl imidazole-2,4-dione), a novel intrinsic antioxidant, against the progression of chronic kidney disease at stages 3 and 4 in rats. *Biol Pharm Bull.* 2010;33:809–815.
- Fine LG, Bandyopadhyay D, Norman JT. Is there a common mechanism for the progression of different types of renal diseases other than proteinuria? Towards the unifying theme of chronic hypoxia. *Kidney Int Suppl.* 2000;75:S22–S26.
- Evans RG, Harrop GK, Ngo JP, Ow CP, O'Connor PM. Basal renal oxygen consumption and the efficiency of oxygen utilization for sodium reabsorption. *Am J Physiol Renal Physiol.* 2014;306:F551–F560.
- van der Loos CM. Multiple immunoenzyme staining: methods and visualizations for the observation with spectral imaging. *J Histochem Cytochem.* 2008;56:313–328.
- Grabias BM, Konstantopoulos K. The physical basis of renal fibrosis: effects of altered hydrodynamic forces on kidney homeostasis. *Am J Physiol Renal Physiol.* 2014;306:F473–F485.

40. Higgins DF, Kimura K, Bernhardt WM, et al. Hypoxia promotes fibrogenesis in vivo via HIF-1 stimulation of epithelial-to-mesenchymal transition. *J Clin Invest*. 2007;117:3810–3820.
41. Wang Z, Zhu Q, Li PL, et al. Silencing of hypoxia-inducible factor-1alpha gene attenuates chronic ischemic renal injury in two-kidney, one-clip rats. *Am J Physiol Renal Physiol*. 2014;306:F1236–F1242.
42. Hanna C, Hubchak SC, Liang X, et al. Hypoxia-inducible factor-2alpha and TGF-beta signaling interact to promote normoxic glomerular fibrogenesis. *Am J Physiol Renal Physiol*. 2013;305:F1323–F1331.
43. Koeners MP, Ow CP, Russell DM, et al. Telemetry-based oxygen sensor for continuous monitoring of kidney oxygenation in conscious rats. *Am J Physiol Renal Physiol*. 2013;304:F1471–F1480.
44. Freeman BA, Crapo JD. Hyperoxia increases oxygen radical production in rat lungs and lung mitochondria. *J Biol Chem*. 1981;256:10986–10992.
45. Schurek HJ, Jost U, Baumgartl H, Bertram H, Heckmann U. Evidence for a preglomerular oxygen diffusion shunt in rat renal cortex. *Am J Physiol*. 1990;259:F910–F915.
46. Evans RG, Gardiner BS, Smith DW, O'Connor PM. Intrarenal oxygenation: unique challenges and the biophysical basis of homeostasis. *Am J Physiol Renal Physiol*. 2008;295:F1259–F1270.
47. Kelly DJ, Zhang Y, Gow R, Gilbert RE. Tranilast attenuates structural and functional aspects of renal injury in the remnant kidney model. *J Am Soc Nephrol*. 2004;15:2619–2629.
48. Bradford MM. A rapid and sensitive method for the quantitation of microgram quantities of protein utilizing the principle of protein-dye binding. *Anal Biochem*. 1976;72:248–254.
49. Ludbrook J. Repeated measurements and multiple comparisons in cardiovascular research. *Cardiovasc Res*. 1994;28:303–311.

CHAPTER 3

**AN IMPROVED METHOD FOR PIMONIDAZOLE-ADDUCT
IMMUNOHISTOCHEMISTRY USING A PRIMARY ANTIBODY RAISED
IN THE RABBIT: APPLICATION TO ADENINE-INDUCED CKD**

3.1 ABSTRACT

Pimonidazole adduct immunohistochemistry, using a mouse monoclonal anti-pimonidazole primary antibody and an anti-mouse secondary antibody, can result in artefactual false-positive staining, particularly in damaged renal tissue. I hypothesized that this false-positive staining could be avoided by use of a primary antibody raised in a non-rodent species. Therefore, I used kidney tissues, collected in the experiments described in Chapter 2 and from additional animals not exposed to pimonidazole, to define the extent of false positive staining generated using a mouse primary antibody and to determine whether superior results can be achieved using a polyclonal primary antibody raised in the rabbit. When the combination of a mouse primary antibody and anti-mouse secondary antibody was used, staining was observed in renal tissues of rats with adenine-induced chronic kidney disease (Ad-CKD) even if the primary antibody was excluded from the incubation or if the rat had not been treated with pimonidazole. Non-specific staining was also observed in vehicle-treated rats, but was confined to the occasional tubular cast in the renal medulla. In contrast, when the combination of a rabbit primary antibody and anti-rabbit secondary antibody was used, positive staining was seen in the cortex, outer medulla and inner medulla of adenine-treated rats, but only if they had received an injection of pimonidazole and the primary antibody was included in the incubation. This staining for pimonidazole-adducts was mostly confined to the tubular epithelium, so was in a close spatial relationship with the interstitial fibrosis characteristic of Ad-CKD. In contrast, staining was considerably less in the kidneys of vehicle-treated rats and was confined to the tubular epithelium of the renal medulla. I conclude that immunohistochemical visualization of pimonidazole adducts using the available mouse monoclonal primary antibody and an anti-mouse secondary antibody is flawed, particularly when applied to damaged renal tissue, because of binding of the secondary antibody to antigens other than those on the primary antibody. However, superior results can be obtained by use of a polyclonal primary antibody raised in rabbits in combination with an anti-rabbit secondary antibody. Nevertheless, our findings using this improved method confirm our previous conclusion that Ad-CKD is associated with renal cellular hypoxia. Moreover, I conclude that the cellular hypoxia is mostly confined to the tubular epithelium and is closely associated with interstitial fibrosis.

3.2 INTRODUCTION

Pimonidazole adduct immunohistochemistry has been used extensively to assess renal hypoxia at the cellular level (14, 24-26, 28). Recently, we used this method to assess renal hypoxia in acute ischemia reperfusion injury (1) and adenine-induced CKD (Ad-CKD) (12). In both cases, there was evidence of artefactual staining of non-cellular components of the tissue, particularly of tubular casts and cellular debris within the tubular lumen. Thus, some caution should be applied to the interpretation of these observations.

In multiple experimental studies (2, 3) including our recent published works (1, 12), pimonidazole-adduct immunohistochemistry has been performed according to two step indirect-immunohistochemical method. Briefly, in these studies tissue sections were incubated with a mouse monoclonal anti-pimonidazole antibody (primary antibody) (step 1). This primary antibody recognizes pimonidazole–protein adducts. These target antigens are formed in tissues, of animals to which pimonidazole has been administered, at an oxygen tension below 10 mmHg (26). The next step in the process is incubation of tissue sections with an anti-mouse secondary antibody conjugated with horseradish peroxidase (HRP) (step 2). This secondary antibody binds to the primary antibody bound to pimonidazole-protein adducts. Addition of the substrate 3,3'-diaminobenzidine then results in the formation of a dark brown reaction product at sites where the secondary antibody has bound. Thus, the HRP conjugated anti-mouse secondary antibody is critical in this indirect-immunodetection method because it generates the signal that facilitates detection of target molecules. However, this anti-mouse secondary antibody may cross-react with rodent tissues, potentially leading to false-positive staining in tissues from mice and rats (9, 27). For example, negative control experiments have been carried out, in the absence of primary antibodies, to study the cross-reaction between HRP-conjugated mouse secondary antibody and endogenous immunoglobulin (Ig) in mouse and rat tissues (9, 27). Positive background staining was observed in paraffin embedded mouse intestinal tissue sections using anti-mouse secondary antibody (9). Similarly, false positive labelling was detected in rat brain tissues with lactate-induced lesions after incubation with rabbit anti-mouse secondary antibody (27). Thus, in the studies described in Chapter 2 (12), it remains possible that the positive staining for pimonidazole adducts in kidney tissues from adenine-treated rats might be confounded by the binding of the anti-mouse secondary antibody to antigens other than pimonidazole adducts.

In multiple experimental studies, an anti-pimonidazole antibody, raised in rabbits, has been used to detect tissue hypoxia (23, 29, 31). Its availability provided an opportunity for us to re-assess

cellular hypoxia in Ad-CKD. Therefore, in the current study I used the experimental material generated in the experiments described in Chapter 2 (12), as well as tissues from additional animals not exposed to pimonidazole, to more precisely define the extent of false-positive staining generated using a mouse primary antibody in conjunction with an anti-mouse secondary antibody. I also determined whether superior results can be achieved using a primary antibody raised in the rabbit in combination with an anti-rabbit secondary antibody. These studies also allowed us to more precisely define the nature of cellular hypoxia in Ad-CKD

3.3 METHODS

3.3.1 Tissue preparation

The perfusion-fixed kidneys of 14 rats (252 ± 10 g) were used in the current studies. All rats received either adenine (100 mg; Sigma-Aldrich, Castle Hill, NSW, Australia) or its vehicle (1 mL of 0.5% w/v methylcellulose; Sigma-Aldrich) for 14 days. On day 15, left kidneys were perfusion fixed as described in Chapter 2 of this thesis. Ten of these kidneys (adenine-treated n=6; vehicle-treated n=4) were generated as part of the experimental studies described in Chapter 2. Thus, all 10 rats received an intraperitoneal injection of pimonidazole hydrochloride (60 mg/kg) 60 min before perfusion fixation. An additional cohort of rats (adenine-treated n=2; vehicle-treated n=2), that did not receive pimonidazole hydrochloride but were otherwise treated identically to those in the studies described in Chapter 2, were included in the current study as negative controls. The kidneys were processed and embedded in paraffin.

3.3.2 Pimonidazole adduct immunohistochemistry

Pimonidazole adduct immunohistochemistry was performed to detect pimonidazole adducts, cellular markers of tissue hypoxia formed in pimonidazole-treated animals at an oxygen tension below 10 mmHg (26). The basic protocol is described in Figure 3.1.

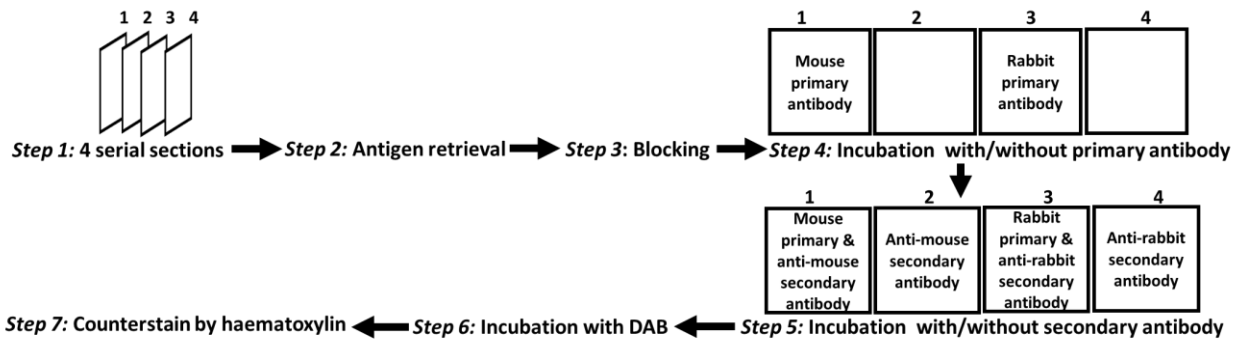


Figure 3.1. Schematic representation of the protocol for pimonidazole adduct immunohistochemistry. *Step 1:* Paraffin embedded kidney samples (n=14) were sectioned at a thickness of 5 μm by a microtome (MicroTec®, CUT4060, micro Tec Laborgeräte GmbH, Germany). Two sets of 4 serial sections from each kidney were collected separately on slides (Superfrost® Plus, Lomb Scientific Pty Ltd, Australia). *Step 2:* Paraffin embedded kidney sections were dewaxed and incubated in citrate buffer (Target Retrieval Solution, DAKO, Denmark), at 90 °C for 30 minutes, for antigen retrieval. After that, sections were cooled to 80 °C before they were washed in Tris-buffered saline with Tween 20 (TBST, DAKO, Denmark). *Step 3:* Tissue peroxidase activity was quenched by incubation with hydrogen peroxide solution (Dako REAL™ Peroxidase-Blocking Solution, DAKO, Denmark) for 10 minutes at room temperature. Subsequently, kidney sections were incubated in a protein block solution (Protein Block Serum-Free, DAKO, Denmark) for 10 minutes, in order to remove non-specific binding, and washed twice in TBST. *Step 4:* The first of four serial sections were incubated with mouse anti-pimonidazole antibody at 1:1000 dilution (Hypoxyprobe™-1 Kit, Lot 1.23.14, Hydroxyprobe Inc, Burlington, MA) while the third sections was incubated with affinity purified rabbit anti-pimonidazole antibody (PAb2627AP) at 1:200 dilution (Hypoxyprobe™-1 Omni Kit, Lot 04.21.16, Hydroxyprobe Inc, Burlington, MA) for 1 hour at room temperature. However, no primary antibody was added to the second and fourth of the serial sections. *Step 5:* Sections with and without primary antibody were washed twice in TBST. Next, the first and second sections were incubated with goat anti-mouse secondary antibody conjugated with horseradish peroxidase (Dako EnVision+System-HRP labelled Polymer anti-mouse, Catalogue K4001, Lot 10127007, DAKO, Denmark) while the third and fourth sections were incubated with goat anti-rabbit secondary antibody conjugated with horseradish peroxidase (Dako EnVision+System-HRP labelled Polymer anti-Rabbit, Catalogue K4003, Lot 10127439, DAKO, Denmark) for 30 minutes. *Step 6:* Slides were then washed twice in TBST and incubated with 3,3'-diaminobenzidine (DAB) (DAKO, Denmark) for 10 minutes. *Step 7:* Sections were counterstained with hematoxylin (Dako

Automations Hematoxyline, DAKO, Denmark) and slides were cover slipped. All kidney sections were scanned using Aperio Scan Scope (Aperio, Vista, CA, USA).

3.3.3 Co-localization of fibrosis and hypoxia in the kidneys of adenine-treated rats

The spatial relationships between renal fibrosis and hypoxia were assessed as described previously in Chapter 2. Briefly, two sets of two serial sections from each kidney were processed so that adjacent section could be stained with Masson's trichrome to detect fibrotic tissue and for pimonidazole adducts for the assessment of cellular hypoxia. For pimonidazole adducts staining rabbit anti-pimonidazole antibody in conjunction with goat anti-rabbit secondary antibody was used.

3.3.4 Hypoxia and patency of renal tubules in the kidneys of adenine-treated rats

The relationship between hypoxia and the state of patency of tubules was examined using the procedure described in detail in Chapter 2 of this thesis. For this study, twenty non-dilated tubules with a visible lumen (open tubules) and twenty tubules with no visible lumen (closed tubules) were randomly selected from each of the kidney sections stained with Masson's trichrome. Then, these tubules were identified in adjacent serial sections processed for pimonidazole adduct immunohistochemistry using the rabbit anti-pimonidazole primary antibody and anti-rabbit secondary antibody. Each tubule was then classified as hypoxic (by the presence of pimonidazole stain) or not hypoxic (by the absence of pimonidazole stain).

3.3.5 Statistical analyses

Data are presented as the mean \pm standard error of the mean (SEM). Dichotomous comparisons were made using Student's paired t-test. Two sided $P \leq 0.05$ was considered statistically significant.

3.4 RESULTS

3.4.1 Cellular staining for pimonidazole adducts

Very little positive staining was observed in the renal cortex of vehicle-treated rats, regardless of the primary antibody used (mouse or rabbit) or whether or not the primary antibody was included in the incubation (Figure 3.2 a & b, e & f, i & j, and m & n). Similarly, very little positive staining was seen in the outer medulla when the mouse antibody was used. In contrast, the rabbit antibody revealed diffuse positive staining in tubular elements in the outer medulla (Figure 3.2 k), which

was not present when only the anti-rabbit secondary antibody was used (Figure 3.2 o). In the inner medulla, positive staining with the mouse antibody was observed chiefly within the lumen of tubular elements (Figure 3.2 d & h). This staining was also observed when the primary mouse antibody was excluded from the incubation, so presumably mainly reflects non-specific staining of tubular casts. In contrast, while some tubular casts were positively stained, by rabbit antibody mainly, most staining was observed within the cytoplasm of the tubular epithelium. None of this staining was present when the primary antibody was excluded from the incubation (Figure 3.2 l & p).

Kidney sections from adenine-treated rats showed positive staining in the cortex, outer medulla and inner medulla after incubation with the mouse primary antibody and anti-mouse secondary antibody (Figure 3.3 a-d). Notably, some positive staining, particularly of glomeruli, apical membranes of the tubules in the cortex and outer medulla, and the interstitium of the inner medulla, was still observed when the primary antibody was excluded from the incubation (Figure 3.3 e-h). There was also widespread positive staining in the kidneys of adenine-treated rats when the rabbit primary antibody and anti-rabbit secondary antibody was used (Figure 3.3 i-l). However, in contrast to the pattern seen with the mouse antibody, this staining was largely confined to the tubular epithelium and was abolished in sections not incubated with the rabbit primary antibody (Figure 3.3 m-p).

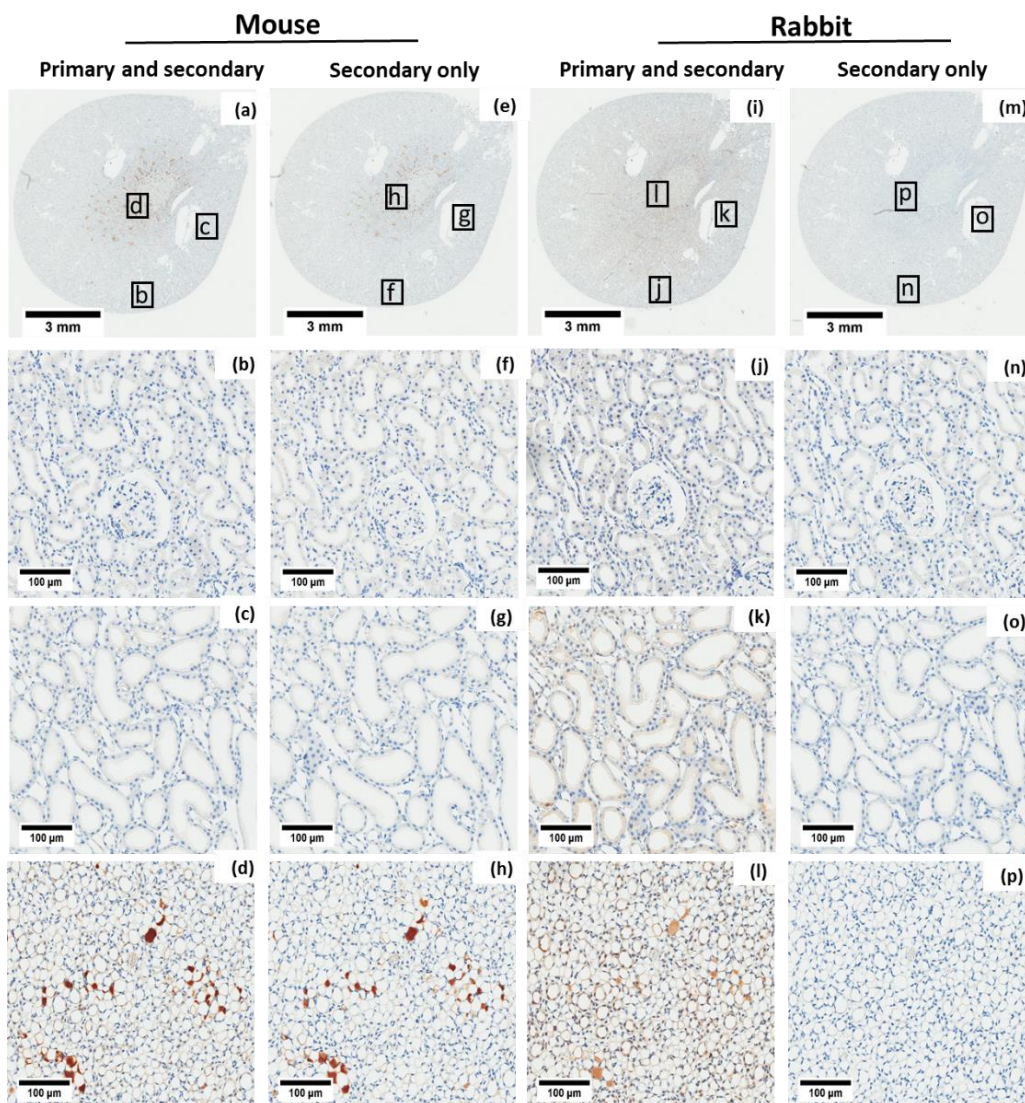


Figure 3.2 Pimonidazole adduct immunohistochemistry of kidney sections after 14 days of vehicle treatment. Micrographs show four serial sections, from the kidney of a vehicle-treated rat, stained with mouse primary antibody and an anti-mouse secondary antibody (a–d), anti-mouse secondary antibody only (e–h), rabbit primary antibody and an anti-rabbit secondary antibody (i–l), or anti-rabbit rabbit secondary only (m–p). Boxes in (a), (e), (i) and (m) show regions presented in (b–d), (f–h), (j–l) and (n–p) respectively. Cortical (b, f, j, n), outer medullary (c, g, k, o) and inner medullary (d, h, l, p) regions are shown. Images are typical of two sets of serial sections taken from each kidney (n=4).

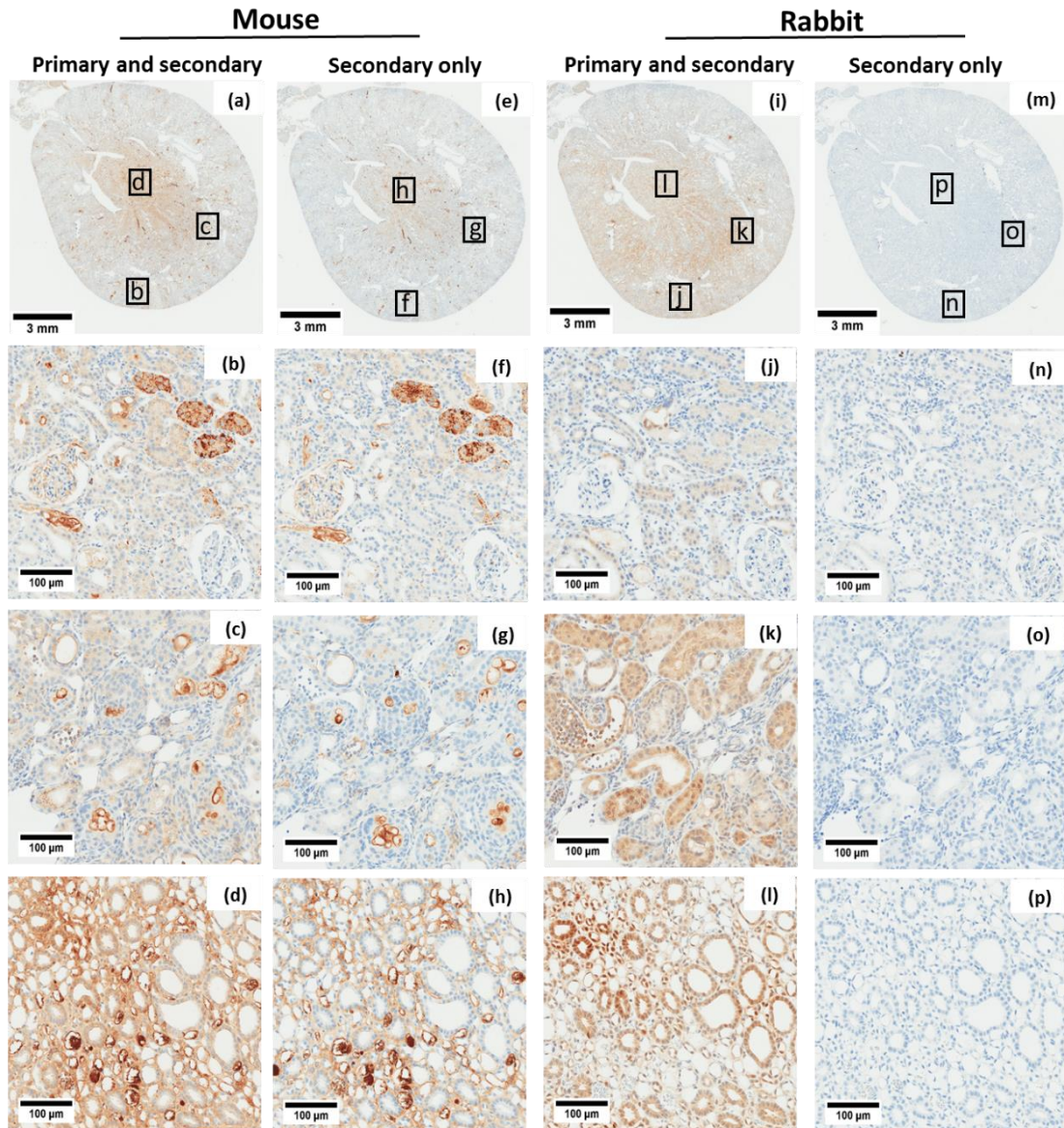


Figure 3.3 Pimonidazole adduct immunohistochemistry of kidney sections after 14 days of adenine treatment. Micrographs show four serial sections from the kidney of an adenine-treated rat, stained with mouse primary antibody and an anti-mouse secondary antibody (a–d), anti-mouse secondary antibody only (e–h), rabbit primary antibody and anti-rabbit secondary antibody (i–l), or anti-rabbit secondary antibody only (m–p). Boxes in (a), (e), (i) and (m) show regions presented in (b–d), (f–h), (j–l) and (n–p) respectively. Cortical (b, f, j, n), outer medullary (c, g, k, o) and inner medullary (d, h, l, p) regions are shown. Images are typical of two sets of serial sections taken from each kidney (n=6).

3.4.2 Staining in renal tissue not exposed to pimonidazole chloride

Pimonidazole adduct immunohistochemistry was performed in kidney sections, from rats not exposed to pimonidazole chloride, as an additional negative control. In sections of the kidneys of vehicle-treated rats that had not been exposed to pimonidazole, no staining was seen in the cortex or outer medulla, regardless of the primary antibody used (mouse or rabbit) or whether or not the primary antibody was included in the incubation (Figure 3.4 a-c, e-g, i-k and m-o). However, when the anti-mouse secondary antibody was used, staining was observed in the inner medulla, in the interstitium, and within the lumen of some tubules that presumably contained casts (Figure 3.4 d and h). This staining was observed regardless of whether the tissue was incubated with the mouse primary antibody. In contrast, no staining was observed in the inner medulla when the rabbit primary antibody and/or the secondary antibody was used (Figure 3.4 l & p).

In kidney sections from adenine-treated rats that were not exposed to pimonidazole chloride, use of the mouse primary antibody resulted in staining throughout the cortex, outer medulla and inner medulla (Figure 3.5 a-d and e-h). Staining was observed in glomeruli, the apical aspects of tubular epithelial cells, tubular casts, and the interstitium. The pattern of staining was similar when the mouse primary antibody was excluded from the incubate. In contrast, no staining was observed in sections of kidneys from adenine-treated rats not exposed to pimonidazole when the rabbit primary antibody was used, or when only the anti-rabbit secondary antibody was used (Figure 3.5 i-l & m-p).

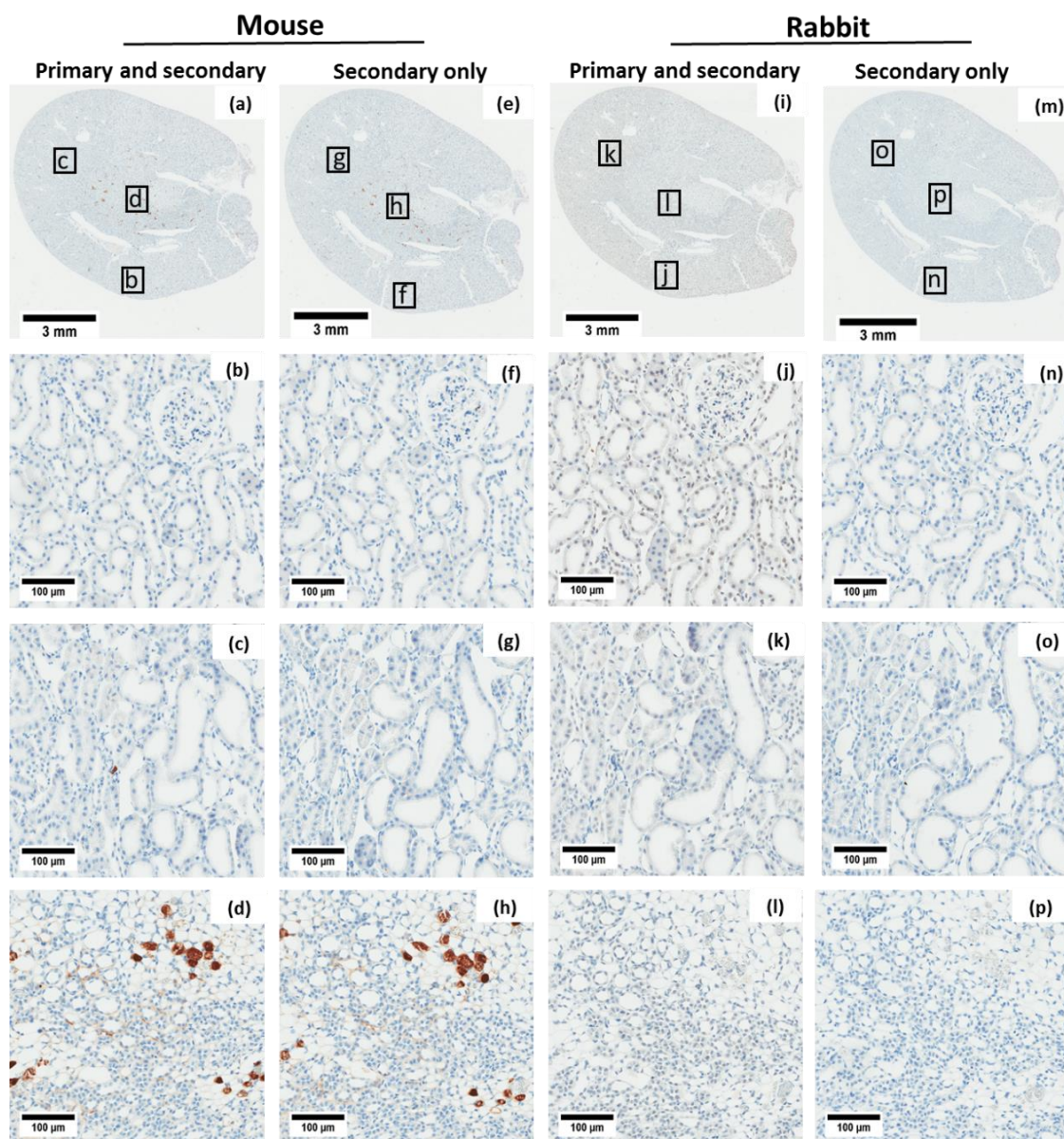


Figure 3.4 Pimonidazole adduct immunohistochemistry of kidney sections from rats, not exposed to pimonidazole chloride, after 14 days of vehicle treatment. Micrographs show four serial sections from the kidney of a vehicle-treated rat, stained with mouse primary antibody and an anti-mouse secondary antibody (a–d), anti-mouse secondary only (e–h), rabbit primary antibody and anti-rabbit secondary antibody (i–l), or anti-rabbit secondary antibody only (m–p). Boxes in (a), (e), (i) and (m) show regions presented in (b–d), (f–h), (j–l) and (n–p) respectively. Cortical (b, f, j, n), outer medullary (c, g, k, o) and inner medullary (d, h, l, p) regions are shown. Images are typical of two sets of serial sections taken from each kidney (n=2).

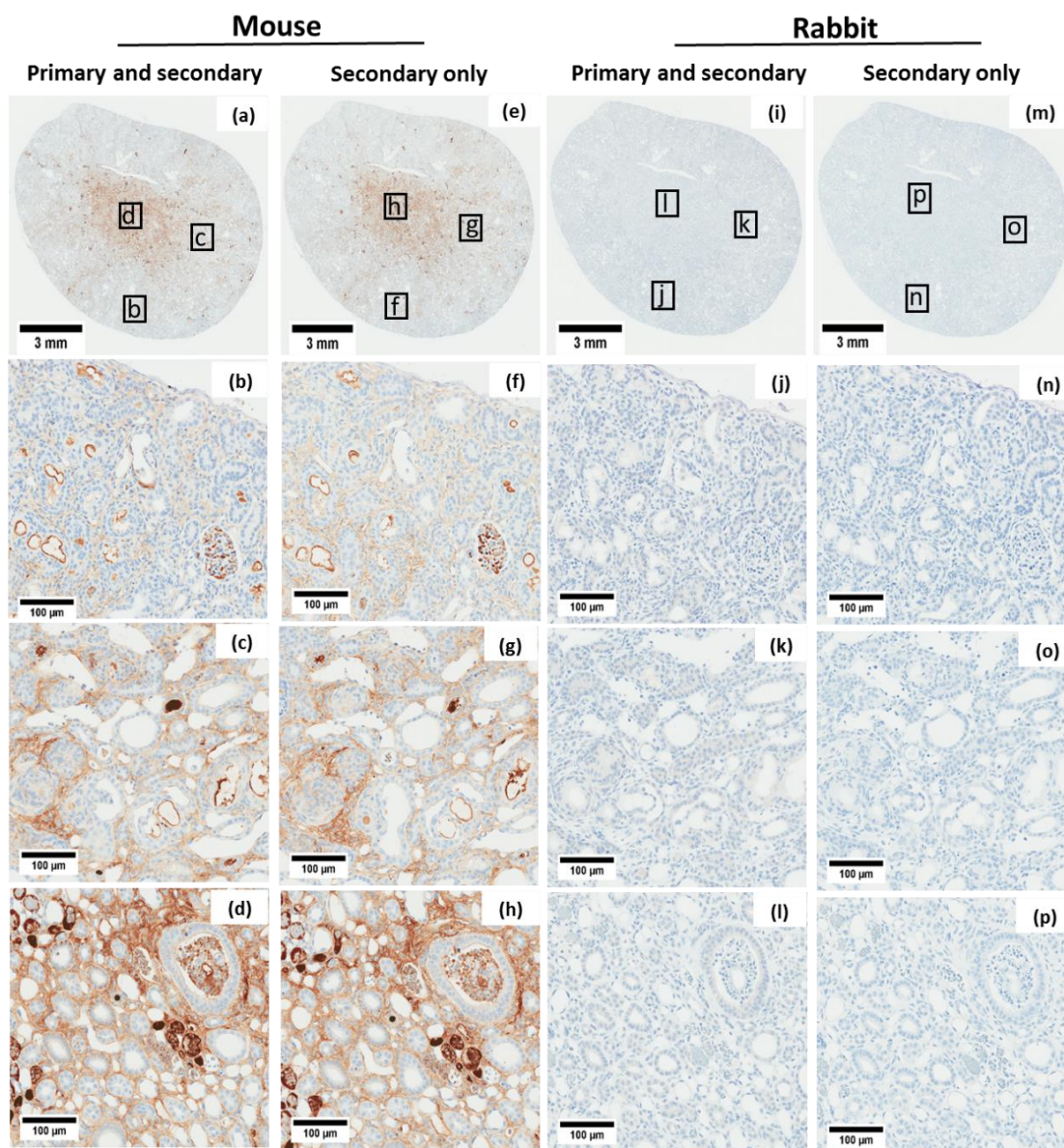


Figure 3.5 Pimonidazole adduct immunohistochemistry of kidney sections of rats, not exposed to pimonidazole chloride, after 14 days of adenine treatment. Micrographs show four serial sections, from the kidney of an adenine-treated rat, stained with mouse primary antibody and an anti-mouse secondary antibody (a–d), anti-mouse secondary antibody only (e–h), rabbit primary antibody and an anti-mouse secondary antibody (i–l), or anti-rabbit secondary antibody only (m–p). Boxes in (a), (e), (i) and (m) show regions presented in (b–d), (f–h), (j–l) and (n–p) respectively. Cortical (b, f, j, n), outer medullary (c, g, k, o) and inner medullary (d, h, l, p) regions are shown. Images are typical of two sets of serial sections taken from each kidney (n=2).

3.4.3 Co-localization of fibrosis and hypoxia

Adjacent serial sections of the kidneys of adenine-treated rats, exposed to pimonidazole chloride, were stained for pimonidazole adducts, using the rabbit primary antibody in combination with an anti-rabbit secondary antibody, and with Masson's trichrome (Figure 3.6). Pimonidazole staining was predominantly seen in tubular epithelial cells. Renal fibrosis, as denoting by blue in Masson's trichrome staining, was observed in the interstitium around these tubules.

3.4.4 Hypoxia and the patency of renal tubules in adenine-induced CKD

Using the anti-pimonidazole antibody raised in rabbits, I re-tested the hypothesis that obstruction of renal tubules causes heterogeneity of tubular oxygen consumption and thus leads to heterogeneity in renal hypoxia in Ad-CKD. As we found using the antibody raised in mice (Chapter two), I could not detect differences between the proportions of open tubules, compared to closed tubules, that stained positive for pimonidazole adducts (Figure 3.7).

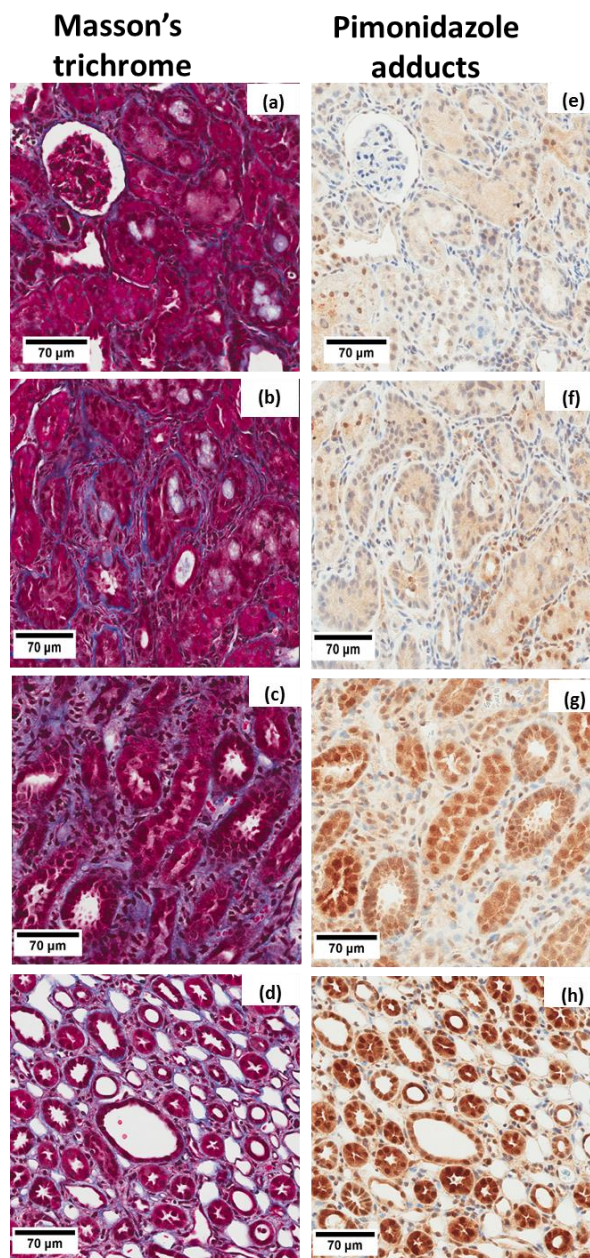


Figure 3.6 Co-localization of fibrosis and hypoxia in kidneys of adenine treated rats. Micrographs show serial sections from the kidney of an adenine-treated rat, stained with Masson's trichrome (a–d) to detect fibrotic tissue (purplish-blue) and for pimonidazole adducts (e–h) for the assessment of cellular hypoxia (brown). Cortical (a, b, e, f) and outer (c & g) and inner (d & h) medullary regions are shown. For pimonidazole adduct staining rabbit anti-pimonidazole antibody was used in conjunction with goat anti-rabbit secondary antibody.

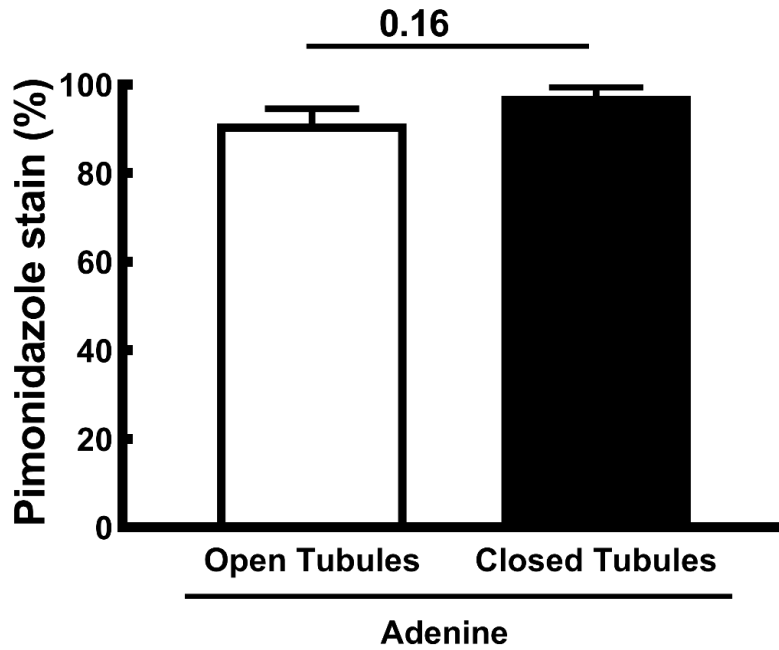


Figure 3.7 Relationship between pimonidazole staining and the patency of tubules in kidneys of adenine-treated rats. Twenty non-dilated tubules with a visible lumen (open tubules) and twenty tubules with no visible lumen (closed tubules) were selected from each of the kidney sections stained with Masson’s trichrome. These tubules were then identified in adjacent serial sections processed for pimonidazole adduct immunohistochemistry using the rabbit anti-pimonidazole primary antibody and anti-rabbit secondary antibody. Each tubule was then classified as hypoxic (by the presence of pimonidazole stain) or not hypoxic (by the absence of pimonidazole stain). Columns and error bars are between-rat mean \pm SEM of $n=4$. The P value is the outcome of a Student’s paired t test.

3.5 DISCUSSION

I compared two combinations of primary and secondary antibodies for immunohistochemical localization of pimonidazole adducts in the kidneys of rats with Ad-CKD, utilizing respectively a mouse primary antibody and a rabbit primary antibody. Our findings indicate that a significant proportion of the staining generated using the mouse primary antibody can be attributed to the binding of the anti-mouse secondary antibody to antigens other than the mouse primary antibody. These ‘off-target’ antigens appear to be particularly prevalent in injured kidney tissue. In contrast, staining generated using the newly available primary antibody raised in rabbits, in conjunction with an anti-rabbit secondary antibody, appears to provide superior specificity of staining for pimonidazole adducts. Using this combination of rabbit primary antibody and anti-rabbit

secondary antibody, I was able to confirm the presence of hypoxia in the kidneys of adenine-treated rats, which appears to be specifically localized to the tubular epithelium. I was also able to confirm the close spatial relationship between tubular hypoxia and interstitial fibrosis in Ad-CKD. Furthermore, as we concluded previously from studies using the mouse antibody, hypoxia in the tubular epithelium appears not to depend upon the patency of renal tubules.

The staining observed using the mouse primary antibody was mostly, but not exclusively, due to non-specific binding of the anti-mouse secondary antibody to damaged renal tissue and tubular casts. This conclusion is supported by our observation that kidney sections from adenine-treated rats were positively stained, regardless of whether the rats had been treated with pimonidazole chloride and regardless of whether the mouse primary antibody was included in the incubation. This false positive staining were observed particularly in glomeruli, apical aspects of the tubular epithelium, tubular casts, and in the interstitium. However, diffuse positive staining was observed in tubular epithelial cells of kidney sections after incubation with the mouse primary antibody and anti-mouse secondary antibody, only when adenine-treated rats were exposed to pimonidazole chloride. The absence of staining in healthy renal tissue (either exposed or not exposed to pimonidazole chloride) after incubation with anti-mouse secondary antibody indicates that tissue damage results in the formation of antigens that cross-react with the anti-mouse secondary antibody. Therefore, immunohistochemical methods for detection of pimonidazole adducts, that employ the combination of a mouse primary antibody and an anti-mouse secondary antibody, are unreliable when deployed in models of kidney damage such as Ad-CKD.

Multiple factors may contribute to development of false positive staining due to off-target binding of secondary antibodies in indirect immunohistochemistry (7). Non-specific epitopes, including those on endogenous immunoglobulins, can form in damaged tissue. It has been proposed that anti-mouse secondary antibodies might cross react with non-specific epitopes exposed by tissue damage (13) or that endogenous immunoglobulins accumulate at the site of tissue damage (7) and thereby form a source of antigens. HRP-conjugated rabbit anti-mouse secondary antibody can cross-react with endogenous immunoglobulins that form in lesions with the rat brain (27). DNA sequence analysis of immunoglobulins shows that there is considerable sequence homology between rat and mouse immunoglobulin G (IgG), in so-called ‘constant regions’. For example, the constant region of rat IgG2b and mouse IgG2a/b is homologous and rat gamma 2c resembles mouse gamma 3 (6). Such homology between rats and mice in terms of these constant regions could lead to false positive staining when anti-mouse secondary antibodies are used in rat tissues or vice versa. Fragment

crystallizable (Fc) receptors are expressed on the cell surface of immune cells (macrophages, neutrophils, mast cell, natural killer cells etc.). These cells can bind to the Fc region (constant region) of the antibody and thus induce an antibody-dependent immune response (22). It is therefore possible that the anti-mouse secondary antibody can bind to the Fc receptors of immune cells which accumulate at the site of the tissue injury, thus resulting in non-specific staining (7). Nevertheless, while our current findings indicate that anti-mouse secondary antibodies can bind to damaged renal tissue of rats, further studies are required to understand the specific cause of this off-target binding.

Our current findings, using an anti-pimonidazole antibody raised in the rabbit indicate that hypoxia in Ad-CKD is localized specifically to renal tubular epithelial cells. Kidney sections from adenine-treated rats, processed using the polyclonal primary antibody raised in rabbits, showed positive staining for pimonidazole-adducts in renal tubular epithelium. Consistent with this finding, diffuse positive staining in tubular elements was also seen with the mouse primary antibody. The presence of hypoxia in the tubular epithelium is consistent with the established high metabolic rate of these tissues (15). In the kidney, peritubular capillaries run alongside the renal tubules, providing oxygen and nutrients to nearby interstitial cells and tubules and thus maintenance of the functional activities of the nephron (18). Most of the supplied oxygen is utilized by $\text{Na}^+\text{-K}^+\text{-ATPase}$ pumps in the basolateral membrane of the renal tubules for reabsorption of filtered sodium (Na^+) (16). The high level of oxygen consumption by the renal tubule is one of the reasons the kidney is susceptible to development of tissue hypoxia if any reduction of oxygen supply occurs from nearby peritubular capillaries to renal tubules (10).

Under pathological conditions, progressive interstitial fibrosis may impair oxygen diffusion from the vasculature to the renal tubules (19). Our current findings indicate that, in Ad-CKD, fibrosis develops in the renal interstitium and is spatially associated with tubular hypoxia. Tubulointerstitial injury, characterized by tubular atrophy and interstitial fibrosis, associated with loss of renal peritubular capillaries, is a common finding in animal models of CKD and in biopsy specimens from human patients with CKD (4, 5, 8, 20). For example, Basile and colleagues demonstrated depletion of peritubular capillary density in the renal outer medulla, 4–8 weeks after reperfusion, in a model of ischemia/reperfusion injury that progresses to CKD. Their findings support the concept that tubulointerstitial fibrosis gradually exacerbates loss of peritubular capillaries and subsequently promotes renal dysfunction (4). Indeed, loss of peritubular capillaries would be expected to restrict blood flow downstream from the glomerular capillaries, restricting oxygen

supply to the renal tubules, thus initiating and/or exacerbating renal hypoxia (17). In addition, accumulation of fibrosis between peritubular capillaries and nearby renal tubules would be expected to decrease oxygen supply from capillaries to renal tubules by increasing the diffusion distance, even if the peritubular capillaries remain intact (11, 19). Thus, the close spatial relationship between interstitial fibrosis and renal tubules might contribute at least in part in development of renal tubular hypoxia in adenine-treated rats.

I found hypoxia in epithelial cells of both open (and thus presumably patent) and closed (and thus presumably obstructed) tubules. Indeed, using the anti-pimonidazole antibody raised in the rabbit, I could not detect differences between the proportions of open tubules, compared to closed tubules, that stained positive for pimonidazole adducts. I hypothesized that tubular obstruction causes decreased oxygen consumption due to decreased solute delivery in occluded tubules downstream from tubular casts. The corollary to this hypothesis is that more severe hypoxia might be expected in open tubules (i.e. those not occluded by tubular casts). As with our previous observations using the antibody raised in mice (Chapter 2), our current observations do not support this proposition.

The current study has both strengths and limitations. Using an anti-pimonidazole antibody raised in the rabbit I was able to confirm the presence of hypoxia in the kidneys of adenine-treated rats. I employed two negative controls; tissues that had not been exposed to pimonidazole and tissues that had been processed without the addition of the primary antibody raised in the rabbit. The complete absence of staining in both sets of negative control tissue provides confidence that the staining observed in the kidneys of rats with Ad-CKD truly reflects the presence of pimonidazole adducts, and thus cellular hypoxia. Furthermore, our use of serial sections provided insight into the nature of the non-specific staining generated using the monoclonal mouse primary antibody that has been deployed by ourselves (1, 12) and others (9, 27) previously. However, an important limitation of pimonidazole adduct immunohistochemistry is that it does not allow quantification of the severity of hypoxia. The dark brown pigment, produced by enzymatic oxidation of 3-diaminobenzidine (DAB), used to visualize pimonidazole adducts, does not follow the Beer-Lambert law (30). As a result, the intensity of staining is not directly proportional to the concentration of pimonidazole adducts in the tissue.

In conclusion, our current findings confirm that renal hypoxia is associated with Ad-CKD. It also confirms the spatial relationship between renal fibrosis and tubular hypoxia. Recently, Ow *et al* argued that, if renal tissue hypoxia is an early driver of pathophysiology of CKD, we should be able to detect renal tissue hypoxia before overt renal dysfunction (21). Ad-CKD may thus be a

useful model to examine the role of renal hypoxia in the initiation and progression of CKD. Therefore, in the studies described in Chapter 4 I deployed multiple methods to assess kidney oxygenation during the first week of adenine treatment.

3.6 REFERENCES

1. **Abdelkader A, Ho J, Ow CP, Eppel GA, Rajapakse NW, Schlaich MP, and Evans RG.** Renal oxygenation in acute renal ischemia-reperfusion injury. *Am J Physiol Renal Physiol* 306: F1026-1038, 2014.
2. **Airley RE, Loncaster J, Raleigh JA, Harris AL, Davidson SE, Hunter RD, West CM, and Stratford IJ.** GLUT-1 and CAIX as intrinsic markers of hypoxia in carcinoma of the cervix: relationship to pimonidazole binding. *Int J Cancer* 104: 85-91, 2003.
3. **Arteel GE, Thurman RG, Yates JM, and Raleigh JA.** Evidence that hypoxia markers detect oxygen gradients in liver: pimonidazole and retrograde perfusion of rat liver. *Br J Cancer* 72: 889-895, 1995.
4. **Basile DP, Donohoe D, Roethe K, and Osborn JL.** Renal ischemic injury results in permanent damage to peritubular capillaries and influences long-term function. *Am J Physiol Renal Physiol* 281: F887-899, 2001.
5. **Bohle A, von Gise H, Mackensen-Haen S, and Stark-Jakob B.** The obliteration of the postglomerular capillaries and its influence upon the function of both glomeruli and tubuli. Functional interpretation of morphologic findings. *Klin Wochenschr* 59: 1043-1051, 1981.
6. **Bruggemann M.** Evolution of the rat immunoglobulin gamma heavy-chain gene family. *Gene* 74: 473-482, 1988.
7. **Burry RW.** Controls for immunocytochemistry: an update. *J Histochem Cytochem* 59: 6-12, 2011.
8. **Choi YJ, Chakraborty S, Nguyen V, Nguyen C, Kim BK, Shim SI, Suki WN, and Truong LD.** Peritubular capillary loss is associated with chronic tubulointerstitial injury in human kidney: altered expression of vascular endothelial growth factor. *Hum Pathol* 31: 1491-1497, 2000.
9. **Eng HY, Wang CI, Xue Y, Lee CY, Zulkifli SB, Chiam PC, Ghadessy FJ, and Lane DP.** Enhanced antigen detection in immunohistochemical staining using a 'digitized' chimeric antibody. *Protein Eng Des Sel* 29: 11-21, 2016.
10. **Evans RG, Ince C, Joles JA, Smith DW, May CN, O'Connor PM, and Gardiner BS.** Haemodynamic influences on kidney oxygenation: clinical implications of integrative physiology. *Clin Exp Pharmacol Physiol* 40: 106-122, 2013.
11. **Fine LG, and Norman JT.** Chronic hypoxia as a mechanism of progression of chronic kidney diseases: from hypothesis to novel therapeutics. *Kidney Int* 74: 867-872, 2008.
12. **Fong D, Ullah MM, Lal JG, Abdelkader A, Ow CP, Hilliard LM, Ricardo SD, Kelly DJ, and Evans RG.** Renal cellular hypoxia in adenine-induced chronic kidney disease. *Clin Exp Pharmacol Physiol* 43: 896-905, 2016.
13. **Fritschy JM.** Is my antibody-staining specific? How to deal with pitfalls of immunohistochemistry. *Eur J Neurosci* 28: 2365-2370, 2008.
14. **Goldfarb M, Rosenberger C, Abassi Z, Shina A, Zilbersat F, Eckardt KU, Rosen S, and Heyman SN.** Acute-on-chronic renal failure in the rat: functional compensation and hypoxia tolerance. *Am J Nephrol* 26: 22-33, 2006.
15. **Gullans SR, and Hebert SC.** Metabolic basis of ion transport. In: *Brenner and Rector's The Kidney*, edited by BM B. Philadelphia, PA: WB Saunders, 1996, p. 211-246.
16. **Lassen NA, Munck O, and Thaysen JH.** Oxygen consumption and sodium reabsorption in the kidney. *Acta Physiol Scand* 51: 371-384, 1961.
17. **Matsumoto M, Tanaka T, Yamamoto T, Noiri E, Miyata T, Inagi R, Fujita T, and Nangaku M.** Hypoperfusion of peritubular capillaries induces chronic hypoxia before progression of tubulointerstitial injury in a progressive model of rat glomerulonephritis. *J Am Soc Nephrol* 15: 1574-1581, 2004.
18. **Molema G, and Aird WC.** Vascular heterogeneity in the kidney. *Semin Nephrol* 32: 145-155, 2012.

19. **Nangaku M.** Chronic hypoxia and tubulointerstitial injury: a final common pathway to end-stage renal failure. *J Am Soc Nephrol* 17: 17-25, 2006.
20. **Ohashi R, Kitamura H, and Yamanaka N.** Peritubular capillary injury during the progression of experimental glomerulonephritis in rats. *J Am Soc Nephrol* 11: 47-56, 2000.
21. **Ow CPC, Ngo JP, Ullah MM, Hilliard LM, and Evans RG.** Renal hypoxia in kidney disease: Cause or consequence? *Acta Physiol* 222: e12999, 2018.
22. **Ra C, Jouvin MH, Blank U, and Kinet JP.** A macrophage Fc gamma receptor and the mast cell receptor for IgE share an identical subunit. *Nature* 341: 752-754, 1989.
23. **Rademakers SE, Lok J, van der Kogel AJ, Bussink J, and Kaanders JHAM.** Metabolic markers in relation to hypoxia; staining patterns and colocalization of pimonidazole, HIF-1 α , CAIX, LDH-5, GLUT-1, MCT1 and MCT4. *BMC Cancer* 11: 167-167, 2011.
24. **Rosenberger C, Goldfarb M, Shina A, Bachmann S, Frei U, Eckardt KU, Schrader T, Rosen S, and Heyman SN.** Evidence for sustained renal hypoxia and transient hypoxia adaptation in experimental rhabdomyolysis-induced acute kidney injury. *Nephrol Dial Transplant* 23: 1135-1143, 2008.
25. **Rosenberger C, Heyman SN, Rosen S, Shina A, Goldfarb M, Griethe W, Frei U, Reinke P, Bachmann S, and Eckardt KU.** Up-regulation of HIF in experimental acute renal failure: evidence for a protective transcriptional response to hypoxia. *Kidney Int* 67: 531-542, 2005.
26. **Rosenberger C, Rosen S, Paliege A, and Heyman SN.** Pimonidazole adduct immunohistochemistry in the rat kidney: detection of tissue hypoxia. *Methods Mol Biol* 466: 161-174, 2009.
27. **Schmidt-Kastner R, Meller D, Bellander BM, Stromberg I, Olson L, and Ingvar M.** A one-step immunohistochemical method for detection of blood-brain barrier disturbances for immunoglobulins in lesioned rat brain with special reference to false-positive labelling in immunohistochemistry. *J Neurosci Methods* 46: 121-132, 1993.
28. **Tanaka T, Kato H, Kojima I, Ohse T, Son D, Tawakami T, Yatagawa T, Inagi R, Fujita T, and Nangaku M.** Hypoxia and expression of hypoxia-inducible factor in the aging kidney. *J Gerontol A Biol Sci Med Sci* 61: 795-805, 2006.
29. **Uddin MI, Evans SM, Craft JR, Capozzi ME, McCollum GW, Yang R, Marnett LJ, Uddin MJ, Jayagopal A, and Penn JS.** In vivo imaging of retinal hypoxia in a model of oxygen-induced retinopathy. *Sci Rep* 6: 31011, 2016.
30. **van der Loos CM.** Multiple immunoenzyme staining: methods and visualizations for the observation with spectral imaging. *J Histochem Cytochem* 56: 313-328, 2008.
31. **Wright WS, McElhatten RM, Messina JE, and Harris NR.** Hypoxia and the expression of HIF-1 α and HIF-2 α in the retina of streptozotocin-injected mice and rats. *Exp Eye Res* 90: 405-412, 2010.

CHAPTER 4

RENAL OXYGENATION DURING THE EARLY STAGES OF ADENINE-INDUCED CHRONIC KIDNEY DISEASE

4.1 ABSTRACT

Renal hypoxia is a characteristic of established adenine-induced chronic kidney disease (CKD). However, the role of hypoxia in the pathogenesis of adenine-induced CKD (Ad-CKD) remains to be determined. I hypothesized that hypoxia is an early event in Ad-CKD which precedes the development of overt renal dysfunction. I used three independent methods to assess kidney oxygenation during the first 7 days of adenine treatment. After a 7 day treatment period, renal oxygen delivery under anesthesia was 50.6% less in adenine-treated rats than in vehicle-treated rats, while renal oxygen consumption was 65.2% less. Cortical tissue PO₂ measured by Clark electrode in anesthetized rats was similar in both adenine-treated (44.5 ± 6.4 mmHg) and vehicle-treated rats (47.6 ± 7.7 mmHg). In contrast, medullary tissue PO₂ was 44% less in adenine-treated rats than in vehicle-treated rats. However, in unanesthetized rats, renal tissue PO₂ measured by radio-telemetry remained relatively stable in adenine-treated rats across a 7 day treatment period. Notably, anesthesia and laparotomy of rats equipped with a telemetry probe in the renal medulla led to greater reductions in medullary tissue PO₂ in rats treated with adenine (36.6%) than in vehicle-treated rats (16.4%). Thus, the apparent medullary hypoxia detected by Clark electrode could be dependent on the use of anesthesia. Consistent with this proposition, levels of hypoxia inducible factor-1 α (HIF-1 α) were less in adenine-treated rats than vehicle-treated rats in the renal cortex, outer medulla and inner medulla, while levels of HIF-2 α did not differ significantly between the two groups of animals. Renal dysfunction was evident by day 7, with glomerular filtration rate 65% less and serum creatinine 183% greater in adenine-treated rats than vehicle-treated rats. Thus, I conclude that renal tissue hypoxia does not precede renal dysfunction in Ad-CKD, so is unlikely to be a major early driver of renal dysfunction in this model.

4.2 INTRODUCTION

Tubulointerstitial hypoxia has been proposed as a ‘final common pathway’ in the development and progression of chronic kidney disease (CKD) (17, 18, 20, 40). According to the so-called ‘chronic hypoxia hypothesis’, during the initial stages of CKD, glomerular injury causes decreased renal blood flow and oxygen delivery via peritubular capillaries, thereby decreasing renal tissue PO₂ (37). Tissue hypoxia, in turn, is proposed to activate multiple signaling pathways that promote tubulointerstitial fibrosis. Simultaneously, the remaining glomerular and peritubular capillaries maintain normal whole kidney (GFR) by increasing single nephron GFR, in part by increased glomerular capillary pressure, which in turn increases damage to the glomerulus and capillary networks and promotes further development of fibrosis (19, 40, 41, 44). CKD is characterized by rarefaction of peritubular capillaries and tubulointerstitial fibrosis (37, 45), regardless of its etiology (2). These processes would be expected to lead to tubulointerstitial hypoxia, thus setting up a vicious cycle driving the progression of CKD (40, 41, 44). However, as we have argued recently, there are still important gaps in our knowledge of the role of hypoxia in the pathogenesis of CKD (49). Most critically, if tubulointerstitial hypoxia is a major driver of pathology in CKD, it should be detectable before overt renal dysfunction (49). This has been observed in some forms of CKD. For example, Franzen and colleagues demonstrated cortical tissue hypoxia, 3 days after induction of type-1 diabetes in mice, using electron paramagnetic resonance oximetry (23). This intrarenal tissue hypoxia was evident before the onset of albuminuria and was sustained until end of the study (23). Cortical tissue hypoxia was also evident as early as 15 h after activation of the renin-angiotensin system in a model of angiotensin II-dependent hypertensive CKD (8). This cortical tissue hypoxia was detected well before the development of renal injury (29).

We recently found evidence, using pimonidazole adduct immunohistochemistry, of tissue hypoxia in adenine-induced CKD (Ad-CKD) (22). Ad-CKD is categorized as a tubular crystal nephropathy (39). Deficiency of the enzyme adenine phosphoribosyl transferase, which leads to accumulation of adenine in the blood, results in an insoluble crystal (2, 8-dihydroxyadenine) precipitate in the renal tubules and obstruction of tubular flow, which initiates renal injury (28, 42, 63). A similar disease phenotype can be induced in rodents by adenine-feeding (22, 51, 64). As is the case in CKD in humans and clinically relevant animal models, Ad-CKD in rodents is characterized by elevated plasma concentrations of urea (38) and creatinine (55) as well as proteinuria (22, 55). Ad-CKD is also characterized by the presence of interstitial fibrosis (22, 28, 38, 42), extensive tubular

dilation (9), degeneration of the proximal tubular epithelium with loss of the brush border (28, 55) and inflammatory cell infiltration (55). One of the advantages of this model is that CKD develops rapidly, within 2 weeks (22), so its time-course can be precisely monitored. In our previous study, tissue hypoxia, evinced by positive staining for pimonidazole adducts, was observed after two weeks of adenine feeding, at a time when CKD was advanced (22). Thus, in that study it was not possible to determine whether tissue hypoxia is an early event in this model, perhaps preceding renal dysfunction.

The current study was designed to test the hypothesis that hypoxia is an early event in Ad-CKD which precedes the development of overt renal dysfunction. I used three independent methods to assess kidney oxygenation in the first 7 days of adenine feeding, each with strengths and limitations. Firstly, I measured renal tissue PO₂ by Clark electrode in anesthetized rats, after 7 days of adenine feeding. This technique allowed us to generate a ‘map’ of tissue PO₂ within the renal cortex and medulla. It also allowed us to determine the effects of adenine feeding on renal oxygen delivery (DO₂) and renal oxygen consumption (VO₂) (47). However, measurements can be made at only a single time-point and are potentially confounded by the effects of anesthesia. Secondly, I used radio-telemetry to assess renal oxygenation continuously, in conscious rats, during 7 days of adenine feeding. This method provides exquisite temporal resolution, but tissue PO₂ can only be measured in relative terms and only in a single point in the kidney in each rat (8, 30, 31). Thirdly, I quantified the effects of 7 days of adenine feeding on expression of the hypoxia inducible factor (HIF) proteins HIF-1 α and HIF-2 α in the cortex, inner medulla and outer medulla. This method provides information about the state of hypoxia signalling cascades (34), although of course these could potentially be modified by factors other than renal oxygenation (26).

4.3 METHODS

4.3.1 Animals

Male Sprague Dawley rats, aged 8-9 weeks (n = 43) were obtained from the Animal Resources Centre (Perth, WA, Australia). The rats were housed individually under standard laboratory conditions; 22 \pm 1°C, 40 \pm 1% humidity and with a 12-hour light/dark cycle (06.00–18.00 hours). Rats were allowed free access to water and were fed a standard laboratory rat chow diet *ad libitum*. Experiments were approved in advance by the Animal Ethics Committee of the Monash University Animal Resources Platform. The experiments were performed in accordance with the Australian Code of Practice for the Care and Use of Animals for Scientific Purposes. Rats were allowed one

week to acclimatize to their housing conditions prior to the commencement of experimental protocols.

4.3.2 Induction of Ad-CKD

Rats received either adenine (n = 23; 100 mg; Sigma Aldrich, Castle Hill, NSW, Australia) or its vehicle (n = 20; 1 ml of 0.5 % w/v methylcellulose (Methyl Cellulose 400 Solution, sterilized, Wako Pure Chemical Industries Ltd., Tokyo, Japan) by oral gavage. Adenine or its vehicle was administered daily, between 9 and 10 am, for a period of seven days.

4.3.3 Protocol 1: Renal tissue oxygenation and its determinants in anesthetized rats

Overview: Renal tissue PO₂ was assessed in anesthetized rats using a Clark electrode (50 µm tip, OX-50, Unisense, Denmark), the day after the final administration of adenine (n = 7) or its vehicle (n = 7). I measured i) cortical tissue PO₂ at six different sites on the dorsal surface of the kidney and ii) tissue PO₂ at 1 mm intervals up to a depth of 10 mm from the cortical surface. In addition, I also assessed renal excretory function and the major determinants of renal tissue PO₂, renal DO₂ and VO₂.

Surgical preparation: Rats were anesthetized with sodium thiobutobarbital (100 mg/kg i.p., Inactin; Sigma Aldrich, St Louis, MO, USA). Once the pedal reflex was abolished, indicating a surgical level of anesthesia, a tracheostomy was performed. Rats were then artificially ventilated with 40% inspired oxygen. A ventilation rate of 90-100 breaths/min and a tidal volume of 3.5 ml were used. A catheter in the left carotid artery was used for measurement of arterial blood pressure and collection of arterial blood. An infusion of 2% w/v bovine serum albumin (BSA, Sigma Aldrich, St Louis, MO, USA) in 154 mM NaCl was administered via a catheter in the jugular vein, during the period of surgical preparation, at a rate of 6 ml/h. Hemoglobin saturation was measured by pulse oximetry with a sensor placed on a hind foot (Mouse Ox, Starr Life Sciences Corporation, Oakmont, PA, USA). The left kidney was exposed via a midline incision. The left renal artery and kidney were isolated and the left kidney was placed in a Lucite cup. A transit-time ultrasound flow probe (Type 0.7 VB, Transonic Systems Inc, Ithaca, NY, USA) was placed around the left renal artery to allow measurement of total renal blood flow (RBF). Urine was collected from a bladder catheter.

Experimental protocol: Bolus doses of [³H]-inulin (10 µCi in 50 µL, Perkin Elmer Australia, Melbourne, Australia) and pancuronium bromide (2 mg/kg, Astra Zeneca Pty Ltd, NSW, Australia)

were administered through the jugular vein once the surgical preparations were complete. A maintenance infusion of 2% w/v bovine serum albumin in 154 mM NaCl was given throughout the experiment at a rate of 2 ml/h. This delivered 676 $\mu\text{Ci/h}$ [^3H]-inulin and 0.1 mg/kg/h pancuronium bromide. After a 1 h equilibration period, a 0.5 ml sample of arterial blood was taken for blood oximetry and chemistry. Renal tissue PO_2 was then measured using a Clark electrode attached to a micromanipulator. In a first series of measurements, cortical tissue PO_2 was determined, 2 mm from the renal surface, at 6 randomly chosen sites on the dorsal surface of the kidney (Figure 4.1A). For the second set of measurements, the electrode was positioned at the mid-point of the dorsal surface of the kidney and advanced in 1 mm steps up to 10 mm below the renal capsule (Figure 4.1B). Thus, a profile of tissue PO_2 at a range of depths below the cortical surface was generated. After these measurements of tissue PO_2 were complete, blood samples were collected from the carotid artery and the renal vein for blood oximetry, blood chemistry, and measurement of the plasma concentration of [^3H]-inulin. Urine produced over the period of measurement of renal tissue PO_2 was also collected to permit measurement of the urinary concentration of [^3H]-inulin, and thus GFR.

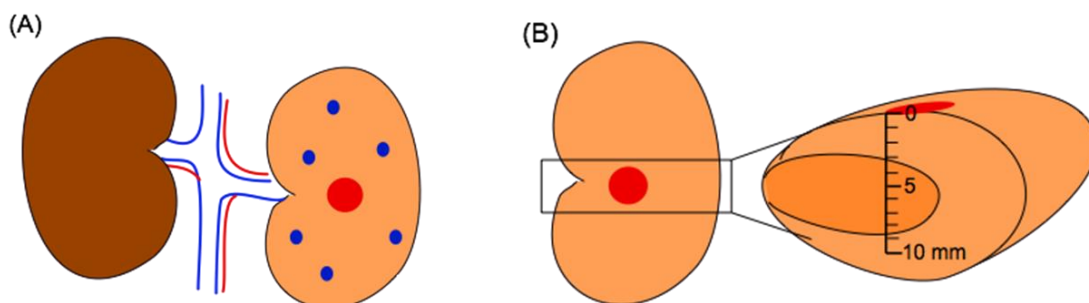


Figure 4.1 Schematic of the protocol for measurement of renal tissue PO_2 in anesthetized rats. Two series of measurements were performed to determine renal tissue PO_2 , in vehicle and adenine-treated rats, using a Clark electrode. Cortical tissue PO_2 was measured in six randomly chosen locations (blue circles) at a depth of 2 mm from the cortical surface (A). A profile of renal tissue PO_2 was then established by measuring tissue PO_2 at 1 mm intervals up to the depth of 10 mm from the cortical surface (B). The red circle represents the point of insertion of the electrode. Images were reproduced from Ow *et al* (47) with permission from the author.

Measurement of hemodynamic variables: The arterial catheter was connected to a pressure transducer (Cobe, Arvarda, CO), the transit-time ultrasound flow probe was connected to a

compatible flowmeter (T108, Transonic Systems), and the Clark electrode was connected to a picoammeter (PA-2000, Unisense). These analog signals were digitized at 500 Hz and continuously displayed by a data-acquisition program (Universal Acquisition, University of Auckland, Auckland, New Zealand), allowing continuous sampling of mean arterial pressure (MAP, mmHg), heart rate (HR, beats/min, derived from the MAP waveform), RBF (ml/min), and PO₂ (mmHg).

Analysis of blood and urine samples: A point-of-care device (iSTAT®, CG8+ Cartridges; Abbott Laboratories, Abbott Park, IL, USA) was used to assess blood oximetry. Arterial and venous blood oxygen content were calculated according to:

$$\begin{aligned} \text{Arterial oxygen content (ml O}_2\text{/dl)} \\ = [0.0139 \times \text{Hb (g/dl)} \times \text{S}_{\text{A}}\text{O}_2 \text{ (\%)}] + [0.003 \times \text{P}_{\text{A}}\text{O}_2 \text{ (mmHg)}] \end{aligned}$$

$$\begin{aligned} \text{Venous oxygen content (ml O}_2\text{/dl)} \\ = [0.0139 \times \text{Hb (g/dl)} \times \text{S}_{\text{V}}\text{O}_2 \text{ (\%)}] + [0.003 \times \text{P}_{\text{V}}\text{O}_2 \text{ (mmHg)}] \end{aligned}$$

Where, Hb is the blood hemoglobin content, S_AO₂ and S_VO₂ are hemoglobin saturation with oxygen in arterial and renal venous blood respectively, and P_AO₂ and P_VO₂ are, respectively, arterial and renal venous blood PO₂.

Renal DO₂ and VO₂ were calculated according to:

$$\text{DO}_2 \text{ (ml O}_2\text{/min)} = \frac{\text{Arterial Oxygen Content ((ml O}_2\text{/dl)} \times \text{RBF (ml/min)}}{100}$$

$$\text{VO}_2 \text{ (ml O}_2\text{/min)} = \frac{(\text{Arterial} - \text{Venous}) \text{ Oxygen Content (ml O}_2\text{/dl)} \times \text{RBF (ml/min)}}{100}$$

Fractional oxygen extraction (FEO₂) was calculated as VO₂ expressed as a percentage of DO₂, *i.e.*

$$\text{FEO}_2 \text{ (\%)} = \frac{\text{DO}_2 \text{ (ml O}_2\text{/min)}}{\text{VO}_2 \text{ (ml O}_2\text{/min)}} \times 100 \%$$

Urine flow was measured gravimetrically. Arterial blood was centrifuged at 3000 g (Eppendorf 5415R, Crown Scientific Pty Ltd, NSW, Australia) at 4 °C for 10 minutes to generate plasma. Glomerular filtration rate (GFR) was determined by the clearance of [³H]-inulin using the following equation:

$$GFR (ml/min) = \frac{(Urine Flow (ml/min) \times [^3H]urine)}{[^3H]plasma}$$

4.3.4 Protocol 2: Temporal changes in renal tissue PO₂ during the first 7 days of treatment with adenine or its vehicle

Overview: Renal cortical or medullary tissue PO₂ were measured in rats treated with adenine or its vehicle, from the day before and for 7 days during treatment with adenine (Figure 4.2). At the end of the experimental protocol, blood, urine and tissue samples were collected for assessment of renal dysfunction and damage.

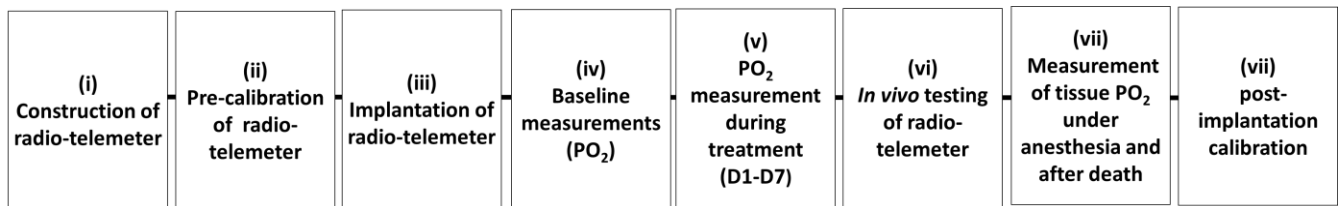


Figure 4.2 Schematic representation of the protocol for measurement of renal tissue PO₂ in unanesthetized rats. The protocol comprised multiple steps: *i) Construction of the radio-telemeter:* the three electrodes (carbon paste electrode, reference and auxiliary electrode) were attached to a radio-telemeter. *ii) Pre-calibration of the radio-telemeter:* This served both to determine whether the device was functional and to assess its responsiveness to changes in PO₂. *iii) Implantation of the radio-telemeter in either the cortex (n =14) or medulla (n =11) of the left kidney:* Electrodes attached to radio-telemeters were implanted in the cortex of 7 rats subsequently treated with adenine and 7 rats subsequently treated with its vehicle. Electrodes attached to radio-telemeters were implanted in the medulla of 6 rats subsequently treated with adenine and 5 rats treated with its vehicle. *iv) Baseline measurements:* Renal tissue PO₂ was measured over a 24 h period before starting the treatment (Pre-treatment). *v) PO₂ measurement during treatment:* Rats received either adenine or its vehicle by oral gavage, daily for a seven day period (D1-D7). Tissue PO₂ was continuously recorded in unanesthetized rats during this treatment period. *vi) In vivo testing of the radio-telemeter:* On day 8, the responsiveness of the radio-telemeter to changes in inspired oxygen was tested in rats with medullary implantation. *vii) Measurement of tissue PO₂ under anesthesia and after death:* Rats were anesthetized and then humanely killed, to assess the effects of anesthesia on tissue oxygenation and the offset current under anoxic conditions (i.e. when PO₂ = 0). *viii) Post-implantation calibration:* The radio-telemeter was explanted and re-calibrated again (as in step ii). Each step is described in detail below.

Construction of the radio-telemeter: This has been described in detail previously (31). Briefly, a functional radio-telemeter (TR57Y, Millar Inc., Houston, TX, USA) consists of two separate units: i) a three electrode system and ii) the telemeter body (31). The three electrodes required for measurement of tissue PO₂ are an oxygen sensing carbon-paste electrode (CPE; Millar, Inc., Texas, USA), a reference electrode, and an auxiliary electrode. The telemeter body contains a battery unit and a potentiostat circuit which maintains a -650 mV potential on the carbon paste electrode to the reference electrode. The potential difference resulting from reduction of oxygen at the tip of the CPE is measured and transmitted wirelessly to a remote receiving station (31).

Prior to implantation of the radio-telemeter, I attached the CPE, reference, and auxiliary electrode to the wires of the probe body. After construction of the telemeter, both the CPE and reference electrode were bent at a 90° angle, ~2 mm (for cortical implantation) or ~5 mm (for medullary implantation) from the electrode tip.

Calibration of the telemeter: An identical procedure was used for calibration of the radio-telemeters before implantation and after explantation. The calibration procedure provides quality control information and allows detection of defects in the manufacturing process. Specifically, improper sealing of the connections between the electrodes and the telemeter wires results in leakage of fluid in the system which causes saturation of current (~ 600 nA) so that the electrodes are unresponsive or poorly responsive to changes in the PO₂ of the phosphate buffered saline (PBS) used during calibration. In such cases, remedial action can be taken to repair the radio-telemetry unit prior to implantation.

In brief, the electrodes of the radio-telemeter were submerged into a small sealed beaker containing 150 ml of 0.1 M PBS at pH 7.4. The PBS was equilibrated with 100% N₂ gas for 30 minutes before submerging the electrodes. In another partially sealed small beaker, 150 ml of 0.1 M PBS was saturated with oxygen by bubbling with 100% O₂. Next, incremental aliquots of 0.1 M PBS equilibrated with 100% O₂ were added to the 0.1 M PBS in the beaker containing the submerged electrodes to achieve cumulative concentrations of 25, 50, 75, 100 and 125 μM O₂. A typical current-time profile of this calibration procedure is given in Figure 4.3.

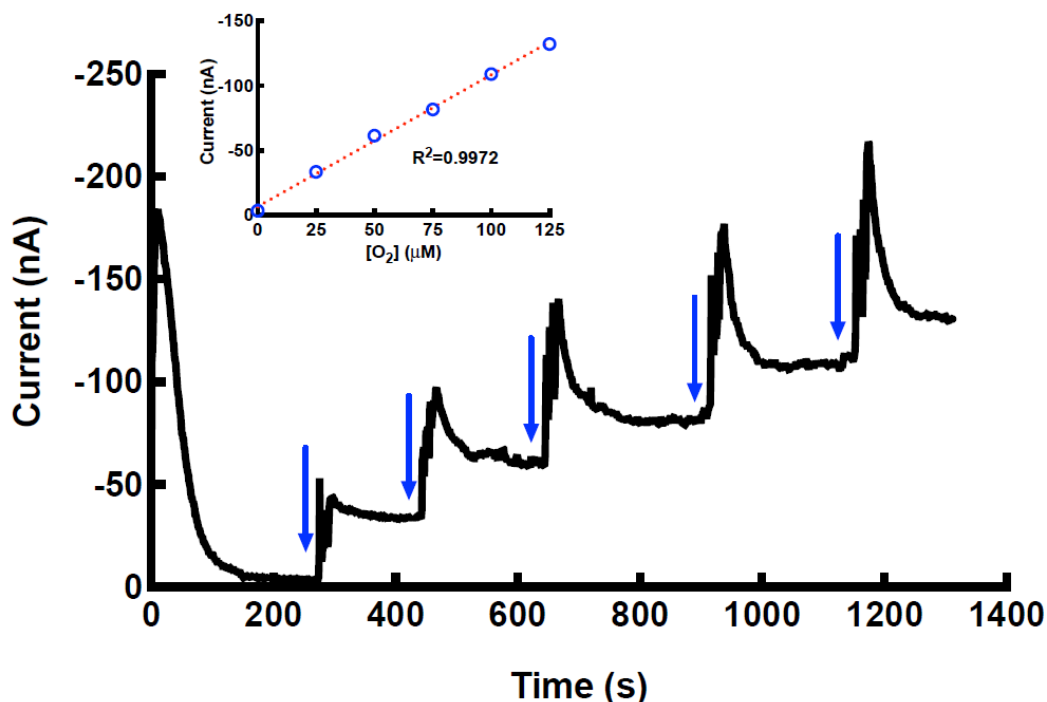


Figure 4.3 An example of a typical trace during the calibration procedure. Current changed incrementally with successive addition of 0.1 M phosphate buffered saline equilibrated with 100 % O₂ to a solution saturated with 100% N₂. Arrows indicate when aliquots were added. The inset represents the relationship between current and oxygen concentration established. Figure was reproduced with permission (46).

Implantation of the radio-telemeter: Radio-telemeters were sterilized with 2% w/v glutaraldehyde (354400-500ML, 25% glutaraldehyde, Merck KGaA, Darmstadt, Germany) in isotonic saline before implantation. The telemeter probe and the wires, up to the joints between the electrodes and the telemeter wires, were submerged in the sterilant for 1 h. The electrodes were kept out of the sterilant, as this could damage the CPE. After 1 h the telemeter probe and wires were rinsed with sterile isotonic saline.

Anesthesia was induced by 5 % v/v isoflurane (IsoFlo™, 05260-05, Abbott Laboratories, IL, USA) supplied in 100 % O₂ (800 ml/min) in an induction box. Once the rat lost consciousness, it was removed from the induction box and isoflurane was supplied through a nose cone at 2.5-3 % v/v for the entire surgical procedure. The rat was placed on a heated pad to facilitate maintenance of body temperature. Rats received a subcutaneous injection of 0.1 ml of an antibiotic suspension containing 80 mg/ml of trimethoprim and 400 mg/ml of sulfadiazine (Tribactral®, Jurox Pty Ltd, NSW, Australia) and a dose 4 mg/kg of carprofen (Rimadyl®, Pfizer, NSW, Australia) for analgesia.

The abdominal aorta and the left kidney were exposed via a midline incision. The wires of the telemeter were sutured onto the adventitia of the abdominal aorta with non-absorbable suture. The CPE and reference electrodes were then inserted into the left kidney so that their tips were either 2 mm below the surface of the renal cortex (renal cortex; n=14) or 5 mm below the surface of the renal cortex (inner medulla; n=11). To allow insertion of the CPE and reference electrode, two small holes were made in the renal capsule, approximately 4 mm apart, using a 30 gauge needle. The electrodes were secured in position with tissue adhesive (3M Vetbond, 3M Animal Care Products, MN, USA) placed onto a small piece of cellulose patch (No. 1469SB, Data Science International, MN, USA) that lay over the electrodes. The auxiliary electrode was attached on the surface of the kidney, away from two other electrodes. As for the CPE and reference electrode, it was secured in place by application of tissue adhesive to a small piece of cellulose patch that lay over the electrode. The telemetry unit was then secured under the right abdominal muscle layer by a suture. Sutures were then used to close the abdominal muscle layer and the skin layer. An antifungal cream (neomycin undenoate, Hamilton Laboratories, Adelaide, SA, Australia) was applied onto the closed wound and the rat was left on a thermal pad for recovery from anesthesia. All rats received subcutaneous injections of carprofen (4 mg/kg; Rimadyl®, Pfizer) for the next three days.

After surgery, the rat was transferred to a standard cage placed on a receiver/recharging device (TR181 SmartPad™, TR181, Millar Inc. Houston, TX, USA), to allow renal tissue PO₂ to be measured continuously across the study period. The SmartPad recharges the battery of the telemeter and also receives and transmits data. The pairing between the radio-telemeter and the smart pad was established by the TR190 Configurator hardware and ConfigSoft™ software (TR190, Millar Inc. Houston, TX, USA).

Responsiveness of the telemeter to changes in renal oxygenation induced by altered inspired oxygen: Rats with electrodes placed in the renal medulla underwent this procedure at the completion of the study (Day 8). For technical reasons I was unable to complete this procedure in rats with electrodes in the renal cortex. The rat cage was placed in a Perspex box, initially with no lid to allow the rat to breathe room air (21% O₂) for 30 minutes (first control period). Next, the Perspex box was closed and 10% O₂ was delivered into the Perspex box for 30 minutes at a rate 5 l/min. Following this first intervention, the lid of the Perspex box was removed and the rat was allowed to breathe at room air for a further 30 minutes (second control period). After that, the lid of the Perspex box was replaced and 100% O₂ was delivered for 30 minutes at a rate of 5 l/min.

This second intervention was followed by a third control period, where the lid of the Perplex box was removed and the rat breathed room air for 30 minutes.

Effects of adenine or its vehicle: All rats received either adenine or its vehicle for a period of 7 days, as described in Section 4.3.2. Body weight and consumption of water were measured daily.

Explantation of the telemeter at day 8: Once responses to altered inspired oxygen content were determined (as described above), rats were then anesthetized by an intraperitoneal injection of 60 mg/kg sodium pentobarbital (Sigma Aldrich). Once a surgical level of anesthesia was achieved, as judged by abolition of pedal reflex, renal tissue PO₂ was recorded for ~7 minutes in order to examine the effect of anesthesia on renal tissue PO₂. Next, a midline incision was made to expose the radio-telemeter and the kidney. Renal tissue PO₂ was then recorded for a further ~5 minutes to investigate the combined effects of anesthesia and laparotomy on renal tissue PO₂. Then, the right renal artery and vein were ligated and the right kidney was removed, decapsulated, weighed and flash frozen in liquid nitrogen and stored at -70°C for later analysis of HIF protein expression by western blot (see below). A 1.5 ml blood sample was then collected from the left ventricle for analysis of blood chemistry (iSTAT, Chem8+ Cartridge; Abbot Laboratories). Each rat subsequently received 2 ml potassium chloride (7 mM) via cardiac puncture to induce cardiac arrest. The current measured by the telemeter rapidly decreased and reached to stable baseline within 30 seconds of death. This stable baseline current (offset value) was subtracted from all data recorded during the experiment. The telemeters, with electrodes attached, were then explanted and calibrated (see *Calibration of the telemeter*, above). The left kidney and heart were removed and weighed. Tissue samples were fixed in 10% neutral buffered formalin solution for further histological studies.

Quantification of tissue PO₂: The current signal from the radio-telemeter was filtered with a 25 Hz low-pass filter. Artefacts were removed when the 1st order derivative of the measured current exceeded a threshold of 5-500 nA/s. The zero-offset current of the radio-telemeters, determined at the end of the experiment after cardiac arrest, was subtracted from all measurement. Therefore, the ‘true current’ measured was calculated as:

$$\text{Current (nA)} = \text{Filtered current(nA)} - \text{Zero offset current (nA)}$$

The current measured at the tip of the electrode is proportional to the concentration of oxygen at the CPE. Renal tissue PO₂ was determined as:

$$\text{Tissue } PO_2 \text{ (mmHg)} = \frac{\text{Current (nA)}}{\text{Calibration of CPE (nA}/\mu\text{m)}} \times 0.631$$

The calibration of the CPE was determined during the pre-calibration procedure. The constant 0.631 is a conversion factor for concentration to partial pressure in aqueous solution at sea level ($1 \mu\text{M} = 0.631 \text{ mmHg}$) (31).

Expression of hypoxia-inducible factors: The right kidneys collected from rats in which kidney tissue PO_2 was measured by radio-telemetry were used for western blot analysis of HIF-1 α and HIF-2 α protein expression. The frozen kidneys were thawed and sliced. The middle slice of each kidney was dissected into three regions (*i.e.* the cortex, outer medulla and inner medulla with papilla).

Tissue samples were homogenized in $8 \mu\text{l}$ per mg of tissue radioimmunoassay-precipitation (RIPA) buffer to lyse cells and allow extraction of proteins from the samples. The RIPA buffer consisted of 25 mM Tris-hydrochloride, 100 mM sodium chloride, 0.1% v/v Triton X-100, 0.5% w/v sodium deoxycholate, 0.1% w/v sodium dodecylsulphate (SDS), 1 mM sodium orthovanadate, 1 mM sodium fluoride, and protease inhibitors (CompleteTM Mini, protease inhibitor cocktail tablets, Roche diagnostics GmbH, Mannheim, Germany). Next, the tissue homogenate was centrifuged at 15,000 g at 4 °C for 20 min. The supernatant was collected and stored -80°C. Prior to western blotting, the amount of protein in each sample was quantified using a commercially available kit (PierceTM BCA Protein Assay Kit #23225, Thermo Scientific, Rockford, IL, USA). After quantification of protein concentration in each sample, the supernatant was added to Laemmli sample buffer (2x Laemmli Sample Buffer #1610737, Bio-Rad Laboratories, CA, USA) and heated at 95 °C for 2 minutes.

Thirty μg of protein from each sample was loaded into each lane of a precast gel (7.5% Mini-PROTEAN[®] TGXTM Precast Protein Gels, 4561025, Bio-Rad Laboratories, CA, USA) and proteins were separated electrophoretically in running buffer (Tris/glycine/SDS) at 300 V for 20 minutes. The fractionated proteins in the precast gel were then transferred onto a polyvinylidene difluoride (PVDF) membrane (Trans-Blot[®] TurboTM RTA Mini PVDF Transfer Kit, 1704272, Bio-Rad Laboratories, CA, USA) using a transfer system (Trans-Blot[®] TurboTM Transfer System, Bio-Rad Laboratories, CA, USA). Next, the PVDF membrane was placed in blocking buffer (5% w/v skim milk in Tris buffered saline with Tween 20 (TBST) buffer) in order to prevent non-specific binding of the detection antibodies.

The PVDF membranes were incubated overnight at 4 °C in the primary antibody (1:1000), either HIF-1 α (NB100-479, Novus Biologicals, CO, USA) or HIF-2 α (NB100-122, Novus Biologicals, CO, USA) in 2.5% w/v bovine serum albumin. After that, the PVDF membranes were washed by TBST buffer. Subsequently, the membranes were incubated in a solution containing secondary antibody at a dilution of 1:4000 (ECL™ anti-rabbit IgG, HRP-linked whole antibody, GE Healthcare UK Limited, UK) and conjugate (1:15,000) (Precision Protein™ StrepTactin-HRP conjugate, Bio-Rad Laboratories, CA, USA) for an hour at room temperature. The membrane was developed by incubation for 3 min with equal parts of Clarity™ Western Peroxide Reagent (Bio-Rad Laboratories, CA, USA) and Clarity™ Western Luminol/Enhancer Reagent (Bio-Rad Laboratories, CA, USA). The intensity of the bands observed on the membrane was quantified using ImageLab software (Bio-Rad) and the intensity of specific bands was corrected to total protein content on the membrane.

Histological assessment of tissue damage and collagen deposition: The formalin-fixed left kidneys were processed, embedded in paraffin and sectioned at 5 μ m. Two sections from each kidney were stained with hematoxylin and eosin (H & E) (1, 22) and picosirius red (7). H & E staining was performed to visualize vascular and tubular structures. Picosirius red staining was used to assess collagen deposition, specifically type I and type III collagen, in the kidney.

All sections were scanned at 40x magnification using Aperio Scan Scope (Aperio, Vista, CA, USA). Quantification of collagen deposition in kidney sections processed for picosirius red staining was performed using the Image Scope Positive Pixel Count Algorithm (Version 9; Aperio). Results are presented as percentage of total area stained with picosirius red.

4.3.5 Statistical analyses

Statistical analyses were performed using SYSTAT (Version 13, Systat Software Inc., Chicago, IL, USA). First, normality was assessed using the Shapiro-Wilk test (58). Data that did not violate normality are presented as mean \pm standard error of the mean (SEM) while data that violated normality are presented as median (25th percentile, 75th percentile). Dichotomous comparisons were made using either Student's t-test with Welch's correction or the Mann-Whitney U-test. Variables measured at multiple time-points were analyzed using repeated measures analysis of variance (ANOVA), with P values conservatively adjusted using the method of Greenhouse and Geisser (35). Two-sided $P \leq 0.05$ was considered statistically significant.

4.4 RESULTS

4.4.1 Protocol 1: Renal tissue oxygenation and its determinants in anesthetized rats

Morphological parameters, body temperature and blood chemistry: Before the treatment period commenced, body weight of rats subsequently treated with adenine (362 ± 14 g) was similar to that of vehicle-treated rats (355 ± 16 g, $P = 0.73$). However, after the 7 day treatment period, adenine-treated rats were significantly lighter (-17%) than vehicle-treated rats (Table 4.1). At the completion of the experimental protocol, left kidney weight was 86% greater in adenine-treated rats than in vehicle-treated rats. Body temperature, blood electrolytes and hematocrit, at the commencement of the terminal experiment under anesthesia, were similar in adenine-treated and vehicle treated rats (Table 4.1). The only exceptions were ionized calcium, which was 7% less in adenine-treated than vehicle-treated rats, and arterial PCO_2 , which showed a tendency ($P = 0.07$) towards hypocapnia in adenine-treated rats.

Table 4.1 Characteristics of vehicle-treated and adenine-treated rats under anesthesia

Parameter	Vehicle	Adenine	P
Morphology			
Body weight, g	391 ± 12	325 ± 11	0.002
Left kidney weight, g	1.4 ± 0.1	2.6 ± 0.1	<0.001
Temperature			
Core temperature, °C	36.5 ± 0.3	36.6 ± 0.3	0.82
Arterial blood chemistry			
Sodium, mM	141.4 ± 1.3	144.7 ± 2.4	0.23
Potassium, mM	4.8 ± 0.1	4.6 ± 0.2	0.29
Ionized calcium, mM	1.29 ± 0.02	1.20 ± 0.02	0.005
Glucose, mM	11.2 ± 1.2	14.5 ± 1.6	0.13
Hematocrit, %	47.2 ± 1.0	46.7 ± 0.6	0.69
PCO_2 , mmHg	37.7 ± 2.4	31.7 ± 1.8	0.07
HCO_3 , mM	25.7 ± 0.6	24.8 ± 0.8	0.43
pH	7.44 ± 0.03	7.50 ± 0.03	0.12

Values are mean \pm SEM (vehicle-treated rats: $n = 7$ for morphology, temperature, and arterial blood chemistry; adenine-treated rats: $n = 9$ for morphology, $n = 7$ for temperature, and $n = 8$ for arterial blood chemistry). P values are the outcomes of Student's unpaired t test with Welch's correction.

Systemic hemodynamics and renal hemodynamics and function under anesthesia: MAP was 24% higher in adenine-treated rats than vehicle-treated rats (Table 4.2). However, neither HR nor SO₂ differed significantly between the two groups. RBF was 51% less, GFR was 65% less and urine flow was 167% greater in adenine treated rats than vehicle-treated rats when these variables were corrected for kidney weight. Filtration fraction did not differ significantly between the two groups.

Table 4.2 Systemic and renal hemodynamic and functional parameters in anesthetized vehicle-treated and adenine-treated rats

Parameters	Vehicle	Adenine	P
Systemic hemodynamic			
MAP, mmHg	107 ± 6	133 ± 5	0.01
HR, bpm	455 ± 30	400 ± 9	0.13
SO ₂ , %	99.0 ± 0.3	97.6 ± 1.4	0.34
Renal hemodynamic			
RBF, ml/min/g KW	1.45 ± 0.24	0.71 ± 0.09	0.02
GFR, ml/min/g KW	0.37 ± 0.05	0.13 ± 0.02	0.003
Urine flow, µl/min/g KW	2.8 ± 0.4	8.3 ± 1.6	0.02
Filtration fraction, %	41.8 ± 6.1	35.4 ± 5.3	0.45

Values are mean ± SEM (vehicle-treated rats: n=7; adenine-treated rats: n=8 for RBF, n=6 for GFR, urine flow and filtration fraction, n=7 for systemic hemodynamics). RBF, renal blood flow; GFR, glomerular filtration rate; FF, filtration fraction; MAP, mean arterial pressure; SO₂, saturation of arterial hemoglobin with oxygen, determined by pulse oximetry. KW: kidney weight. P values are outcomes of Student's unpaired t-test with Welch's correction.

Blood oxygen content: Arterial and renal venous blood hemoglobin, PO₂, SO₂ and blood oxygen content were similar in rats treated with adenine to their levels in vehicle-treated rats (Table 4.3). The only exception was that arterial SO₂ was slightly but significantly greater in adenine-treated rats than vehicle-treated rats.

Table 4.3 Blood oxygenation in anesthetized vehicle-treated and adenine-treated rats

Parameters	Vehicle	Adenine	P
Arterial blood			
Hemoglobin, g/dl	16.2 ± 0.5	15.8 ± 0.2	0.51
PO ₂ , mmHg	127.6 ± 10.8	139.0 ± 4.8	0.36
SO ₂ , %	98.8 ± 0.2	99.4 ± 0.1	0.03
O ₂ content, ml O ₂ /dl	21.9 ± 0.5	21.7 ± 0.4	0.77
Renal venous blood			
Hemoglobin, g/dl	14.8 ± 0.4	14.8 ± 0.5	0.99
PO ₂ , mmHg	43.7 ± 4.8	53.0 ± 5.0	0.21
SO ₂ , %	76.0 ± 7.9	86.4 ± 4.9	0.29
O ₂ content, ml O ₂ /dl	16.5 ± 1.6	18.7 ± 1.3	0.30

Values are mean ± SEM (vehicle-treated rats: n = 7; adenine-treated rats: n = 7). SO₂, saturation of hemoglobin with oxygen. P values are the outcomes of Student's unpaired t-test with Welch's correction.

Renal oxygen supply and utilization: Renal DO₂ was 51% less, and renal VO₂ was 65% less, in rats treated with adenine compared to vehicle-treated rats, when these variables were corrected for kidney weight (Figure 4.4). In contrast, fractional extraction of oxygen (FEO₂) did not differ significantly between the two groups.

Spatial distribution of renal tissue PO₂ in anesthetized vehicle-treated and adenine-treated rats:

Cortical tissue PO₂, measured by Clark electrode at a depth of 2 mm below the renal capsule, was heterogeneous across the left kidney in both vehicle-treated and adenine-treated rats. The lowest tissue PO₂ in the cortical region was measured at 2.7 mmHg and the highest tissue PO₂ was 133.7 mmHg (Figure 4.5A). However, the average cortical tissue PO₂ in the group of rats treated with adenine did not differ significantly from that in the corresponding vehicle-treated group (Figure 4.5B). Tissue PO₂ was consistently lower, from the cortico-medullary junction to a depth of 9 mm below the renal capsule, in adenine-treated rats compared to vehicle-treated rats (Figure 4.5C). Notably, the average medullary tissue PO₂, between 4-6 mm depth, was 44% less in adenine-treated rats than vehicle-treated rats, whereas cortical tissue PO₂ (average of 1-2 mm depth) was comparable between adenine-treated (44.5 ± 6.4 mmHg) and vehicle-treated (47.6 ± 7.7 mmHg) rats (Figure 4.5D).

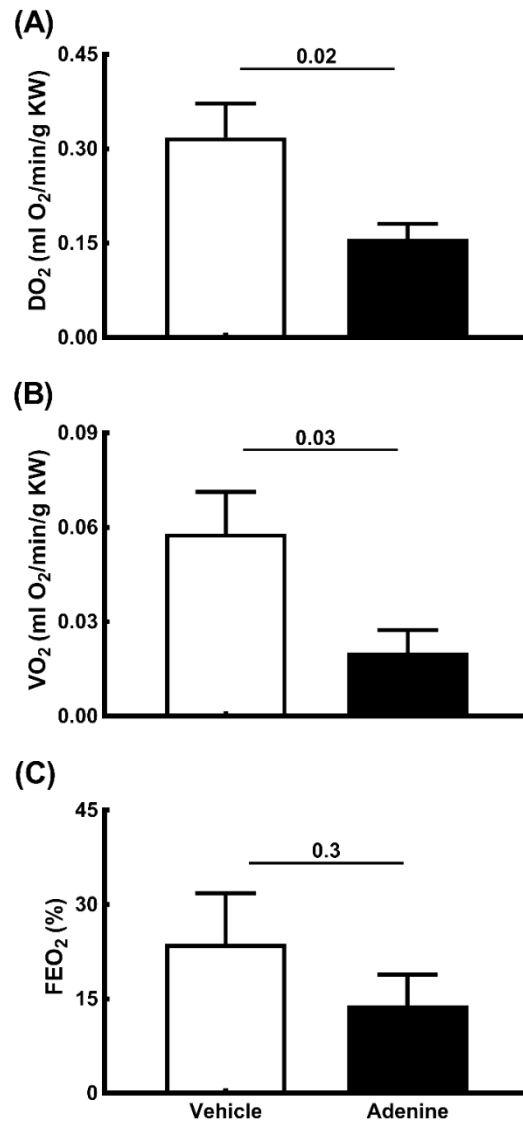


Figure 4.4 Whole kidney oxygenation in vehicle-treated and adenine-treated rats. Columns and error bars represent mean \pm SEM (vehicle-treated rats: $n = 7$; adenine-treated-rats: $n = 7$). A: renal oxygen delivery (DO_2). B: renal oxygen consumption (VO_2). C: fractional extraction of oxygen (FEO_2). KW: kidney weight. P values are the outcomes of Student's unpaired t-test with Welch's correction.

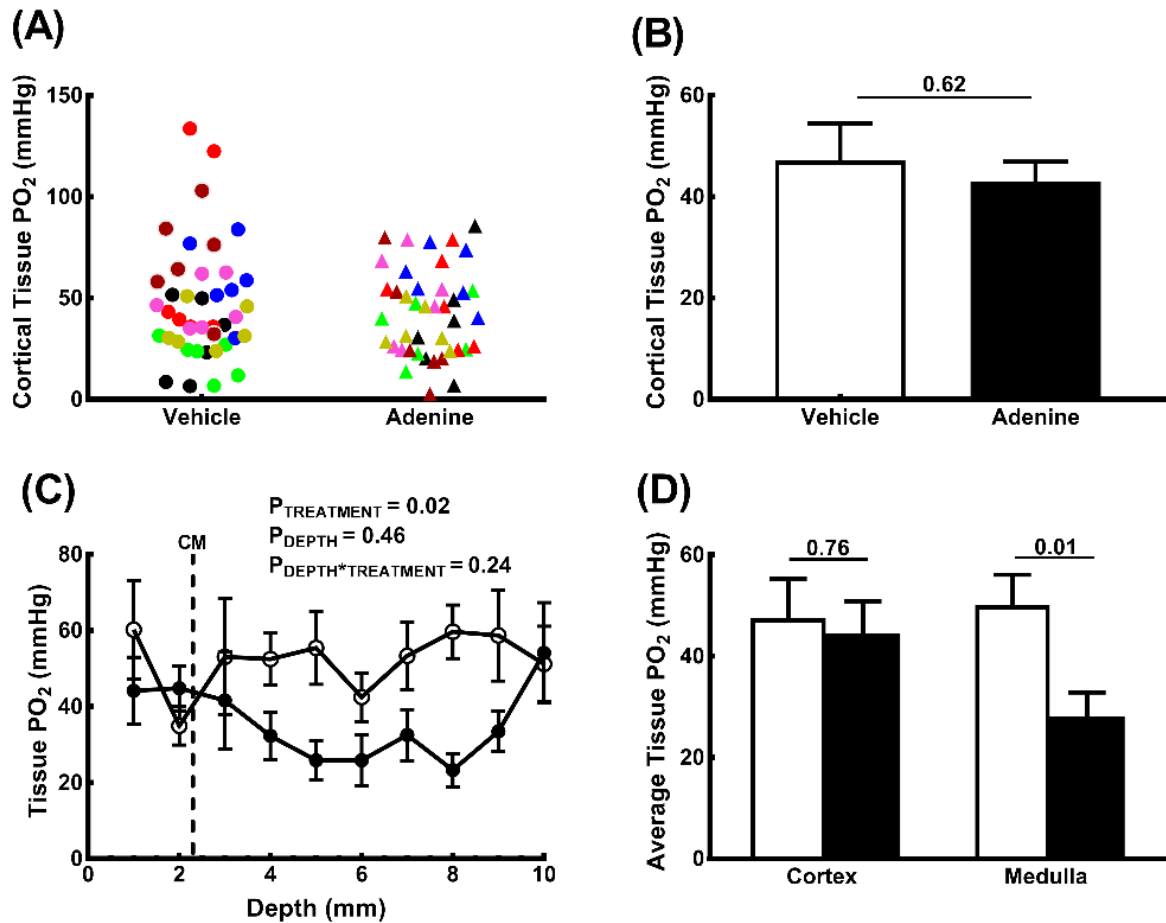


Figure 4.5 Assessment of renal tissue PO₂ in vehicle-treated rats (n = 7) and adenine-treated rats (n = 7) under anesthesia. **A:** Measurements of tissue PO₂ at a depth of 2 mm below the cortical surface at six random spots across the left kidney. Each color represents a different rat. **B:** Measurements of cortical tissue PO₂ for each rat were averaged. Columns and error bars represent mean ± SEM. P values are the outcomes of Student's unpaired t-test with Welch's correction. **C:** A tissue PO₂ profile with depth was established by advancing the Clark electrode from the cortical surface at 1 mm increments up to a depth of 10 mm below the cortical surface. Circles and error bars represent mean ± SEM (vehicle-treated rats: open circles; adenine-treated rats: closed circles). P values (P_{Depth}, P_{Treatment} and P_{Depth*Treatment}) are the outcomes of repeated measures analysis of variance with factors depth and treatment. **D:** Cortical tissue PO₂ (1-2 mm depth) and medullary tissue PO₂ (4 to 6 mm depth) were averaged. Columns and error bars represent mean ± SEM (vehicle-treated rats: open bar; adenine-treated rats: filled bar). P values are the outcomes of Student's unpaired t-test with Welch's correction. PO₂: tissue oxygen tension, CM: cortico-medullary junction.

4.4.2 Protocol 2: Temporal changes in renal tissue PO₂ during the first 7 days of treatment with adenine or its vehicle

Body weight and water intake: Body weight differed significantly between two groups across the 7 day treatment period (Figure 4.6A). At the completion of the study protocol, body weight had increased by $7.8 \pm 1.3\%$ in vehicle-treated rats whereas in adenine-treated rats it had decreased by $5.9 \pm 3.8\%$ compared to their respective baseline values.

Daily water intake by rats treated with vehicle remained stable across the 7 day study period (Figure 4.6B). However, water intake in adenine-treated rats had increased by $47.4 \pm 20.2\%$ at day 2 and remained consistently greater than baseline levels across the remainder of the 7 day treatment period.

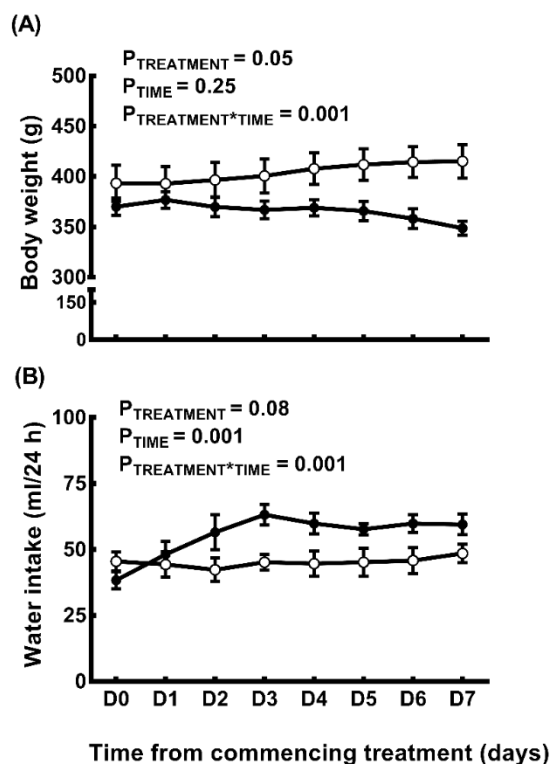


Figure 4.6 Body weight and water intake in vehicle-treated and adenine-treated rats during the 7 day treatment period. Circles and error bars represent mean \pm SEM. **A:** Body weight (vehicle treated rats: $n = 7$; open circles; adenine-treated rats: $n = 7$; closed circles) was recorded before (D0) and during the treatment period (D1-D7) **B:** Daily water intake was recorded (vehicle-treated rats: $n = 6$; open circles and adenine-treated rats: $n = 6$; closed circles) before and during the treatment period. P ($P_{TREATMENT}$, P_{TIME} and $P_{TREATMENT * TIME}$) values are the outcomes of repeated measures analysis of variance.

Temporal changes of renal tissue PO₂ in unanesthetized rats: Neither cortical nor medullary tissue PO₂ measured by telemetry differed significantly between the adenine-treated and vehicle-treated groups across the 7 day treatment period (Figure 4.7).

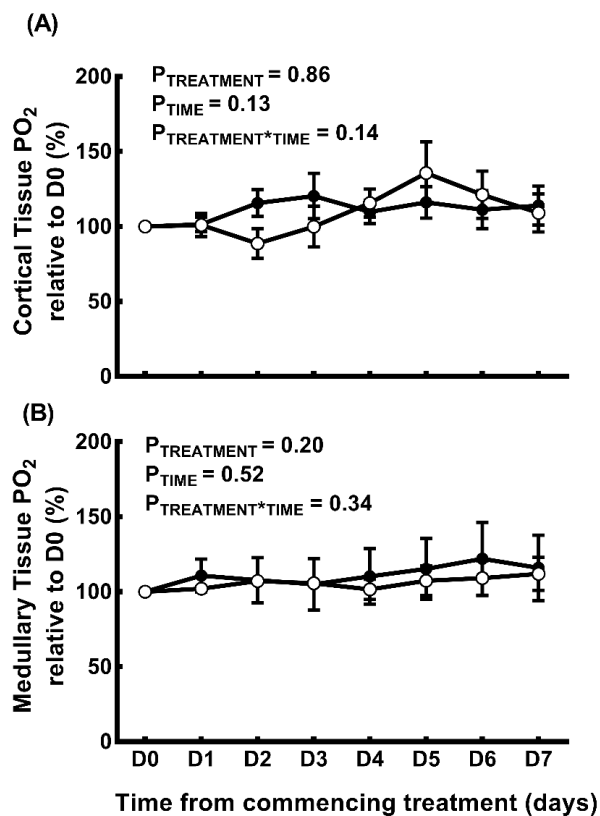


Figure 4.7 Temporal changes of cortical and medullary tissue PO₂ in vehicle-treated and adenine-treated rats. Tissue PO₂, averaged over 24 h, was recorded before (D0) and during the treatment period (D1-D7). Tissue PO₂ is expressed as percentage relative to the day before the treatment. Circles and error bars represent mean ± SEM. **A:** Cortical tissue PO₂ (vehicle treated rats: n = 7, open circle; adenine-treated rats: n = 7; closed circles). **B:** Medullary tissue PO₂ (vehicle-treated rats: n = 5, open circles; adenine-treated rats: n = 6, closed circles). D; day. P (P_{TREATMENT}, P_{TIME} and P_{TREATMENT*TIME}) values are the outcomes of repeated measures analysis of variance with factors time and treatment.

Responsiveness of radio-telemeters to altered inspired oxygen: At the completion of the experimental protocol, the responsiveness of radio-telemeters to altered inspired oxygen inducing hyperoxia (100% O₂) and hypoxia (10% O₂) was tested in unanesthetized rats (Figure 4.8). When rats were exposed to hyperoxia, medullary tissue PO₂ increased by 21 ± 11% in vehicle-treated rats

and $29 \pm 4\%$ and adenine-treated rats respectively. When rats were exposed to hypoxia, medullary tissue PO_2 decreased by $19 \pm 10\%$ in vehicle-treated rats and $27 \pm 4\%$ in adenine-treated rats.

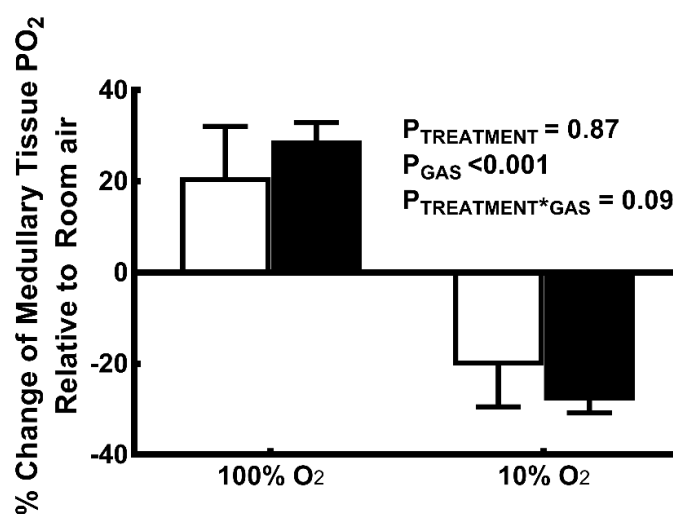


Figure 4.8 Responsiveness of radio-telemeters to changes in inspired oxygen content in unanesthetized rats. Columns and error bars represent mean \pm SEM (vehicle-treated rats: $n = 3$, open bar; adenine-treated rats: $n = 4$, closed bar). Rats were subjected to two intervention periods in which they inspired either 100% O_2 or 10% O_2 for 30 minutes, bracketed by control periods (room air; 21% O_2 for 30 minutes). P ($P_{TREATMENT}$, P_{GAS} and $P_{TREATMENT*GAS}$) values are the outcomes of 2-way repeated measures analysis of variance with factors gas (10% or 100% O_2) and treatment. PO_2 : partial pressure of oxygen.

Effects of anesthesia and laparotomy on renal tissue PO_2 : Cortical tissue PO_2 was reduced under anesthesia and was further reduced after laparotomy in both treatment groups. The magnitude of the reduction in cortical tissue PO_2 after laparotomy was similar between adenine-treated rats ($38 \pm 5\%$) and vehicle-treated rats ($34 \pm 2\%$) (Figure 4.9 A). In the renal medulla, anesthesia was accompanied by a $12 \pm 1\%$ reduction in tissue PO_2 in adenine-treated rats and a similar ($14 \pm 8\%$) reduction in vehicle-treated rats (Figure 4.9 B). However, after laparotomy, a greater reduction in medullary tissue PO_2 was observed in adenine-treated rats ($36.6 \pm 6.6\%$) than vehicle-treated rats ($16.4 \pm 3.6\%$).

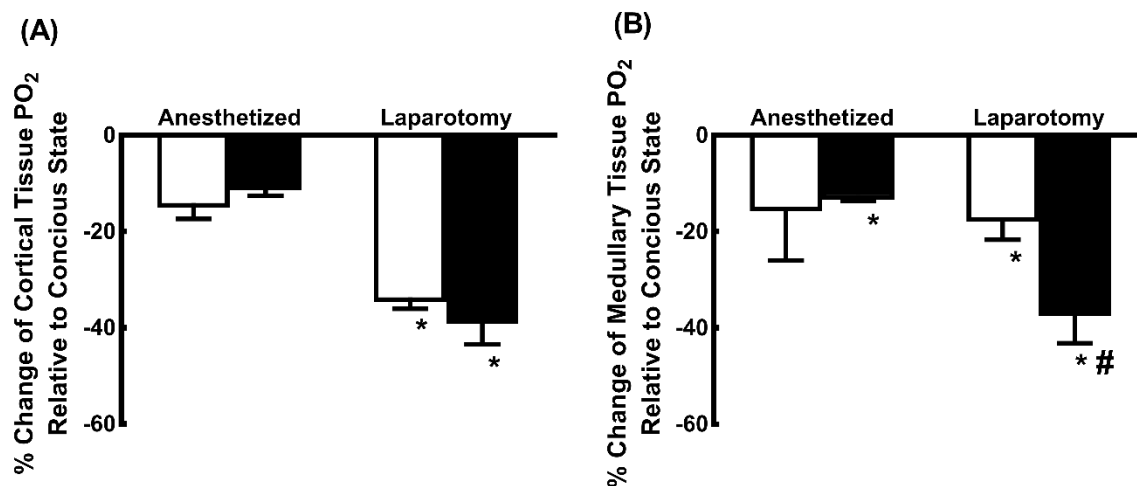


Figure 4.9. Effects of anesthesia and laparotomy on renal tissue PO₂ in vehicle-treated and adenine-treated rats. Columns and error bars represent mean \pm SEM. At the completion of the experiment, renal tissue PO₂ was recorded by radio-telemetry for \sim 7 minutes after a surgical level of anesthesia was achieved (Anesthetized). After laparotomy, renal tissue PO₂ was recorded for \sim 5 minutes. **A:** Cortical tissue PO₂ (vehicle-treated rats: n = 5, open bar; adenine-treated rats: n = 5, filled bar). **B:** Medullary tissue PO₂ (vehicle-treated rats: n = 5, open bar; adenine-treated rats: n = 5, filled bar). *P \leq 0.05 conscious state vs anesthetized state (Student's paired *t*-test) and #P \leq 0.05 adenine vs vehicle (Student's unpaired *t*-test with Welch's correction).

Morphological parameters and blood chemistry: After the 7 day treatment period, adenine-treated rats were significantly lighter (-13%) than vehicle-treated rats (Table 4.4). In contrast, left kidney and right kidney weights were 83.7% and 90.6% greater, respectively, in adenine-treated rats than in vehicle-treated rats. Plasma electrolyte concentrations, hematocrit and hemoglobin concentration were comparable between the two treatment groups (Table 4.4). Blood urea nitrogen (BUN) was 283% greater, and plasma creatinine concentration was 183% greater, in adenine-treated rats than vehicle-treated rats.

Table 4.4 Characteristics of vehicle-treated and adenine-treated rats after the 7 day treatment period

Parameters	Vehicle	Adenine	P
Morphology			
Body weight, g	422 ± 9	369 ± 10	<0.001
Left kidney, g	1.35 ± 0.05	2.48 ± 0.09	<0.001
Right kidney, g	1.39 ± 0.06	2.65 ± 0.13	<0.001
Heart weight, g	1.10 ± 0.05	1.08 ± 0.07	0.81
Blood chemistry			
Sodium, mM	136.6 ± 0.9	136.1 ± 2.8	0.89
Potassium, mM	4.0 ± 0.1	4.0 ± 0.3	0.94
Chloride, mM	100.7 ± 1.3	98.7 ± 2.4	0.47
Ionized calcium, mM	1.28 ± 0.03	1.16 ± 0.07	0.13
Glucose, mM	9.5 ± 0.2	8.7 ± 0.4	0.07
Hematocrit, %	37.0 ± 0.9	35.9 ± 1.3	0.47
Hemoglobin, g/dl	12.6 ± 0.3	12.2 ± 0.4	0.47
Anion gap, mM	12.6 ± 1.3	15.0 ± 0.7	0.14
TCO ₂ , mM	28.6 ± 0.7	27.6 ± 0.6	0.31
BUN, mM	4.5 ± 0.3	17.2 ± 1.9	<0.001
Creatinine, mg/dl	0.46 ± 0.05	1.30 ± 0.14	<0.001

Values are mean ± SEM (vehicle-treated rats: n = 14 for morphology, and n = 7 for arterial blood chemistry; adenine-treated rats: n = 14 for morphology, and n = 7 for arterial blood chemistry). TCO₂: total carbon dioxide, BUN: blood urea nitrogen. P values are outcomes of the Student's unpaired t-test with Welch's correction.

Histological assessment of tissue damage and collagen deposition: Renal cortical and medullary tissue from vehicle-treated rats appeared relatively normal (Figure 4.10 a-d). In the cortex the glomeruli were intact with no apparent abnormalities of Bowman's space (Figure 4.10 b). Renal tubules were closely spaced and the interstitial space was not prominent in both the cortex and medulla. (Figure 4.10 b,c). In contrast, tissue architecture of kidneys of adenine-treated rats was abnormal (Figure 4.10 e-h). Adenine treatment induced marked tubular dilation and disintegration of the brush border of the apical surface of renal tubules in both the cortex and medulla (Figure 4.10 f, g and h). Nevertheless, the glomeruli remained intact with no apparent abnormalities of Bowman's space. Renal tubular casts were observed in the kidneys of adenine-treated rats.

Renal tissue sections from vehicle-treated rats showed very little picosirius red staining. Red staining was observed in the perivascular region, associated with the normal presence of perivascular adventitia. However, there was very little red stain in the interstitium (Figure 4.11 a-d). In contrast, kidney sections from adenine-treated rats show considerable red staining in the interstitium of the cortex and outer medulla (Figure 4.11 e and g). Quantification indicated that picosirius red staining was 155% greater in the cortex and 58.3% greater in the medulla of adenine-treated rats compared to vehicle-treated rats (Figure 4.12).

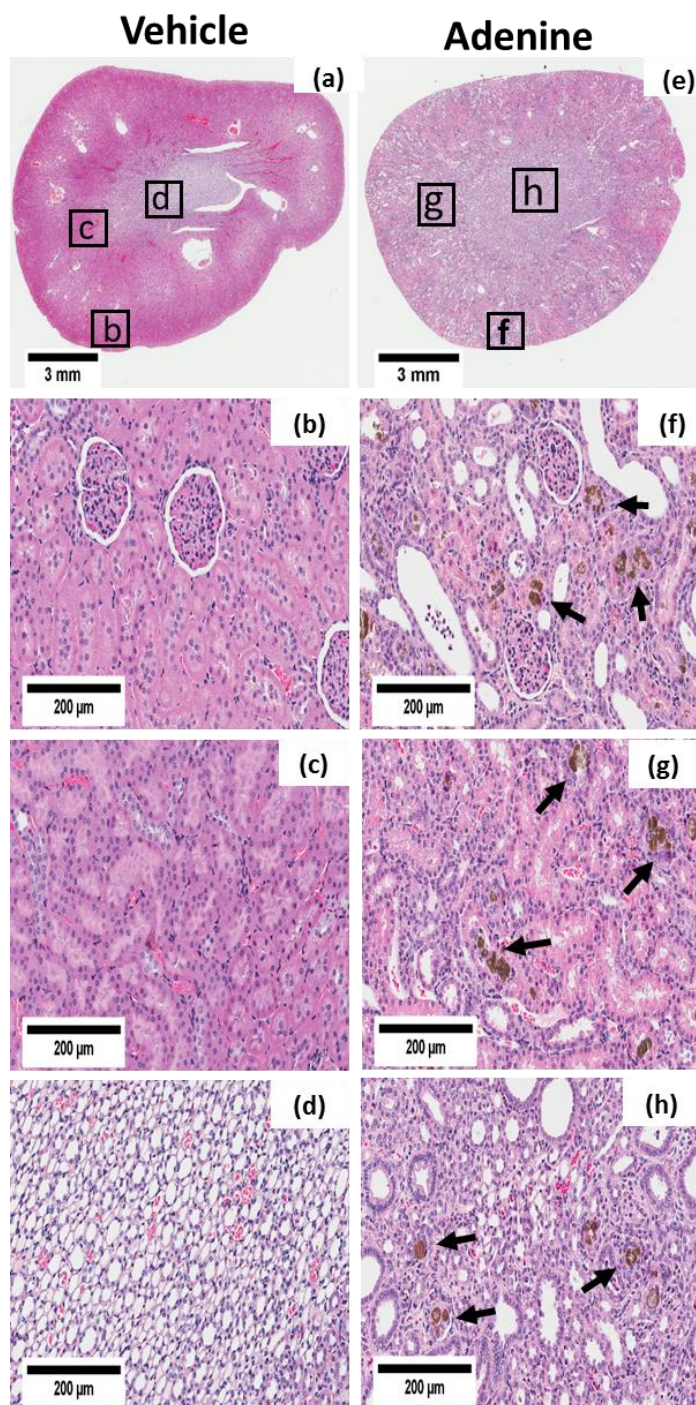


Figure 4.10 Micrographs of kidney sections from rats treated with vehicle (a–d) or adenine (e–h), stained with hematoxylin and eosin. Cortical (b, f), outer medullary (c, g) and inner medullary regions (d, h) are shown. Boxes in (a) and (e) show regions presented in (b–d) and (f–h). Images are typical of two sections taken from each kidney. Here, n = 5 in each group. Note presence of tubular casts (arrows) formed from precipitation of 2, 8- dihydroxyadenine.

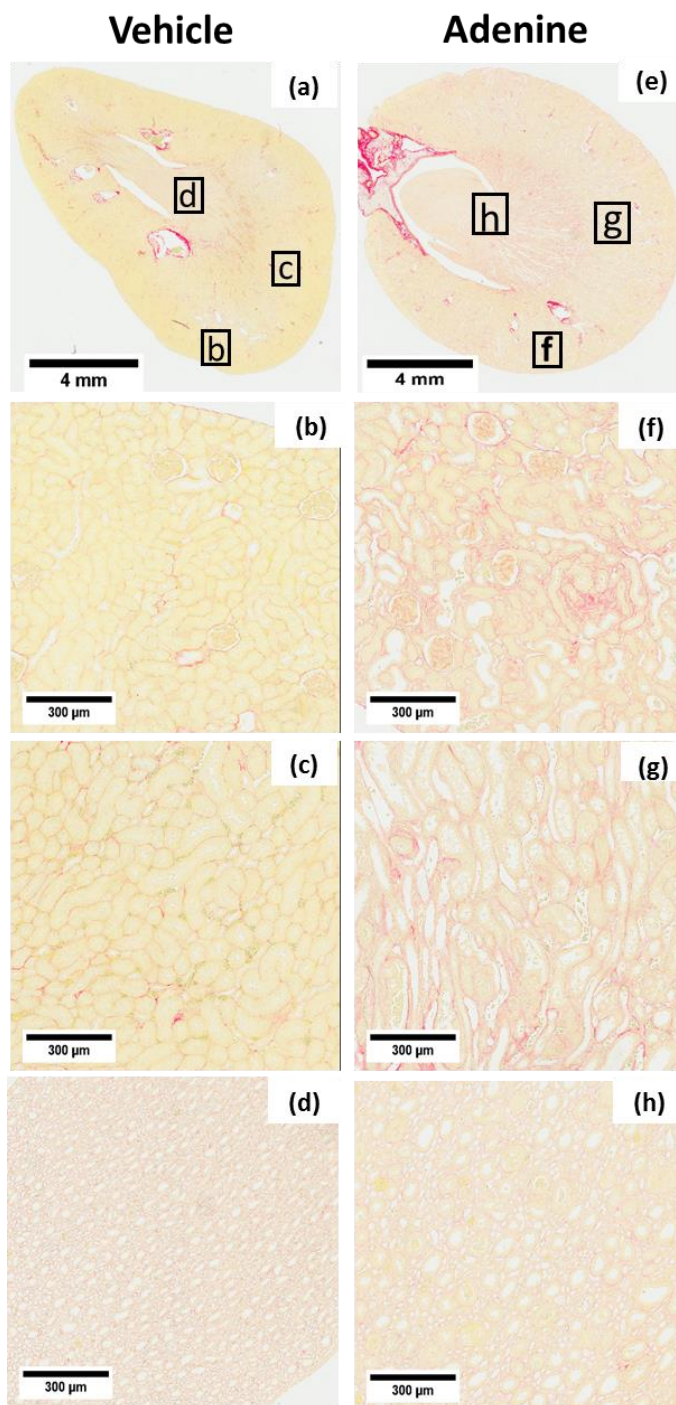


Figure 4.11 Micrographs of kidney sections from rats treated with vehicle (a–d) or adenine (e–h), stained with picosirius red. Cortical (b, f), outer medullary (c, g) and inner medullary regions (d, h) are shown. Boxes in (a) and (e) show regions presented in (b–d) and (f–h). Images are typical of two sections taken from each kidney. Here, $n = 5$ in each group. Note intense red staining in kidneys of adenine-treated rats representing collagen accumulation in the interstitium, whereas vehicle-treated rats show only faint staining around glomeruli and normal staining of the adventitia surrounding arteries and veins.

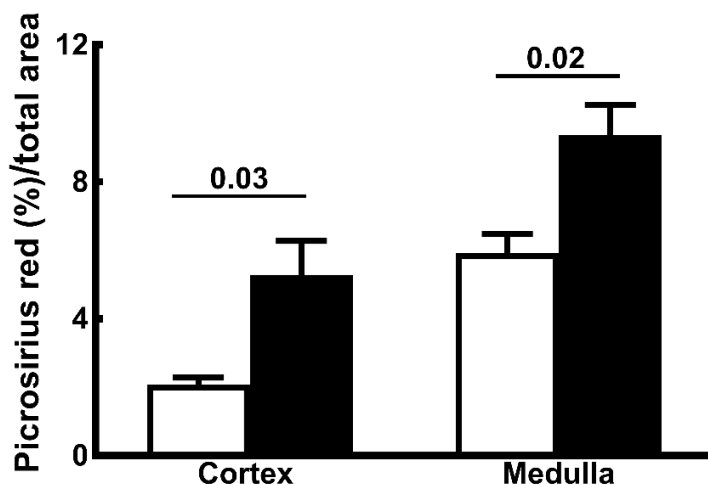


Figure 4.12 Quantification of collagen deposition in the cortex and medulla. Two sections were analyzed from each kidney. Values are mean \pm SEM for vehicle-treated rats (n = 5: open bars) and adenine-treated rats (n = 5: filled bars). P values are the outcomes of Student's unpaired t-test with Welch's correction.

Expression of hypoxia inducible factors: After the 7 day treatment period, levels of HIF-1 α protein were 40% less in the cortex, 58% less in the outer medulla, and 75% less in the inner medulla, in adenine-treated rats than in vehicle-treated rats (Figure 4.13). In contrast, protein levels of HIF-2 α did not differ significantly between the two groups in any of the three regions of the kidney (Figure 4.14).

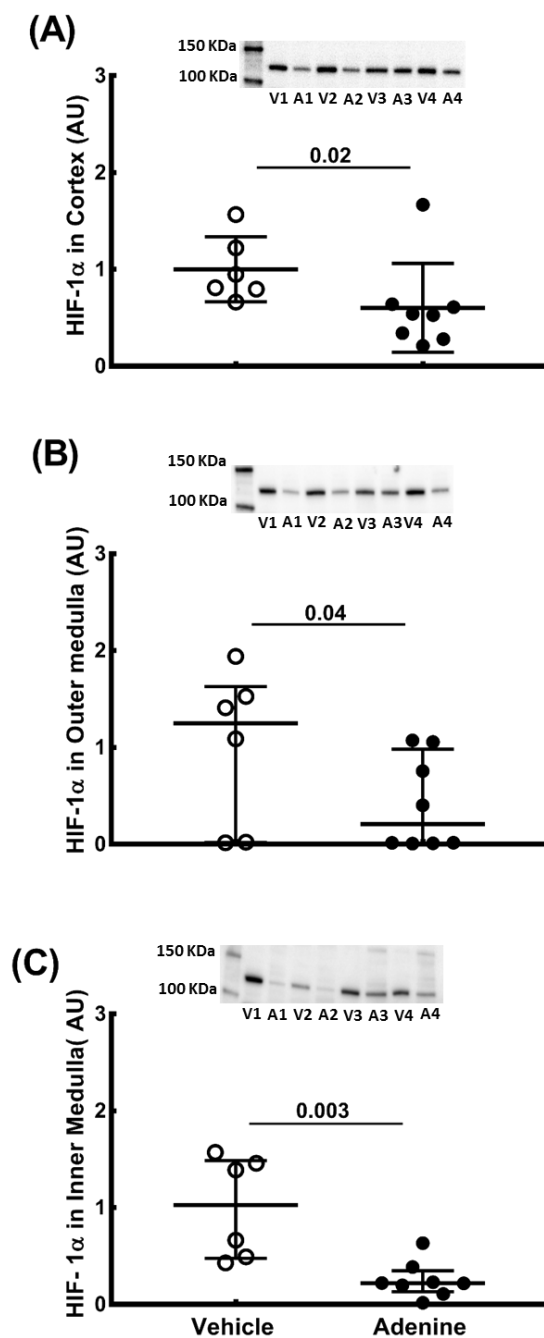


Figure 4.13 Levels of HIF-1 α protein in vehicle-treated and adenine-treated rats after the 7 day treatment period. Protein levels of HIF-1 α are shown in both graphs and immunoblots for (A) the cortex, (B) the outer medulla and (C) the inner medulla of the left kidneys. Vehicle-treated rats: n = 6 (open circles) and adenine-treated-rats: n = 8 (closed circles). Values are expressed as median (25th percentile, 75th percentile). P values are outcomes of the Mann-Whitney U-test. HIF-1 α : hypoxia-inducible factor-1 α , V: vehicle-treated rat, A: adenine-treated rat, KDa: kilodalton, AU: arbitrary unit.

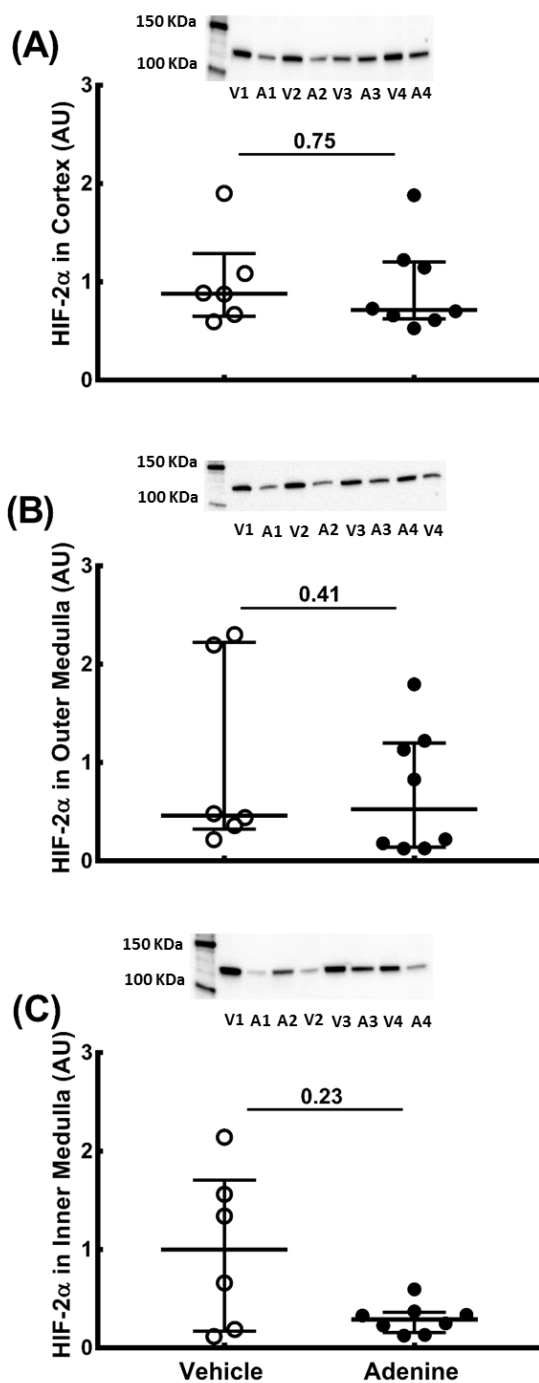


Figure 4.14 Levels of HIF-2 α protein in vehicle-treated and adenine-treated rats after the 7 day treatment period. Protein levels of HIF-2 α are shown in both graphs and immunoblots for (A) the cortex, (B) the outer medulla and (C) the inner medulla of the left kidneys. Vehicle-treated rats: n = 6 (open circles) and adenine-treated-rats: n = 8 (closed circles). Values are expressed as median (25th percentile, 75th percentile). P values are outcomes of the Mann-Whitney U-test. HIF-2 α : hypoxia-inducible factor-2 α , V: vehicle-treated rat, A: adenine-treated rat, KDa: kilodalton, AU: arbitrary unit.

4.5 DISCUSSION

In the current study, I used three independent methods to assess kidney oxygenation during the first week of development of Ad-CKD. I found no evidence of hypoxia in the renal cortex of adenine-treated rats, as assessed either by Clark electrode in anesthetized rats at the end of a 7 day treatment period, by radiotelemetry in unanesthetized rats across the course of the 7 day treatment period, or by post-mortem assessment of HIF-1 α and HIF-2 α protein expression. Similarly, I found no evidence of hypoxia in the renal medulla using radiotelemetry or post-mortem assessment of HIF-1 α and HIF-2 α protein expression. In contrast, in anesthetized rats I found that medullary tissue PO₂, measured by Clark electrode, was less in adenine-treated than vehicle-treated rats. However, our observations in rats instrumented with radio-telemeters indicate that this observation could be confounded by the effects of anesthesia and laparotomy. Critically, impairment of renal function and interstitial fibrosis were found to be present as early as 7 days after commencement of adenine treatment. Thus, renal tissue hypoxia might not be an early characteristic of Ad-CKD so may not be a primary driver of pathology in this model.

Renal tissue hypoxia is not a prominent feature during the first 7 days of development of Ad-CKD. Using radio-telemetry in unanesthetized rats, I found that tissue PO₂ in both the cortex and medulla was maintained across a 7 day treatment period. This observation does not support the hypothesis that renal tissue hypoxia precedes renal pathology, at least in this experimental model of CKD. Our failure to detect hypoxia using radiotelemetry is unlikely to be due to a deficit in the sensitivity of the method. As we have shown previously (30), we could detect tissue hypoxia and hyperoxia in the rats we studied when they were subjected to acute changes in inspired oxygen content. Furthermore, Emans and colleagues were able to detect cortical tissue hypoxia as early as 15 h after activation of the renin-angiotensin system in a rat model of angiotensin II-dependent hypertensive CKD (8). Thus, cortical tissue hypoxia associated with activation of the renin-angiotensin system was apparent in unanesthetized rats well before the development of renal injury (29). Our current findings indicate that this is not the case for Ad-CKD.

The absence of renal tissue hypoxia in the early stages of Ad-CKD could be due to relatively well-balanced changes in renal DO₂ and VO₂. Renal DO₂ is the product of total RBF and the quantity of oxygen carried in arterial blood (10). In this current study, I determined that RBF (indexed to kidney weight) in adenine-treated rats was approximately half that of vehicle-treated rats, whereas blood hemoglobin concentration and both arterial PO₂ and SO₂ were similar to that in vehicle-treated rats. Thus, renal ischemia is the major factor driving the deficit in renal DO₂ in the early

stages of Ad-CKD. Previous studies have demonstrated deficits in RBF (27, 54) and anemia (51) in Ad-CKD when rats were treated with adenine for longer periods (i.e. 2 weeks or more). However, to our knowledge our current observations represent the first available quantification of renal DO_2 and VO_2 in Ad-CKD. Critically, our findings indicate that renal VO_2 is also reduced in Ad-CKD, to a similar extent to the deficit in DO_2 . It is also relevant to consider that renal tissue hypoxia observed in other models of CKD has consistently been found to be associated with imbalanced changes in DO_2 and VO_2 . For example, renal tissue hypoxia in polycystic kidney disease is associated with reduced renal DO_2 but little reduction in renal VO_2 (47). Furthermore, renal cortical hypoxia associated with intravenous infusion of angiotensin II was found to be associated with decreased renal DO_2 but relatively well-maintained renal VO_2 (8). Indeed, renal hypoxia is associated with disruption of the balance between renal DO_2 and VO_2 in multiple forms of CKD and acute kidney injury (6, 33, 50, 62). Consistent with the concept that kidney tissue oxygenation is governed by the balance between local tissue DO_2 and consumption VO_2 (12), our current findings indicate that the relative preservation of renal tissue PO_2 within the first 7 days of adenine treatment may be due to the fact that the deficit in renal VO_2 (65%) matched the deficit in DO_2 (51%).

The very marked deficit in GFR I observed in rats treated with adenine (66%) likely provided some protection against development of renal hypoxia by limiting renal VO_2 (which was reduced by 65%). We recently observed a very similar scenario in rats during the sub-acute phase of severe renal ischemia-reperfusion injury (48). That is, renal tissue hypoxia could not be detected and both GFR and renal VO_2 were significantly reduced. There is a close association between renal VO_2 and GFR (52, 59), as the latter determines the tubular sodium load and thus tubular sodium reabsorption (11). For example, Redfors and colleagues found, in human patients after cardiac surgery, that increased GFR after administration of mannitol was associated with increased tubular sodium reabsorption and renal VO_2 (52). Thus, one could envisage scenarios in which renal tissue is normoxic, hypoxic, or even hyperoxic at various stages during development and progression of both acute kidney injury and CKD, depending on the relative changes in DO_2 and VO_2 and their determinants (13). For local tissue oxygen delivery, determinants include RBF and the intrarenal distribution of perfusion, blood hemoglobin concentration and arterial PO_2 . For VO_2 , determinants include total sodium reabsorption and the distribution of tubular reabsorption across the various nephron segments, and the metabolic efficiency of tubular sodium reabsorption. The latter, in turn, depends on a range of factors including the degree of damage to the integrity and polarity of endothelial cells and the presence of oxidative stress (13).

I could not detect renal medullary hypoxia in the first week of Ad-CKD in unanesthetized rats, using telemetry. However, in anesthetized rats medullary tissue PO₂ measured by Clark electrode was less after 7 days of adenine treatment than in corresponding vehicle-treated rats. How can we explain the difference between these two sets of findings? One possibility is that anesthesia and subsequent laparotomy confounded our measurements made with Clark electrodes. In rats equipped for radio-telemetric measurement of cortical or medullary tissue PO₂ I found that both cortical and medullary tissue PO₂ were reduced by anesthesia and laparotomy. Importantly, medullary tissue PO₂ fell more after laparotomy in adenine-treated rats than vehicle-treated rats. It is well established that anesthetic agents, including barbiturates such as pentobarbital and thiobutabarbital, can depress systemic and renal hemodynamics during the time of anesthesia and after skin incision (3, 4, 60, 61). It is also likely that laparotomy can alter neurohumoral function. Regardless, our current findings suggest that the relative hypoxia in the renal medulla of adenine-treated rats, as measured by Clark electrode under anesthesia, may not reflect the situation in conscious animals.

The recognition that anesthesia and laparotomy markedly reduce both cortical and medullary tissue PO₂ is important because, until recently, the only available direct measurements of renal tissue PO₂ had been made in anesthetized animals and man. Telemetric methods are now available, such as the system used in the current study. However, this method is limited by the fact that it is not really possible to generate a reliable estimate of absolute tissue PO₂. Rather, this method really only allows changes in tissue PO₂ to be assessed. Similarly, blood oxygen level dependent magnetic resonance imaging (BOLD-MRI) really only provides a measure of blood oxygenation within kidney tissue (15), which may vary independently of tissue PO₂ (14). Nevertheless, it is now possible to directly measure renal tissue PO₂ in conscious, albeit large, animals using fiber-optic probes (5). Further development and use of methods for monitoring renal tissue oxygenation in conscious animals, and the extension of their use to smaller species such as rats, should lead to considerable advances in our knowledge of the physiology and pathophysiology of renal oxygenation.

Under normoxic conditions, oxygen regulated HIF- α subunits are constitutively expressed and subsequently degraded by the ubiquitin-proteasome system (57). Consequently, hypoxia is often associated with increased tissue expression of HIF- α protein ((16, 53). In our current study, renal expression of HIF-2 α protein did not differ between adenine-treated and vehicle-treated rats. Moreover, HIF-1 α protein was downregulated in kidneys of adenine-treated rats. These

observations are consistent with our overall conclusion that renal tissue is not hypoxic during the first 7 days of Ad-CKD. The marked downregulation of HIF-1 α throughout the kidney in Ad-CKD is of particular interest because it indicates that oxygen-independent pathways might be important in regulating HIF activity in early Ad-CKD. We were unable to investigate the nature of these oxygen-independent pathways, which could conceivably lead to reduced HIF-1 α synthesis by reducing the expression of its gene, or increased rate of breakdown of HIF-1 α . Some examples of the latter have recently been identified. For example, Koh and colleagues found that hypoxia-associated factor (HAF), an E3 ubiquitin ligase, binds to HIF-1 α but not HIF-2 α and initiates its proteasomal degradation by oxygen independent mechanism (32). Furthermore, multiple lines of evidence indicate that post-translational modification of HIF-subunits at specific residues, such as phosphorylation (21) and acetylation (24, 25) may affect HIF protein stability and transactivation activity.

Renal dysfunction appears to precede the development of renal tissue hypoxia in Ad-CKD. We previously found evidence of hypoxia, assessed by pimonidazole adduct immunohistochemistry, after 14 days of treatment with adenine (Chapters 2 and 3). However, in the current study, using multiple methods, I have provided compelling evidence that tissue hypoxia is not present after 7 days of adenine treatment. Nevertheless, administration of adenine caused kidney dysfunction by day 7, as manifested by the presence of marked increases in the plasma concentrations of urea (282%) and creatinine (183%), along with decreased GFR measured by inulin clearance. In addition, pathological changes were visible at the tissue level after 7 days of adenine treatment as reflected by interstitial fibrosis and tubular dilatation, in accord with similar, but more marked, changes observed in rats treated with adenine for 14 days (22). Presumably, the pathophysiological mechanisms underlying the development of renal dysfunction are dominated by the influence of tubular obstruction caused by tubular casts (probably 2,8-dihydroxyadenine crystals) as shown in H & E stained kidney sections in our current report and previously by others (64, 65). In gentamicin-induced acute renal failure, proximal tubular free-flow pressure (intratubular hydrostatic pressure), measured by micropuncture, was found to be increased in association with reduced tubular flow (43). The tubular obstruction and higher intratubular hydrostatic pressure would be expected to lower the net hydraulic pressure gradient across the glomerular capillary wall and thereby decrease GFR (56). Thus, the renal tubular obstruction observed in the early stages of Ad-CKD in the current study might be a major cause of reduced GFR and thus reduced excretion of uremic toxins.

Our study has several strengths and limitations. The radio-telemetric technique I used to measure renal tissue PO₂ provided relatively stable and reproducible measurements of cortical or medullary tissue PO₂ in the absence of confounding effects of anesthesia. In addition, I showed that the technique could detect acute changes in medullary tissue PO₂ induced by systemic hypoxia and hyperoxia. These observations are consistent with those of previous studies in unrestrained rats (8, 30). However, we can only measure renal tissue PO₂ in one site in each animal and tissue PO₂ can be expressed only in relative terms. I was also unable to measure renal DO₂ and VO₂ in unanesthetized rats, so measured these variables in rats under barbiturate anesthesia. This experiment also allowed us to deploy a Clark electrode to generate a spatial profile of renal tissue PO₂. Nevertheless, anesthesia may confound the measurement of renal tissue PO₂, particularly in the medulla. Together, use of Clark electrodes and radiotelemetry enabled us to establish both temporal and spatial profiles of renal tissue PO₂ during the early stages of Ad-CKD. For technical reasons I could not determine renal sodium clearance and consequently changes in total sodium reabsorption. Nonetheless, it seems reasonable to conclude that the major cause of the 65.2% reduction in renal VO₂ in anesthetized adenine-treated rats was probably reduced sodium reabsorption as a consequence of the 65.5% reduction in GFR. Furthermore, our quantification of the protein levels of HIF-1 α and HIF-2 α also indicate that renal hypoxia is not present in the early stages of Ad-CKD. However, interpretation of these observations must be tempered by the recognition that factors other than tissue PO₂, which I was unable to interrogate in the current study, also contribute to the regulation of HIF signaling (26).

Our current findings provide evidence against a role for renal hypoxia in the initial stages of Ad-CKD, but cannot be generalized to other forms of CKD. For example, Manotham and coworkers (36) demonstrated the presence of renal tubular hypoxia in the early stages of the remnant kidney model of CKD, before any histological evidence of tubulointerstitial damage could be observed. This was indicated by the presence of positive staining for pimonidazole adducts, upregulation of expression of HIF-1 α protein, and by increased transcription of hypoxia target genes (36). Similarly, Matsumoto *et al* provided evidence of tubular hypoxia in the early stage of model of rat glomerulonephritis (37). In that study, the overall structure of the renal tubules was observed to remain normal during the evolution of renal hypoxia. Renal tissue hypoxia has also been observed before the onset of nephropathy in diabetic mice (23) and in rats in which the renin-angiotensin system was activated (8). Nevertheless, the observation of an association between hypoxia and later development of CKD does not demonstrate causation. Furthermore, the absence of renal tissue

hypoxia in the early stages of Ad-CKD does not rule out a role for hypoxia in the later progression of this disease.

In conclusion, our present findings indicate that renal tissue hypoxia does not precede renal dysfunction in the early stages of Ad-CKD. The relative preservation of renal tissue PO_2 in this model might be a consequence of the well maintained balance between renal DO_2 and VO_2 . Our findings also provide further evidence that anesthesia can confound measurement of renal tissue PO_2 .

4.6 REFERENCES

1. **Abdelkader A, Ho J, Ow CP, Eppel GA, Rajapakse NW, Schlaich MP, and Evans RG.** Renal oxygenation in acute renal ischemia-reperfusion injury. *Am J Physiol Renal Physiol* 306: F1026-1038, 2014.
2. **Babickova J, Klinkhammer BM, Buhl EM, Djudjaj S, Hoss M, Heymann F, Tacke F, Floege J, Becker JU, and Boor P.** Regardless of etiology, progressive renal disease causes ultrastructural and functional alterations of peritubular capillaries. *Kidney Int* 91: 70-85, 2017.
3. **Blake DW, Way D, Trigg L, Langton D, and McGrath BP.** Cardiovascular effects of volatile anesthesia in rabbits: influence of chronic heart failure and enalaprilat treatment. *Anesth Analg* 73: 441-448, 1991.
4. **Calzavacca P, Bailey M, Velkoska E, Burrell LM, Ramchandra R, Bellomo R, and May CN.** Effects of renal denervation on regional hemodynamics and kidney function in experimental hyperdynamic sepsis. *Crit Care Med* 42: e401-409, 2014.
5. **Calzavacca P, Evans RG, Bailey M, Lankadeva YR, Bellomo R, and May CN.** Long-term measurement of renal cortical and medullary tissue oxygenation and perfusion in unanesthetized sheep. *Am J Physiol Regul Integr Comp Physiol* 308: R832-839, 2015.
6. **Deng A, Tang T, Singh P, Wang C, Satriano J, Thomson SC, and Blantz RC.** Regulation of oxygen utilization by angiotensin II in chronic kidney disease. *Kidney Int* 75: 197-204, 2009.
7. **Ding A, Kalaighanasundaram P, Ricardo SD, Abdelkader A, Witting PK, Broughton BR, Kim HB, Wyse BF, Phillips JK, and Evans RG.** Chronic treatment with tempol does not significantly ameliorate renal tissue hypoxia or disease progression in a rodent model of polycystic kidney disease. *Clin Exp Pharmacol Physiol* 39: 917-929, 2012.
8. **Emans TW, Janssen BJ, Pinkham MI, Ow CP, Evans RG, Joles JA, Malpas SC, Krediet CT, and Koeners MP.** Exogenous and endogenous angiotensin-II decrease renal cortical oxygen tension in conscious rats by limiting renal blood flow. *J Physiol* 594: 6287-6300, 2016.
9. **Engle SJ, Stockelman MG, Chen J, Boivin G, Yum MN, Davies PM, Ying MY, Sahota A, Simmonds HA, Stambrook PJ, and Tischfield JA.** Adenine phosphoribosyltransferase-deficient mice develop 2,8-dihydroxyadenine nephrolithiasis. *Proc Natl Acad Sci* 93: 5307-5312, 1996.
10. **Evans RG, Gardiner BS, Smith DW, and O'Connor PM.** Methods for studying the physiology of kidney oxygenation. *Clin Exp Pharmacol Physiol* 35: 1405-1412, 2008.
11. **Evans RG, Harrop GK, Ngo JP, Ow CP, and O'Connor PM.** Basal renal O₂ consumption and the efficiency of O₂ utilization for Na⁺ reabsorption. *Am J Physiol Renal Physiol* 306: F551-560, 2014.
12. **Evans RG, Ince C, Joles JA, Smith DW, May CN, O'Connor PM, and Gardiner BS.** Haemodynamic influences on kidney oxygenation: clinical implications of integrative physiology. *Clin Exp Pharmacol Physiol* 40: 106-122, 2013.
13. **Evans RG, Lankadeva YR, Cochrane AD, Marino B, Iguchi N, Zhu MZL, Hood SG, Smith JA, Bellomo R, Gardiner BS, Lee CJ, Smith DW, and May CN.** Renal haemodynamics and oxygenation during and after cardiac surgery and cardiopulmonary bypass. *Acta Physiol* 222: 2018.
14. **Evans RG, Leong CL, Anderson WP, and O'Connor PM.** Don't be so BOLD: Potential limitations in the use of BOLD MRI for studies of renal oxygenation. *Kidney Int* 71: 1327-1328, 2007.
15. **Evans RG, Smith JA, Gardiner BS, Smith DW, Thrift AG, May CN, Lankadeeva YR, and Cochrane AD.** Hypoxia as a Biomarker of Kidney Disease. In: *Biomarkers in Kidney Disease*, edited by Patel VB. Dordrecht: Springer Netherlands, 2015, p. 1-23.

16. **Fahling M, Mathia S, Scheidl J, Abramovitch R, Milman Z, Paliege A, Peters H, Persson PB, Heyman SN, and Rosenberger C.** Cyclosporin a induces renal episodic hypoxia. *Acta Physiol* 219: 625-639, 2017.
17. **Fine LG, Bandyopadhyay D, and Norman JT.** Is there a common mechanism for the progression of different types of renal diseases other than proteinuria? Towards the unifying theme of chronic hypoxia. *Kidney Int* 57: S22-S26, 2000.
18. **Fine LG, and Norman JT.** Chronic hypoxia as a mechanism of progression of chronic kidney diseases: from hypothesis to novel therapeutics. *Kidney Int* 74: 867-872, 2008.
19. **Fine LG, Ong AC, and Norman JT.** Mechanisms of tubulo-interstitial injury in progressive renal diseases. *Eur J Clin Invest* 23: 259-265, 1993.
20. **Fine LG, Orphanides C, and Norman JT.** Progressive renal disease: the chronic hypoxia hypothesis. *Kidney Int Suppl* 65: S74-78, 1998.
21. **Flugel D, Gorlach A, Michiels C, and Kietzmann T.** Glycogen synthase kinase 3 phosphorylates hypoxia-inducible factor 1alpha and mediates its destabilization in a VHL-independent manner. *Mol Cell Biol* 27: 3253-3265, 2007.
22. **Fong D, Ullah MM, Lal JG, Abdelkader A, Ow CP, Hilliard LM, Ricardo SD, Kelly DJ, and Evans RG.** Renal cellular hypoxia in adenine-induced chronic kidney disease. *Clin Exp Pharmacol Physiol* 43: 896-905, 2016.
23. **Franzen S, Pihl L, Khan N, Gustafsson H, and Palm F.** Pronounced kidney hypoxia precedes albuminuria in type 1 diabetic mice. *Am J Physiol Renal Physiol* 310: F807-809, 2016.
24. **Geng H, Harvey CT, Pittsenbarger J, Liu Q, Beer TM, Xue C, and Qian DZ.** HDAC4 protein regulates HIF1alpha protein lysine acetylation and cancer cell response to hypoxia. *J Biol Chem* 286: 38095-38102, 2011.
25. **Geng H, Liu Q, Xue C, David LL, Beer TM, Thomas GV, Dai MS, and Qian DZ.** HIF1alpha protein stability is increased by acetylation at lysine 709. *J Biol Chem* 287: 35496-35505, 2012.
26. **Haase VH.** Hypoxia-inducible factors in the kidney. *Am J Physiol Renal Physiol* 291: F271-281, 2006.
27. **Johns EJ, and Rutkowski B.** The action of atriopeptin III on renal function in two models of chronic renal failure in the rat. *Br J Pharmacol* 99: 317-322, 1990.
28. **Kaartinen K, Hemmila U, Salmela K, Raisanen-Sokolowski A, Kouri T, and Makela S.** Adenine phosphoribosyltransferase deficiency as a rare cause of renal allograft dysfunction. *J Am Soc Nephrol* 25: 671-674, 2014.
29. **Kantachuvesiri S, Fleming S, Peters J, Peters B, Brooker G, Lammie AG, McGrath I, Kotelevtsev Y, and Mullins JJ.** Controlled hypertension, a transgenic toggle switch reveals differential mechanisms underlying vascular disease. *J Biol Chem* 276: 36727-36733, 2001.
30. **Koeners MP, Ow CP, Russell DM, Abdelkader A, Eppel GA, Ludbrook J, Malpas SC, and Evans RG.** Telemetry-based oxygen sensor for continuous monitoring of kidney oxygenation in conscious rats. *Am J Physiol Renal Physiol* 304: F1471-1480, 2013.
31. **Koeners MP, Ow CPC, Russell DM, Evans RG, and Malpas SC.** Prolonged and continuous measurement of kidney oxygenation in conscious rats. *Methods Mol Biol* 1397: 93-111, 2016.
32. **Koh MY, Darnay BG, and Powis G.** Hypoxia-associated factor, a novel E3-ubiquitin ligase, binds and ubiquitinates hypoxia-inducible factor 1 α , leading to its oxygen-independent degradation. *Mol Biol Cell* 28: 7081-7095, 2008.
33. **Legrand M, Almac E, Mik EG, Johannes T, Kandil A, Bezemer R, Payen D, and Ince C.** L-NIL prevents renal microvascular hypoxia and increase of renal oxygen consumption after ischemia-reperfusion in rats. *Am J Physiol Renal Physiol* 296: F1109-1117, 2009.
34. **Liu J, Wei Q, Guo C, Dong G, Liu Y, Tang C, and Dong Z.** Hypoxia, HIF, and associated signaling networks in chronic kidney disease. *Int J Mol Sci* 18: 2017.

35. **Ludbrook J.** Repeated measurements and multiple comparisons in cardiovascular research. *Cardiovasc Res* 28: 303-311, 1994.
36. **Manotham K, Tanaka T, Matsumoto M, Ohse T, Miyata T, Inagi R, Kurokawa K, Fujita T, and Nangaku M.** Evidence of tubular hypoxia in the early phase in the remnant kidney model. *J Am Soc Nephrol* 15: 1277-1288, 2004.
37. **Matsumoto M, Tanaka T, Yamamoto T, Noiri E, Miyata T, Inagi R, Fujita T, and Nangaku M.** Hypoperfusion of peritubular capillaries induces chronic hypoxia before progression of tubulointerstitial injury in a progressive model of rat glomerulonephritis. *J Am Soc Nephrol* 15: 1574-1581, 2004.
38. **Milman Z, Axelrod JH, Heyman SN, Nachmansson N, and Abramovitch R.** Assessment with unenhanced MRI techniques of renal morphology and hemodynamic changes during acute kidney injury and chronic kidney disease in mice. *Am J Nephrol* 39: 268-278, 2014.
39. **Mulay SR, and Anders HJ.** Crystal nephropathies: mechanisms of crystal-induced kidney injury. *Nat Rev Nephrol* 13: 226-240, 2017.
40. **Nangaku M.** Chronic hypoxia and tubulointerstitial injury: a final common pathway to end-stage renal failure. *J Am Soc Nephrol* 17: 17-25, 2006.
41. **Nangaku M, and Eckardt KU.** Hypoxia and the HIF system in kidney disease. *J Mol Med* 85: 1325-1330, 2007.
42. **Nasr SH, Sethi S, Cornell LD, Milliner DS, Boelkins M, Broviac J, and Fidler ME.** Crystalline nephropathy due to 2,8-dihydroxyadeninuria: an under-recognized cause of irreversible renal failure. *Nephrol Dial Transplant* 25: 1909-1915, 2010.
43. **Neugarten J, Aynedjian HS, and Bank N.** Role of tubular obstruction in acute renal failure due to gentamicin. *Kidney Int* 24: 330-335, 1983.
44. **Norman JT, and Fine LG.** Intrarenal oxygenation in chronic renal failure. *Clin Exp Pharmacol Physiol* 33: 989-996, 2006.
45. **Ohashi R, Kitamura H, and Yamanaka N.** Peritubular capillary injury during the progression of experimental glomerulonephritis in rats. *J Am Soc Nephrol* 11: 47-56, 2000.
46. **Ow CP.** Renal Tissue Hypoxia in Kidney Diseases. PhD Thesis. Monash University, 2017.
47. **Ow CP, Abdelkader A, Hilliard LM, Phillips JK, and Evans RG.** Determinants of renal tissue hypoxia in a rat model of polycystic kidney disease. *Am J Physiol Regul Integr Comp Physiol* 307: R1207-1215, 2014.
48. **Ow CPC, Ngo JP, Ullah MM, Barsha G, Meex RCR, Watt MJ, Hilliard LM, Koeners MP, and Evans RG.** Absence of renal hypoxia in the subacute phase of severe renal ischemia reperfusion injury. *Am J Physiol Renal Physiol* 315: F1358-F1369, 2018.
49. **Ow CPC, Ngo JP, Ullah MM, Hilliard LM, and Evans RG.** Renal hypoxia in kidney disease: Cause or consequence? *Acta Physiol* 222: e12999, 2018.
50. **Palm F, Cederberg J, Hansell P, Liss P, and Carlsson PO.** Reactive oxygen species cause diabetes-induced decrease in renal oxygen tension. *Diabetologia* 46: 1153-1160, 2003.
51. **Rahman A, Yamazaki D, Sufiun A, Kitada K, Hitomi H, Nakano D, and Nishiyama A.** A novel approach to adenine-induced chronic kidney disease associated anemia in rodents. *PLoS One* 13: e0192531, 2018.
52. **Redfors B, Sward K, Sellgren J, and Ricksten SE.** Effects of mannitol alone and mannitol plus furosemide on renal oxygen consumption, blood flow and glomerular filtration after cardiac surgery. *Intensive Care Med* 35: 115-122, 2009.
53. **Rosenberger C, Khamaisi M, Abassi Z, Shilo V, Weksler-Zangen S, Goldfarb M, Shina A, Zibertrest F, Eckardt KU, Rosen S, and Heyman SN.** Adaptation to hypoxia in the diabetic rat kidney. *Kidney Int* 73: 34-42, 2008.
54. **Saeed A, DiBona GF, Grimberg E, Nguy L, Mikkelsen ML, Marcussen N, and Guron G.** High-NaCl diet impairs dynamic renal blood flow autoregulation in rats with adenine-induced chronic renal failure. *Am J Physiol Regul Integr Comp Physiol* 306: R411-419, 2014.

55. **Santana AC, Degaspari S, Catanozi S, Delle H, de Sa Lima L, Silva C, Blanco P, Solez K, Scavone C, and Noronha IL.** Thalidomide suppresses inflammation in adenine-induced CKD with uraemia in mice. *Nephrol Dial Transplant* 28: 1140-1149, 2013.
56. **Selkurt EE, Deetjen P, and Brechtelsbauer H.** Tubular pressure gradients and filtration dynamics during urinary stop flow in the rat. *Pflugers Arch Gesamte Physiol Menschen Tiere* 286: 19-35, 1965.
57. **Semenza GL.** HIF-1, O₂, and the 3 PHDs: how animal cells signal hypoxia to the nucleus. *Cell* 107: 1-3, 2001.
58. **Shapiro SS, and Wilk MB.** An analysis of variance test for normality (complete samples). *Biometrika* 52: 591-611, 1965.
59. **Sward K, Valsson F, Sellgren J, and Ricksten SE.** Differential effects of human atrial natriuretic peptide and furosemide on glomerular filtration rate and renal oxygen consumption in humans. *Intensive Care Med* 31: 79-85, 2005.
60. **Walker LA, Buscemi-Bergin M, and Gellai M.** Renal hemodynamics in conscious rats: effects of anesthesia, surgery, and recovery. *Am J Physiol* 245: F67-74, 1983.
61. **Walker LA, Gellai M, and Valtin H.** Renal response to pentobarbital anesthesia in rats: effect of interrupting the renin-angiotensin system. *J Pharmacol Exp Ther* 236: 721-728, 1986.
62. **Welch WJ, Baumgärtl H, Lübbers D, and Wilcox CS.** Renal oxygenation defects in the spontaneously hypertensive rat: Role of AT1 receptors. *Kidney Int* 63: 202-208, 2003.
63. **Wyngaarden JB, and Dunn JT.** 8-Hydroxyadenine as the intermediate in the oxidation of adenine to 2, 8-dihydroxyadenine by xanthine oxidase. *Arch Biochem Biophys* 70: 150-156, 1957.
64. **Yokozawa T, Zheng PD, Oura H, and Koizumi F.** Animal model of adenine-induced chronic renal failure in rats. *Nephron* 44: 230-234, 1986.
65. **Zhao YY, Cheng XL, Wei F, Xiao XY, Sun WJ, Zhang Y, and Lin RC.** Serum metabolomics study of adenine-induced chronic renal failure in rats by ultra performance liquid chromatography coupled with quadrupole time-of-flight mass spectrometry. *Biomarkers* 17: 48-55, 2012.

CHAPTER 5

TRANSCUTANEOUS MEASUREMENT OF GLOMERULAR FILTRATION RATE IN CONSCIOUS RATS DURING THE PROGRESSION OF STREPTOZOTOCIN-INDUCED TYPE 1 DIABETES

5.1 ABSTRACT

I hypothesized that glomerular hyperfiltration is an early and sustained event in streptozotocin (STZ)-induced diabetes that could contribute to the renal tissue hypoxia observed in this model of type 1 diabetes. To test this hypothesis I employed a transcutaneous technique to measure the clearance of fluorescein isothiocyanate-abelled (FITC)-sinistrin in conscious, free moving rats across a 4 week experimental protocol. I compared four different kinetic models to calculate the excretion half-life ($t_{1/2}$) of FITC-sinistrin and thus allow estimation of glomerular filtration rate (GFR). This included a one-compartment kinetic model (1-COM), a two-compartment kinetic model (2-COM), a three-compartment kinetic model (3-COM) and a three-compartment kinetic model with baseline correction (3-COMB). Glomerular hyperfiltration was detected in STZ-induced diabetes by using either the 2-COM model or the 3-COMB model at day 14 and by using the 3-COM model at day 3 and 14, after induction of diabetes. However, glomerular hyperfiltration could not be detected using the 1-COM model at any time across the four week experimental protocol. From a theoretical perspective I reasoned that the 3-COMB model provides a better estimate of $t_{1/2}$ than the three other models. Linear regression analysis of the data generated using the 3-COMB model showed a statistically significant relationship between blood glucose and calculated GFR at the day 14 ($P = 0.004$) and day 28 ($P = 0.01$) time-points, along with a strong tendency for a relationship at the day 3 time-point ($P = 0.06$). In addition, there was no evidence of renal dysfunction as shown by the absence of significant albuminuria and interstitial fibrosis four weeks post-induction of diabetes in STZ-diabetic rats. Thus, it seems reasonable to conclude that hyperfiltration is an early and persistent phenomenon in the STZ model of type 1 diabetes in rats that may contribute to the development of renal tissue hypoxia.

5.2 INTRODUCTION

There is evidence that renal tissue hypoxia is an early and persistent event in diabetes (8, 38). Renal hypoxia was detected in anesthetized rats with STZ-induced diabetes within two days of STZ administration, both by direct measurement of tissue oxygen tension using fiber optic probes and by blood-oxygen-level dependent magnetic resonance imaging (BOLD-MRI) (8). In these animals renal hypoxia persisted 5, 14, and 28 days after induction of diabetes. Recently, Franzen and colleagues detected cortical tissue hypoxia in anesthetized mice, by 3 days after induction of diabetes with STZ, using electron paramagnetic resonance oximetry (14). Tissue hypoxia in these mice persisted until the end of the experimental protocol, 2 weeks after administration of STZ.

Glomerular hyperfiltration might be a potential contributing factor to development of renal tissue hypoxia in diabetes (34). Glomerular hyperfiltration is thought to be driven by increased proximal tubular reabsorption of electrolytes (Na^+ , Cl^- , and K^+), which has been observed in both experimental models of diabetes mellitus (37, 50, 51) and human patients with insulin-dependent diabetes mellitus (IDDM) (20, 53). This increased reabsorption of electrolytes in the proximal tubule (51) appears to diminish the tubuloglomerular feedback response (49), resulting in an increased single nephron glomerular filtration rate (GFR). Furthermore, increased reabsorption in the proximal tubule could lower the glomerular hydrostatic pressure in Bowman's space (26, 51). This reduction of hydrostatic pressure may also contribute to glomerular hyperfiltration by increased net filtration pressure (26, 51). Under normal physiological conditions, approximately 80% of the oxygen utilization in the kidney is for reabsorption of Na^+ (9). Thus, the increased filtered load of Na^+ associated with hyperfiltration would be expected to increase oxygen utilization in the proximal tubule, thus promoting the development of tissue hypoxia.

Hyperfiltration is a characteristic of experimental type 1 diabetes (24, 25, 43, 51), but the time-point at which it occurs in the progression of the disease remains controversial. For example, Bak and colleagues observed glomerular hyperfiltration at day 7 after STZ administration using the steady state constant infusion technique in unanesthetized rats (2). In that study GFR was measured across the 7 days after induction of diabetes. Similarly, Tucker *et al* found that GFR was significantly greater 24 hours after STZ administration and remained increased across the 15 days of their experimental protocol (47). In contrast, in two other studies glomerular hyperfiltration could not be detected in STZ-diabetic rats, either with the steady state constant infusion technique (11) or the single injection technique (35), across the 3-4 week experimental protocol. However, in one of those studies, a significant elevation in GFR was detected in STZ-diabetic rats when GFR

was indexed to body weight (35). Thus, the precise time-course of development of glomerular hyperfiltration in conscious rats after induction of diabetes remains controversial. Furthermore, the techniques used to assess GFR in those studies require surgical preparation for catheter implantation, collection of multiple blood and/or urine samples and laboratory analysis of those samples in order to calculate GFR (2, 7). Thus the techniques are invasive, cumbersome and time consuming.

In the current study, I used transcutaneous measurement of fluorescein isothiocyanate (FITC)–sinistrin clearance in conscious rats to test the hypothesis that glomerular hyperfiltration is an early and sustained event in type 1 diabetes. If this hypothesis is correct, our findings could provide the basis for further studies to investigate the mechanistic link between hyperfiltration and hypoxia in the diabetic kidney. The transcutaneous based measurement of GFR involves injection of FITC–sinistrin and detection of the clearance of this marker in a conscious animal by a transcutaneous device (17, 21, 40, 42). This technique has advantages over traditional clearance-based techniques, including the fact that no blood or urine samples are required, no further time consuming laboratory analysis is required, and GFR can be calculated immediately after completion of the clearance procedure (32, 41). Nevertheless, this technique does have limitations, most notably the fact that specific mathematical models must be applied to the data generated by measurement of the clearance of FITC–sinistrin, in order to generate the excretion half-life ($t_{1/2}$) value from which GFR is calculated (17, 42). Thus, assumptions must be made regarding the distribution of FITC–sinistrin within the various fluid compartments (15). Consideration of the impact of these assumptions on the values of GFR determined in diabetic and non-diabetic rats may thus help us more precisely define the time-course of hyperfiltration in experimental type 1 diabetes.

In the current study I employed four different mathematical models of FITC–sinistrin clearance: a one compartment kinetic model (1-COM) (16, 41, 42), a two-compartment kinetic model (2-COM) (16, 42), a three-compartment kinetic model (3-COM) (16) and a three-compartment kinetic model with baseline correction (3-COMB) (16, 17), to calculate the $t_{1/2}$ from the data obtained during FITC–sinistrin clearance. Each of these models has inherent limitations. For example, the 1-COM model is based on the assumption that FITC–sinistrin is cleared without distribution throughout the body, which is unlikely to be true (39). The 2-COM and 3-COM models are likely more accurate than the 1-COM model because they incorporate the assumption that FITC–sinistrin is distributed within the extracellular space (16). However, the 1-COM, 2-COM and 3-COM models cannot incorporate the influence of skin auto-fluorescence (10) or changes in skin perfusion (30) that

might arise as a result of attachment of the transcutaneous device, and thus alter the intensity of the signal. These factors might influence the baseline signal generated during transcutaneous measurement and thus influence the calculation of $t_{1/2}$ and the resultant estimate of GFR (17). Recently, Friedemann *et al* showed that the $t_{1/2}$ derived by the 3-COMB model is comparable with that determined by the ‘gold standard’ constant infusion technique (17). This mathematical algorithm describes the complete course of clearance kinetics for FITC-sinistrin which includes the point of injection of the marker, the distribution and mixing of the marker within the blood stream as well as the excretion kinetics of the marker (17). In addition, this 3-COMB model also incorporates automated correction for drifts of the baseline signal. Thus, from a theoretical perspective, this model should provide a more accurate estimate of $t_{1/2}$. I compared these available kinetic models for calculating the clearance of FITC-sinistrin, to determine whether the choice of model could influence the conclusions drawn from our study of the time-course of changes in GFR in experimental type 1 diabetes.

5.3 METHODS

5.3.1 Animals

Sixteen male Sprague Dawley rats, aged 10 weeks, were obtained from the Monash Animal Research Platform (Monash University, Melbourne, Victoria, Australia). The rats were housed individually under standard laboratory conditions; $22 \pm 1^\circ\text{C}$, $40 \pm 1\%$ humidity and with a 12-hour light/dark cycle (06.00–18.00 hours). Rats were allowed free access to water and were fed a sodium-controlled diet (0.25% sodium chloride; Specialty Feeds, Glen Forrest, Western Australia, Australia) *ad libitum*. Experiments were approved by the Animal Ethics Committee of the Monash University Animal Research Platform. The experiments were performed in accordance with the Australian Code of Practice for the Care and Use of Animals for Scientific Purposes. Rats were allowed one week to acclimatize to their housing conditions prior to the commencement of the experimental protocol.

5.3.2 Induction of diabetes

Diabetes was induced in 11 week old male Sprague Dawley rats by a single intravenous injection of STZ (Sigma- Aldrich Pty. Ltd. Castle Hill, NSW, Australia), at a dose of 50 mg/kg body weight, dissolved in 0.1 M citrate buffer at pH 4.5. Vehicle-treated rats received citrate buffer only (1 ml/kg, i.v.). The STZ was administered by tail vein injection under light anesthesia. Rats were

anesthetized with the inhalation anesthetic, isoflurane (IsoFlo™, 05260-05, Abbott Laboratories, IL, USA) maintained at 2.5 – 3.0% (v/v) using a vaporizer. Forty eight hours after injection of STZ, the blood concentration of glucose was measured in the non-fasting state using a glucometer and glucose test strips (Nova Stat Strip Xpress, Nova Biomedical Corporation, Waltham, MA, USA) from blood obtained from a needle prick of the tail vein. Rats with blood glucose >15 mM were considered diabetic.

Insulin therapy: Rats with diabetes were administered insulin (HUMULIN® NPH; Isophane – NPH – human insulin; recombinant DNA origin suspension, Eli Lilly Australia Pty. Limited, NSW, Australia) subcutaneously to maintain a moderately elevated blood concentration of glucose (27 to 28 mM). The specific dose of insulin was titrated according to the measured concentration of blood glucose of each individual rat (Table 5.1).

Table 5.1 Insulin regimen according to the concentration of blood glucose.

Blood glucose concentration	Units of insulin
<27 mM	No insulin
27-28 mM	2 units every second day
28 -31 mM	3 units every second day
32 mM	4 units every second day

For all rats (diabetic and vehicle) in this study, blood glucose concentration was measured at two day intervals until completion of the study.

5.3.3 Experimental protocol



Figure 5.1. Time line of the experimental protocol. Glomerular filtration rate (GFR) of each rat (vehicle or diabetic) was measured at 4 time points across the duration of the study. Baseline GFR

was measured at day -1 (i.e. before administration of streptozotocin (STZ) or the citrate buffer vehicle). GFR was then measured 3, 14 and 28 days after injection of either citrate buffer or STZ.

5.3.4 Measurement of glomerular filtration rate

GFR was estimated in conscious rats by measuring the clearance of FITC-labeled sinistrin (17, 21). Signal intensity of FITC-sinistrin was assessed transcutaneously using a non-invasive clearance (NIC)-Kidney Device (Mannheim Pharma and Diagnostics GmbH, Mannheim, Germany) (17). The battery of the NIC-Kidney Device was charged 24 h before measurement of GFR. The FITC-sinistrin (Fresenius Kabi Austria GmbH, Linz, Austria) solution was prepared by dissolving FITC-sinistrin (5 mg/100 g body weight) in 0.9% w/v sodium chloride solution. It was stored at -20°C , away from light and then thawed on the day of use.

5.3.5 Experimental procedure

Rats were lightly and briefly anesthetized (2.5 – 3.0% v/v isoflurane) and placed on a heated pad to maintain body temperature at 37.5°C . Then, a small area of fur on the flank of the rat, slightly larger than the surface area of the NIC-Kidney device, was removed using an electric shaver followed by application of depilatory cream. This was necessary because rat fur can auto-fluoresce and thus interfere with measurement of the concentration of FITC-sinistrin. Following fur removal, the area of depilatory cream was washed thoroughly and a strip of adhesive tape (Leukosilk® tape; BSN medical GmbH, Hamburg, Germany) was placed beneath the abdomen of the rat. Next, the NIC-Kidney Device was turned on via connection to a lithium polymer rechargeable battery which was adhered to the top of the device with an adhesive sticker. The NIC-Kidney Device-battery unit was then attached to the depilated skin on the back of the rat using a double-sided adhesive patch and adhesive tape. This minimized movement artefacts and prevented the rat from interfering with the device. Before administration of FITC-sinistrin, a 3 minute recording period was allowed to account for the background signal generated within the skin. Then, a bolus of FITC-sinistrin (5 mg/100 g body weight made up in 0.9% w/v sodium chloride solution) was administered via the tail vein. The isoflurane anesthesia was then withdrawn and the rat was kept on a heated pad until it became conscious (usually ~2 min). The rat was returned to an experimental chamber (containing bedding chips from the rat's home cage only) for a period of 2 hours during which the elimination kinetics of FITC-sinistrin were recorded. These chambers were used as they were larger than the rat's home cages and thus reduced the likelihood of dislodgement of the device from the back of the rat. At the end of the recording period, the tape and device were

gently removed from each rat under light isoflurane anesthesia, and the rat was returned to its home cage.

5.3.6 Data analyses

The battery was detached from the device and the device was connected to a computer via a micro USB cable. The data were downloaded as a .csv file, which can be opened and modified in Microsoft Excel and read by the MPD Studio software package (Mannheim Pharma and Diagnostics GmbH, Mannheim, Germany) (17). The software generated the elimination kinetics curve of FITC-sinistrin from which the $t_{1/2}$ of FITC-sinistrin was calculated using mathematically derived models. In this study $t_{1/2}$ was determined using 1-COM (16, 41), 2-COM (16, 42), 3-COM (16, 46) and 3-COMB (16, 17) models. A detailed discussion of the theoretical basis of the various models is given in the Chapter 1, Section 1.5.4, of this thesis. Each model was applied to the kinetics curve of FITC-sinistrin to calculate the $t_{1/2}$ (17, 41, 42, 45). The elimination rate constant (λ), an expression of GFR indexed to extracellular fluid volume, was calculated using the following equation (17).

$$\lambda (\text{minute}^{-1}) = t_{1/2} \times \ln(2)$$

Where, $t_{1/2}$ represents the excretion half-life and $\ln(2)$ is the natural logarithm of 2, which is approximately 0.693.

The $t_{1/2}$ was used for the calculation GFR according to the following formula (17):

$$GFR = \frac{21.33}{t_{1/2}}$$

Where GFR is in the units ml/min/100 g body weight, the numerator 21.33 (ml/100 g body weight) is an empirically derived conversion factor for GFR calculation for rats (17) and $t_{1/2}$ is the excretion half-life of FITC-sinistrin.

5.3.7 Metabolic cage studies

Each rat was housed individually in a metabolic cage for 2-3 hours after each GFR measurement, to obtain urine samples. A day prior to the first study, each rat was housed in a cage for a 6-hour training period for acclimatization. Urine samples were stored at -20°C for later measurement of urinary albumin-to-creatinine ratio (ACR).

At the completion of the experimental protocol, rats were deeply anesthetized by an intraperitoneal injection of sodium pentobarbital (60 mg/kg, Sigma Aldrich, NSW, Australia) and a 1 ml blood sample was collected via cardiac puncture. Blood was centrifuged at 3000 g at 4°C for 10 minutes and the plasma stored at -20°C for later measurement of plasma electrolytes, creatinine and urea. A 2 ml bolus of potassium chloride (7 mM) was then delivered by cardiac puncture to induce death by cardiac arrest. The kidneys and heart were removed from each rat and weighted. The right kidney was flash frozen and the left kidney and heart were fixed in 10% neutral buffered formalin solution.

5.3.8 Analysis of urine and plasma samples

The urinary ACR was quantified using a rat urinary albumin enzyme-linked immunosorbent assay kit (NEPHRAT; Exocell Inc., Suite 200, Philadelphia, PA, USA) and a urinary creatinine assay kit (The Creatinine Companion; Exocell Inc., Suite 200, Philadelphia, PA, USA) according to the manufacturer's instructions. Plasma electrolytes, creatinine and urea were measured using a point-of-care device (iSTAT, Chem8+ Cartridge; Abbot Laboratories, Abbott Park, IL, USA).

5.3.9 Histological assessment of tissue damage and collagen deposition

The formalin fixed kidneys were processed, embedded in paraffin and sectioned at 5 µm. Two sections from each kidney were stained with hematoxylin and eosin (H & E) (1, 13) and picrosirius red (6). All sections were scanned at 40x magnification using Aperio Scan Scope (Aperio, Vista, CA, USA). Quantification of fibrosis in kidney sections processed for picrosirius red staining was performed using the Image Scope Positive Pixel Count Algorithm (Version 9; Aperio). Results are presented as percentage of total area stained with picrosirius red.

5.3.10 Statistical analyses:

Statistical and graphical analyses were performed using the software SYSTAT (Version 13, Systat Software Inc., Chicago, IL, USA) and GraphPad Prism (Version 7, GraphPad Software Inc., La Jolla, CA, USA), respectively. Normality was assessed using the Shapiro-Wilk test (44). Data that did not violate normality are presented as mean ± standard error of the mean (SEM). Data that violated normality were log₁₀-transformed, and after confirmation that these log-transformed data did not violate normality, subjected to parametric statistical analysis. Variables measured at multiple time-points were analyzed using repeated measures analysis of variance (ANOVA), with P values conservatively adjusted using the Greenhouse-Geisser correction (29). To protect against

increased risk of type 1 error from the use of multiple comparisons either Tukey's test (when all possible comparisons were made) or Dunnett's test (when multiple time-points were compared to a control condition) were applied (31). Ordinary least squares regression analysis was performed to determine the linear relationships between concentration of blood glucose and GFR (28). Student's unpaired t-test with Welch's correction was used for dichotomous comparisons. Two sided $P \leq 0.05$ was considered statistically significant.

5.4 RESULTS

5.4.1 Body weight and blood glucose concentrations

The body weight of vehicle-treated rats increased gradually over the four weeks of the protocol, to be $17 \pm 1\%$ greater than its baseline level by 28 days after vehicle injection (Figure 5.2A). In contrast, body weight had decreased in rats with diabetes ($5 \pm 1\%$) by day 3 after injection of STZ and then remained relatively constant for the rest of the period of observation.

Vehicle-treated rats maintained a narrow range of blood glucose concentration (5.4 – 6.0 mM) across the duration of the experimental protocol (Figure 5.2B). In contrast blood glucose concentration had increased 3.7-fold by day 3 after STZ injection and was maintained at this elevated level thereafter.

5.4.2 Glomerular filtration rate

Baseline GFR: Baseline GFR differed significantly according to the model used for calculation of the $t_{1/2}$ of FITC-sinistrin (Figure 5.3). In general, the $t_{1/2}$ was least, while the rate constant and GFR were greater, for the 2-COM model compared to the other models. Indeed, the $t_{1/2}$ calculated by 2-COM was $22.6 \pm 7.6\%$ less than that determined by the 3-COM model while the GFR determined by the 2-COM model was $21.3 \pm 8.8\%$ greater than that determined by the 1-COM model and $22.8 \pm 7.6\%$ greater than that determined by the 3-COM model. Neither the $t_{1/2}$ calculated by the 3-COM model nor the rate constant or GFR determined by the 3-COM model differed significantly from that derived using the other models (1-COM, 2-COM and 3-COM).

Temporal profile of GFR: The profile of changes in GFR across the course of the experimental protocol varied somewhat according to the method used to calculate $t_{1/2}$ (Figure 5.4 and Table 5.2). In vehicle-treated rats, regardless of the method used, $t_{1/2}$ and so consequently both the rate constant and calculated GFR, remained relatively stable across the four week period of observation. The

only exceptions were for the 28-day time-point, at which time $t_{1/2}$ was significantly greater than baseline according to the 2-COMB and 3COMB models but not the 1-COM or 3-COM models. In contrast, after administration of STZ, $t_{1/2}$ fell and the rate constant and GFR increased when the 2COM, 3-COM or 3-COMB methods were used, although no significant changes were detected when the 1-COM method was used. The time-points at which these changes became statistically significant differed according to the method used to calculate GFR. The increase from baseline was significant only at the 14 day time point for the 2-COM ($46.8 \pm 26.8\%$) and 3-COMB ($32.7 \pm 9.6\%$) models. However, it was significant at both the 3 day ($29.3 \pm 11.6\%$) and 14 day ($43.4 \pm 11.6\%$) time points when the 3-COM method was used. At the 28 day time-point, no significant difference in GFR, from baseline, was detected with any of the four models.

During transcutaneous measurement of FITC-sinistrin, the intensity of the fluorescent signal can be influenced by skin autofluorescence and changes of skin perfusion induced by attachment of device (30). These factors might affect the baseline signal generated by the device and thus influence the actual value of GFR. The 3-COMB model provides automated correction for baseline drift (17). Theoretically, a model that both corrects for changes in baseline signal and incorporates a more realistic set of assumptions about the nature of the compartments that FITC-sinistrin is distributed in, should be superior to the 1-COM, 2-COM and 3-COM models. Therefore, data obtained by the 3-COMB model were subjected to linear regression analysis to determine the relationship between blood glucose concentration and GFR.

Relationship between concentration of blood glucose and glomerular filtration rate: Linear regression established positive relationships between blood glucose concentration and GFR in vehicle-treated and STZ-diabetic rats (Figure 5.5). The proportion of the variance in calculated GFR, explained by these relationships, was least on day 3 (22%) and most at day 14 (45%).

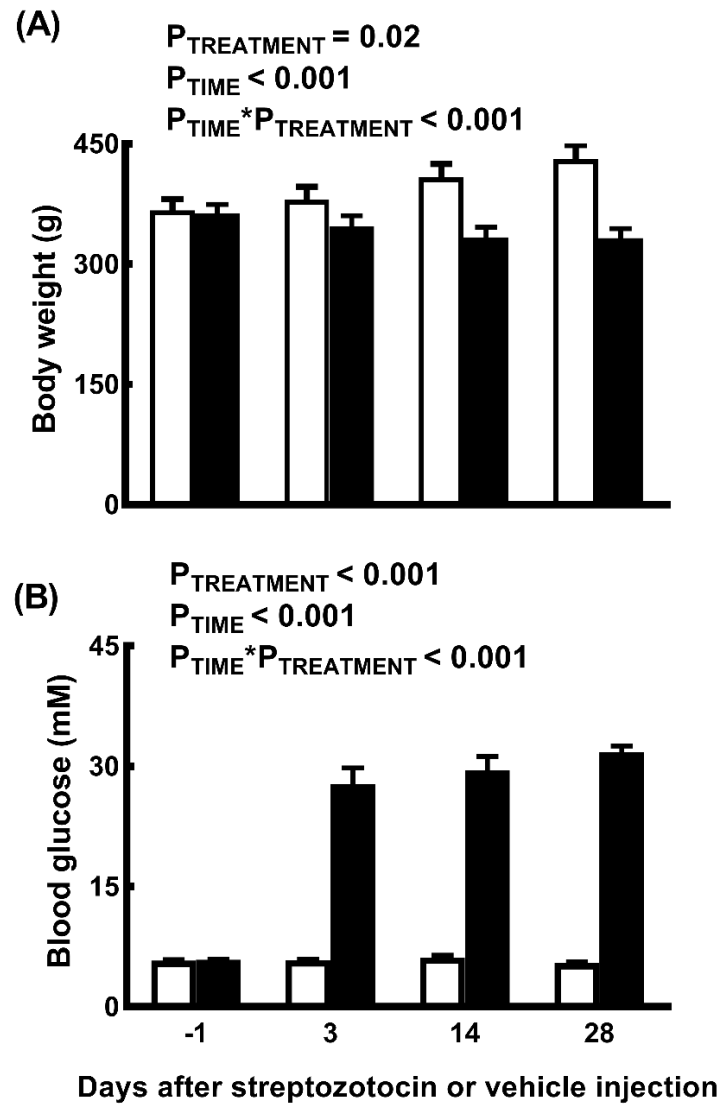


Figure 5.2 Body weight (A) and blood glucose (B) in vehicle-treated and diabetic rats during the 4 week experimental protocol. Columns and bars represent mean \pm SEM of $n = 8$ (vehicle; opened bar) and $n = 8$ (diabetic; filled bar). P values were derived from repeated measures analysis of variance.

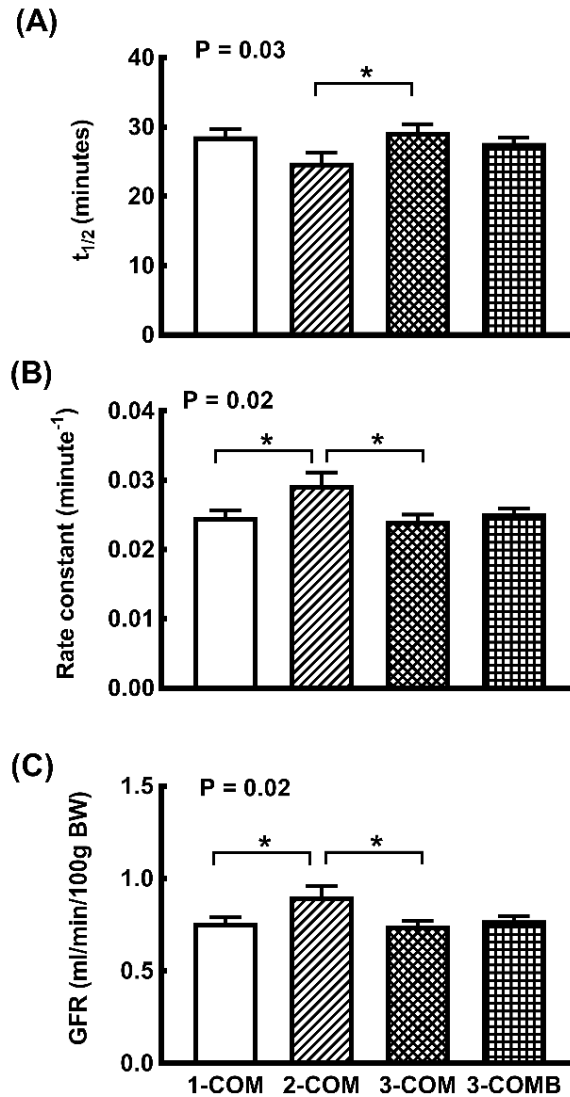


Figure 5.3 Renal clearance of FITC-sinistrin at baseline. Baseline renal clearance of FITC-sinistrin for all rats ($n = 16$) was calculated and expressed in three different forms (A) $t_{1/2}$ = excretion half-life (minutes), (B) rate constant (minute^{-1}) and (C) GFR indexed to body weight ($\text{ml}/\text{min}/100\text{ g body weight}$). Excretion half-life of FITC-sinistrin was calculated using a one compartment kinetic model (1-COM), a two compartment kinetic model (2-COM), a three compartment kinetic model (3-COM) and a three compartment kinetic model with baseline correction (3-COMB). Columns and error bars represent mean \pm SEM. P values were derived from repeated measures analysis of variance. * $P \leq 0.05$ (Tukey's post hoc test).

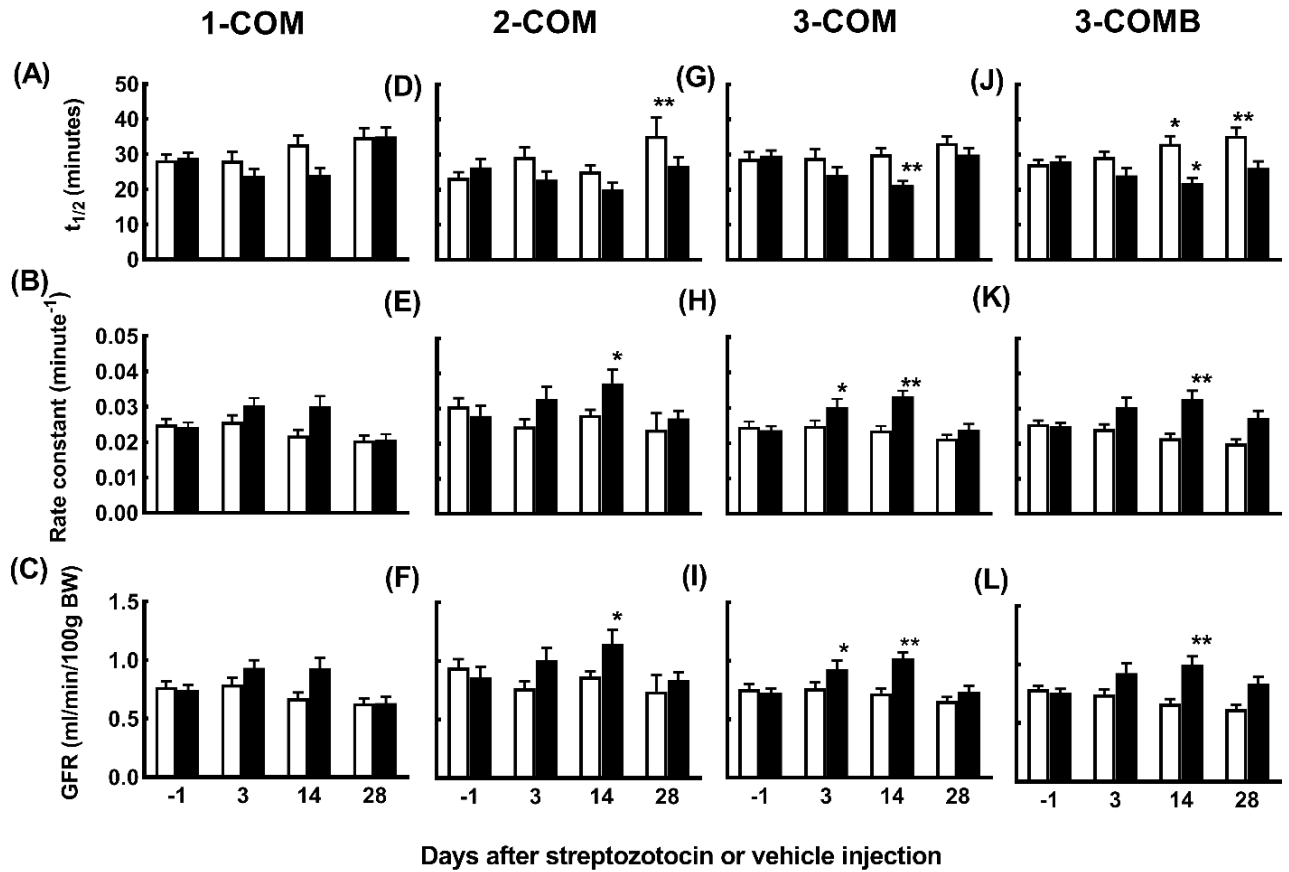


Figure 5.4. Temporal profile of renal clearance of FITC-sinistrin in vehicle-treated and diabetic rats during the 4 week experimental protocol. Renal clearance of FITC-sinistrin was calculated and expressed in three different forms: $t_{1/2}$ = excretion half-life (minutes), rate constant (minute^{-1}), and GFR indexed to body weight ($\text{ml}/\text{min}/100\text{ g}$ body weight). Excretion half-life of FITC-sinistrin was calculated using a one compartment kinetic model (1-COM; panels A-C), a two compartment kinetic model (2-COM; panels D-F), a three compartment kinetic model (3-COM; panels G-I) and a three compartment kinetic model with baseline correction (3-COMB; panels J-L). Columns and error bars represent mean \pm SEM of $n = 8$ (vehicle; opened bar) and $n = 8$ (diabetic; filled bar). *P \leq 0.05, and **P < 0.001 compared to the corresponding baseline value (Dunnett's test).

Table 5.2 Outcomes of repeated-measures ANOVA for the data shown in Figure 5.4

	P_{Treat}	P_{Time}	P_{Interaction}
1-COM			
T _(1/2)	0.11	0.001	0.10
Rate constant	0.06	0.002	0.06
GFR	0.06	0.002	0.06
2-COM			
T _(1/2)	0.08	0.03	0.16
Rate constant	0.09	0.14	0.19
GFR	0.17	0.07	0.09
3-COM			
T _(1/2)	0.05	0.004	0.03
Rate constant	0.006	0.002	0.01
GFR	0.006	0.002	0.01
3-COMB			
T _(1/2)	0.002	0.06	0.003
Rate constant	0.001	0.14	0.02
GFR	0.001	0.03	0.001

P values represent the outcomes of repeated measures analysis of variance. T_{1/2}, excretion half-life; GFR, glomerular filtration rate; Treat, treatment; 1-COM, one compartment kinetic model; 2-COM, two compartment kinetic model; 3-COM, three compartment kinetic model; 3-COMB, three compartment kinetic model with baseline correction. Bolded P values are ≤ 0.05 .

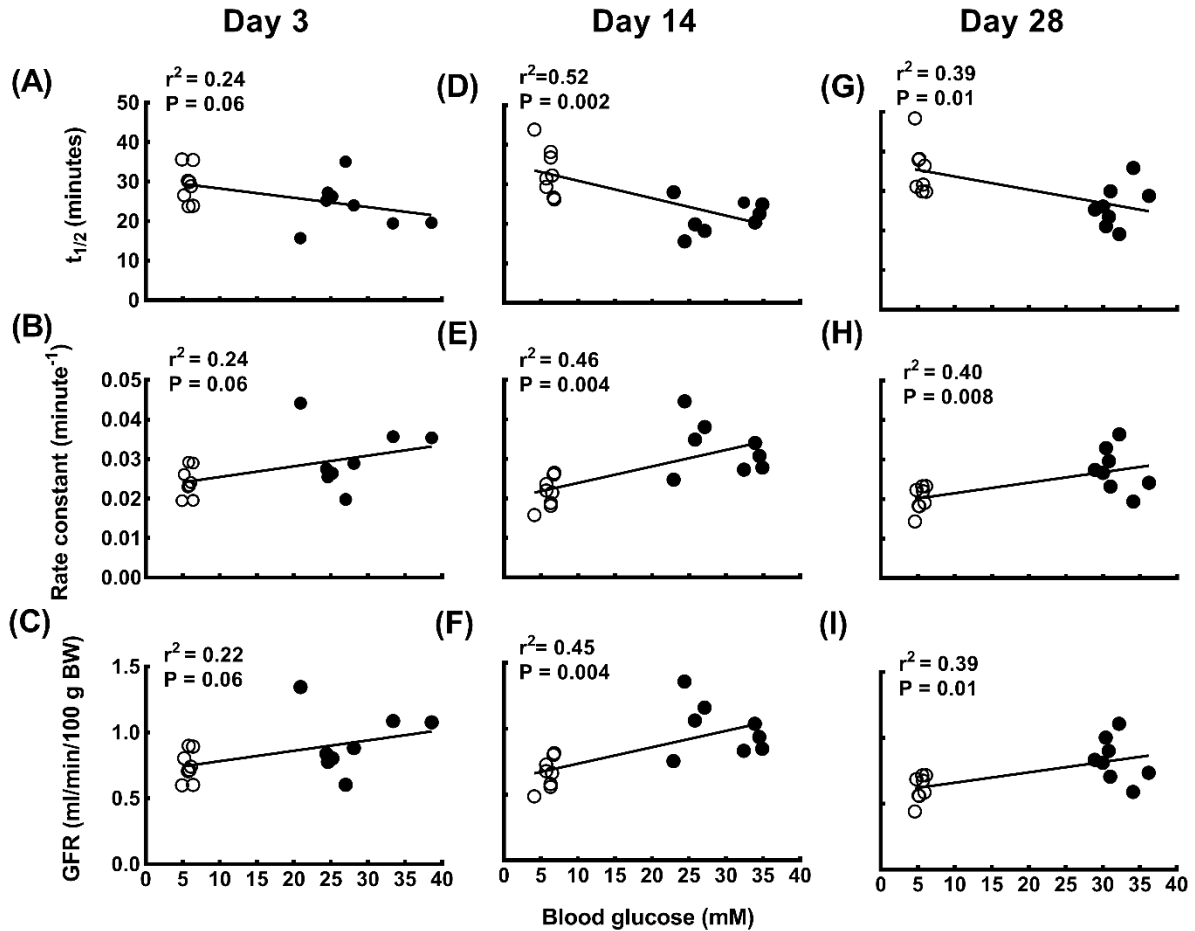


Figure 5.5 Relationships between concentrations of blood glucose and excretion half-life ($t_{1/2}$), rate constant, and glomerular filtration rate in diabetic and non-diabetic rats. Excretion half-life of FITC-sinistrin was calculated using a three compartment kinetic model with base line correction (3-COMB). Data for concentrations of blood glucose and $t_{1/2}$ were collected at baseline and 3, 14 and 28 days after injection of streptozotocin (STZ) or its vehicle. Open circles represent data for vehicle-treated rats and closed circles represent corresponding data in rats rendered diabetic by administration of STZ. Lines of best fit were generated by ordinary least squares linear regression analysis (28). Coefficient of determination (r^2) and the associated P value (testing the null hypothesis that the slope is zero) are shown for each relationship.

5.4.3 Blood and urine chemistry

Urinary albumin to creatinine ratio (ACR) did not differ significantly between rats treated with STZ and those treated with vehicle, throughout the experimental protocol (Figure 5.6).

At the end of the 4 week experimental protocol, the plasma concentration of sodium was 6.4% less, and plasma chloride was 9% less, in STZ-diabetic rats than vehicle-treated rats (Table 5.3). However, plasma concentrations of potassium and ionized calcium did not differ significantly between the two groups. Plasma urea concentration was 50.4% greater after STZ injection than after vehicle injection. However, there was no significant difference between the groups in the plasma concentration of creatinine.

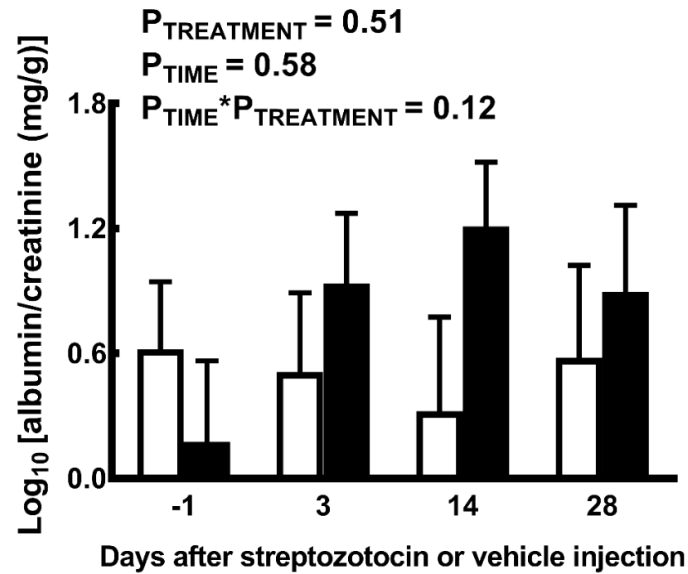


Figure 5.6 Logarithmic transformed urinary albumin to creatinine ratio in vehicle-treated rats and diabetic rats during the four week experimental protocol. Columns and error bars represent mean \pm SEM of $n = 7$ (vehicle; opened bar) and $n = 7$ (diabetic; filled bar). P values were derived from repeated measures analysis of variance. Sufficient urine samples could not be collected for two rats at multiple time points. Thus I only included rats from which I collected urine at 4 time points.

5.4.4 Kidney and heart weight

The kidneys of STZ-diabetic rats were 47% (left) and 34% (right) heavier than the kidneys of vehicle-treated rats (Table 5.3). Heart weight did not differ significantly between the two groups at the end of 4 week experimental protocol.

Table 5.3 Characteristics of rats four weeks after injection of vehicle or streptozotocin

Variables	n	Vehicle	Diabetic	P
<i>Plasma analysis</i>				
Sodium, mM	8	137.1 ± 1.4	128.4 ± 2.4	0.009
Potassium, mM	8	5.1 ± 0.2	4.6 ± 0.1	0.09
Chloride, mM	8	96.5 ± 0.6	87.8 ± 2.1	0.004
Ionized calcium, mM	8	0.90 ± 0.12	1.02 ± 0.06	0.36
Urea, mM	8	4.9 ± 0.3	7.4 ± 0.4	<0.001
Creatinine, mg/dl	8	0.33 ± 0.03	0.30 ± 0.02	0.29
<i>Kidney and Heart weight</i>				
Left kidney weight, g	8	1.22 ± 0.06	1.80 ± 0.08	<0.001
Right kidney weight, g	8	1.35 ± 0.14	1.81 ± 0.07	0.02
Heart weight, g	8	1.10 ± 0.06	1.03 ± 0.04	0.37

Values are mean ± SEM. P values represent the outcomes of Student's unpaired t- test with Welch's correction. n indicates sample number in each group. Bolded P values are ≤ 0.05.

5.4.5 Histological assessment of tissue damage and collagen deposition

Hematoxylin and eosin staining was performed to visualize renal tissue structure (Figure 5.7). Kidney tissue from rats treated with vehicle appeared relatively normal (Figure 5.7 a-d). The glomeruli were intact with regular Bowman's space (Figure 5.7 b). Renal tubules were closely spaced and the brush border of the apical surface of the renal tubules appeared normal in both the cortex and medulla. (Figure 5.7 b,c,d). In contrast, in the cortex of STZ-diabetic rats, the glomerular tufts were expanded and Bowman's space appeared narrow (Figure 5.7 f). Tubular dilation was observed in both the cortex and medulla (Figure 5.7 f, g and h).

Renal tissue sections from vehicle-treated rats and STZ-diabetic rats were stained with picrosirius red (Figure 5.8). In kidney sections from both groups, positive red stain was observed around the perivascular adventitia surrounding the arteries and veins and glomeruli. Quantification indicated that picrosirius red staining of kidney sections did not differ significantly between the two groups in either the cortex or medulla (Figure 5.9).

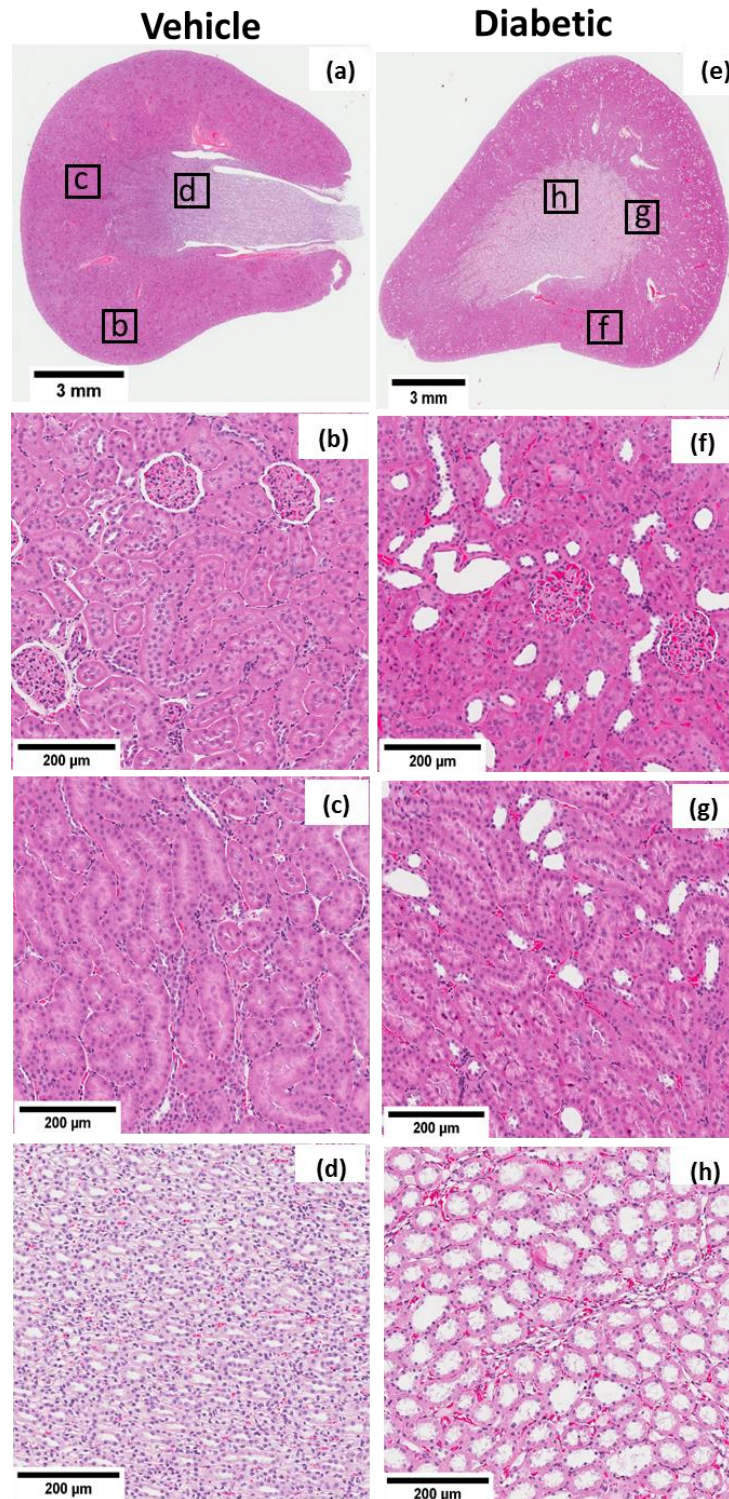


Figure 5.7 Micrographs of kidney sections, stained with hematoxylin and eosin, taken from vehicle-treated rats (a–d) and diabetic rats (e–h) at the end of the four week experimental protocol. Cortical (b, f), outer medullary (c, g) and inner medullary (d, h) regions are shown. Boxes in (a) and (e) show regions presented in (b–d) and (f–h)

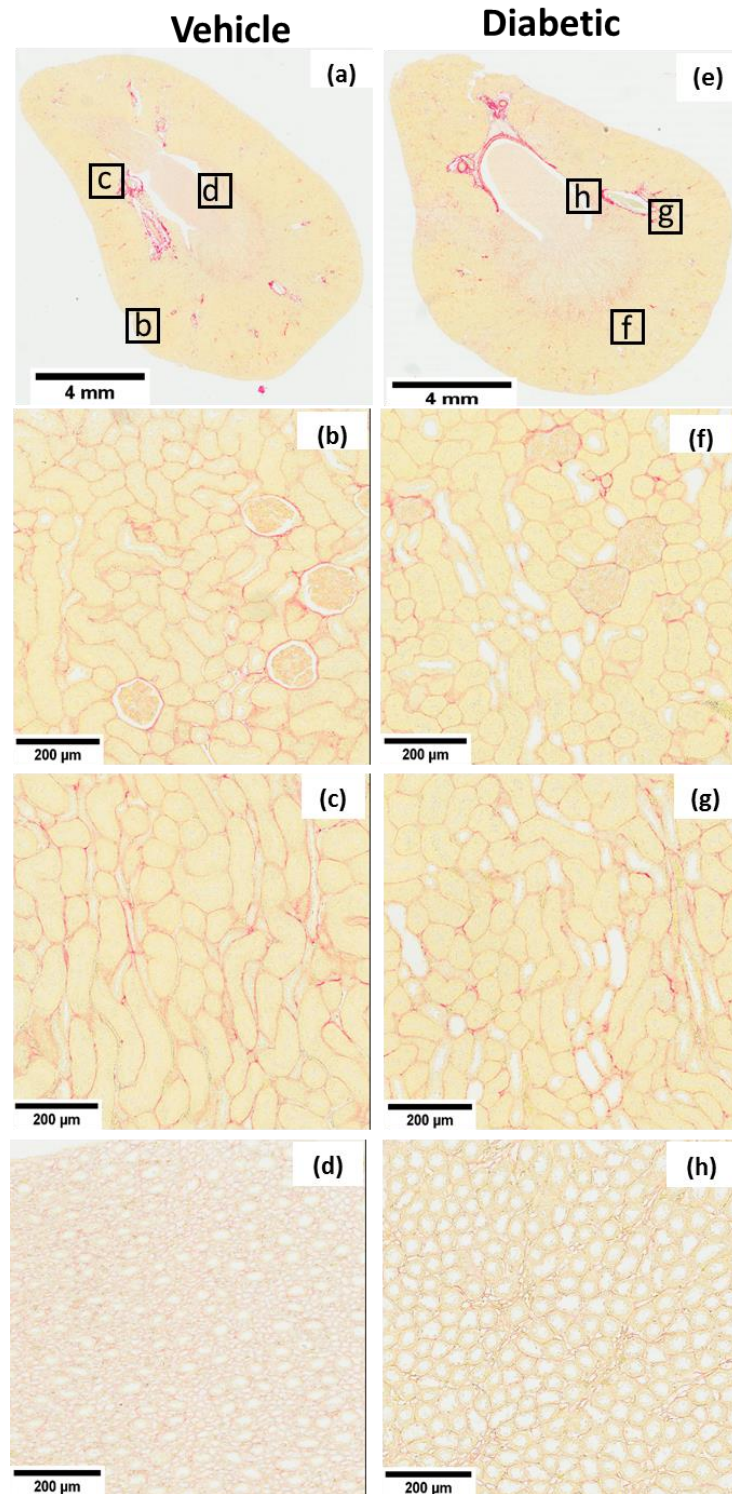


Figure 5.8 Micrographs of kidney sections, stained with picosirius red, taken from vehicle-treated rats (a–d) and diabetic rats (e–h) at the end of the four week experimental protocol. Cortical (b, f), outer medullary (c, g) and inner medullary (d, h) regions are shown. Boxes in (a) and (e) show regions presented in (b–d) and (f–h).

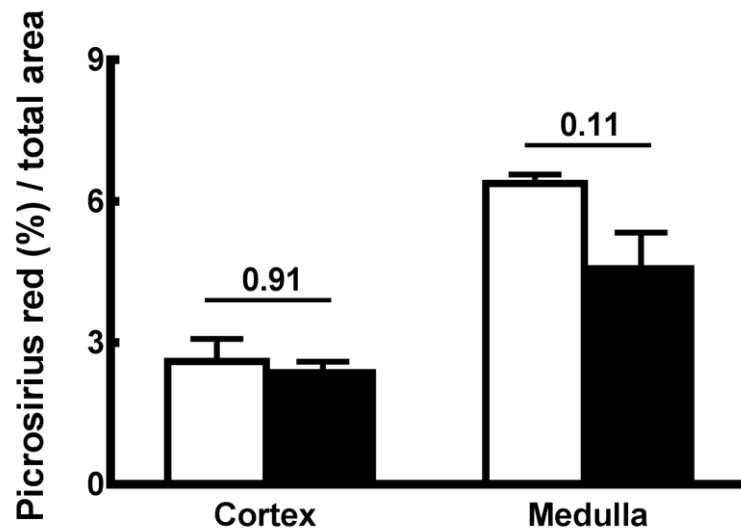


Figure 5.9 Quantification of collagen deposition in the cortex and medulla at the end of the 4 week experimental protocol. Two sections were analysed from each kidney. Values are between-rat mean \pm SEM for vehicle-treated rats (n=5; opened bars) and diabetic rats (n = 5; filled bars). P values are outcomes of Student's unpaired t-test with Welch's correction.

5.5 DISCUSSION

The major findings in our current study are that (i) glomerular hyperfiltration was detected in rats using both the 2-COM and 3-COMB models at day 14 and using the 3-COM model at day 3 and day 14, after injection of STZ, (ii) linear regression analysis of data obtained using the 3-COMB model demonstrated a significant relationship between blood glucose and GFR at day 14 and day 28, along with a strong tendency for a relationship at day 3, and (iii) there was no evidence of overt renal dysfunction or damage as shown by the absence of albuminuria and tubulointerstitial fibrosis at day 28 after induction of diabetes. Thus, our current findings support the proposition that hyperfiltration is a prominent characteristic of the early stages of STZ-induced type 1 diabetes and thus is a potential driver of diabetic nephropathy. Our findings also indicate that the choice of kinetic model for calculation of $t_{1/2}$ can have a profound impact on the conclusions drawn from studies in which FITC-sinistrin clearance is used to estimate GFR in conscious rats. From a theoretical perspective I propose that the 3-COMB model provides the most valid $t_{1/2}$ and thereby calculation of GFR. Thus, I recommend that this model be employed in future studies in which GFR is estimated in conscious rats using FITC-sinistrin clearance.

Our current findings indicate that hyperfiltration can be detected in conscious rats, using FITC-sinistrin clearance, during the early stages of type 1 diabetes induced by injection of STZ. However, the method used to calculate $t_{1/2}$ appears to be an important consideration in studies such as these. For example, calculated GFR was significantly increased as early as 3 days after STZ administration when the 3-COM method was used, but the apparent increase at this time-point was not statistically significant when the 1-COM, 2-COM, or 3-COMB methods were used. I reasoned that the 3-COMB method is the most valid of these four approaches. The 1-COM model has several limitations despite its wide application in experimental studies to assess GFR (22, 41). For example, the 1-COM model does not incorporate the complete clearance kinetics of FITC-sinistrin. It uses the later part of the kinetics curve (33), which represents the excretion phase of the marker, to calculate $t_{1/2}$. Thus, it excludes the data obtained after injection and distribution of the marker (33). The 2-COM method, modified from the original 2-COM method of Schock-Kusch *et al* (42), incorporates the complete course of measurement, including from the time of injection of the marker to complete excretion of the marker. However the recognized error of this model is that the model leads to a systematic deviation in the curve fitting, particularly in the peak area (16). This deviation provided a significantly higher $t_{1/2}$ value compared to any other methods (16). In addition, during transcutaneous measurement of GFR, the intensity of the fluorescence signal can be affected by changes in skin perfusion induced by attachment of the transcutaneous device (30) or by autofluorescence of the skin by photo bleaching (10). These factors might affect the baseline signal generated by the transcutaneous device and thus affect the calculation of $t_{1/2}$, when the 1-COM, 2-COM or 3-COM models are used. Friedemann and colleagues developed the 3-COMB model, which describes the distribution and mixing of an exogenous marker within the blood stream, as well as its excretion kinetics (16, 17). Furthermore, they also improved the model by introducing a baseline correction term, which compensates for the drifts of the baseline signal due to a rat's movements or autofluorescence of the rat's skin (17). Most importantly, the GFR measured by the 3-COMB model (0.87 ± 0.11 ml/min/100 g body weight) was found to be comparable with the GFR measured by the 'gold standard' constant infusion technique (0.94 ± 0.13 ml/min/100 g body weight) (17). Thus from theoretical point of view, the 3-COMB model should provide more accurate $t_{1/2}$ values compared to other methods (1-COM, 2-COM and 3-COM).

Another limitation of the transcutaneous based measurement of renal function is that an empirically-derived conversion factor is used, based on the assumption that the extracellular fluid volume is similar in both vehicle-treated rats and STZ-treated rats. This conversion factor is used to derive GFR (ml/min/100 g body weight) from $t_{1/2}$. Experimental evidence demonstrates an

alteration of extracellular fluid volume in poorly controlled STZ-induced diabetic rats compared to the vehicle-treated rats (24, 47). Extracellular fluid volume was decreased by one day after STZ-injection and was consistently less across the 15 day study periods in both the insulin-treated rats and untreated rats compared to their control rats (47). However, there are also reports of either increased (24) or unaltered extracellular fluid volume (48) in STZ-induced diabetic rats compared to the vehicle-treated rats. Thus, in the absence of direct measurement of extracellular fluid volume in the current study, it is not possible to assess the impact of this potential confounder on calculated GFR.

Hyperglycemia might alter the extracellular fluid volume either (i) by increasing serum osmolality which subsequently increases movement of water from cells to extracellular space (23, 27) or (ii) by inducing osmotic-diuresis (5, 27). Interestingly, a study by Tucker et al demonstrated that STZ-diabetic rats maintained a similar extracellular fluid volume to control rats, 60 days after STZ-injection (48). In that study, the euvoletic state in STZ-induced diabetic rats was associated with hyponatremia, osmotic diuresis and natriuresis. Similar to previous studies (4, 48), I also observed hyponatremia in STZ-diabetic rats as shown by the decreased plasma sodium concentration compare to the vehicle-treated rats.

Our inability to consistently detect a significant increase in GFR at the 3 day and 28 day time-points after administration of STZ could represent a type II error, given both the relatively small sample size in our current study ($n = 8$ per group) and the possible variability in levels of blood glucose in STZ-diabetic rats. Therefore, I subjected the data generated using the 3-COMB method to linear regression analysis. This revealed statistically significant relationships between blood glucose and calculated GFR at the 14 day ($P = 0.004$) and 28 day ($P = 0.01$) time-points, along with a strong tendency for a relationship at the 3 day time-point ($P = 0.06$). Thus, it seems reasonable to conclude that in our current study hyperfiltration is an early and persistent phenomenon in the STZ model of type 1 diabetes in rats. Tucker *et al*, using the constant infusion technique, showed that GFR in STZ-diabetic rats not receiving insulin supplementation was significantly greater as early as 24 hours after induction of diabetes when compared to control rats. In that study GFR was found to remain increased in STZ-diabetic rats during the entire 15 day experimental protocol (47). Bell *et al* detected elevated GFR in STZ-diabetic rats compared to the respective control group, when GFR was assessed at day 4 and day 12 after induction of diabetes (3). However the major drawbacks of the constant infusion techniques include the fact that surgical preparation is needed for catheter implantation, multiple blood and/or urine samples are required,

and laboratory analysis of the samples must be conducted at the conclusion of the experiment (2, 7). To our knowledge our current observations are the first available measurements of GFR using the transcutaneous-based technique, across a 4 week experimental protocol, during the early stage of diabetes in STZ-treated rats.

It has been argued that renal tissue hypoxia is an early and persistent phenomenon in diabetes (8, 14, 38). In STZ-diabetic mice, cortical tissue hypoxia was detected, as early 3 days after induction of diabetes, using electron paramagnetic resonance oximetry (14). In that study renal tissue hypoxia persisted across a 2 week experimental protocol. Nordquist and co-workers (2015) found that both cortical and medullary tissue PO₂ were reduced significantly in rats with diabetes compared to their respective control rats, 28 days after induction of diabetes (34).

Our current findings are consistent with a potential role of hyperfiltration in the development of renal tissue hypoxia in diabetes. Glomerular hyperfiltration is associated with increased proximal tubular reabsorption of sodium (50, 51). Under normal physiological conditions, approximately 80% of renal oxygen consumption is utilized for sodium reabsorption (9). Thus, increased reabsorption of sodium in the proximal tubule, associated with glomerular hyperfiltration, would be expected to increase renal oxygen consumption and thus potentially contribute to reduced renal tissue PO₂. Consistent with this proposition, O'Neill *et al* found that acute inhibition of proximal tubular reabsorption by administration of phlorizin, an inhibitor of sodium dependent glucose transporters, could attenuate both cortical hypoxia and glomerular hyperfiltration in STZ-diabetic rats (36). The results of this acute study indicate that increased sodium reabsorption in the proximal tubule, associated with glomerular hyperfiltration, may play an important role in development of cortical hypoxia in rats with diabetes.

Our current study was focused on the early period of diabetes, before development of overt renal dysfunction and tissue damage. Accordingly, I found no evidence of albuminuria or tubulointerstitial fibrosis in STZ-diabetic rats. Flynn *et al* found that the level of urinary albumin excretion in Sprague Dawley rats with diabetes did not differ from that of corresponding control rats at 4 and 8 weeks after induction of diabetes (12). However in that study rats with diabetes exhibited albuminuria, compared to their control group, at 12 weeks after injection of STZ. In a separate study, Gilbert and colleagues reported albuminuria in STZ-diabetic rats by 4 weeks after induction of diabetes and this albuminuria persisted for the 16 week experimental protocol (19). In both studies albuminuria was associated with the development of tubulointerstitial fibrosis (12, 19). Renal tubulointerstitial fibrosis has also been demonstrated in STZ diabetic rats by 3 weeks

after induction of diabetes (18). However, in that study the levels of urinary protein excretion and plasma creatinine were comparable between STZ-diabetic rats and their corresponding control rats at the end of the 3 week protocol. In our current study, urinary ACR and plasma creatinine were comparable between STZ-diabetic rats and their corresponding control rats at the end of the four week experimental protocol. Thus in our current study renal dysfunction was not an early event in STZ-diabetic rats as indicated by the absence of albuminuria or tubulointerstitial fibrosis. However, there was some evidence from our histological analysis of relatively minor changes in tissue structure such as expansion of glomerular capillary tufts and tubular dilation. Surprisingly, I also found evidence of modest uremia in STZ-diabetic rats, despite hyperfiltration and the absence of an increase in plasma creatinine concentration. I speculate this might be due to an increase in food intake and thus protein intake, as rats with diabetes are polyphagic (52).

In conclusion, our current findings indicate that hyperfiltration is an early event in type 1 diabetes. Diabetic hyperfiltration can be detected in conscious rats using FITC-sinistrin. However, the method used to calculate $t_{1/2}$ can influence the findings of studies of this type. I recommend use of the 3-COMB model for analysis of FITC-sinistrin clearance because this model describes the complete course of clearance kinetics for FITC-sinistrin, from the point of injection, with automated baseline correction.

5.6 REFERENCES

1. **Abdelkader A, Ho J, Ow CP, Eppel GA, Rajapakse NW, Schlaich MP, and Evans RG.** Renal oxygenation in acute renal ischemia-reperfusion injury. *Am J Physiol Renal Physiol* 306: F1026-F1038, 2014.
2. **Bak M, Thomsen K, Christiansen T, and Flyvbjerg A.** Renal enlargement precedes renal hyperfiltration in early experimental diabetes in rats. *J Am Soc Nephrol* 11: 1287-1292, 2000.
3. **Bell TD, DiBona GF, Wang Y, and Brands MW.** Mechanisms for renal blood flow control early in diabetes as revealed by chronic flow measurement and transfer function analysis. *J Am Soc Nephrol* 17: 2184, 2006.
4. **Chen L, LaRocque LM, Efe O, Wang J, Sands JM, and Klein JD.** Effect of Dapagliflozin Treatment on Fluid and Electrolyte Balance in Diabetic Rats. *Am J Med Sci* 352: 517-523, 2016.
5. **Chiasson JL, Aris-Jilwan N, Belanger R, Bertrand S, Beaugerard H, Ekoe JM, Fournier H, and Havrankova J.** Diagnosis and treatment of diabetic ketoacidosis and the hyperglycemic hyperosmolar state. *Cmaj* 168: 859-866, 2003.
6. **Ding A, Kalaighanasundaram P, Ricardo SD, Abdelkader A, Witting PK, Broughton BR, Kim HB, Wyse BF, Phillips JK, and Evans RG.** Chronic treatment with tempol does not significantly ameliorate renal tissue hypoxia or disease progression in a rodent model of polycystic kidney disease. *Clin Exp Pharmacol Physiol* 39: 917-929, 2012.
7. **Dixon JJ, Lane K, Dalton RN, Turner C, Grounds RM, MacPhee IA, and Philips BJ.** Validation of a continuous infusion of low dose iohexol to measure glomerular filtration rate: randomised clinical trial. *J Transl Med* 13: 58, 2015.
8. **dos Santos EA, Li LP, Ji L, and Prasad PV.** Early changes with diabetes in renal medullary hemodynamics as evaluated by fiberoptic probes and BOLD magnetic resonance imaging. *Invest Radiol* 42: 157-162, 2007.
9. **Evans RG, Harrop GK, Ngo JP, Ow CP, and O'Connor PM.** Basal renal O₂ consumption and the efficiency of O₂ utilization for Na⁺ reabsorption. *Am J Physiol Renal Physiol* 306: F551-F560, 2014.
10. **Ferulova I, Lihachev A, and Spigulis J.** Photobleaching effects on in vivo skin autofluorescence lifetime. *J Biomed Opt* 20: 051031, 2015.
11. **Fitzgerald SM, and Brands MW.** Nitric oxide may be required to prevent hypertension at the onset of diabetes. *Am J Physiol Endocrinol Metab* 279: E762-E768, 2000.
12. **Flynn ER, Marbury DC, Sawyer RT, Lee J, Teutsch C, Kauser K, and Maric-Bilkan C.** Amlodipine reduces inflammation despite promoting albuminuria in the streptozotocin-induced diabetic rat. *Nephron Extra* 2: 205-218, 2012.
13. **Fong D, Ullah MM, Lal JG, Abdelkader A, Ow CP, Hilliard LM, Ricardo SD, Kelly DJ, and Evans RG.** Renal cellular hypoxia in adenine-induced chronic kidney disease. *Clin Exp Pharmacol Physiol* 43: 896-905, 2016.
14. **Franzen S, Pihl L, Khan N, Gustafsson H, and Palm F.** Pronounced kidney hypoxia precedes albuminuria in type 1 diabetic mice. *Am J Physiol Renal Physiol* 310: F807-F809, 2016.
15. **Frennby B, and Sterner G.** Contrast media as markers of GFR. *Eur Radiol* 12: 475-484, 2002.
16. **Friedemann J.** Development of a pharmacokinetic model to describe the distribution and excretion kinetics of a renal function marker using transcutaneously obtained data in rats (Doctoral dissertation). In: *Medizinische Fakultät Mannheim* Germany: University of Heidelberg, 2015, p. 117.

17. **Friedemann J, Heinrich R, Shulhevich Y, Raedle M, William-Olsson L, Pill J, and Schock-Kusch D.** Improved kinetic model for the transcutaneous measurement of glomerular filtration rate in experimental animals. *Kidney Int* 90: 1377-1385, 2016.
18. **Fujisawa G, Okada K, Muto S, Fujita N, Itabashi N, Kusano E, and Ishibashi S.** Spironolactone prevents early renal injury in streptozotocin-induced diabetic rats. *Kidney Int* 66: 1493-1502, 2004.
19. **Gilbert RE, Zhang Y, Williams SJ, Zammit SC, Stapleton DI, Cox AJ, Krum H, Langham R, and Kelly DJ.** A purpose-synthesised anti-fibrotic agent attenuates experimental kidney diseases in the rat. *PLoS One* 7: e47160, 2012.
20. **Hannedouche TP, Delgado AG, Gnionsahe DA, Boitard C, Lacour B, and Grunfeld JP.** Renal hemodynamics and segmental tubular reabsorption in early type 1 diabetes. *Kidney Int* 37: 1126-1133, 1990.
21. **Herrera Perez Z, Weinfurter S, and Gretz N.** Transcutaneous assessment of renal function in conscious rodents. *J Vis Exp* e53767, 2016.
22. **Hilliard LM, and Denton KM.** Transcutaneous assessment of glomerular filtration rate in unanesthetized rats using a small animal imager: impact on arterial pressure, heart rate, and activity. *Physiological Reports* 4: e12723, 2016.
23. **Hillier TA, Abbott RD, and Barrett EJ.** Hyponatremia: evaluating the correction factor for hyperglycemia. *Am J Med* 106: 399-403, 1999.
24. **Hostetter TH, Troy JL, and Brenner BM.** Glomerular hemodynamics in experimental diabetes mellitus. *Kidney Int* 19: 410-415, 1981.
25. **Jensen PK, Christiansen JS, Steven K, and Parving HH.** Renal function in streptozotocin-diabetic rats. *Diabetologia* 21: 409-414, 1981.
26. **Leysac PP, Karlson FM, and Skott O.** Role of proximal tubular reabsorption for the intrarenal control of GFR. *Kidney Int Suppl* 32: S132-135, 1991.
27. **Liamis G, Liberopoulos E, Barkas F, and Elisaf M.** Diabetes mellitus and electrolyte disorders. *World journal of clinical cases* 2: 488-496, 2014.
28. **Ludbrook J.** Linear regression analysis for comparing two measurers or methods of measurement: but which regression? *Clin Exp Pharmacol Physiol* 37: 692-699, 2010.
29. **Ludbrook J.** Repeated measurements and multiple comparisons in cardiovascular research. *Cardiovasc Res* 28: 303-311, 1994.
30. **Martin P, Debreczenya, Rebecca Batesb, Rick M. Fitchb, Karen P. Galenb, Jiajia Geb, B. R, and Dorshow.** Human skin auto-fluorescence decay as a function of irradiance and skin type. *Proc of SPIE* 7897-78971T-2: 2011.
31. **McHugh ML.** Multiple comparison analysis testing in ANOVA. *Biochem Med* 21: 203-209, 2011.
32. **Mondritzki T, Steinbach SML, Boehme P, Hoffmann J, Kullmann M, Schock-Kusch D, Vogel J, Kolkhof P, Sandner P, Bischoff E, Huser J, Dinh W, and Truebel H.** Transcutaneous glomerular filtration rate measurement in a canine animal model of chronic kidney disease. *J Pharmacol Toxicol Methods* 90: 7-12, 2018.
33. **Murray AW, Barnfield MC, Waller ML, Telford T, and Peters AM.** Assessment of glomerular filtration rate measurement with plasma sampling: a technical review. *J Nucl Med Technol* 41: 67-75, 2013.
34. **Nordquist L, Friederich-Persson M, Fasching A, Liss P, Shoji K, Nangaku M, Hansell P, and Palm F.** Activation of hypoxia-inducible factors prevents diabetic nephropathy. *J Am Soc Nephrol* 26: 328-338, 2015.
35. **O'Brien RC, Allen TJ, Cooper ME, Bach L, and Jerums G.** Glomerular filtration rate in early experimental diabetes. *J Diabet Complications* 2: 8-11, 1988.

36. **O'Neill J, Fasching A, Pihl L, Patinha D, Franzen S, and Palm F.** Acute SGLT inhibition normalizes O₂ tension in the renal cortex but causes hypoxia in the renal medulla in anaesthetized control and diabetic rats. *Am J Physiol Renal Physiol* 309: F227-F234, 2015.
37. **Pollock CA, Lawrence JR, and Field MJ.** Tubular sodium handling and tubuloglomerular feedback in experimental diabetes mellitus. *Am J Physiol* 260: 946-952, 1991.
38. **Ries M, Basseau F, Tyndal B, Jones R, Deminiere C, Catargi B, Combe C, Moonen CW, and Grenier N.** Renal diffusion and BOLD MRI in experimental diabetic nephropathy. Blood oxygen level-dependent. *J Magn Reson Imaging* 17: 104-113, 2003.
39. **Sapirstein LA, Vidt DG, Mandel MJ, and Hanusek G.** Volumes of distribution and clearances of intravenously injected creatinine in the dog. *Am J Physiol* 181: 330-336, 1955.
40. **Schock-Kusch D, Geraci S, Ermeling E, Shulhevich Y, Sticht C, Hesser J, Stsepankou D, Neudecker S, Pill J, Schmitt R, and Melk A.** Reliability of transcutaneous measurement of renal function in various strains of conscious mice. *PLoS One* 8: e71519, 2013.
41. **Schock-Kusch D, Sadick M, Henninger N, Kraenzlin B, Claus G, Kloetzer HM, Weiss C, Pill J, and Gretz N.** Transcutaneous measurement of glomerular filtration rate using FITC-sinistrin in rats. *Nephrol Dial Transplant* 24: 2997-3001, 2009.
42. **Schock-Kusch D, Xie Q, Shulhevich Y, Hesser J, Stsepankou D, Sadick M, Koenig S, Hoecklin F, Pill J, and Gretz N.** Transcutaneous assessment of renal function in conscious rats with a device for measuring FITC-sinistrin disappearance curves. *Kidney Int* 79: 1254-1258, 2011.
43. **Scholey JW, and Meyer TW.** Control of glomerular hypertension by insulin administration in diabetic rats. *J Clin Invest* 83: 1384-1389, 1989.
44. **Shapiro SS, and Wilk MB.** An analysis of variance test for normality (complete samples). *Biometrika* 52: 591-611, 1965.
45. **Shmarlouski A, Schock-Kusch D, Shulhevich Y, Buschmann V, Rohlicke T, Herdt D, Radle M, Hesser J, and Stsepankou D.** A novel analysis technique for transcutaneous measurement of glomerular filtration rate with ultralow dose marker concentrations. *IEEE Trans Biomed Eng* 63: 1742-1750, 2016.
46. **Shmarlouski A, Shulhevich Y, Geraci S, Friedemann J, Gretz N, Neudecker S, Hesser J, and Stsepankou D.** Automatic artifact removal from GFR measurements. *Biomed Signal Process Control* 14: 30-41, 2014.
47. **Tucker BJ, Collins RC, Ziegler MG, and Blantz RC.** Disassociation between glomerular hyperfiltration and extracellular volume in diabetic rats. *Kidney Int* 39: 1176-1183, 1991.
48. **Tucker BJ, Mendonca MM, and Blantz RC.** Contrasting effects of acute insulin infusion on renal function in awake nondiabetic and diabetic rats. *J Am Soc Nephrol* 3: 1686-1693, 1993.
49. **Vallon V.** Tubuloglomerular feedback and the control of glomerular filtration rate. *News Physiol Sci* 18: 169-174, 2003.
50. **Vallon V, Blantz RC, and Thomson S.** Homeostatic efficiency of tubuloglomerular feedback is reduced in established diabetes mellitus in rats. *Am J Physiol* 269: 876-883, 1995.
51. **Vallon V, Richter K, Blantz RC, Thomson S, and Osswald H.** Glomerular hyperfiltration in experimental diabetes mellitus: potential role of tubular reabsorption. *J Am Soc Nephrol* 10: 2569-2576, 1999.
52. **Wei M, Ong L, Smith MT, Ross FB, Schmid K, Hoey AJ, Burstow D, and Brown L.** The streptozotocin-diabetic rat as a model of the chronic complications of human diabetes. *Heart Lung Circ* 12: 44-50, 2003.
53. **Wiseman MJ, Mangili R, Alberetto M, Keen H, and Viberti G.** Glomerular response mechanisms to glycemic changes in insulin-dependent diabetics. *Kidney Int* 31: 1012-1018, 1987.

CHAPTER 6

**ASSESSMENT OF THE SPATIAL RELATIONSHIPS BETWEEN
PERITUBULAR CAPILLARIES AND RENAL TUBULES IN THE RAT
KIDNEY: A PILOT STUDY**

6.1 ABSTRACT

I conducted a pilot study to investigate the feasibility of using multiphoton microscopy of slices of renal tissue to generate three dimensional (3-D) reconstructions of the spatial relationships between peritubular capillaries and tubules. This information is required for further refinement of computational models of oxygen transport in the kidney. The kidneys of rats were perfusion fixed and then filled with a gelatin solution containing albumin conjugated with fluorescein isothiocyanate (FITC). Fluorescence could be detected in the vasculature of kidneys filled with gelatin containing FITC conjugated albumin. Superior filling of the vasculature was achieved at an inflow rate of 3 ml/min than at 1 ml/min. In 400 μm thick slices of kidney tissue, fluorescent labeling of glomerular and peritubular capillaries could be detected by confocal microscopy of optically cleared tissue, enabling 3-D reconstruction of vascular morphology. I also attempted to label renal tubules in these slices using a pan cytokeratin antibody, but this was not successful. However, renal tubules could be visualized to a certain extent using their autofluorescent properties, although this approach did not provide adequate resolution of tubular structure in 3-D reconstructions of kidney tissue. Nevertheless, future refinement of imaging relying on tubular autofluorescence, or use of alternative approaches to label the tubules with antibodies, could overcome the limitations of our current method.

6.2 INTRODUCTION

Chronic kidney disease (CKD) is associated with progressive loss of peritubular capillaries (PTCs) as shown in both experimental animal models (1, 30, 31) and human patients (6, 15). Recently, Babickova and colleagues showed that both ultrastructural and functional abnormalities in PTCs are common in multiple forms of CKD, regardless of etiology (1). In their study, the ratio of capillary density to renal tubular segments progressively decreased in mouse models of unilateral ureteral obstruction, unilateral ischemia-reperfusion injury, and Alport syndrome (Col4a3-deficient mice). These findings followed on from the seminal observations of Basile and colleagues, who demonstrated depletion of PTCs in the outer medulla by utilizing Microfil® infusion into rat kidneys 4–40 weeks after ischemia-reperfusion injury (3). They also provided evidence that tubulointerstitial fibrosis gradually exacerbates and induces the loss of PTCs and subsequently promotes renal dysfunction.

The integrity of PTCs is essential for maintenance of kidney function. PTCs run alongside the renal tubules and provide nutrients and oxygen to nearby renal tubules which in turn is utilized to generate ATP for maintenance of tubular function, especially reabsorption of electrolytes (24). Under normal physiological conditions approximately 80% of renal oxygen consumption is utilized for sodium reabsorption by $\text{Na}^+\text{-K}^+\text{-ATPase}$ at the basolateral membrane of renal tubules (10). This high oxygen consumption in renal tubules renders the kidney susceptible to development of hypoxia (11) if any reduction of oxygen supply occurs from PTCs to tubules due to an increase in diffusion distances between renal tubules and PTCs or loss of PTCs (12, 26). There is good evidence for a causal pathway between the decline in PTC density and the development of renal hypoxia in experimental models of CKD (23, 30). For example, renal tubular hypoxia occurs at an early stage (by 2 weeks) in a rat model of glomerulonephritis, which is associated with loss of PTCs (structural rarefaction) and reduced blood flow (functional rarefaction) in remaining PTCs (23).

Despite the evidence of association between loss of PTCs and development of renal hypoxia in multiple forms of CKD, our current knowledge of the impact of capillary rarefaction on oxygen delivery to renal tubular elements is poor. Indeed, the complex spatial relationships between the renal vasculature (the source of oxygen) and the renal tubules (the major oxygen sink in the kidney) has been a major barrier to our understanding of the dynamics of renal oxygenation (9). Computational models of renal oxygen transport provide an opportunity to overcome some of this complexity. Our

research group and collaborators have developed a series of computational models of oxygen transport in the kidney (13, 14, 17, 19-21, 28). These computational models are based on the principle of multi-scale modeling. That is, each component of the model (e.g. diffusion of oxygen from a glomerulus) is modeled separately but simultaneously. Consequently, the quality of the data generated from model simulations depend on accurate information regarding renal function and structure (19-21). Currently, the major shortcoming of these models is their relatively simple representation of oxygen diffusion between PTCs and the renal tubules (19-21). This limitation is a consequence of the lack of accurate anatomical information regarding PTC morphology and the geometrical relationships between PTCs and tubules.

The spatial relationships between PTCs and renal tubules is poorly defined due to difficulties in identifying these structures at high resolution in three dimensions. Immunostaining of the endothelium of blood vessels is commonly used in experimental studies for assessing the surface area of PTCs and for quantifying the number of PTCs within a particular area of tissue (16, 33). CD31, an endothelial marker, is commonly used for this purpose. However, this antigen is also expressed in non-vascular tissues (e.g. lymphatic vessels) so labeling of tissues by anti-CD31 antibody may over-estimate vascular density (18). Previous observations generated in our laboratory indicate that histochemical and immunohistochemical technique have limited utility in identification of artery and vein pairs in rat kidney (27). Synchrotron-based micro-computed tomography has also been used to characterize the vascular geometry within the kidney (17, 29). After filling the vasculature with Microfil®, a radio-opaque substance, synchrotron-based micro-CT allows visualization of the renal vasculature in three-dimensions (3-D) (27). However, this technique is also limited by resolution. In addition I cannot visualize renal tubules using this method as the Microfil® is only present in the renal vasculature. A method of filling the vasculature with gelatin containing fluorescein isothiocyanate (FITC) conjugated albumin (gelatin-FITC) has been shown to be useful in staining the vascular network of the mouse brain (8, 22). This fluorescent gel material, gelatin-FITC, was retained in the vascular lumen during and after optical clearing processes (8, 22). This method allows the blood vessels to be clearly distinguished from surrounding tissues under confocal microscopy. In the experiments described in this chapter I performed a series of pilot studies in an attempt to modify the use of gelatin-FITC for use in the kidney. I reasoned that filling the renal circulation with gelatin-FITC and labeling tubules by immunofluorescence might allow the identification of not only the renal vasculature, but also its association with tubules at high resolution. To this end, I determined the feasibility of combining the

labeling of the vasculature with gelatin–FITC with labeling of the renal tubules with a monoclonal pan-cytokeratin antibody conjugated with Alexa Fluor 647.

6.3 METHODS

6.3.1 Animals

Male Sprague-Dawley rats, aged 12–13 weeks ($n=7$, body weight = 390 ± 12 g), were obtained from the Monash Animal Research Platform (Monash University, Melbourne, Victoria, Australia). The rats were housed individually under standard laboratory conditions; $22 \pm 1^\circ\text{C}$, $40 \pm 1\%$ humidity and with a 12-hour light/dark cycle (06.00–18.00 hours). Rats were allowed free access to water and were fed a standard laboratory rat chow diet *ad libitum*. Experiments were approved in advance by the Animal Ethics Committee of the Monash University Animal Resources Platform. The experiments were performed in accordance with the Australian Code of Practice for the Care and Use of Animals for Scientific Purposes. Rats were allowed 1 week to acclimatize to their housing conditions prior to the commencement of experimental protocols.

6.3.2 Protocol: Staining of renal vasculature and renal tubules

Preparation of gelatin containing FITC-conjugated albumin: I adopted the protocol from Tsai *et al* for staining the renal vascular lumen (32). The staining solution was prepared in two steps. In step 1, a 2% (w/v) solution of gelatin (from porcine skin, type A, G1890, Sigma Aldrich, St Louis, MO, USA) was prepared in 0.1 M phosphate buffered saline (PBS) at 60°C . The solution was continuously stirred and heated at 60°C until the gelatin fully dissolved and the solution became clear. Then the gelatin solution was allowed to cool to 35 to 36°C with constant stirring. In step 2, a solution of 1% (w/v) FITC-albumin (albumin–fluorescein isothiocyanate conjugate, A9771, Sigma Aldrich, St Louis, MO, USA) was prepared in 0.1 M PBS (at 4°C). This FITC-albumin solution was filtered using a sterile syringe filter (pore size $0.22\ \mu\text{m}$). Finally, the FITC-albumin solution (step 2) was combined with the gelatin solution (step 1) at a ratio of 1:10. The mixed solution was stirred at $\sim 36^\circ\text{C}$ before perfusion into the rat kidneys. The temperature was kept below 37°C because Banks *et al* have shown that the FITC-conjugate is poorly stable at 37°C (2). This is due to hydrolysis of the chemical bond between FITC and the α -amino group of lysine (2).

Perfusion flow rate and temperature: I used a peristaltic pump (Masterflex® pumps, serial no 670649, Cole-Parmer Instrument Company, Chicago, IL, USA) and silicon tubing (Masterflex® 6411-13, Cole-Parmer Instrument Company) for perfusion of the gelatin-FITC (gelatin-FITC–albumin) into the rat’s kidney. In a bench-top experiment, I first assessed the outflow temperature at two different perfusion flow rates (1 ml/min and 3 ml/min; Figure 6.1).

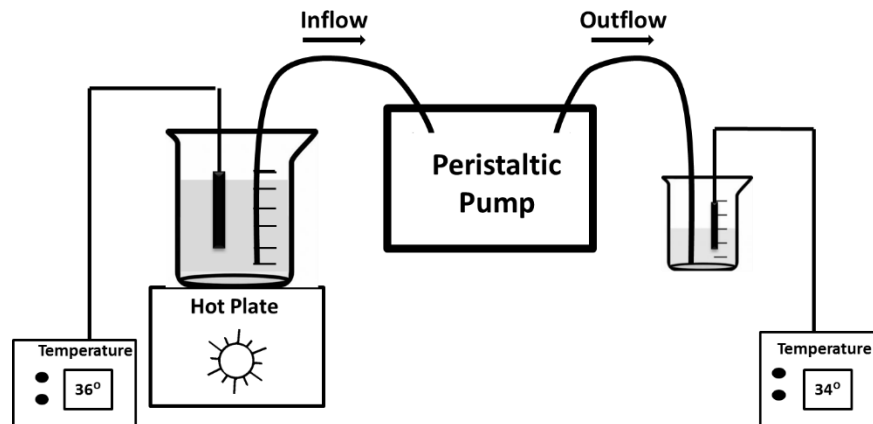


Figure 6.1 Schematic of a benchtop experiment for determination of outflow temperature of the gelatin-FITC at specific flow rates. For this experiment a 2% (w/v) gelatin solution was prepared in 0.1 M PBS at 60°C and then the solution was cooled down to ~36°C. The gelatin containing beaker was kept on a hot plate and inflow temperature for the gelatin solution was maintained at ~36°C. The temperature was monitored continuously using a thermometer. The outflow temperature was determined in triplicate at flow rates of 1 and 3 ml/min.

I identified that the averaged outflow temperature was ~23°C at a flow rate of 1 ml/min and ~28°C at a flow rate of 3 ml/min. I repeated the bench top experiment again, but this time I wrapped the tube with aluminum foil and primed the peristaltic tube for 10 minutes with gelatin solution (outflow temperature ~36°C). This produced an outflow temperature of ~30°C at a flow rate of 1 ml/min and ~34°C at a flow rate of 3 ml/min. Based on the perfusion flow rate, I divided rats into two groups. Group A received gelatin-FITC (n=2) or its vehicle gelatin (n=1) at a flow rate of 1 ml/min. Group B received gelatin-FITC (n=2) or vehicle gelatin (n=2) at a flow rate of 3 ml/min. Each rat received 30 ml of either gelatin-FITC or its vehicle.

Perfusion fixation and filling of the vasculature with gelatin: Rats were anesthetized by an intraperitoneal injection of sodium pentobarbital (60 mg/kg, Sigma Aldrich, NSW, Australia). Once

the pedal reflex was abolished, indicating a surgical level of anesthesia, a midline incision was made to expose the abdominal cavity. The abdominal aorta, inferior vena cava, and left and right kidney were isolated and freed from surrounding fat and connective tissue. Two silk ligatures (3/0, Dysilk, Dynek Pty Ltd, SA, Australia) were placed around the abdominal aorta and vena cava, one ligature just below the level of the left kidney and the other placed just above the level of the right kidney. Next, the abdominal aorta was catheterized below the level of the left renal artery using a polyethylene catheter (PE 90, Becton Dickinson and Company, NJ, USA). This catheter permitted retrograde perfusion of the aorta and thus perfusion of the renal arteries. The catheter was connected to a perfusion apparatus by a three way valve. The kidneys were perfused with 150-200 ml of cold 0.1 M PBS followed by 150-200 ml of 10% neutral buffered formalin at 150 mmHg. After that, the kidneys were slowly filled with 30 ml of gelatin-FITC at a flow rate of either 1 ml/min or 3 ml/min at an inflow temperature of ~36 °C. Immediately after perfusion, 50 ml of ice cold saline (0°C) was poured on each kidney for 15 minutes to solidify the gel. After that, the kidneys were removed, decapsulated and kept overnight in 10% neutral buffered formalin at 4°C.

Visualization of fluorescent signals after perfusion fixation: Slices of both the left and right post-fixed kidneys were visualized under a fluorescence microscope (Leica DFC450 C, Leica Microsystems, Switzerland) in order to check the quality of filling of the vascular lumen. Each kidney was sliced as shown in Figure 6.2, to generate 400 µm thick slices, with a series of razor blades evenly spaced at 400 µm. Three randomly selected thick sections from each kidney were visualized under a microscope. Images were taken at a wavelength of 488 nm using a 1.25X objective lens. Images were stored as 1280x960 pixel frames.

I have identified that kidney slices from rats that received gelatin-FITC at a flow rate of 3 ml/min were filled better compared to kidney slices processed after perfusion at a flow rate of 1 ml/min. Therefore I used kidney slices processed after perfusion at a flow rate of 3 ml/min for further immunohistochemistry and optical clearing.

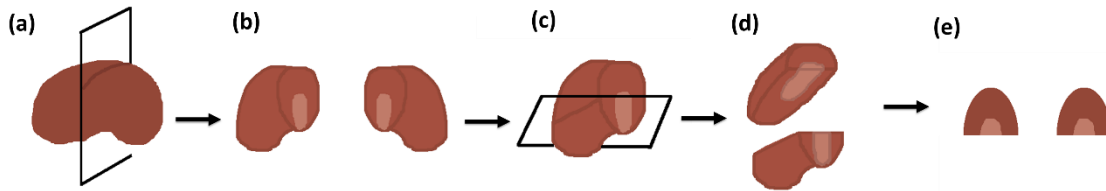


Figure 6.2 Schematic diagram for processing of kidney slices. Each kidney was cut perpendicularly to the longitudinal axis (a) and resulted in two halves (b). Next, each half of the kidney was cut horizontally in the transverse plane (c). Finally, the resulting portions (d) of the kidney were then sliced to generate 400 µm thick slices (e). Images were reproduced from (27).

Tubular labeling by immunohistochemistry: I used a monoclonal pan cytokeratin antibody conjugated with the fluorescent dye Alexa Fluor 647 (Pan Cytokeratin Antibody (AE1 + AE3) [Alexa Fluor® 647] NBP2-33200AF647, lot number: MSM2-371PBX180306-083018-AF 647, Novus Biologicals USA) for labeling of renal tubular epithelium. Two sets of four thick (400 µm) slices from each kidney were used for immunohistochemistry. Briefly, the kidney slices were rinsed thrice with 0.1 M PBS. Next, the kidney slices were incubated for 10 minutes in a solution containing 0.1% (vol/vol) Tween 20 in 0.1 M PBS. After that, the kidney slices were incubated in a 1% (w/v) bovine serum albumin (BSA) for 2 h at room temperature, with rocking. Subsequently, the kidney slices were transferred to a solution containing the monoclonal pan cytokeratin antibody conjugated with Alexa Fluor 647 and incubation was performed either at room temperature or at 36°C for 6 days on an orbital shaker. The antibody solution was prepared in 1% (w/v) BSA. Each kidney slice was incubated with one of four concentrations of antibody solution (0, 1, 4, and 16 µg antibody/ml BSA).

Optical clearing: After a 6 day incubation period, the kidney slices were washed with 0.1 M PBS for 30 minutes on an orbital shaker. Next, the kidney slices were transferred to a glass petri dish and embedded in 2% (w/v) low-melting point agarose solution in water. The agarose solution was allowed to cool and formed an agarose disk. After that, the embedded kidney slices were dehydrated by incubation in a series of increasing ethanol concentrations, 50% (vol/vol) for 2 h, 70% (vol/vol) for 2 h and 100% (vol/vol) for 2 h. Finally, the kidney slices were incubated overnight in fresh 100% (vol/vol) ethanol. After overnight incubation, the ethanol was removed from the petri dish and cyanoacrylate glue (Tarzan's Grip Shockproof Super Glue, Selleys Pty Ltd, Australia) was applied to

the borders of the agarose disk in order to prevent the movement of the disk in the petri dish. Finally, 10 to 15 ml of ethyl cinnamate (catalog no W243000; Sigma Aldrich) was added to the petri dish and incubated at room temperature for 4 h. After the 4 h incubation the agarose and tissues were optically cleared and used for imaging.

Microscopy: I used a Leica SP8 Confocal Microscope (Leica Microsystems) fitted with a 20X objective lens (0.95 numerical aperture; 1950 μm working distance) for acquiring optical images. For excitation of FITC, a 488 nm laser was used and emitted light was detected at 500-550 nm. For exciting Alexa Fluor 647, a 650 nm laser was used and emitted light was detected at 655-671 nm. Representative images (optical section 1.944 μm) were obtained using a constant gain intensity and stored as 1024x1024 pixel frames. Serial optical images (z stack, 230 μm) were acquired at 1 μm intervals and stored as 1024x1024 pixel frames.

Fiji imaging software (Max-Planck Institute of Molecular Cell Biology and Genetics, Dresden, Germany) was used for image reconstruction. For 3-D reconstruction of the renal vasculature and tubular network Imaris (version 9.2.1, Bitplane AG, Zürich, Switzerland) was used. During 3-D reconstruction the display adjustment was set to auto settings for two color channels (green and red).

6.4 RESULTS

6.4.1 Visualization of kidney slices after perfusion with gelatin or gelatin-FITC

Under fluorescence microscopy, kidney slices filled with gelatin-FITC showed fluorescence (green fluorescence from gelatin-FITC-albumin) (Figure 6.3). Gelatin-FITC was not distributed throughout the kidney when a flow rate of 1 ml/min was used, as shown by the presence of scattered green fluorescence (Figure 6.3 b). In contrast, gelatin-FITC was distributed across the kidney at a flow rate of 3 ml/min, as shown by the distribution of green fluorescence throughout the kidney slices (Figure 6.3 d). Green fluorescence was absent in kidney slices perfused with gelatin alone either at 1 ml/min or 3 ml/min (Figure 6.3 a, c).

6.4.2 Labeling of renal blood vessels and tubules

In optical sections of kidneys filled with gelatin-FITC, renal tubules showed red autofluorescence while the renal vasculature showed green fluorescence from the FITC (Figure 6.4). Kidney slices,

incubated either at room temperature or 36°C, showed the presence of red fluorescence in renal tubules even in the absence of the monoclonal pan cytokeratin antibody conjugated with Alexa Fluor 647 (Figure 6.4 a,e). Similar staining of renal tubules was present in kidney slices incubated, either at room temperature or 36°C, with the antibody at various concentrations (Figure 6.4 b-d and f-h). Glomeruli and PTCs were stained green, suggesting that the gelatin-FITC-albumin remains within the renal vasculature after clearing of kidney tissue with ethyl cinnamate.

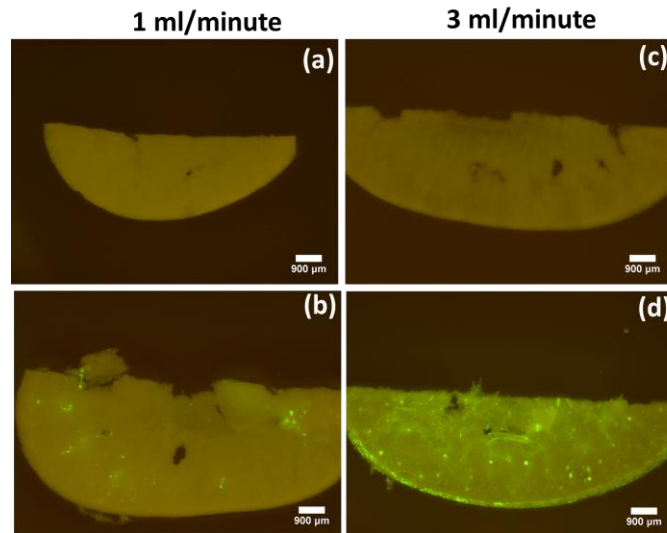


Figure 6.3 Micrographs of kidney slices after perfusion with gelatin or gelatin-FITC. Kidneys were perfused either at a flow rate of 1 ml/min with gelatin (a) or gelatin-FITC (b) or at a flow rate of 3 ml/min with gelatin (c) or gelatin-FITC (d). Images are typical of 3 thick slices taken from each kidney. Note, perfusion with gelatin-FITC resulted in green fluorescence (b,d). In contrast, green fluorescence was absent in kidney tissue perfused with gelatin only (a,c). Images were taken at a wavelength of 488 nm using a 1.25X objective lens.

6.4.3 Three-dimensional visualization of renal vasculature and tubules

A 3-D reconstruction of the renal vasculature and tubules was performed to visualize their geometric relationship (Figure 6.5 and Supplementary Video 6.1). In the 3-D reconstructions, the renal vasculature network was clearly identified by the presence of green fluorescence (Figure 6.5 a,b and video 6.1). In contrast, I could not identify a distinct network of renal tubules in the kidney by using either the monoclonal pan cytokeratin antibody conjugated with Alexa Fluor 647 or tissue endogenous autofluorescence (Figure 6.5 c and Supplementary Video 6.1).

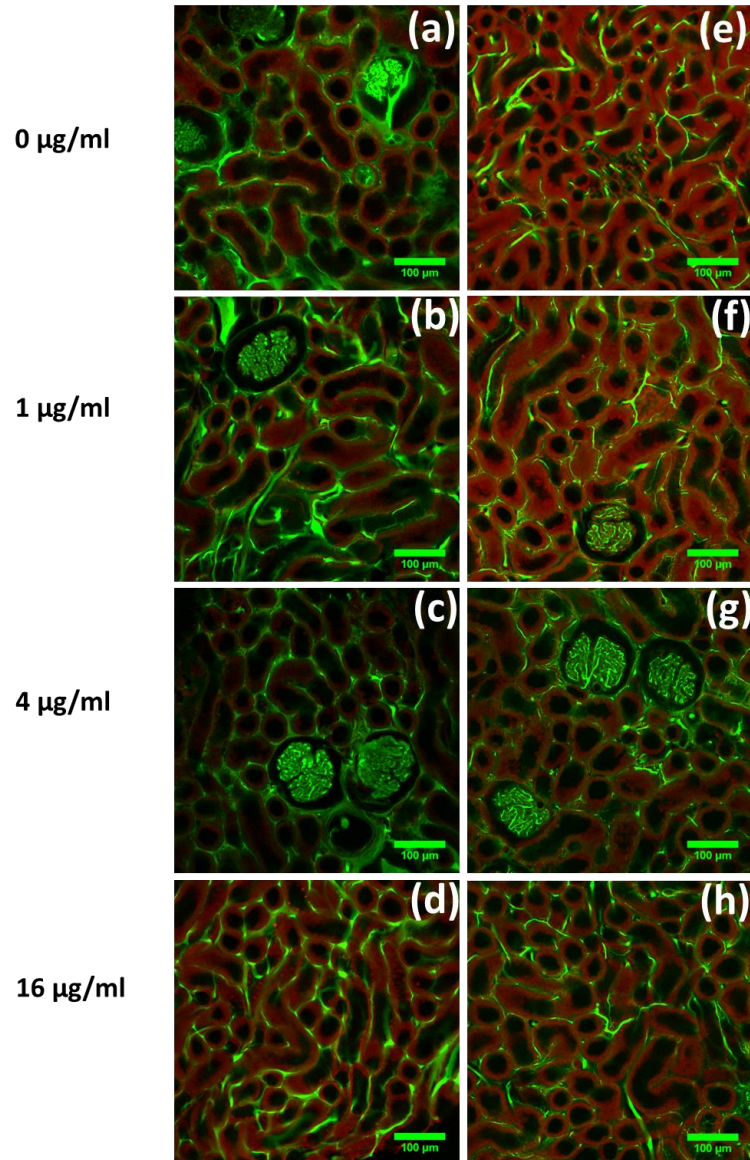


Figure 6.4 Visualization of vascular and tubular elements in kidney slices after optical clearing.

Kidney slices filled with gelatin-FITC were incubated with monoclonal pan cytokeratin antibody conjugated with Alexa Fluor 647 either at room temperature (a-d) or at 36°C (e-h) for 6 days. Kidney slices were incubated at 4 different concentrations of antibody i.e. 0 µg/ml (a,e), 1 µg/ml (b,f), 4 µg/ml (c,g) and 16 µg/ml (d,h). After 6 days of incubation, kidney slices were optically cleared and images were taken on an SP8 multiphoton microscope fitted with a 20X objective lens. Note, micrographs of single optical sections (1.94 µm) of a kidney slice show that glomeruli and PTCs were stained green (FITC-albumin) and tubules were stained red, regardless of the concentration of the pan cytokeratin antibody.

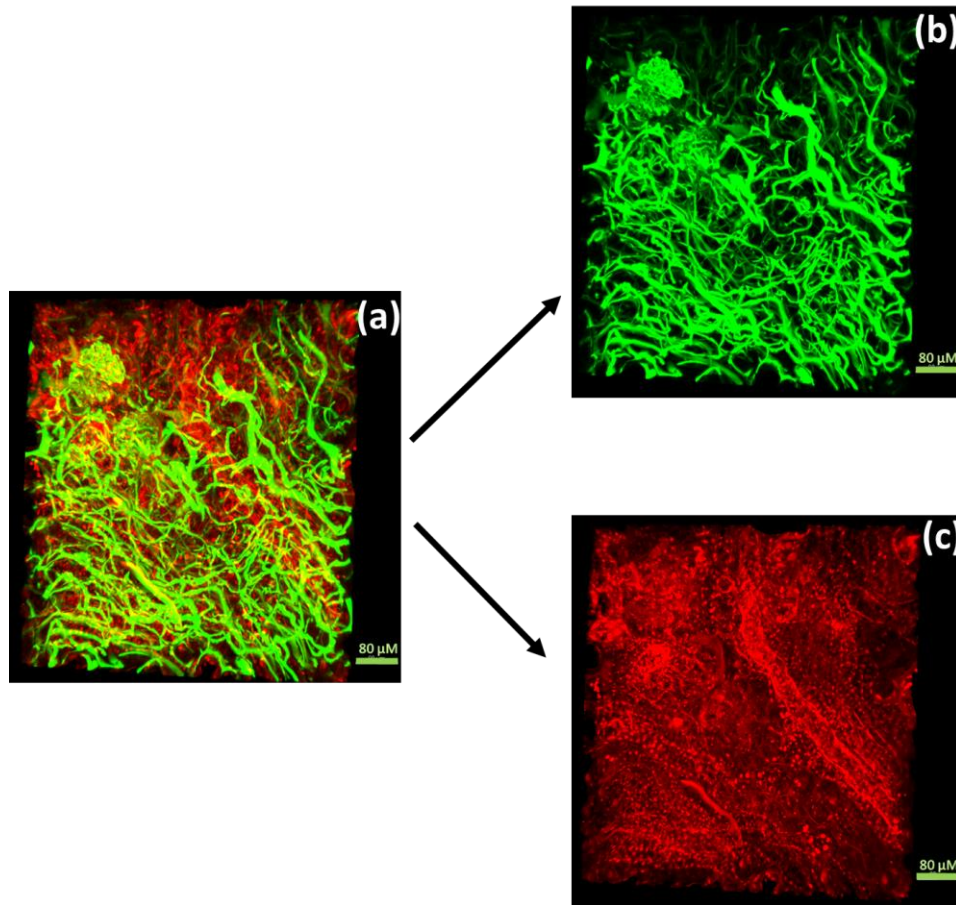


Figure 6.5 Visualization of vascular and tubular architecture of the rat kidney. (a) A 3-D reconstruction of the renal vasculature (green fluorescence) and tubules (red fluorescence) was performed using Imaris, a 3-D rendering and analysis software, from a z-stack (230 μm steps obtained at 1 μm intervals). In the color settings of Imaris, either the red channel was turned off for (b) visualization of the vasculature or the green channel was turned off (c) for visualization of renal tubules. Note, during 3-D reconstruction by Imaris the display adjustment settings for both the red and green colors were kept in the auto mode.

Supplementary video 6.1 3-D rendering of renal vasculatures and tubules of rats kidney. Serial optical sections (z-stack; 230 μm steps obtained at 1 μm intervals) were generated using an SP8 multiphoton microscope. A 3-D reconstruction was generated from a z-stack using Imaris, version 9.2.1. The video frame rate was 20 frames/second. (Video link: https://figshare.com/articles/3D_rendering_of_renal_vasculatures_and_tubules_of_rats_kidney_mp4/7314248).

6.5 DISCUSSION

The major findings of the current pilot experiment were that i) I could get better filling of the kidney with gelatin-FITC at the flow rate of 3 ml/min compared to the flow rate of 1 ml/minute, ii) gelatin-FITC remained within the renal vasculature after optical clearing with ethyl cinnamate, iii) glomeruli and PTCs were labeled by gelatin-FITC and a 3-D PTC network could be reconstructed from a series of optical sections, and iv) I was unable to label renal tubules within kidney slices using a pan cytokeratin antibody. However, renal tubules could be identified to at least some extent using their autofluorescent property. Consequently, I could visualize, albeit incomplete, a 3-D tubular network. Our current findings provide some initial progress in development of methods to assess the spatial arrangement between renal tubules and the renal vascular network. The method I developed could be used, for example, to quantify glomerular volume, and PTC diameter and surface area, both in healthy rats and rats with CKD. However, further studies are required to generate effective methods to label the renal tubules within slices of kidney to allow 3-D reconstruction of tubular morphology to allow quantification of the spatial arrangement between renal tubules and PTCs.

Our current study demonstrates the applicability of gelatin-FITC in combination with confocal microscopy for imaging PTCs in rats. The technique of labeling the microvasculature by gelatin-FITC has previously been successfully applied to the intact whole mouse brain (8) and whole ischemic mouse brain (22). In optically cleared whole mouse brain, the brain capillaries were clearly visible under light sheet microscopy and the smallest capillary diameter was measured to be 5 μm (22). However, there is an additional challenge associated with labeling the vasculature in the kidney because gelatin can pass through the glomerular membrane once it is degraded to smaller particles (25). Our solution was to use FITC conjugated to albumin. I expected this to be confined to the vascular compartment, since it should not be filtered at the glomerular membrane. Our expectation was confirmed by our current observations. Thus, renal blood vessels, including PTCs, could be visualized by high resolution microscopy to generate images of the fine structure of the vasculature. I was able to reconstruct the 3-D renal microvasculature network from z-stacked images (serial optical sections of cleared thick tissue) using Imaris, a 3-D rendering and analysis software.

A number of issues related to our use of gelatin-FITC require resolution. Firstly, while we can visualize PTCs using this technique, we do not yet know whether this technique provides an accurate

representation of their morphology. Shrinkage of the gelatin could be a particular problem because it would lead to under-estimation of the true diameter of PTCs. Previously, our group has used comparison with histological images generated by standard light microscopy to validate synchrotron-based micro-computer tomography of the renal vasculature (29). A similar approach could be taken to determine the degree to which shrinkage or other changes in tissue morphology confound our ability to generate accurate quantitative information about the renal vasculature from 3-D reconstructions generated using the gelatin-FITC method. An additional challenge will be the development of automated methods for analysis of these 3-D reconstructions. Our group has recently developed a method for automated analysis of the geometry of artery-vein pairs from synchrotron-based micro-computed tomography (17). A similar approach should be feasible for analysis of capillary networks.

The current method of labelling renal peritubular capillaries using gelatin-FITC might not provide complete labelling of the renal vasculature under disease conditions. For example, in kidneys with glomerular nephritis, gelatin-FITC might cross the filtration barrier during perfusion and thus may poorly fill downstream peritubular capillaries. In future, alternative methods could be used to generate more effective staining of the renal vasculature in injured kidneys. Potential approaches include (i) immunostaining of a novel protein of capillary basal lamina (cablin) (4, 5) in kidney slices or (ii) genetic labelling of endothelial cell (tyrosine protein kinase receptor; Tie 2) (4, 7) at the whole kidney level.

I was unable to generate a valid method for labeling of tubules with a pan cytokeratin antibody. This may reflect the slow penetration of antibody solutions into slices of tissue. In future studies alternative antibodies, longer incubation times, and variations in the thickness of tissue slices should be deployed, in an attempt to generate more effective staining. Nevertheless, the presence of autofluorescence in tubular elements may provide an alternative method for visualization of renal tubules. The intensity of this autofluorescence generated by our current methods was not sufficient for high resolution 3-D imaging of the renal tubules. However, it may be possible to refine the imaging conditions in the future to improve the visualization of tubules through autofluorescence.

In conclusion, in this pilot study I demonstrated the feasibility of using FITC-labelled albumin suspended within a solution of gelatin to label the renal vasculature, including the peritubular capillaries. However, I was unable to generate a method for high resolution imaging of the renal

tubules. Nevertheless, refinement of our approach may generate a method that can be used to quantify the geometry of the relationships between PTCs and tubules within the kidney. Such a method could provide the information required to accurately model oxygen transport between PTCs and tubules in both the healthy and diseased kidney, opening up a new avenue for understanding the roles of capillary rarefaction and fibrosis in the initiation and progression of CKD.

6.6 REFERENCES

1. **Babickova J, Klinkhammer BM, Buhl EM, Djudjaj S, Hoss M, Heymann F, Tacke F, Floege J, Becker JU, and Boor P.** Regardless of etiology, progressive renal disease causes ultrastructural and functional alterations of peritubular capillaries. *Kidney Int* 91: 70-85, 2017.
2. **Banks PR, and Paquette DM.** Comparison of three common amine reactive fluorescent probes used for conjugation to biomolecules by capillary zone electrophoresis. *Bioconjug Chem* 6: 447-458, 1995.
3. **Basile DP, Donohoe D, Roethe K, and Osborn JL.** Renal ischemic injury results in permanent damage to peritubular capillaries and influences long-term function. *Am J Physiol Renal Physiol* 281: F887-899, 2001.
4. **Basile DP, Friedrich JL, Spahic J, Knipe N, Mang H, Leonard EC, Changizi-Ashtiyani S, Bacallao RL, Molitoris BA, and Sutton TA.** Impaired endothelial proliferation and mesenchymal transition contribute to vascular rarefaction following acute kidney injury. *Am J Physiol Renal Physiol* 300: F721-733, 2011.
5. **Charron AJ, Xu W, Bacallao RL, and Wandinger-Ness A.** Cablin: a novel protein of the capillary basal lamina. *Am J Physiol* 277: H1985-1996, 1999.
6. **Choi YJ, Chakraborty S, Nguyen V, Nguyen C, Kim BK, Shim SI, Suki WN, and Truong LD.** Peritubular capillary loss is associated with chronic tubulointerstitial injury in human kidney: altered expression of vascular endothelial growth factor. *Hum Pathol* 31: 1491-1497, 2000.
7. **De Palma M, Venneri MA, Galli R, Sergi L, Politi LS, Sampaolesi M, and Naldini L.** Tie2 identifies a hematopoietic lineage of proangiogenic monocytes required for tumor vessel formation and a mesenchymal population of pericyte progenitors. *Cancer Cell* 8: 211-226, 2005.
8. **Di Giovanna AP, Tibo A, Silvestri L, Mullenbroich MC, Costantini I, Allegra Mascaro AL, Sacconi L, Frasconi P, and Pavone FS.** Whole-brain vasculature reconstruction at the single capillary level. *Sci Rep* 8: 12573, 2018.
9. **Evans RG, Gardiner BS, Smith DW, and O'Connor PM.** Intrarenal oxygenation: unique challenges and the biophysical basis of homeostasis. *Am J Physiol Renal Physiol* 295: F1259-1270, 2008.
10. **Evans RG, Harrop GK, Ngo JP, Ow CP, and O'Connor PM.** Basal renal O₂ consumption and the efficiency of O₂ utilization for Na⁺ reabsorption. *Am J Physiol Renal Physiol* 306: F551-F560, 2014.
11. **Evans RG, Ince C, Joles JA, Smith DW, May CN, O'Connor PM, and Gardiner BS.** Haemodynamic influences on kidney oxygenation: clinical implications of integrative physiology. *Clin Exp Pharmacol Physiol* 40: 106-122, 2013.
12. **Fine LG, and Norman JT.** Chronic hypoxia as a mechanism of progression of chronic kidney diseases: from hypothesis to novel therapeutics *Kidney Int* 74: 867-872, 2008.
13. **Gardiner BS, Smith DW, O'Connor PM, and Evans RG.** A mathematical model of diffusional shunting of oxygen from arteries to veins in the kidney. *Am J Physiol Renal Physiol* 300: F1339-1352, 2011.
14. **Gardiner BS, Thompson SL, Ngo JP, Smith DW, Abdelkader A, Broughton BR, Bertram JF, and Evans RG.** Diffusive oxygen shunting between vessels in the preglomerular renal vasculature: anatomic observations and computational modeling. *Am J Physiol Renal Physiol* 303: F605-618, 2012.

15. **Ishii Y, Sawada T, Kubota K, Fuchinoue S, Teraoka S, and Shimizu A.** Injury and progressive loss of peritubular capillaries in the development of chronic allograft nephropathy. *Kidney Int* 67: 321-332, 2005.
16. **Kang DH, Hughes J, Mazzali M, Schreiner GF, and Johnson RJ.** Impaired angiogenesis in the remnant kidney model: II. Vascular endothelial growth factor administration reduces renal fibrosis and stabilizes renal function. *J Am Soc Nephrol* 12: 1448-1457, 2001.
17. **Khan Z, Ngo JP, Le B, Evans RG, Pearson JT, Gardiner BS, and Smith DW.** Three-dimensional morphometric analysis of the renal vasculature. *Am J Physiol Renal Physiol* 314: F715-F725, 2018.
18. **Kriehuber E, Breiteneder-Geleff S, Groeger M, Soleiman A, Schoppmann SF, Stingl G, Kerjaschki D, and Maurer D.** Isolation and characterization of dermal lymphatic and blood endothelial cells reveal stable and functionally specialized cell lineages. *J Exp Med* 194: 797-808, 2001.
19. **Lee CJ, Gardiner BS, Evans RG, and Smith DW.** A model of oxygen transport in the rat renal medulla. *Am J Physiol Renal Physiol* 2018.
20. **Lee CJ, Gardiner BS, Ngo JP, Kar S, Evans RG, and Smith DW.** Accounting for oxygen in the renal cortex: a computational study of factors that predispose the cortex to hypoxia. *Am J Physiol Renal Physiol* 313: F218-F236, 2017.
21. **Lee CJ, Ngo JP, Kar S, Gardiner BS, Evans RG, and Smith DW.** A pseudo-three-dimensional model for quantification of oxygen diffusion from preglomerular arteries to renal tissue and renal venous blood. *Am J Physiol Renal Physiol* 313: F237-F253, 2017.
22. **Lugo-Hernandez E, Squire A, Hagemann N, Brenzel A, Sardari M, Schlechter J, Sanchez-Mendoza EH, Gunzer M, Faissner A, and Hermann DM.** 3D visualization and quantification of microvessels in the whole ischemic mouse brain using solvent-based clearing and light sheet microscopy. *J Cereb Blood Flow Metab* 37: 3355-3367, 2017.
23. **Matsumoto M, Tanaka T, Yamamoto T, Noiri E, Miyata T, Inagi R, Fujita T, and Nangaku M.** Hypoperfusion of peritubular capillaries induces chronic hypoxia before progression of tubulointerstitial injury in a progressive model of rat glomerulonephritis. *J Am Soc Nephrol* 15: 1574-1581, 2004.
24. **Molema G, and Aird WC.** Vascular heterogeneity in the kidney. *Semin Nephrol* 32: 145-155, 2012.
25. **Nahman NS, Drost WT, Bhatt UY, Sferra TJ, Johnson A, Gamboa P, Hinkle GH, Haynam A, Bergdall V, Hickey C, Bonagura JD, Brannon-Peppas L, Ellison JS, Mansfield A, Shie S, and Shen N.** Biodegradable microparticles for in vivo glomerular targeting: Implications for gene therapy of glomerular disease. *Biomed Microdevices* 4: 189-195, 2002.
26. **Nangaku M.** Chronic hypoxia and tubulointerstitial injury: a final common pathway to end-stage renal failure. *J Am Soc Nephrol* 17: 17-25, 2006.
27. **Ngo JP.** The structural basis of kidney oxygenation (Doctoral dissertation). In: *Department of Physiology*. Australia: Monash University, 2016.
28. **Ngo JP, Kar S, Kett MM, Gardiner BS, Pearson JT, Smith DW, Ludbrook J, Bertram JF, and Evans RG.** Vascular geometry and oxygen diffusion in the vicinity of artery-vein pairs in the kidney. *Am J Physiol Renal Physiol* 307: F1111-1122, 2014.
29. **Ngo JP, Le B, Khan Z, Kett MM, Gardiner BS, Smith DW, Melhem MM, Maksimenko A, Pearson JT, and Evans RG.** Micro-computed tomographic analysis of the radial geometry of intrarenal artery-vein pairs in rats and rabbits: Comparison with light microscopy. *Clin Exp Pharmacol Physiol* 44: 1241-1253, 2017.

30. **Ohashi R, Kitamura H, and Yamanaka N.** Peritubular capillary injury during the progression of experimental glomerulonephritis in rats. *J Am Soc Nephrol* 11: 47-56, 2000.
31. **Ohashi R, Shimizu A, Masuda Y, Kitamura H, Ishizaki M, Sugisaki Y, and Yamanaka N.** Peritubular capillary regression during the progression of experimental obstructive nephropathy. *J Am Soc Nephrol* 13: 1795-1805, 2002.
32. **Tsai PS, Kaufhold JP, Blinder P, Friedman B, Drew PJ, Karten HJ, Lyden PD, and Kleinfeld D.** Correlations of neuronal and microvascular densities in murine cortex revealed by direct counting and colocalization of nuclei and vessels. *J Neurosci* 29: 14553-14570, 2009.
33. **Yuan HT, Li XZ, Pitera JE, Long DA, and Woolf AS.** Peritubular capillary loss after mouse acute nephrotoxicity correlates with down-regulation of vascular endothelial growth factor-A and hypoxia-inducible factor-1 alpha. *Am J Pathol* 163: 2289-2301, 2003.

CHAPTER 7

PERSPECTIVES AND FUTURE DIRECTIONS

The central theme of the studies described in this thesis is renal hypoxia and its role in the pathophysiology of chronic kidney disease (CKD). As we recently identified, in a major review of this topic (50) reproduced in Appendix 1, this is a field in which many important questions remain. In the studies described in this thesis, I have investigated the following questions to generate more definitive evidence to confirm or refute the chronic hypoxia hypothesis. These are:

- 1) Is renal tissue hypoxia associated with adenine-induced CKD (Ad-CKD)? (Chapters 2 and 3)
- 2) Are renal tubular hypoxia and interstitial fibrosis spatially associated in Ad-CKD? (Chapters 2 and 3)
- 3) Does hypoxia precede renal dysfunction in Ad-CKD? (Chapter 4)
- 4) Is glomerular hyperfiltration, which would be expected to drive renal hypoxia, an early event in type 1 diabetes? (Chapter 5)
- 5) Is it feasible to use multiphoton microscopy, to quantify the spatial relationships between peritubular capillaries (PTCs) and renal tubules, and so support further development of computational models of renal oxygen transport? (Chapter 6)

To answer the above questions we need reliable methods to assess renal oxygenation with high temporal and/or spatial resolution. We also require reliable methods to quantify the factors that determine renal oxygen delivery (e.g. renal perfusion and renal vascular geometry) and renal oxygen consumption (e.g. glomerular filtration rate (GFR) and thus the filtered load of sodium). In the studies described in this thesis I have refined such methods and applied them to better understand the role of renal hypoxia in the pathophysiology of CKD. For example, pimonidazole adduct immunohistochemistry was used for assessing cellular hypoxia in Ad-CKD (Chapters 2 and 3). This technique provides excellent spatial resolution of renal tissue PO_2 but does not provide direct quantification. Tissue PO_2 can be quantified using Clark electrodes. In anesthetized rats, renal tissue PO_2 was measured by Clark electrode while renal oxygen delivery and consumption were determined by measurement of renal blood flow, renal arterial and venous blood oxygen content (Chapter 4). The Clark electrode allowed us to generate a map of renal tissue PO_2 (spatial resolution) within the renal cortex and medulla. However renal tissue PO_2 can only be measured at one time point, thus providing limited temporal resolution. To determine the time course of changes of renal tissue PO_2 (temporal resolution) I used radiotelemetry in conscious and free living animals across a 7 day adenine treatment period (Chapter 4). Together, these methods provided

high levels of temporal and spatial resolution of renal oxygenation in Ad-CKD. I used transcutaneous measurement of fluorescein isothiocyanate (FITC)-sinistrin clearance to assess the time-course of development of glomerular hyperfiltration in conscious rats rendered diabetic by administration of streptozotocin (STZ) (Chapter 5). These studies allowed me to investigate the potential for hyperfiltration to be an early driver of renal tissue hypoxia in diabetes. In addition, I performed a preliminary study with the aim of developing a new approach to quantify the 3-dimensional arrangement of renal PTCs and tubules, which could be used to support further development of computational models of oxygen transport to renal tissue (Chapter 6).

7.1 IS RENAL TISSUE HYPOXIA ASSOCIATED WITH ADENINE-INDUCED CHRONIC KIDNEY DISEASE?

It has been two decades since Fine *et al* proposed the chronic hypoxia hypothesis, implicating tubulointerstitial hypoxia as a ‘final common pathway’ for the initiation and progression of CKD (17). Over the past two decades, renal hypoxia has been observed in multiple forms of CKD, including diabetic nephropathy (18, 52, 57, 60), hypertensive CKD (72, 73), the remnant kidney model (38), polycystic kidney disease (9, 48), and CKD after ischemia/reperfusion injury (53). However, these studies could not demonstrate the precise time-point of development of renal hypoxia or a causal relationship between hypoxia and renal damage in experimental models of CKD. This is at least partly due to the relatively slowly developing nature of CKD (3, 29). I reasoned that, to examine the temporal and spatial relationships between renal hypoxia and the development of CKD, we need a rodent model of CKD in which pathological changes in the kidney develop rapidly.

In the experiments described in Chapters 2 and 3 of this thesis I found that rats treated with 100 mg adenine/day over a 15 day period exhibited characteristics of CKD similar to those observed in CKD in humans and in clinically relevant animal models of CKD. For example, adenine-treated rats exhibited elevated plasma concentrations of urea and creatinine, proteinuria and renal tubulointerstitial fibrosis. The most important finding was that Ad-CKD is associated with renal tissue hypoxia, as indicated by the presence of positive pimonidazole staining in renal tissue 15 day after commencing adenine feeding.

Pimonidazole adduct immunohistochemistry has been used for assessing renal cellular hypoxia in multiple forms of CKD (21, 58, 59, 61, 66). In the experiments described in Chapter 3, I identified that pimonidazole adduct immunohistochemistry, using the standard monoclonal mouse anti-

pimonidazole antibody, can produce artefactual staining of non-cellular components of the kidney tissue of adenine-treated rats. This artefactual staining was particularly prominent in tubular casts and cellular debris within the tubular lumen. Our findings indicated that it is caused by non-specific binding of the anti-mouse secondary antibody to damaged renal tissue and tubular casts. I solved this problem by using a combination of an anti-pimonidazole antibody raised in rabbit and an anti-rabbit secondary antibody. Using this new method I was able to confirm the presence of hypoxia (as shown in Chapter 2) in the kidneys of adenine-treated rats, which appears to be specifically localized to the tubular epithelium. Thus, I was able to demonstrate that CKD develops within two weeks of adenine-feeding and that Ad-CKD is associated with renal hypoxia. Thus, I established the potential that this model could be used to examine the temporal relationship between hypoxia and the development of CKD.

7.2 ARE RENAL TUBULAR HYPOXIA AND INTERSTITIAL FIBROSIS SPATIALLY ASSOCIATED IN ADENINE-INDUCED CHRONIC KIDNEY DISEASE?

Ow *et al* argued that, to characterize the role of renal tissue hypoxia in progression of CKD, I need a better understanding of the spatial relationship between renal tissue hypoxia and tissue damage. To date, this issue has received little attention.

In the experiments described in Chapters 2 and 3 of this thesis I generated evidence that renal tubular hypoxia is spatially associated with renal fibrosis in Ad-CKD. Under normal physiological conditions almost 80% of oxygen consumption in the kidney is utilized for sodium reabsorption by the Na-K-ATPase pumps located on the basolateral surface of the renal tubules (14). This high consumption of oxygen is one of the factors that render the kidney susceptible to hypoxia if oxygen supply from capillaries to renal tubules is restricted. Interstitial fibrosis would be expected to impair oxygen diffusion from peritubular capillaries to renal tubules by increasing the diffusion distance (16, 40). Furthermore, there is now strong evidence that tubulointerstitial fibrosis is associated with progressive loss of peritubular capillaries in experimental model of CKD (1, 3, 47). In the fibrotic kidney the gradual loss of PTCs appears to be preceded by changes in their ultrastructure, such as swelling of endothelial cells, loss of endothelial fenestrations, and formation of subendothelial electron-lucent spaces (1). These structural alterations of PTCs are associated with downregulation of vascular endothelial growth factor (1, 27, 47), the proangiogenic factor required for maintenance of renal PTCs under normal physiological conditions (8). Loss of PTCs would be expected to further restrict the downstream blood flow from glomerular capillaries and thus limit oxygen supply to the renal tubules (35). Thus, interstitial fibrosis likely has a dual action

to promote hypoxia, both by directly impeding the diffusion of oxygen from peritubular capillaries to tubules and indirectly by promoting loss of the microvasculature.

Despite the evidence of association between renal fibrosis and development of renal hypoxia in multiple forms of CKD, a causal association between renal fibrosis and hypoxia has not been determined yet. This might be due to a lack of effective therapeutic agents for prevention of renal fibrosis. Pirfenidone, an anti-fibrotic agent, has received considerable attention due to its beneficial effects in prevention of fibrosis in numerous disorders including idiopathic pulmonary fibrosis (23, 24) and fibrotic renal disorder (6, 55). This therapeutic agent reduces fibrosis most likely by suppressing the transcription of the gene for transforming growth factor- β (23), the master regulator of fibrosis (39). I hypothesize that amelioration of development of renal fibrosis by pirfenidone or related anti-fibrotic therapies could maintain the structure of PTCs and thus inhibit the progression of renal hypoxia in Ad-CKD. This hypothesis could be tested in the rat model of Ad-CKD used in the studies described in this thesis. Radiotelemetry could be a particularly useful method to examine the effects of anti-fibrotic therapy in Ad-CKD, since it allows long-term and continuous monitoring. It could also be used to guide the choice of time-points for collection of renal tissue, from separate groups of animals, for assessment of the structure and density of PTCs (e.g. using techniques similar to those described in Chapter 6 of this thesis), quantification of fibrosis (e.g. picosirious red staining), and analysis of the signaling cascades that drive fibrosis and capillary rarefaction.

7.3 DOES HYPOXIA PRECEDE RENAL DYSFUNCTION IN ADENINE-INDUCED CHRONIC KIDNEY DISEASE?

If renal hypoxia is a pathogenic factor in the initiation and progression of CKD, we should be able to detect renal hypoxia before overt renal dysfunction (50). This appears to be the case in the remnant kidney model of CKD (38), in diabetic nephropathy (51, 60) and in hypertensive CKD associated with activation of the renin-angiotensin system (12). However, this issue has not been addressed in detail, in part due to the unavailability, until recently, of methods that allow changes of renal tissue PO₂ to be monitored continuously in freely living animals. A newly developed radiotelemetric method for measurement of renal oxygenation in unanesthetized rats now provides a method for characterizing the time-course of changes in renal tissue PO₂ in rodent models of CKD (31, 32).

In the experiments described in Chapter 4 of this thesis, I found no evidence of renal hypoxia during the first week of development of Ad-CKD in unanesthetized rats. This conclusion was supported both by observations generated using the newly developed radiotelemetric technique and by assessing expression of hypoxia-inducible factor-1 α and -2 α protein. Our inability to detect renal hypoxia using radiotelemetry is unlikely to be due to a deficit in the sensitivity of the method. Koeners *et al* (31) showed that radiotelemetry could detect acute changes in renal tissue PO₂ when rats were subjected to acute changes in inspired oxygen content (hyperoxia or hypoxia) (31). Furthermore, Emans *et al* (12) were able to detect renal cortical hypoxia within the first 15 h after activation of the endogenous renin-angiotensin system in an animal model in which overt CKD does not develop until 4 weeks later. In contradistinction to our findings in unanesthetized rats using radiotelemetry, in anesthetized adenine-treated rats medullary tissue PO₂, measured by the 'gold standard' Clark electrode technique, was less compared to the medullary tissue PO₂ in corresponding control rats. However, our findings indicate that the relative medullary hypoxia observed in anesthetized adenine-treated rats might be due to effects of anesthesia and laparotomy on medullary oxygenation, which appear to be altered by chronic adenine-feeding.

Our inability to detect renal hypoxia in the early stages of Ad-CKD might be a consequence of the nature of the pathophysiology in this disease model. Ad-CKD is a model of crystal-induced nephropathy (41). Deficiency of the enzyme adenine phosphoribosyl transferase (26, 41, 62) or excessive dietary adenine (54, 75) leads to accumulation of adenine in the blood, which further results in formation of insoluble crystals of 2,8-dihydroxyadenine in the renal tubules (74). These tubular casts cause obstruction of tubular flow, which in turn initiates renal disease (4, 11). The tubular obstruction would be expected to increase proximal tubular free-flow pressure (intratubular hydrostatic pressure) (43) and subsequently might lower the net hydraulic pressure gradient across the glomerular capillary wall and thereby decrease GFR (64). In our study the marked deficit of GFR (66%) in adenine-treated rats likely provide some protection against development of renal hypoxia by limiting renal oxygen consumption (VO₂, which was reduced by ~65% in adenine-treated rats). Similar observations have been made in rats during the sub-acute phase of renal ischemia/reperfusion injury (49). In that study renal hypoxia could not be detected in the first 5 days after reperfusion and both GFR and renal VO₂ were reduced significantly. Renal VO₂ and GFR are closely associated (56, 65), as the latter determines the tubular load and thereby sodium reabsorption.

Renal oxygenation is maintained by the balance between renal oxygen delivery (DO_2) and VO_2 (15). Disruption of this balance has been shown to be associated with renal hypoxia in multiple forms of CKD (7, 37, 51). In our study the relative preservation of renal tissue PO_2 within the first 7 days of adenine treatment may be because the deficit in VO_2 (65.2%) matched or exceeded that of DO_2 (50.6%).

Our findings also raise some important questions about the time-course of development of renal hypoxia in Ad-CKD. As demonstrated in the experiments described in Chapters 2 and 3, renal tissue hypoxia is clearly evident after two weeks of adenine feeding. However, renal hypoxia appears not to be present after 7 days of adenine feeding. It would be of great interest to identify the point at which hypoxia begins to develop. I hypothesize that this transition point should occur when the deficit in renal tissue oxygen delivery exceeds that of renal tissue oxygen consumption. If this prediction holds we could more confidently accept the proposition that kidney disease could be associated with renal hyperoxia, normoxia or hypoxia, depending on the balance in changes in local renal tissue oxygen delivery and consumption. However, there are a number of technical barriers to the successful completion of such an experiment. Firstly, we should ideally be able to measure whole kidney DO_2 and VO_2 in the conscious animal. Such experimental measurements are technically feasible in large animals (5) but are far more difficult in rodents. Another current methodological limitation is the lack of methods for assessing local oxygen delivery and consumption (13, 50). If these technical limitations could be overcome, it should be feasible to more precisely define the biophysical basis of renal oxygenation in CKD.

Our current observations are not consistent with a role of renal hypoxia as a pathogenic factor in the early stages of Ad-CKD, but this conclusion cannot be generalized to other forms of CKD. For example, renal hypoxia was demonstrated, using electron paramagnetic resonance oximetry, as early as three days after induction of diabetes by STZ in mice (18). In that study, renal hypoxia was observed well before the onset of diabetic nephropathy. However, the major limitation of that study, and indeed most other previous studies of the role of renal hypoxia in the pathogenesis of CKD, is that renal oxygenation was measured in anesthetized animals, and only over a brief period of time. Thus, a potentially confounding effect of anesthesia could not be excluded. Our radiotelemetric technique may overcome this limitation. In future, radiotelemetry could be used to monitor the changes of renal tissue PO_2 in rodent models of type 1 diabetes and other forms of CKD. This method provides a means to identify the precise time-point of development of renal hypoxia and thereby the temporal relationship between renal hypoxia and progression of CKD.

7.4 IS GLOMERULAR HYPERFILTRATION, WHICH WOULD BE EXPECTED TO DRIVE RENAL HYPOXIA, AN EARLY EVENT IN TYPE 1 DIABETES?

Renal hypoxia is an early and persistent characteristic of experimental type 1 diabetes (10, 57). Glomerular hyperfiltration, also a characteristic of type 1 diabetes (22, 25, 63, 71), may contribute to the development of renal hypoxia in type 1 diabetes. Under normal physiological conditions, approximately 80% of renal VO_2 is utilized for tubular sodium reabsorption (14). Hyperfiltration would be expected to promote renal hypoxia by increasing the filtered load of sodium and thereby reabsorption of sodium by Na-K-ATPase pumps on the basolateral membrane of renal tubules. To examine the causal relationship between glomerular hyperfiltration and development of renal hypoxia, it would first be necessary to assess the time courses of development of these phenomena. Thus, the first step in this process was to characterize the time-course of changes in GFR in an experimental model of type 1 diabetes.

In the experiment described in Chapter 5 of this thesis I employed transcutaneous measurement of fluorescein isothiocyanate (FITC)-sinistrin clearance in conscious rats to calculate the excretion half-life ($t_{1/2}$) of FITC-sinistrin and thus allow estimation of GFR. I compared four different kinetic models to calculate the $t_{1/2}$ of FITC-sinistrin and thus estimation of GFR. This included a one-compartment kinetic model (1-COM), a two-compartment kinetic model (2-COM), a three-compartment kinetic model (3-COM) and a three-compartment kinetic model with baseline correction (3-COMB). From a theoretical prospective, I reasoned that the 3-COMB method is the most valid of these four approaches as this model describes the complete course of clearance kinetics for FITC-sinistrin, from the point of injection, with automated baseline correction. Using the 3-COMB method I found that glomerular hyperfiltration is a prominent characteristic of the early stages of STZ-induced type 1 diabetes and thus is a potential driver of diabetic nephropathy. In ongoing studies, our group is using blood oxygen level-dependent magnetic resonance imaging (BOLD-MRI) to characterize the time course of development of renal hypoxia in STZ-induced diabetes. Comparison of these data sets should provide a unique insight into the temporal relationship between glomerular hyperfiltration and renal hypoxia in type 1 diabetes. Nevertheless, while both these methods allow repeated measurements to be made in the same animals, they are limited to snap-shots in time. Thus, as discussed above, it would also be of considerable interest to apply radiotelemetry to more precisely define the time-course of development of renal hypoxia in type 1 diabetes.

Our findings may also provide the basis for further investigation of the mechanistic link between hyperfiltration and hypoxia in the diabetic kidney. This causal relationship could be investigated using a sodium-dependent glucose co-transporter 2 (SGLT-2) inhibitor (42), a new class of antidiabetic agent, in STZ-diabetic rats equipped with a radiotelemeter for measurement of renal tissue PO₂. SGLT-2, located on the luminal aspects of the proximal tubule, is responsible for reabsorption of ~90% of proximal tubular glucose in animals and humans under normoglycemic conditions (69, 70). In diabetes, the high concentration of glucose in glomerular filtrate, and thus the large quantity of glucose reabsorbed in the proximal tubule, leads to increased reabsorption of sodium in the proximal tubule (2). Inhibition of SGLT-2 reduces reabsorption of both glucose and sodium in the proximal tubule, increasing distal solute delivery, and thus ameliorating the tubuloglomerular feedback signal that drives hyperfiltration (68). Collectively, these actions should ameliorate renal hypoxia, at least in the cortex. Consistent with this idea, O'Neill *et al* showed that the non-specific inhibitor of both SGLT1 and SGLT2, phlorizin, increased renal cortical tissue PO₂ in anesthetized rats with type 1 diabetes (46). Telemetric measurement of renal tissue PO₂ provides an opportunity to examine this effect in the absence of the confounding effects of anesthesia and with exquisite temporal resolution. Such future studies are warranted.

7.5 SPATIAL ARRANGEMENT OF PERITUBULAR CAPILLARIES AND RENAL TUBULES.

Computational models have made a particularly important contribution to renal physiology (67). In part, this can be attributed to the complexity of renal physiological processes. In the case of renal oxygenation, this complexity is writ large (15, 33). Over recent years, models of oxygen transport in the kidney have been developed with ever-increasing complexity. In the case of our research group and collaborators, this process started with development of a one-dimensional model only incorporating the axial geometry of the pre-glomerular circulation (19). Two-dimensional models were then developed that incorporated first idealized (20), and then realistic (44), representations of the radial geometry of artery-vein pairs. More recently, these models were combined into a pseudo three-dimensional model of oxygen transport in the renal cortex (35, 36) that allows estimation of oxygen fluxes throughout the renal cortex. Most recently, this has been combined with a computational model of oxygen transport in the renal medulla (34).

These evolving computational models all operate on the principle of multiscale modelling. That is, to describe the system, individual components are modelled separately but simultaneously. The quality of these individual models depends heavily on the accuracy of the information they are

based on, including anatomical details. In the case of the renal circulation, we now have very detailed anatomical information upon which to base models of oxygen transport in the pre-glomerular circulation (28, 44, 45) and in the renal medulla (34). However, our understanding of the geometric relationship between peritubular capillaries and renal tubules remains poor. This information is critical because, even in the healthy kidney, oxygen delivery to cortical tissue appears to be ‘diffusion limited’ by capillary surface area (35). Furthermore, microvascular loss and thus capillary rarefaction is a common characteristic of CKD, regardless of the etiology of the disease (1).

In the experiments described in Chapter 6 I performed a preliminary investigation to generate high resolution reconstructions of the spatial relationships between peritubular capillaries and their associated tubules. We were able to visualize peritubular capillaries by filling the renal vasculature with a solution of gelatin containing fluorescein isothiocyanate (FITC) conjugated albumin. Consequently, we reconstructed a 3-D network of peritubular capillaries from a series of optical sections. I was unable to label the renal tubules within kidney by using monoclonal pan cytokeratin antibody conjugated with Alexa Fluor 647. However, we could identify the renal tubular network to some extent, albeit incompletely, by using endogenous autofluorescence. Our preliminary experiment provides some initial progress in development of methods to assess the spatial arrangement between renal tubules and the renal vascular network. A number of challenges remain if we are to develop a method for high throughput analysis of renal vascular geometry so that we can apply the imaging methods developed in the experiments described in Chapter 6 to models of CKD.

The first challenge is the labeling of renal tubules within the kidney for visualization and subsequently 3-D reconstruction of the renal tubular network. Labeling of renal tubules could be achieved using either specific fluorescently labeled antibodies or by relying on the endogenous autofluorescence of renal tubules. A number of specific antibodies for labeling the tubular epithelium are available, which target members of the cadherin superfamily (transmembrane proteins; e.g. anti-N cadherin conjugated to Alexa Fluor[®] 647, anti-E cadherin conjugated to Alexa Fluor[®] 647) or members of the claudin family (tight junction membrane proteins; e.g. anti-claudin-4 conjugated to Alexa-Fluor[®]-594), which could be used to label renal tubules within the kidney. A major challenge in the use of such antibodies in thick slices of tissue, particularly when antigen retrieval methods must be avoided to maintain tissue integrity, is ensuring penetration of the antibody into the tissue slice. In future studies, the effects of variations in both the thickness of the

kidney slices and the length of the incubation period should be investigated in an effort to optimize staining. Alternatively, it may be possible to utilize endogenous tubular autofluorescence for identifying renal tubules. Thus, future investigations to optimize the imaging conditions, including wavelengths of emitted and detected light and gain setting, could potentially allow imaging of the renal tubules without the need for a specific fluorescent antibody.

An additional challenge will be the accurate measurement of diameter of PTCs after optical clearing of tissue. Fixation and optical clearing might cause shrinkage of tissue and/or of the gelatin within the renal vasculature (30). In our study shrinkage of the gelatin could be a particular problem because it might lead to under-estimation of the true diameter of PTCs. Previously, our group has used comparison with histological images generated by standard light microscopy to validate synchrotron-based micro-computed tomography of the renal vasculature (45). A similar approach could be taken to determine the degree to which shrinkage or other changes in tissue morphology confound our ability to generate accurate quantitative information about the renal vasculature from 3-D reconstructions generated using the gelatin-FITC method. Refinement of our current experimental approach may generate an imaging method that could be used to quantify the geometry of the relationships between PTCs and tubules within the kidney in both the healthy and diseased condition. Such a method could open a new avenue for understanding the roles of capillary rarefaction and fibrosis in the initiation and progression of CKD.

In conclusion, in the experiments described in this thesis I investigated the roles of renal hypoxia in the initiation and progression of Ad-CKD. I deployed a suite of methods for assessing renal oxygenation and its determinants. Taken collectively, my findings support the concept that renal tissue hypoxia is a common characteristic of CKD. The major drivers of this hypoxia probably differ depending on the etiology of the CKD. For example, fibrosis may be a critical event in driving hypoxia in Ad-CKD while hyperfiltration may be a critical early event that drives hypoxia in diabetic CKD. The fact that renal dysfunction can be detected in Ad-CKD before renal hypoxia does not support the idea that renal hypoxia is an absolute requirement for progression of CKD. Thus, perhaps in answer to the question we recently posed (50): hypoxia might sometimes be a cause, sometimes a consequence, and sometimes both a cause and consequence, of CKD.

7.6 REFERENCES

1. **Babickova J, Klinkhammer BM, Buhl EM, Djudjaj S, Hoss M, Heymann F, Tacke F, Floege J, Becker JU, and Boor P.** Regardless of etiology, progressive renal disease causes ultrastructural and functional alterations of peritubular capillaries. *Kidney Int* 91: 70-85, 2017.
2. **Bank N, and Aynedjian HS.** Progressive increases in luminal glucose stimulate proximal sodium absorption in normal and diabetic rats. *J Clin Invest* 86: 309-316, 1990.
3. **Basile DP, Donohoe D, Roethe K, and Osborn JL.** Renal ischemic injury results in permanent damage to peritubular capillaries and influences long-term function. *Am J Physiol Renal Physiol* 281: F887-899, 2001.
4. **Bollee G, Dollinger C, Boutaud L, Guillemot D, Bensman A, Harambat J, Deteix P, Daudon M, Knebelmann B, and Ceballos-Picot I.** Phenotype and genotype characterization of adenine phosphoribosyltransferase deficiency. *J Am Soc Nephrol* 21: 679-688, 2010.
5. **Calzavacca P, Evans RG, Bailey M, Lankadeva YR, Bellomo R, and May CN.** Long-term measurement of renal cortical and medullary tissue oxygenation and perfusion in unanesthetized sheep. *Am J Physiol Regul Integr Comp Physiol* 308: R832-839, 2015.
6. **Cho ME, and Kopp JB.** Pirfenidone: an anti-fibrotic therapy for progressive kidney disease. *Expert opinion on investigational drugs* 19: 275-283, 2010.
7. **Deng A, Tang T, Singh P, Wang C, Satriano J, Thomson SC, and Blantz RC.** Regulation of oxygen utilization by angiotensin II in chronic kidney disease. *Kidney Int* 75: 197-204, 2009.
8. **Dimke H, Sparks MA, Thomson BR, Frische S, Coffman TM, and Quaggin SE.** Tubulovascular cross-talk by vascular endothelial growth factor maintains peritubular microvasculature in kidney. *J Am Soc Nephrol* 26: 1027-1038, 2015.
9. **Ding A, Kalaiganasundaram P, Ricardo SD, Abdelkader A, Witting PK, Broughton BR, Kim HB, Wyse BF, Phillips JK, and Evans RG.** Chronic treatment with tempol does not significantly ameliorate renal tissue hypoxia or disease progression in a rodent model of polycystic kidney disease. *Clin Exp Pharmacol Physiol* 39: 917-929, 2012.
10. **dos Santos EA, Li LP, Ji L, and Prasad PV.** Early changes with diabetes in renal medullary hemodynamics as evaluated by fiberoptic probes and BOLD magnetic resonance imaging. *Invest Radiol* 42: 157-162, 2007.
11. **Edvardsson V, Palsson R, Olafsson I, Hjaltadottir G, and Laxdal T.** Clinical features and genotype of adenine phosphoribosyltransferase deficiency in iceland. *Am J Kidney Dis* 38: 473-480, 2001.
12. **Emans TW, Janssen BJ, Pinkham MI, Ow CP, Evans RG, Joles JA, Malpas SC, Krediet CT, and Koeners MP.** Exogenous and endogenous angiotensin-II decrease renal cortical oxygen tension in conscious rats by limiting renal blood flow. *J Physiol* 594: 6287-6300, 2016.
13. **Evans RG, Gardiner BS, Smith DW, and O'Connor PM.** Methods for studying the physiology of kidney oxygenation. *Clin Exp Pharmacol Physiol* 35: 1405-1412, 2008.
14. **Evans RG, Harrop GK, Ngo JP, Ow CP, and O'Connor PM.** Basal renal O₂ consumption and the efficiency of O₂ utilization for Na⁺ reabsorption. *Am J Physiol Renal Physiol* 306: F551-560, 2014.
15. **Evans RG, Ince C, Joles JA, Smith DW, May CN, O'Connor PM, and Gardiner BS.** Haemodynamic influences on kidney oxygenation: clinical implications of integrative physiology. *Clin Exp Pharmacol Physiol* 40: 106-122, 2013.
16. **Fine LG, and Norman JT.** Chronic hypoxia as a mechanism of progression of chronic kidney diseases: from hypothesis to novel therapeutics. *Kidney Int* 74: 867-872, 2008.
17. **Fine LG, Orphanides C, and Norman JT.** Progressive renal disease: the chronic hypoxia hypothesis. *Kidney Int Suppl* 65: S74-78, 1998.

18. **Franzen S, Pihl L, Khan N, Gustafsson H, and Palm F.** Pronounced kidney hypoxia precedes albuminuria in type 1 diabetic mice. *Am J Physiol Renal Physiol* 310: F807-809, 2016.
19. **Gardiner BS, Smith DW, O'Connor PM, and Evans RG.** A mathematical model of diffusional shunting of oxygen from arteries to veins in the kidney. *Am J Physiol Renal Physiol* 300: F1339-1352, 2011.
20. **Gardiner BS, Thompson SL, Ngo JP, Smith DW, Abdelkader A, Broughton BR, Bertram JF, and Evans RG.** Diffusive oxygen shunting between vessels in the preglomerular renal vasculature: anatomic observations and computational modeling. *Am J Physiol Renal Physiol* 303: F605-618, 2012.
21. **Goldfarb M, Rosenberger C, Abassi Z, Shina A, Zilbersat F, Eckardt KU, Rosen S, and Heyman SN.** Acute-on-chronic renal failure in the rat: functional compensation and hypoxia tolerance. *Am J Nephrol* 26: 22-33, 2006.
22. **Hostetter TH, Troy JL, and Brenner BM.** Glomerular hemodynamics in experimental diabetes mellitus. *Kidney Int* 19: 410-415, 1981.
23. **Iyer SN, Gurujeyalakshmi G, and Giri SN.** Effects of pirfenidone on transforming growth factor-beta gene expression at the transcriptional level in bleomycin hamster model of lung fibrosis. *J Pharmacol Exp Ther* 291: 367-373, 1999.
24. **Iyer SN, Wild JS, Schiedt MJ, Hyde DM, Margolin SB, and Giri SN.** Dietary intake of pirfenidone ameliorates bleomycin-induced lung fibrosis in hamsters. *J Lab Clin Med* 125: 779-785, 1995.
25. **Jensen PK, Christiansen JS, Steven K, and Parving HH.** Renal function in streptozotocin-diabetic rats. *Diabetologia* 21: 409-414, 1981.
26. **Kaartinen K, Hemmila U, Salmela K, Raisanen-Sokolowski A, Kouri T, and Makela S.** Adenine phosphoribosyltransferase deficiency as a rare cause of renal allograft dysfunction. *J Am Soc Nephrol* 25: 671-674, 2014.
27. **Kairaitis LK, Wang Y, Gassmann M, Tay YC, and Harris DC.** HIF-1alpha expression follows microvascular loss in advanced murine adriamycin nephrosis. *Am J Physiol Renal Physiol* 288: F198-206, 2005.
28. **Khan Z, Ngo JP, Le B, Evans RG, Pearson JT, Gardiner BS, and Smith DW.** Three-dimensional morphometric analysis of the renal vasculature. *Am J Physiol Renal Physiol* 314: F715-F725, 2018.
29. **Kiran G, Nandini CD, Ramesh HP, and Salimath PV.** Progression of early phase diabetic nephropathy in streptozotocin-induced diabetic rats: evaluation of various kidney-related parameters. *Indian J Exp Biol* 50: 133-140, 2012.
30. **Klingberg A, Hasenberg A, Ludwig-Portugall I, Medyukhina A, Mann L, Brenzel A, Engel DR, Figge MT, Kurts C, and Gunzer M.** Fully automated evaluation of total glomerular number and capillary tuft size in nephritic kidneys using lightsheet microscopy. *J Am Soc Nephrol* 28: 452-459, 2017.
31. **Koeners MP, Ow CP, Russell DM, Abdelkader A, Eppel GA, Ludbrook J, Malpas SC, and Evans RG.** Telemetry-based oxygen sensor for continuous monitoring of kidney oxygenation in conscious rats. *Am J Physiol Renal Physiol* 304: F1471-1480, 2013.
32. **Koeners MP, Ow CPC, Russell DM, Evans RG, and Malpas SC.** Prolonged and continuous measurement of kidney oxygenation in conscious rats. *Methods Mol Biol* 1397: 93-111, 2016.
33. **Layton AT.** Recent advances in renal hypoxia: insights from bench experiments and computer simulations. *Am J Physiol Renal Physiol* 311: F162-165, 2016.
34. **Lee CJ, Gardiner BS, Evans RG, and Smith DW.** A model of oxygen transport in the rat renal medulla. *Am J Physiol Renal Physiol* 2018.

35. **Lee CJ, Gardiner BS, Ngo JP, Kar S, Evans RG, and Smith DW.** Accounting for oxygen in the renal cortex: a computational study of factors that predispose the cortex to hypoxia. *Am J Physiol Renal Physiol* 313: F218-F236, 2017.
36. **Lee CJ, Ngo JP, Kar S, Gardiner BS, Evans RG, and Smith DW.** A pseudo-three-dimensional model for quantification of oxygen diffusion from preglomerular arteries to renal tissue and renal venous blood. *Am J Physiol Renal Physiol* 313: F237-F253, 2017.
37. **Legrand M, Almac E, Mik EG, Johannes T, Kandil A, Bezemer R, Payen D, and Ince C.** L-NIL prevents renal microvascular hypoxia and increase of renal oxygen consumption after ischemia-reperfusion in rats. *Am J Physiol Renal Physiol* 296: F1109-1117, 2009.
38. **Manotham K, Tanaka T, Matsumoto M, Ohse T, Miyata T, Inagi R, Kurokawa K, Fujita T, and Nangaku M.** Evidence of tubular hypoxia in the early phase in the remnant kidney model. *J Am Soc Nephrol* 15: 1277-1288, 2004.
39. **Meng XM, Nikolic-Paterson DJ, and Lan HY.** TGF-beta: the master regulator of fibrosis. *Nat Rev Nephrol* 12: 325-338, 2016.
40. **Nangaku M.** Chronic hypoxia and tubulointerstitial injury: a final common pathway to end-stage renal failure. *J Am Soc Nephrol* 17: 17-25, 2006.
41. **Nasr SH, Sethi S, Cornell LD, Milliner DS, Boelkins M, Broviac J, and Fidler ME.** Crystalline nephropathy due to 2,8-dihydroxyadeninuria: an under-recognized cause of irreversible renal failure. *Nephrol Dial Transplant* 25: 1909-1915, 2010.
42. **Nespoux J, and Vallon V.** SGLT2 inhibition and kidney protection. *Clin Sci* 132: 1329-1339, 2018.
43. **Neugarten J, Aynedjian HS, and Bank N.** Role of tubular obstruction in acute renal failure due to gentamicin. *Kidney Int* 24: 330-335, 1983.
44. **Ngo JP, Kar S, Kett MM, Gardiner BS, Pearson JT, Smith DW, Ludbrook J, Bertram JF, and Evans RG.** Vascular geometry and oxygen diffusion in the vicinity of artery-vein pairs in the kidney. *Am J Physiol Renal Physiol* 307: F1111-1122, 2014.
45. **Ngo JP, Le B, Khan Z, Kett MM, Gardiner BS, Smith DW, Melhem MM, Maksimenko A, Pearson JT, and Evans RG.** Micro-computed tomographic analysis of the radial geometry of intrarenal artery-vein pairs in rats and rabbits: Comparison with light microscopy. *Clin Exp Pharmacol Physiol* 44: 1241-1253, 2017.
46. **O'Neill J, Fasching A, Pihl L, Patinha D, Franzen S, and Palm F.** Acute SGLT inhibition normalizes O₂ tension in the renal cortex but causes hypoxia in the renal medulla in anaesthetized control and diabetic rats. *Am J Physiol Renal Physiol* 309: F227-234, 2015.
47. **Ohashi R, Shimizu A, Masuda Y, Kitamura H, Ishizaki M, Sugisaki Y, and Yamanaka N.** Peritubular capillary regression during the progression of experimental obstructive nephropathy. *J Am Soc Nephrol* 13: 1795-1805, 2002.
48. **Ow CP, Abdelkader A, Hilliard LM, Phillips JK, and Evans RG.** Determinants of renal tissue hypoxia in a rat model of polycystic kidney disease. *Am J Physiol Regul Integr Comp Physiol* 307: R1207-1215, 2014.
49. **Ow CPC, Ngo JP, Ullah MM, Barsha G, Meex RCR, Watt MJ, Hilliard LM, Koeners MP, and Evans RG.** Absence of renal hypoxia in the subacute phase of severe renal ischemia reperfusion injury. *Am J Physiol Renal Physiol* 315: F1358-F1369, 2018.
50. **Ow CPC, Ngo JP, Ullah MM, Hilliard LM, and Evans RG.** Renal hypoxia in kidney disease: Cause or consequence? *Acta Physiol* 222: e12999, 2018.
51. **Palm F, Cederberg J, Hansell P, Liss P, and Carlsson PO.** Reactive oxygen species cause diabetes-induced decrease in renal oxygen tension. *Diabetologia* 46: 1153-1160, 2003.
52. **Palm F, Ortsater H, Hansell P, Liss P, and Carlsson PO.** Differentiating between effects of streptozotocin per se and subsequent hyperglycemia on renal function and metabolism in the streptozotocin-diabetic rat model. *Diabetes Metab Res Rev* 20: 452-459, 2004.

53. **Papazova DA, Friederich-Persson M, Joles JA, and Verhaar MC.** Renal transplantation induces mitochondrial uncoupling, increased kidney oxygen consumption, and decreased kidney oxygen tension. *Am J Physiol Renal Physiol* 308: F22-28, 2015.
54. **Rahman A, Yamazaki D, Sufiun A, Kitada K, Hitomi H, Nakano D, and Nishiyama A.** A novel approach to adenine-induced chronic kidney disease associated anemia in rodents. *PLoS One* 13: e0192531, 2018.
55. **RamachandraRao SP, Zhu Y, Ravasi T, McGowan TA, Toh I, Dunn SR, Okada S, Shaw MA, and Sharma K.** Pirfenidone is renoprotective in diabetic kidney disease. *J Am Soc Nephrol* 20: 1765-1775, 2009.
56. **Redfors B, Sward K, Sellgren J, and Ricksten SE.** Effects of mannitol alone and mannitol plus furosemide on renal oxygen consumption, blood flow and glomerular filtration after cardiac surgery. *Intensive Care Med* 35: 115-122, 2009.
57. **Ries M, Basseau F, Tyndal B, Jones R, Deminiere C, Catargi B, Combe C, Moonen CW, and Grenier N.** Renal diffusion and BOLD MRI in experimental diabetic nephropathy. Blood oxygen level-dependent. *J Magn Reson Imaging* 17: 104-113, 2003.
58. **Rosenberger C, Goldfarb M, Shina A, Bachmann S, Frei U, Eckardt KU, Schrader T, Rosen S, and Heyman SN.** Evidence for sustained renal hypoxia and transient hypoxia adaptation in experimental rhabdomyolysis-induced acute kidney injury. *Nephrol Dial Transplant* 23: 1135-1143, 2008.
59. **Rosenberger C, Heyman SN, Rosen S, Shina A, Goldfarb M, Griethe W, Frei U, Reinke P, Bachmann S, and Eckardt KU.** Up-regulation of HIF in experimental acute renal failure: evidence for a protective transcriptional response to hypoxia. *Kidney Int* 67: 531-542, 2005.
60. **Rosenberger C, Khamaisi M, Abassi Z, Shilo V, Weksler-Zangen S, Goldfarb M, Shina A, Zibertrest F, Eckardt KU, Rosen S, and Heyman SN.** Adaptation to hypoxia in the diabetic rat kidney. *Kidney Int* 73: 34-42, 2008.
61. **Rosenberger C, Rosen S, Paliege A, and Heyman SN.** Pimonidazole adduct immunohistochemistry in the rat kidney: detection of tissue hypoxia. *Methods Mol Biol* 466: 161-174, 2009.
62. **Sahota A, Chen J, Behzadian MA, Ravindra R, Takeuchi H, Stambrook PJ, and Tischfield JA.** 2,8-Dihydroxyadenine lithiasis in a Japanese patient heterozygous at the adenine phosphoribosyltransferase locus. *Am J Hum Genet* 48: 983-989, 1991.
63. **Scholey JW, and Meyer TW.** Control of glomerular hypertension by insulin administration in diabetic rats. *J Clin Invest* 83: 1384-1389, 1989.
64. **Selkurt EE, Deetjen P, and Brechtelsbauer H.** Tubular pressure gradients and filtration dynamics during urinary stop flow in the rat. *Pflugers Arch Gesamte Physiol Menschen Tiere* 286: 19-35, 1965.
65. **Sward K, Valsson F, Sellgren J, and Ricksten SE.** Differential effects of human atrial natriuretic peptide and furosemide on glomerular filtration rate and renal oxygen consumption in humans. *Intensive Care Med* 31: 79-85, 2005.
66. **Tanaka T, Kato H, Kojima I, Ohse T, Son D, Tawakami T, Yatagawa T, Inagi R, Fujita T, and Nangaku M.** Hypoxia and expression of hypoxia-inducible factor in the aging kidney. *J Gerontol A Biol Sci Med Sci* 61: 795-805, 2006.
67. **Thomas SR, Layton AT, Layton HE, and Moore LC.** Kidney modeling: Status and perspectives. *Proceedings of the IEEE* 94: 740-752, 2006.
68. **Thomson SC, Rieg T, Miracle C, Mansoury H, Whaley J, Vallon V, and Singh P.** Acute and chronic effects of SGLT2 blockade on glomerular and tubular function in the early diabetic rat. *Am J Physiol Regul Integr Comp Physiol* 302: R75-83, 2012.
69. **Vallon V, Rieg T, Cunard R, and H. K.** Impaired proximal tubular and kidney glucose reabsorption in gene-targeted mice lacking SGLT1. *Am Soc Nephrol* 21: 262A: 2010.

70. **Vallon V, Platt KA, Cunard R, Schroth J, Whaley J, Thomson SC, Koepsell H, and Rieg T.** SGLT2 mediates glucose reabsorption in the early proximal tubule. *J Am Soc Nephrol* 22: 104-112, 2011.
71. **Vallon V, Richter K, Blantz RC, Thomson S, and Osswald H.** Glomerular hyperfiltration in experimental diabetes mellitus: potential role of tubular reabsorption. *J Am Soc Nephrol* 10: 2569-2576, 1999.
72. **Welch WJ, Baumgartl H, Lubbers D, and Wilcox CS.** Nephron pO₂ and renal oxygen usage in the hypertensive rat kidney. *Kidney Int* 59: 230-237, 2001.
73. **Welch WJ, Baumgartl H, Lubbers D, and Wilcox CS.** Renal oxygenation defects in the spontaneously hypertensive rat: role of AT1 receptors. *Kidney Int* 63: 202-208, 2003.
74. **Wyngaarden JB, and Dunn JT.** 8-Hydroxyadenine as the intermediate in the oxidation of adenine to 2, 8-dihydroxyadenine by xanthine oxidase. *Arch Biochem Biophys* 70: 150-156, 1957.
75. **Yokozawa T, Zheng PD, Oura H, and Koizumi F.** Animal model of adenine-induced chronic renal failure in rats. *Nephron* 44: 230-234, 1986.

APPENDIX 1

REVIEW ARTICLE

Renal hypoxia in kidney disease: Cause or consequence?

C. P. C. Ow | J. P. Ngo | M. M. Ullah | L. M. Hilliard | R. G. Evans

Cardiovascular Disease Program,
Biomedicine Discovery Institute and
Department of Physiology, Monash
University, Melbourne, Vic., Australia

Correspondence

R. G. Evans, Department of Physiology,
Monash University, Melbourne, Vic.,
Australia.

Email: roger.evans@monash.edu

Funding information

The authors' work was supported by grants from the National Health and Medical Research Council of Australia (GNT1050672 and GNT1122455), the National Heart Foundation of Australia (VG-2016-101377) and the Australian Research Council (DP140103045).

Abstract

Tissue hypoxia has been proposed as an important factor in the pathophysiology of both chronic kidney disease (CKD) and acute kidney injury (AKI), initiating and propagating a vicious cycle of tubular injury, vascular rarefaction, and fibrosis and thus exacerbation of hypoxia. Here, we critically evaluate this proposition by systematically reviewing the literature relevant to the following six questions: (i) Is kidney disease always associated with tissue hypoxia? (ii) Does tissue hypoxia drive signalling cascades that lead to tissue damage and dysfunction? (iii) Does tissue hypoxia per se lead to kidney disease? (iv) Does tissue hypoxia precede pathology? (v) Does tissue hypoxia colocalize with pathology? (vi) Does prevention of tissue hypoxia prevent kidney disease? We conclude that tissue hypoxia is a common feature of both AKI and CKD. Furthermore, at least under in vitro conditions, renal tissue hypoxia drives signalling cascades that lead to tissue damage and dysfunction. Tissue hypoxia itself can lead to renal pathology, independent of other known risk factors for kidney disease. There is also some evidence that tissue hypoxia precedes renal pathology, at least in some forms of kidney disease. However, we have made relatively little progress in determining the spatial relationships between tissue hypoxia and pathological processes (i.e. colocalization) or whether therapies targeted to reduce tissue hypoxia can prevent or delay the progression of renal disease. Thus, the hypothesis that tissue hypoxia is a “common pathway” to both AKI and CKD still remains to be adequately tested.

KEYWORDS

acute kidney injury, chronic kidney disease, hypoxia, hypoxia-inducible factors, oxygen consumption, oxygen delivery

1 | INTRODUCTION

Renal tissue hypoxia has been proposed as a critical mediator of both acute kidney injury (AKI) and chronic kidney disease (CKD).^{1–3} For example, in 1998, Fine et al^{4,5} proposed the “chronic hypoxia hypothesis” for the pathogenesis of CKD. Their argument was largely based on the proposition that tubulointerstitial injury (especially fibrosis and capillary rarefaction) is a hallmark of all progressive renal diseases and that hypoxia drives fibrogenesis in the kidney. Thus, they proposed that any insult that induces either hypoxia or tubulointerstitial injury has the

potential to initiate a vicious cycle. More recently, considerable evidence has been generated to support associations between tissue hypoxia and multiple forms of CKD. However, as discussed in detail herein, direct evidence of causation is rather limited.

It has also been proposed that tissue hypoxia plays a critical role in the initiation and progression of AKI.^{6,7} In hospital settings, AKI commonly occurs in sepsis,⁸ and after procedures associated with temporary cessation of renal perfusion or reduced renal blood flow or oxygen delivery. Such procedures include renal transplantation,⁹ cardiac and other major surgery,¹⁰ resection of renal mass¹¹

and reparation of an aneurysm.¹² The heavily respiring outer medulla is particularly sensitive to acute reductions in renal oxygen delivery.^{13,14} Outer medullary hypoxia can then result in tubular necrosis, tubular and capillary obstruction,¹⁵ loss of mitochondrial integrity¹⁶ and oxidative stress.¹⁷ In the longer term, tissue hypoxia could contribute to the interstitial fibrosis and vascular rarefaction that characterizes progression from AKI to CKD,¹⁸ as predicted by the chronic hypoxia hypothesis.

In this review, we critically evaluate the evidence that dysregulation of renal tissue oxygenation plays specific roles in the pathogenesis of both CKD and AKI. Thus, we focus more on the identification of the gaps in our knowledge than on the evidence supporting the roles of hypoxia. To achieve this aim, we performed a systematic review of the literature related to the potential roles of hypoxia in renal pathology. In a MEDLINE search, we used the Medical Subject Headings (MeSH) and keywords “AKI” (44509 results) or “acute renal failure” (48552 results) or “CKD” (37883 results) or “polycystic kidney disease (PKD)” (10820 results) and “hypoxia” or “anoxia” (140468), giving a combined return of 10914 results (from 1956 to November 2017). Additional articles were sourced from the references of articles obtained from the search and from an examination of articles that cited the papers identified in our search. The final analysis included only original studies with at least an abstract written in English.

With analogy to Koch’s¹⁹ postulates regarding the roles of specific bacteria in infectious disease, we propose six lines of evidence that are required in order to confirm or refute the hypothesis that renal tissue hypoxia initiates and drives the progression of CKD and AKI. These are presented below as a series of questions, which we then address in turn.

- 1). Is kidney disease always associated with tissue hypoxia?
- 2). Does tissue hypoxia drive signalling cascades that lead to tissue damage and dysfunction?
- 3). Does tissue hypoxia per se lead to kidney disease?
- 4). Does tissue hypoxia precede pathology?
- 5). Does tissue hypoxia colocalize with pathology?
- 6). Does prevention of tissue hypoxia prevent kidney disease?

2 | IS THE DEVELOPMENT OF KIDNEY DISEASE ALWAYS ASSOCIATED WITH TISSUE HYPOXIA?

Before directly addressing this question, we must consider the strengths and limitations of the various techniques used for the assessment of renal tissue oxygenation. These have

previously been reviewed in detail.^{20,21} In brief, polarographic electrodes such as the Clark-type electrode can directly quantify tissue oxygen tension (PO₂).²² This method is highly invasive so does not allow for long-term measurements or studies in freely moving animals. It is also not suitable for use in the clinical setting. Immunohistochemical methods such as pimonidazole adduct immunohistochemistry provide qualitative assessment of tissue hypoxia with high spatial resolution.²³ This technique has been relatively well validated for the detection of cellular hypoxia in cultured tumour cells that were <10 mmHg.²⁴ Caveats that should be applied to this method include that it can only be applied at discrete time-points, is not quantitative and can be confounded by false-positive staining in the injured kidney,²⁵ and in other tissues under relatively well-oxygenated conditions.^{26,27}

Blood oxygen level-dependent magnetic resonance imaging (BOLD-MRI) is non-invasive and can be used in experimental and clinical settings over multiple time-points. Thus, BOLD-MRI has the potential to characterize the evolution of renal hypoxia during the development of kidney disease. Its major limitation arises from the fact that it provides a measure of the ratio of deoxyhaemoglobin to oxyhaemoglobin in the blood²⁸ and thus only provides a semi-quantitative and indirect measurement of tissue PO₂. Similar to BOLD-MRI, electron paramagnetic resonance utilizes the paramagnetic nature of oxygen to attenuate magnetic resonance. This method requires the invasive implantation of a paramagnetic probe into the tissue of interest.²⁹ Once implanted, it allows for the direct quantification of tissue PO₂ over extended periods non-invasively³⁰ and thus potentially allows for determination of the temporal relationship between tissue hypoxia in the pathogenesis of kidney diseases.

Assessment of the expression of hypoxia-inducible factors (HIF) and their downstream targets provides information regarding the cellular responses to hypoxia rather than hypoxia itself, which likely vary depending on physiological and pathological conditions.³¹ Most recently, methods have been described that allow continuous measurement of renal tissue PO₂ in unanaesthetized experimental animals.³²⁻³⁵ These techniques promise to deliver exquisite temporal resolution of kidney oxygenation in both small and large animal models of kidney disease. However, they are yet to be widely employed to study models of kidney disease.³⁶⁻³⁸

2.1 | Chronic kidney disease

Chronic kidney disease is a complex and multifactorial disease often complicated by comorbidities such as diabetes and hypertension. However, despite the seemingly varying underlying aetiology across different forms of CKD, tissue hypoxia almost always develops at some stage during progression of the disease (Figure 1).

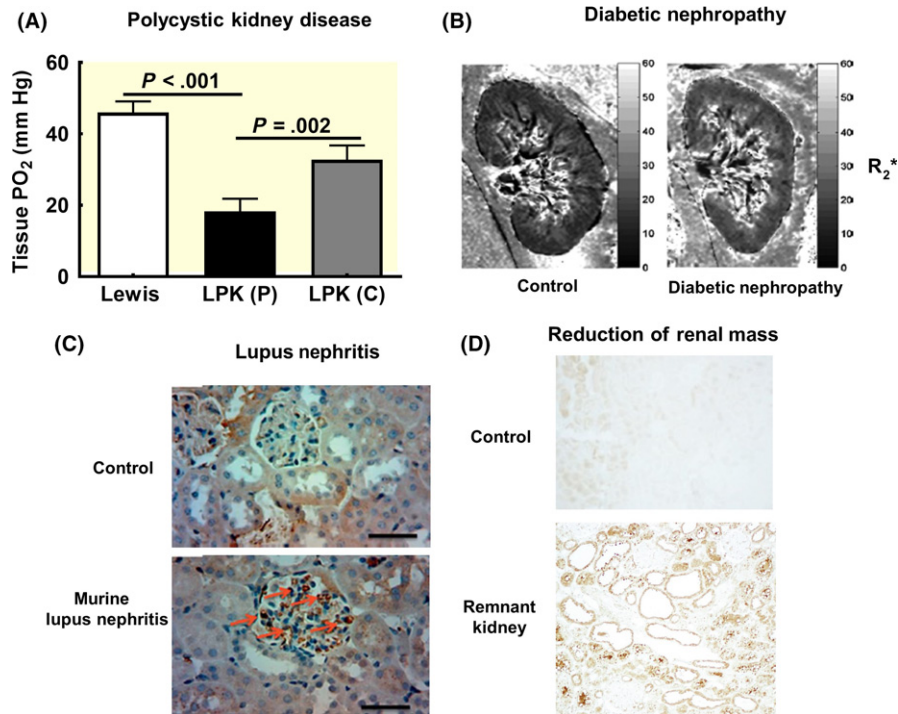


FIGURE 1 Evidence of renal hypoxia in various forms of chronic kidney disease (CKD). Panel A shows cortical tissue oxygen tension (PO₂) measured by Clark electrode in control rats (Lewis), and in the renal parenchyma (LPK(P)) and within the renal cysts (LPK(C)) in a rat model of polycystic kidney disease. Panel B shows images generated by blood oxygen level-dependent magnetic resonance imaging (BOLD-MRI) from patients with and without diabetic nephropathy. Note the greater proportion of deoxyhaemoglobin (indicated by the greater R₂*) in the blood within the kidney in the individual with diabetic nephropathy than the control subject. Panel C shows glomeruli in renal sections from a mouse with lupus nephritis (LN) and a control mouse. Note the positive (brown) staining for hypoxia-inducible factor-1 α in the glomerulus from the mouse with LN. Panel D shows immunohistochemical staining for pimonidazole adducts (brown) in kidney tissue from a control rat and a rat with CKD induced by the removal of 5/6th of the kidney (remnant kidney). Images were reproduced from (A)⁴²; (B)⁵³; (C)⁴⁷; (D)⁶³ with permission

Polycystic kidney disease, the most common genetic form of CKD, is characterized by excessive and uncontrolled tubular epithelial proliferation resulting in the formation of fluid-filled cysts³⁹ and thus renomegaly.⁴⁰ The increased total kidney volume, in conjunction with increased angiogenesis, results in flattened and tortuous capillaries and arterioles.⁴¹ Vascular remodelling and the expansion of the tubules in PKD not only has the potential to decrease tissue perfusion, it also has the potential to increase the distance over which oxygen must diffuse to reach renal tissue. There is also evidence that oxygen demand, at least in proportion to the level of sodium reabsorption, is augmented in PKD.⁴² Thus, both decreased oxygen supply to the tissue and inappropriately high oxygen consumption likely contribute to the severe tissue hypoxia that has been observed using both quantitative (Figure 1A)⁴² and qualitative^{43,44} methods.

Systemic lupus erythematosus is a polygenic autoimmune disorder of non-cystic nature characterized by the presence of antinuclear antibodies indicative of an aberrant immune response to autoantigens.⁴⁵ In lupus nephritis (LN), inflammatory cytokines mediate fibrogenesis.⁴⁶ The resultant

expansion of extracellular matrix could promote tissue hypoxia by increasing the distance for diffusion of oxygen to tissue. Deng et al⁴⁷ showed the upregulation of glomerular hypoxia-inducible factor 1- α (HIF-1 α) in renal biopsies obtained from patients with LN. HIF-1 α expression was positively correlated with severity of the disease and proliferative index in LN.⁴⁷ Critically, the expression of HIF-1 α can be upregulated in the presence of IL-6, even under normoxic conditions, suggestive of molecular crosstalk between inflammatory mediators and induction of HIFs.⁴⁸ However, we are not aware of studies in which renal oxygenation has been examined in LN using more direct methods.

Cellular⁴⁹ and tissue^{50,51} hypoxia in the kidney is a common finding in animal models of diabetic nephropathy. Treatment with insulin abolished cellular hypoxia, suggesting that the hypoxia is dependent on hyperglycaemia.⁴⁹ Extending these observations to the clinical setting, several studies using BOLD-MRI have provided evidence of hypoxia in the cortex and medulla in patients with diabetic nephropathy.^{52,53} In contrast, using the same technique, Wang et al⁵⁴ could not detect differences in the BOLD signal in the renal cortex of patients with diabetic

nephropathy compared to healthy volunteers (Figure 1B). Indeed, the medulla actually appeared to be better oxygenated in patients with diabetic nephropathy than in controls.⁵⁴ Additionally, renal hypoxia was also not detected in a recent BOLD-MRI study of patients with CKD, inclusive of patients with diabetic nephropathy.⁵⁵

The discrepancies in these clinical observations may be due to (i) the relative sensitivity of the BOLD-MRI technique to changes in tissue oxygenation per se and/or (ii) differences in the severity of CKD in the populations included in the various studies. Importantly, the disparity in observations using BOLD-MRI in human diabetic nephropathy indicates that the relationship between tissue hypoxia and progression of the disease is likely complex. The absence of tissue hypoxia during any particular stage cannot rule out a pathogenic role during an earlier or later stage. On the other hand, the presence of hypoxia, even if throughout the natural history of kidney disease, does not provide evidence that hypoxia contributes mechanistically to the development of diabetic nephropathy.

Reduction in renal mass reduces the number of viable nephrons, resulting in compensatory increases in single nephron glomerular filtration rate (GFR).⁵⁶ The increase in single nephron GFR appears to drive increased oxygen consumption in the remaining viable nephrons.^{56,57} This, and other factors such as fibrosis^{58,59} and oxidative stress,^{60,61} may drive the development of tubulointerstitial hypoxia (Figure 1D). In these so-called remnant kidney models, hypoxia has been observed in both the cortex⁶¹⁻⁶³ and medulla.⁶² In contrast, Priyadarshi et al⁶⁴ observed that cortical and medullary tissue PO₂ was greater, 6-8 weeks following renal mass reduction. The discrepancy between these observations may be related to the time-course of progression of the disease. That is, tissue hypoxia may be important in the acute and subacute phases following reduction in renal mass, but not in the longer term. Nevertheless, the balance of evidence suggests that tissue hypoxia is a characteristic of the remnant kidney model.

In renovascular disease, once the narrowing of the main renal artery or its proximal branches reaches a critical stage, marked reductions in renal blood flow occur.⁶⁵ Examination of renal tissue oxygenation in animal models of renovascular disease has yielded conflicting results, likely due to differences in severity and the time-course of progression of the disease. Palm et al found, in a rat model of renovascular disease, that cortical hypoxia developed 3 weeks after stenosis and was accompanied by a reduction in renal blood flow.^{66,67} In contrast, Rognant et al,⁶⁸ using BOLD-MRI, found that renal blood oxygenation changed little in the 4 weeks following stenosis. In the clinical setting, patients with renovascular disease had rather well-oxygenated renal blood in comparison with the contralateral kidney, despite reductions in cortical and

medullary blood flow.⁶⁹⁻⁷¹ However, it appears that cortical hypoxia may develop once the stenosis reaches a critical level (>70%) so that cortical blood flow is markedly reduced.⁷² The explanation for these disparate findings may lie in the effect of a stenosis on the balance between oxygen delivery and oxygen demand. Importantly, reductions in GFR induced by a stenosis should act to reduce renal oxygen demand for sodium reabsorption and so reduce the risk of renal hypoxia.⁶

In summary, renal hypoxia is a common, but not universal, characteristic of CKD. It is also relevant here to consider recent evidence that interstitial fibrosis, microvascular dysfunction and capillary rarefaction are characteristics of CKD, regardless of its aetiology.⁷³

2.2 | Acute kidney injury

Acute kidney injury is associated with increased morbidity, increased length of stay in hospital in the case of hospital-acquired AKI and increased risk of death.⁷⁴ Furthermore, patients who recover from AKI are at increased risk of development of CKD and end-stage renal disease.^{75,76} Evidence of renal tissue hypoxia has been observed in multiple forms of AKI (Figure 2).

Ischaemia-reperfusion injury (IRI) is the leading cause of AKI in the hospital setting.⁷⁷ Flow to the kidney is temporarily occluded during surgical procedures such as renal transplantation (cold ischaemia), or resection of a renal tumour or reparation of an abdominal aneurysm (warm ischaemia). Consequentially, oxygen delivery to the kidney ceases and the kidney becomes anoxic. Following reperfusion, the kidney, particularly the medulla, has been observed to be hypoperfused.⁷⁸ Hypoperfusion is likely driven by multiple factors, including capillary obstruction resulting from infiltration of immune cells, vasoconstriction and loss of endothelial integrity.^{15,79,80} Hypoperfusion following reperfusion compromises renal oxygen delivery^{25,78,81,82} and thus promotes tissue hypoxia.^{78,82-85}

Cardiac surgery, particularly when requiring cardiopulmonary bypass (CPB), is a major cause of AKI.⁸⁶ Ischaemia and reperfusion injury likely make an important contribution to the pathophysiology of AKI in this setting. Renal oxygen delivery is decreased by ~20% during CPB in humans.⁸⁶ However, renal oxygenation during CPB has only been measured directly in experimental animals. Stafford-Smith et al, using a blood gas probe, examined medullary oxygen tension in a porcine model of CPB. They found that 30 minutes into CPB, medullary PO₂ was markedly reduced.⁸⁷ Medullary hypoxia in these pigs did not appear to recover 30 minutes post-CPB,⁸⁷ suggesting the presence of persistent medullary hypoxia after CPB. Medullary hypoxia was also observed to develop in rats during CPB and was augmented by anaemia.⁸⁸

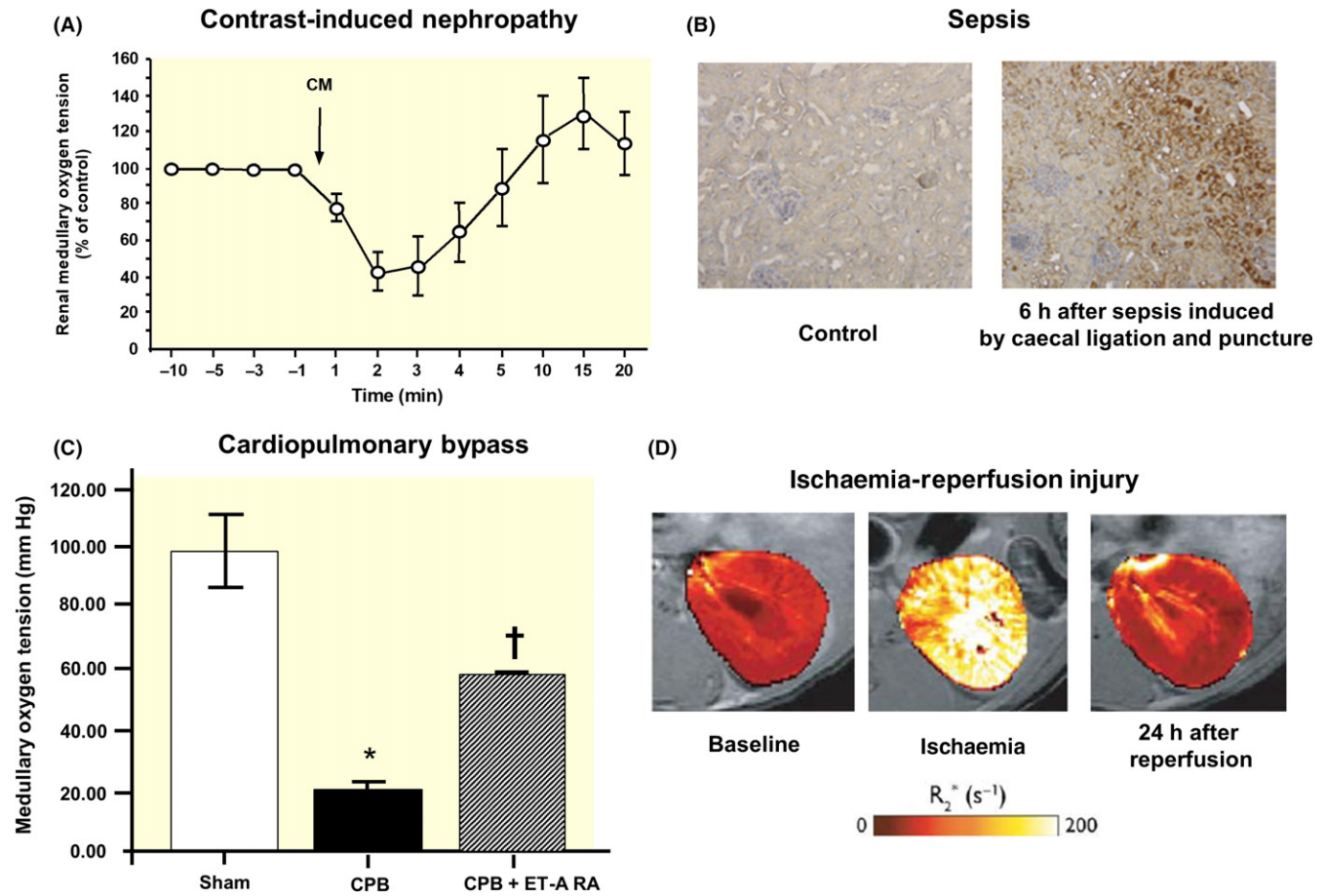


FIGURE 2 Evidence of renal hypoxia in various forms of acute kidney injury. Panel A shows the response of medullary tissue oxygen tension (PO_2), measured by Clark electrode in rats, to administration of an iodinated radiocontrast agent (CM). Panel B shows immunohistochemical staining for pimonidazole adducts (brown) in a control mouse and a mouse with sepsis induced by caecal puncture and ligation. Panel C shows medullary tissue PO_2 in pigs, measured by fibre-optic probe, 24 h after cardiopulmonary bypass (CPB), CPB and treatment with endothelin A receptor antagonist (CPB + ET-A RA) or sham surgery. Panel D shows images generated by blood oxygen level-dependent magnetic resonance imaging in at baseline, during renal ischaemia and 24 h after reperfusion. Note the greater proportion of deoxyhaemoglobin in the blood within the kidney during ischaemia. Images were reproduced from (A)⁹⁵; (B)¹⁰⁹; (C)²⁰⁵; (D)⁸⁴ with permission

Mathematical models have also predicted that haemodynamic conditions associated with CPB, including haemodilution and hypotension, render the medulla susceptible to hypoxia.^{89,90}

Renal hypoxia in AKI that occurs after CPB might be associated with abnormalities in both renal oxygen delivery and consumption. In a prospective study, Redfors et al compared renal oxygen delivery and consumption in patients with AKI relative to those with normal postoperative renal function following cardiac surgery requiring CPB. They demonstrated that renal blood flow (~40%) and hence renal oxygen delivery were markedly reduced in patients with AKI compared to those without AKI.⁹¹ GFR and hence tubular sodium reabsorption were also greatly decreased. Interestingly, the reduction in tubular workload had no detectable effect on renal oxygen consumption.⁹¹ This may be indicative of inefficient oxygen utilization for

sodium reabsorption in AKI, which could be an important contributor to renal tissue hypoxia. Renal tissue hypoxia has also been observed after CPB in experimental animals.^{87,88,92} In pigs, Patel et al⁹² found that 24 hours after CPB, total renal blood flow was decreased and the medulla was hypoxic. Taken collectively, these experimental and modelling studies provide evidence for medullary hypoxia during and after CPB.

Administration of iodinated contrast agents can lead to AKI.⁹³ Medullary hypoxia has been consistently observed in animals administered contrast agents.⁹⁴⁻⁹⁸ Furthermore, administration of contrast agents was associated with increased deoxyhaemoglobin content in the medulla of healthy human subjects.⁹⁹ The mechanisms mediating medullary hypoxia after contrast administration remain to be definitively established. Contrast agents have been shown to promote constriction of vasa recta, at least in part

due to endothelial dysfunction.⁹³ Tubular dilation associated with contrast administration may also promote compression of vasa recta.⁹³ Increased tubular sodium reabsorption, and thus oxygen consumption, could also play a role.⁹³ Thus, renal tissue hypoxia may contribute to the pathogenesis of contrast-induced nephropathy. However, other factors are also likely to be important, including direct toxic effects of contrast agents¹⁰⁰ and their propensity to increase intratubular pressure secondary to their viscosity (reviewed in⁹³).

Sepsis is one of the most common causes of AKI in the intensive care unit (ICU), with an incidence of 10%–48% in the ICU.¹⁰¹ The mortality rate for septic AKI of ~70% is considerably greater than AKI of non-septic nature (~45%)¹⁰² or sepsis alone (~35%).¹⁰³ Rodent models of septic AKI are characterized by global vasoconstriction and consequently renal hypoperfusion.¹⁰⁴ But sepsis in these models is most commonly induced by infusion of lipopolysaccharide (LPS), a component of the outer surface membrane of gram-negative bacteria, resulting in systemic inflammation and ultimately renal vasoconstriction.¹⁰⁵ In LPS-induced septic AKI, renal blood flow is markedly reduced, so it is unsurprising that renal hypoxia has been observed in this setting using multiple methods.^{106–110} In contrast, Tran et al¹¹¹ could not detect renal hypoxia using BOLD-MRI in mice with septic AKI induced by LPS. Clinically, sepsis is caused by bacterial infection. This can be associated with a hyperdynamic state.¹¹² Using a clinically relevant ovine model of sepsis induced by infusion of live *Escherichia Coli*, Calzavacca et al³⁶ recently demonstrated selective ischaemia and hypoxia in the renal medulla, despite systemic and global renal hyperaemia and well-maintained cortical perfusion and oxygenation. Thus, even in the absence of global renal ischaemia, hypoxia in the renal medulla appears to be a common characteristic of septic AKI.

In summary, renal hypoxia, particularly in the medulla, appears to be a common characteristic of AKI. However, in both AKI and CKD, the presence of hypoxia does not necessarily show it has pathophysiological roles. Below, we turn our attention more specifically to the issue of causation.

3 | DOES TISSUE HYPOXIA DRIVE SIGNALLING CASCADES THAT LEAD TO TISSUE DAMAGE AND DYSFUNCTION?

Upregulation of HIFs has been observed in multiple forms of kidney disease in both humans^{47,83,113,114} and experimental animals.^{115,116} HIFs are heterodimeric transcription factors consisting of an oxygen-sensitive α subunit and a

constitutively expressed β subunit.¹¹⁷ In response to hypoxia, the α subunit is stabilized and subsequently translocates to the nucleus. Dimerization of the α and β subunits results in the downstream transcription of hypoxia-responsive elements.^{117,118} There are many known HIF target genes, including but not limited to *EPO*, *VEGF*, *TGF- β* , *ET-1*, *MMP*, *NOS2* and *Bcl-2*. Hence, HIFs have complex effects on cellular activities (Table 1).^{119,120} The downstream activation of hypoxia response genes in response to the activation of HIFs can be beneficial in some cases, but deleterious in others.¹²¹

3.1 | HIFs and erythropoietin

Erythropoietin, transcribed from the *EPO* gene, is the master regulator for the production of erythrocytes.¹²² HIF is the key factor that directs transcription of the *EPO* gene within peritubular fibroblasts in the kidney.¹²³ Thus, arterial hypoxaemia and/or anaemia cause renal hypoxia,⁶ and thus increased synthesis and release of erythropoietin.¹²² The general consensus is that, during a hypoxic event, the stabilization of HIF-2 α results in the transcription of *EPO* and the subsequent production of erythrocytes.^{124,125} The importance of this pathway is further highlighted by the observation that mutations in HIFs themselves, or factors involved in stabilization/degradation of HIFs, often result in erythrocytosis.¹²³ Further to its role in the production of red blood cells, it appears that erythropoietin may modulate tissue injury after an ischaemic event by exerting anti-apoptotic^{126,127} and anti-inflammatory¹²⁸ effects. It thus appears that hypoxia-induced production of erythropoietin may be renoprotective. However, there is emerging evidence of deleterious outcomes in the longer term that may contribute to worsening/predisposition to CKD. For example, Gobe et al¹²⁹ recently found that administration of recombinant human erythropoietin at the time of reperfusion after ischaemia exacerbated the later development of renal fibrosis. Taken together, the available data indicate that erythropoietin may be an effective treatment during the acute phase of IRI but may contribute to development of CKD in the longer term.

3.2 | HIFs and fibrogenesis

Fibrosis and associated microvascular rarefaction is a hallmark of CKD.⁷³ Together, these phenomena are predicted to impede the diffusion of oxygen into renal tissue, thus exacerbating hypoxia.⁵

There is a delicate balance between the production of extracellular matrix (ECM) and its destruction. In response to tissue hypoxia in vitro, expression of genes for the production of collagen, *Coll-1* and *TGF- β* , increases.^{130–132} There is also upregulation of the other constituents of the

TABLE 1 The adaptive and maladaptive responses to downstream transcription of various hypoxia-responsive genes induced by the activation of hypoxia-inducible factors (HIF)

Target gene of HIF activation	Function	Adaptive response	Reference	Maladaptive consequence	Reference
Erythropoietin	Erythropoiesis	Increased erythrocyte production, anti-apoptosis, anti-inflammatory	123, 188, 189	Increased fibrosis	129
Vascular endothelial growth factor	Angiogenesis	Increased vascular growth	190	Pro-inflammation	191
Transforming growth factor β	Cellular survival			Increased fibrosis	192
Endothelin-1	Vascular tone			Increased vasoconstriction	193
Matrix metalloproteinases	Extracellular matrix metabolism			Epithelial-mesenchymal transition, metastasis	194, 195
Nitric oxide synthase	Vascular tone	Vasodilatory		Pro-inflammation	196
Insulin-like growth factor 1	Cellular proliferation	Mediator for growth hormone and thus repair		Stimulate production of extracellular matrix proteins and thus fibrosis	197, 198, 199
Haem oxygenase 1	Oxidative stress regulation	Anti-apoptotic and anti-autophagic	200, 201	Arrest of cellular growth	202
Glucose transporter 1	Glucose metabolism	Increased anaerobic glycolysis	203	Increased tubular reabsorption of glucose	204

ECM such as fibronectin.¹³³ The profibrotic matrix metalloproteinases (MMPs) such as MMP-9 and MMP-2, whose production is regulated by the activity of transforming growth factor β (TGF- β), can degrade the basement membrane.¹³⁴ This may in turn result in a chemotactic response, attracting neutrophils and macrophages.¹³⁵ The influx of immune complexes may ultimately result in the remodelling of the ECM, so contributing to the pathology of various kidney diseases.¹³⁶ The activity of MMP inhibitors, the TIMPs, has been reported to increase in kidney diseases.¹³⁶ It appears that the activities of TIMP-1 and TIMP-2 increase in response to hypoxic conditions, in association with increased TGF- β and Coll-1.¹³⁷ Thus, hypoxia-dependent stabilization of HIF-1 α and consequent translation of downstream genes that promote fibrogenesis may be a critical pathogenic event in the progression of CKD.

3.3 | HIFs and the innate immune system

The activation (or overactivation) of the innate immune system, and its priming for the activation of the adaptive immune system following injury, may be detrimental to the cell.⁷⁹ Rama et al¹³⁸ found that exposure of immature dendritic cells to hypoxia (0.5% O₂) resulted in their differentiation and maturation, which was associated with a threefold increase in HIF-1 α mRNA. This observation suggests that the activation of innate immunity may be dependent on hypoxia-induced stabilization of HIF-1 α .¹³⁸ Furthermore, HIF-1 α activation in response to hypoxia results in the upregulation of translation of mRNA for Toll-like receptors

2 and 6 on human dendritic cells, ultimately resulting in the production of the pro-inflammatory cytokine interleukin-6.¹³⁹ In response to the oxygen-starved cellular environment, neutrophils are upregulated by HIF-1 α -dependent regulation of nuclear factor (NF)- κ B.^{140,141} On the other hand, the accumulation of macrophages at sites of tissue injury, under hypoxic conditions, increases the gene expression of numerous proangiogenic, pro-inflammatory, cytotoxic and immunosuppressive factors.¹⁴² The expression of these immune complexes can in turn be modulated through the stabilization of HIF-1 α in hypoxic conditions. Thus, the activation of innate immunity during hypoxia has a wide range of downstream effects including mechanical plugging of the vasculature by immune cells, possibly further compromising blood flow. Consequentially, further recruitment of immune cells may result in propagative tissue injury and deranged cellular integrity.^{143,144}

One of the caveats to consider with regard to the observations described above is that many of these studies were performed under *in vitro* conditions. As such, immortalized cells are often used and they may not mimic the normal physiology of renal cells *in vivo*. Furthermore, cultured cells may adapt to incubation conditions, so may respond to stimuli in a different manner to the cellular response *in vivo*. Therefore, it is imperative that we extend these studies to *in vivo* conditions that closely represent the physiological adaptations and responses to hypoxic conditions. One way that we can examine the role of the activation of HIFs and its contribution to the maladaptive responses to IRI *in vivo* is through imaging studies. The

improvements in multiphoton imaging in recent years have greatly improved our ability to image the kidney in living, albeit anaesthetized, rodents.^{145,146} It is now possible to simultaneously examine multiple physiological parameters such as blood flow,¹⁴⁷ mitochondrial energetics,¹⁴⁸ oxidative stress¹⁴⁹ and leucocyte activity¹⁵⁰ in vivo. Harnessing the advantages of this imaging technique, one could examine the involvement of HIFs by examining these parameters in renal disease using multiphoton imaging in models of HIF knockout, HIF inhibition or HIF activation. One limitation of this method is that, because of the limitation in tissue penetration of the light source, imaging of the kidney is often restricted to the renal cortex.¹⁵¹ Nevertheless, the combination of multiphoton imaging and models of altered HIF activity might shed more light on the role of HIFs in the initiation and progression of kidney disease.

3.4 | HIFs, VEGF and angiogenesis

The relationships between VEGF, HIF and capillary angiogenesis are likely complex. There are indeed many reports documenting close correlation between microvascular rarefaction and tissue hypoxia.^{62,152} VEGF is one of the many HIF-induced target genes. Tissue hypoxia as a result of microvascular rarefaction might be expected to upregulate HIF and thus VEGF, thereby reversing microvascular loss. Indeed, expression of VEGF was shown to be strongly induced in cultured proximal tubular epithelial cells¹⁵³ and human epithelial cells¹⁵⁴ exposed to hypoxia. Furthermore, TGF- β and hypoxia appear to act independently and synergistically to upregulate VEGF.¹⁵³ But VEGF can be downregulated in CKD. For example, in murine adriamycin nephrosis, expression of VEGFA was found to be reduced despite induction of HIF-1.¹⁵⁵ Furthermore, in a remnant kidney model, Kang et al¹⁵⁶ found peritubular capillary rarefaction was associated with decreased VEGF expression. VEGF administration in this model reduced renal fibrosis and stabilized renal function.¹⁵⁷ Treatment with VEGF-121, given at the time of reperfusion, also ameliorated capillary rarefaction in the chronic phase of IRI.¹⁵⁸ On the other hand, upregulation of VEGF in the tubules of adult mice led to fibrosis, cyst formation and glomerular hypertrophy, along with proliferation of peritubular capillaries.¹⁵⁹ Thus, VEGF remains an attractive target to combat hypoxia-induced microvasculature loss, but off-target effects may limit its utility.

3.5 | Protective effects of HIF activation

Given the potential beneficial effects of HIF activation on renal pathology, upregulation of HIF abundance by inhibition of prolyl hydroxylase domain-containing protein (PHD), which mediates degradation of HIF-1 α , is an attractive

therapeutic target. However, these therapies have had mixed success. It seems that the effectiveness of PHD inhibition depends critically on the time at which interventions are given during the course of disease, and also on the specific pathological features of the renal disease in question.

In terms of AKI, Bernhardt et al¹⁶⁰ demonstrated amelioration of graft injury and improved survival in a rat model of allogenic renal transplant, by prophylactic treatment of donor rats with the PHD inhibitor FG-4497. The same group demonstrated amelioration of renal IRI by prophylactic treatment with FG-4497 or 2-(1-chloro-4-hydroxyisoquinoline-3-carboxamido) acetate (ICA).¹⁶¹ However, PHD inhibition was not effective when given after the ischaemic insult.¹⁶²

In terms of CKD, Nordquist et al¹⁶³ found that upregulation of HIFs by chronic treatment with cobalt chloride blunted diabetic nephropathy in rats. It also ameliorated renal hypermetabolism and renal tissue hypoxia. Cobalt chloride also inhibited tubulointerstitial injury in Thy1 nephropathy.¹⁶⁴ There is also some evidence that HIF activation can blunt progression from AKI to CKD, as reviewed by Tanaka et al¹⁶⁴ However, in a model of hypertension and CKD induced by blockade of nitric oxide synthase and a high salt diet, the PHD inhibitor dimethyloxallyl glycine exacerbated hypertension and urinary protein excretion.¹⁶⁵

4 | DOES TISSUE HYPOXIA PER SE LEAD TO KIDNEY DISEASE?

The available evidence relating to this question is scarce. Friederich-Persson et al^{166,167} used the mitochondrial uncoupler 2,4-dinitrophenol and the thyroid hormone triiodothyronine to induce tissue hypoxia by increasing renal oxygen consumption independent of tubular workload. Chronic treatment of rats with either 2,4-dinitrophenol or triiodothyronine resulted in increased renal oxygen consumption (Figure 3A) and renal tissue hypoxia (Figure 3B).^{166,167} Interestingly, tissue hypoxia in this model was associated with proteinuria (Figure 3C).^{166,167} Additionally, they found that renal tissue hypoxia induced by treatment with 2,4-dinitrophenol was associated with nephropathy even in the absence of confounding factors such as diabetes, hypertension, oxidative stress or tubular damage.¹⁶⁷ Thus, chronic tissue hypoxia per se may drive tissue injury independent of traditional risk factors for CKD. Arguably, these studies provide the strongest available evidence for a causative role of tissue hypoxia in CKD.

A major impediment to further progress in our understanding of the role of tissue hypoxia in the development of kidney disease relates to the nature of the models we study. Most experimental methods for inducing kidney disease inevitably also induce tissue hypoxia. For example, in

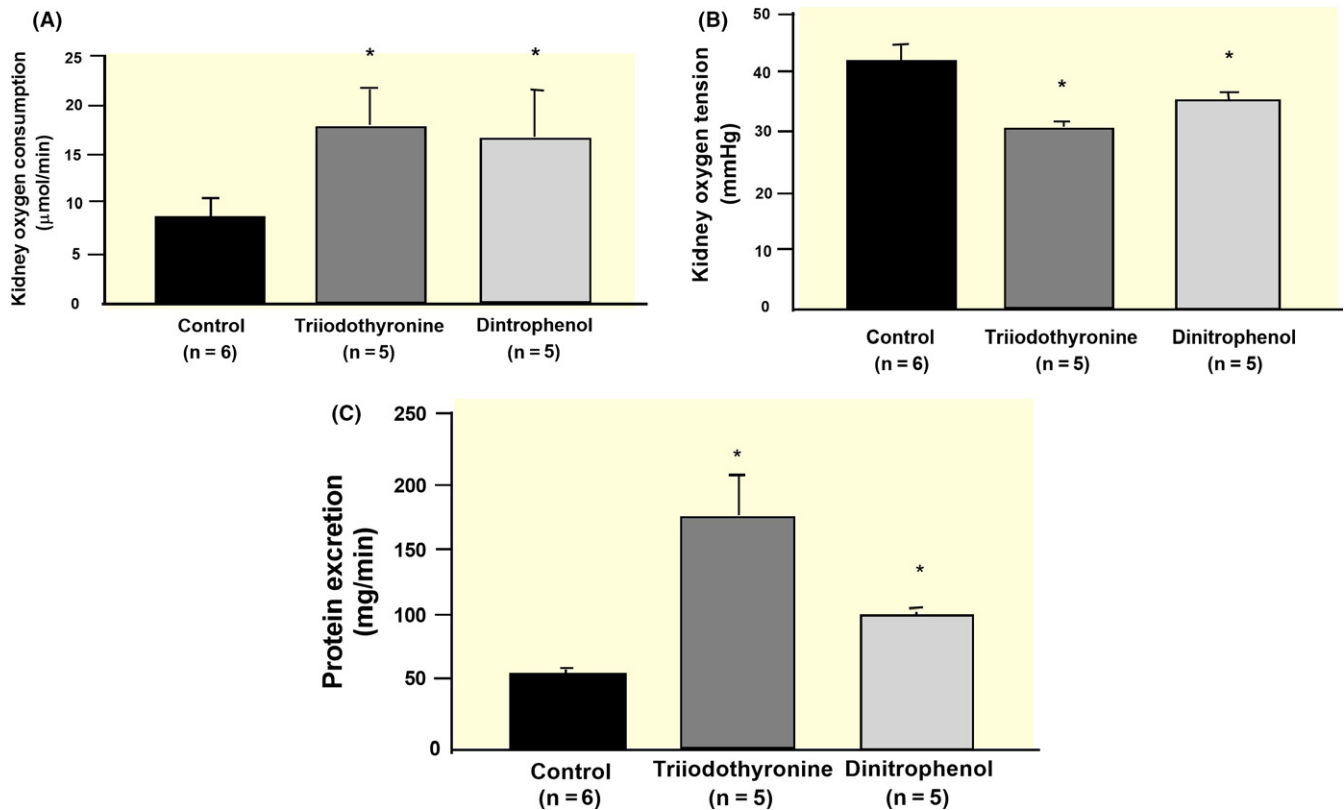


FIGURE 3 Evidence that renal tissue hypoxia per se leads to kidney disease. Panel A shows the renal oxygen consumption in rats that underwent chronic treatment with either triiodothyronine, dinitrophenol or their vehicle (control). At the end of the treatment regimen, renal cortical tissue oxygenation was assessed using a Clark electrode under anaesthesia (B). Panel C shows protein excretion at the end of the study. Images were reproduced from Ref. (166) with permission

IRI, blood flow, and thus oxygen delivery to the kidney, temporarily ceases. Similarly, removal of 5/6th of renal mass results in hyperfiltration and thus presumably increased oxygen consumption by individual tubules.⁵⁶ Along the same lines, CKD is often accompanied by the development of anaemia.¹⁶⁸ Anaemia, in turn, reduces renal oxygen delivery and promotes renal tissue hypoxia. Nevertheless, correction of anaemia by erythropoietin therapy has not been shown to delay progression of CKD.¹⁶⁹ Thus, it is often hard to delineate whether tissue hypoxia is a cause or consequence, or both, of the kidney disease. New experimental models of kidney disease, and new methods to follow the temporal and spatial relationships between hypoxia and renal damage, are required to overcome this limitation.

5 | DOES TISSUE HYPOXIA PRECEDE PATHOLOGY?

One of the important factors to consider for the development of therapeutic interventions to mitigate renal tissue hypoxia (discussed later in detail) is the timing of the intervention. Thus, it would be valuable to assess the time-course of development of tissue hypoxia relative to tissue injury.

Traditional and emerging biomarkers of AKI and CKD such as kidney injury molecule-1, neutral gelatinase-associated lipocalin and cystatin C are markers of kidney injury. Thus, if hypoxia causes kidney injury, we would expect hypoxia to precede the increased expression of these molecules. Unfortunately, to the best of our knowledge, there have been no reports of the temporal relationship between the onset of tissue hypoxia and the earliest time-point where upregulation of markers of kidney damage can be detected.

Due to the highly invasive nature of most methods for the direct assessment of tissue oxygenation in animal models of kidney disease, renal tissue oxygenation is often only assessed at single time-points, providing only “snapshots” of the natural progression of disease. Recently, this technical limitation has been addressed through development of new methods.

Electron paramagnetic resonance oximetry provides a partial solution to the limitation described above. Franzen et al⁵⁰ recently used this technique to demonstrate tissue hypoxia as early as 3 days after induction of type 1 diabetes that was sustained for at least 15 days (Figure 4A). Critically, tissue hypoxia in this model of type 1 diabetes was evident before the onset of significant albuminuria (Figure 4B).¹⁷⁰

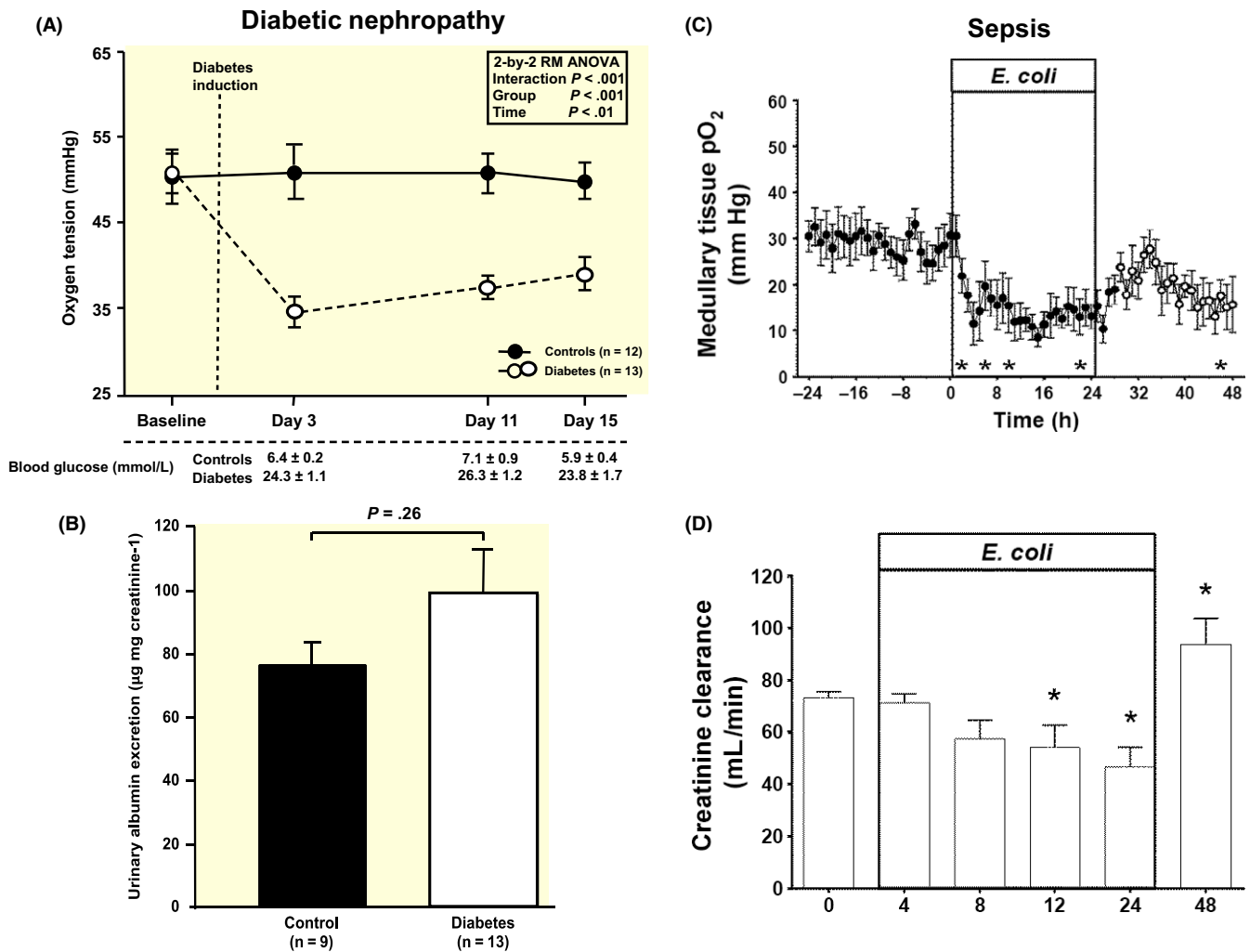


FIGURE 4 Evidence that renal tissue hypoxia precedes renal dysfunction in diabetic nephropathy and sepsis. Panel A shows the responses of renal tissue oxygen tension (PO_2), measured by paramagnetic resonance in mice, across a 15-d period in control mice and before and after administration of alloxan to render them diabetic. Panel B shows urinary albumin excretion in the same mice at the end of the study. Panel C shows medullary tissue PO_2 , measured by fibre-optic probe, in sheep rendered septic by intravenous infusion of live *Escherichia coli*. Panel D shows the time-course of creatinine clearance in the same sheep. Images were reproduced from: (A) and (B),⁵⁰ (C) and (D)³⁶ with permission

A telemetric method has been developed for use in unrestrained rats that allows continuous measurement of renal tissue oxygen tension via the electrochemical reduction of oxygen at the tip of an implanted carbon paste electrode.^{34,35} Using this technique, Emans et al³⁷ found that cortical tissue hypoxia developed 15 hours after the activation of the endogenous renin-angiotensin system in Cyp1a1Ren2 transgenic rats, a model of angiotensin II-dependent hypertensive CKD. Importantly, tissue hypoxia in this model of CKD was present well before the development of renal damage, consistent with the proposition that renal hypoxia could contribute to CKD induced by activation of the renin-angiotensin system.^{171,172}

Calzavacca et al³³ used chronically implantable fibre-optic probes to investigate the time-course of development of tissue hypoxia in an ovine model of sepsis. In conscious sheep, they demonstrated reduced medullary tissue perfusion and PO_2 in response to infusion of live bacteria

(Figure 4C).³⁶ Critically, medullary hypoxia developed before overt changes in creatinine clearance occurred (Figure 4D), suggesting that medullary hypoxia precedes the development of renal dysfunction in this model of AKI.³⁶

The recent observations described above, using techniques that allow long-term measurement of renal tissue PO_2 , are consistent with the hypothesis that tissue hypoxia is a driver of pathophysiology of various forms of kidney disease. However, they do not yet constitute a “smoking gun.”¹⁷³ There is considerable scope for further use of these methods to generate more detailed information regarding the temporal relationships between hypoxia, the molecular drivers of kidney disease, and renal damage and dysfunction. However, we also require information regarding the spatial relationship between tissue hypoxia and renal pathology, and most of all, on the efficacy of treatments for AKI and CKD that target renal hypoxia.

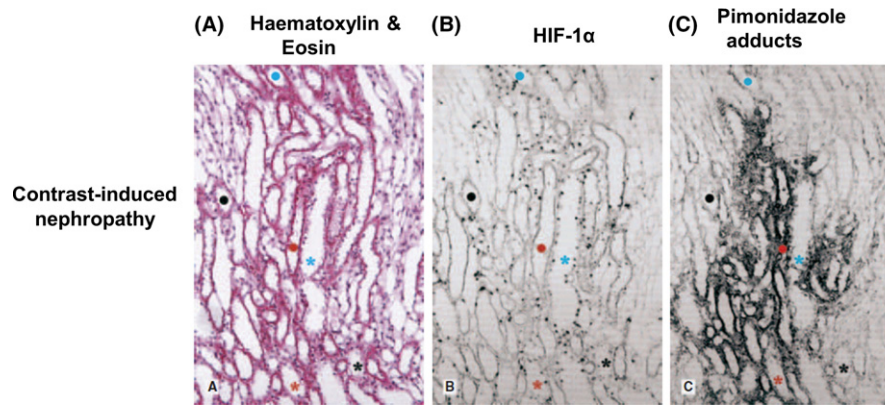


FIGURE 5 Evidence of colocalization of tissue hypoxia and pathology. Shown are serial sections of renal medullary tissue from a rat with contrast-induced nephropathy. The serial sections were stained with (A) haematoxylin and eosin, (B) hypoxia-inducible factor-1 α (HIF-1 α) and (C) pimonidazole adducts. HIF-1 α present in tubules was colocalized with areas of moderate (blue asterisk and circle) and extensive (red asterisk and circle) staining of pimonidazole adducts but not in areas where there was absence of pimonidazole adducts (black asterisk and circle). Images were reproduced from Ref. ¹⁷⁷ with permission

6 | DOES TISSUE HYPOXIA COLOCALIZE WITH PATHOLOGY?

To better characterize the role of tissue hypoxia in kidney damage and dysfunction, we require a better understanding of the spatial relationships between tissue hypoxia and tissue damage. Of the many methods available for the examination of tissue hypoxia, most either have limited spatial resolution or are indirect indicators of tissue hypoxia.²⁰ One method that overcomes the lack of spatial resolution is pimonidazole adduct immunohistochemistry. However, this method is not without limitations. Pimonidazole, a 2-nitroimidazole, has been used extensively in studies of tumour biology.^{174,175} Pimonidazole is given *in vivo* and forms adducts in tissues where the oxygen tension is <10 mmHg.²⁴ These adducts can be detected by immunohistochemistry once the tissue of interest is excised.¹⁷⁶ Thus, this method does not allow quantification of the severity of tissue hypoxia. An additional caveat is that upregulation of some nitroreductases may lead to deposition of pimonidazole adducts even under normoxic conditions.²⁷ Furthermore, the potential for detection of hypoxia in the renal cortex is rather limited as tissue PO₂ is probably rarely <10 mmHg in viable cortical tissue. On the other hand, this method provides excellent spatial resolution. Despite the limitations of pimonidazole adduct immunohistochemistry, it is currently the only available direct marker of cellular hypoxia in the kidney. This method was adapted for use in the kidney and was optimized by Rosenberger et al.¹⁷⁶ Since then, it has been used to demonstrate renal tissue hypoxia in many studies where direct quantification of tissue PO₂ is not available/not feasible. Indeed, Rosenberger et al.¹⁷⁷ observed the colocalization of pimonidazole adducts and HIF-1 α in the medulla but not in the cortex in

a model of contrast-induced nephropathy (Figure 5). This suggests that the tissue hypoxia arising from administration of radiocontrast agents is associated with downstream activation of HIF-dependent signalling pathways.

To better characterize the spatial relationships between tissue hypoxia and tissue injury in kidney disease, it should be possible to stain serial sections of kidney tissue for pimonidazole adducts and markers for tissue injury. It should also be possible to tag pimonidazole adducts and markers of tissue injury with fluorophores to compare their localization in three-dimensional rendering of fluorescence imaging. Some markers of interest that may indicate tissue damage are periodic acid-Schiff stain, Masson's trichrome, vimentin, CD31 and CD34.

7 | DOES PREVENTION OF TISSUE HYPOXIA PREVENT KIDNEY DISEASE?

If indeed tissue hypoxia is the critical driver of kidney diseases, then abrogation of hypoxia should delay the progression of, or even prevent, kidney disease. Unfortunately, there are currently few therapeutic options for abrogating tissue hypoxia. One proposed therapy is normobaric or hyperbaric hyperoxia, which could increase renal oxygen delivery. Normobaric hyperoxic treatment in a rat model of haemorrhagic shock reduced renal tubular damage and abrogated cellular hypoxia, although it did appear to exacerbate renal oxidative stress.¹⁷⁸ Hyperbaric hyperoxia, applied in a rat model of sepsis, markedly reduced tubular and glomerular damage but did not result in oxidative stress.¹⁷⁹ Thus, there is scope to further explore the potential benefits of this approach. But, critically, observations

in most of these studies were generated in animal models that may not necessarily reflect kidney disease in humans. Therefore, the next step might be phase 1 and phase 2 clinical trials of normobaric/hyperbaric hyperoxia in patients with certain forms of AKI or even CKD.

The acute effects of normobaric hyperoxia on cardiovascular function in patients with CKD have been assessed, but have generated rather conflicting findings. Hering et al¹⁸⁰ subjected patients with CKD to brief normobaric hyperoxia. They showed that the abnormally high muscle sympathetic nerve activity was significantly attenuated following 15 minutes of exposure to passive breathing of 100% O₂.¹⁸⁰ In contrast, van der Bel et al¹⁸¹ reported increases in systemic vascular resistance in response to normobaric hyperoxia. Thus, it seems likely that the cardiovascular response to hyperoxia depends on the balance of changes in chemoreflex (reduced sympathetic vasomotor drive) and local (vasoconstrictor) control of the circulation. The question of whether hyperoxia can ameliorate AKI or delay the progression of CKD remains to be determined. Such longer-term trials might be problematic, given the established toxic effects of oxygen.¹⁸²

Aside from increasing renal oxygen delivery, the alternative approach to abrogating tissue hypoxia is by reducing renal oxygen consumption. Indeed, inhibition of tubular reabsorption may improve medullary tissue oxygenation¹⁸³ and reduce renal damage.¹⁸⁴ For example, the diuretic furosemide has also been shown to abrogate renal damage and dysfunction in a rat model of contrast-induced nephropathy.¹⁸⁵ It is also possible that the beneficial effects of protein restriction on progression of CKD¹⁸⁶ could at least be partly mediated by improved oxygenation of the renal outer medulla.¹⁸⁷

8 | SUMMARY AND CONCLUSIONS

The proposal that chronic hypoxia as an important driver in the pathogenesis of kidney disease was first developed two decades ago.⁴ Since then, much evidence has been produced to show that (i) hypoxia is a common feature of both AKI and CKD, (ii) that at least under in vitro conditions, renal tissue hypoxia drives signalling cascades that lead to tissue damage and dysfunction and that (iii) tissue hypoxia itself can lead to renal pathology, independent of other known risk factors for kidney disease. There is also some evidence that (iv) tissue hypoxia precedes renal pathology, at least in some forms of AKI and CKD. However, we have made relatively little progress in determining (v) the spatial relationships between tissue hypoxia and pathological processes (i.e. colocalization) or (vi) whether therapies targeted to reduce tissue hypoxia can prevent or delay the progression of renal

disease. These questions remain the greatest challenges for the field.

CONFLICT OF INTEREST

The authors report no conflict of interest.

REFERENCES

- Eckardt K-U, Bernhardt WM, Weidermann A, et al. Role of hypoxia in the pathogenesis of renal disease. *Kidney Int.* 2005;68:S46-S51.
- Heyman SN, Khamaisi M, Rosen S, Rosenberger C. Renal parenchymal hypoxia, hypoxia response and the progression of chronic kidney disease. *Am J Nephrol.* 2008;28:998-1006.
- Nangaku M. Chronic hypoxia and tubulointerstitial injury: a final common pathway to end-stage renal failure. *J Am Soc Nephrol.* 2006;17:17-25.
- Fine LG, Orphanides C, Norman JT. Progressive renal disease: the chronic hypoxia hypothesis. *Kidney Int Suppl.* 1998;65:S74-S78.
- Fine LG, Norman JT. Chronic hypoxia as a mechanism of progression of chronic kidney diseases: from hypothesis to novel therapeutics. *Kidney Int.* 2008;74:867-872.
- Evans RG, Ince C, Joles JA, et al. Hemodynamic influences on kidney oxygenation: clinical implications of integrative physiology. *Clin Exp Pharmacol Physiol.* 2013;40:106-122.
- Singh P, Ricksten S, Bragadottir G, Redfors B, Nordquist L. Renal oxygenation and haemodynamics in acute kidney injury and chronic kidney disease. *Clin Exp Pharmacol Physiol.* 2013;40:138-147.
- Bellomo R, Kellum JA, Ronco C. Acute kidney injury. *Lancet.* 2012;380:756-766.
- Kosieradzki M, Rowinski W. Ischemia/reperfusion injury in kidney transplantation: mechanisms and prevention. *Transplant Proc.* 2008;40:3279-3288.
- O'Neal JB, Shaw AD, Billings FT 4th. Acute kidney injury following cardiac surgery: current understanding and future directions. *Crit Care.* 2016;20:187.
- Secin FO. Importance and limits of ischemia in renal partial surgery: experimental and clinical research. *Adv Urol.* 2008;1-10:2008.
- Munshi R, Hsu C, Himmelfarb J. Advances in understanding ischemic acute kidney injury. *BMC Med.* 2011;9:11-16.
- Brezis M, Rosen S. Mechanisms of disease: hypoxia of the renal medulla - Its implications for disease. *N Engl J Med.* 1995;332:647-655.
- Fry BC, Edwards A, Sgouralis I, Layton AT. Impact of renal medullary three-dimensional architecture on oxygen transport. *Am J Physiol Renal Physiol.* 2014;307:F263-F272.
- Devarajan P. Update on mechanisms of ischemic acute kidney injury. *J Am Soc Nephrol.* 2006;17:1503-1520.
- Tanaka T, Miyata T, Inagi R, et al. Hypoxia-induced apoptosis in cultured glomerular endothelial cells: involvement of mitochondrial pathways. *Kidney Int.* 2003;64:2020-2032.
- Kim J, Seok YM, Jung K, Park KM. Reactive oxygen species/oxidative stress contributes to progression of kidney fibrosis following transient kidney injury in mice. *Am J Physiol Renal Physiol.* 2009;297:F461-F470.

18. Basile DP, Bonventre JV, Mehta RL, et al. Progression after AKI: understanding maladaptive repair processes to predict and identify therapeutic treatments. *J Am Soc Nephrol*. 2016;27:687-697.
19. Koch R. Die aetiologie der tuberculose. *Berl Klin Wochenschr*. 1882;19:221.
20. Evans RG, Gardiner BS, Smith DW, O'Connor PM. Methods for studying the physiology of kidney oxygenation. *Clin Exp Pharmacol Physiol*. 2008;35:1405-1412.
21. Hirakawa Y, Tanaka T, Nangaku M. Renal hypoxia in CKD; Pathophysiology and detecting methods. *Front Physiol*. 2017;8:99.
22. Clark LC, Mishrahy G, Fox RP. Chronically implanted polarographic electrodes. *J Appl Physiol*. 1958;13:85-91.
23. Urtasun RC, Koch CJ, Franko AJ, Raleigh JA, Chapman JD. A novel technique for measuring human tissue pO₂ at the cellular level. *Br J Cancer*. 1986;54:453-457.
24. Gross MW, Karbach U, Groebe K, Franko AJ, Mueller-Klieser W. Calibration of misonidazole labeling by simultaneous measurement of oxygen tension and labeling density in multicellular spheroids. *Int J Cancer*. 1995;61:567-573.
25. Abdelkader A, Ho J, Ow CPC, et al. Renal oxygenation in acute renal ischemia-reperfusion injury. *Am J Physiol Renal Physiol*. 2014;306:F1026-F1038.
26. Cobb LM, Hacker T, Nolan J. NAD(P)H nitroblue tetrazolium reductase levels in apparently normoxic tissues: a histochemical study correlating enzyme activity with binding of radiolabelled misonidazole. *Br J Cancer*. 1990;61:524-529.
27. Janssen HLK, Hoebbers FJ, Sprong D, et al. Differentiation-associated staining with anti-pimonidazole antibodies in head and neck tumors. *Radiother Oncol*. 2004;70:91-97.
28. Prasad PV. Evaluation of intra-renal oxygenation by BOLD MRI. *Nephron Clin Pract*. 2006;103:c58-c65.
29. Ahmad R, Kuppusamy P. Theory, instrumentation, and applications of EPR Oximetry. *Chem Rev*. 2010;110:3212-3236.
30. Khan N, Williams BB, Hou H, Li H, Swartz HM. Repetitive tissue PO₂ measurements by electron paramagnetic resonance oximetry: current status and future potential for experimental and clinical studies. *Antioxid Redox Signal*. 2007;9:1169-1182.
31. Nangaku M, Eckardt K-U. Hypoxia and the HIF system in kidney disease. *J Mol Med*. 2007;85:1325-1330.
32. Calzavacca P, Evans RG, Bailey M, Bellomo R, May CN. Variable responses of regional renal oxygenation and perfusion to vasoactive agents in awake sheep. *Am J Physiol Regul Integr Comp Physiol*. 2015;309:R1226-R1233.
33. Calzavacca P, Evans RG, Bailey M, Lankadeva Y, Bellomo R, May CN. Long-term measurement of renal cortical and medullary tissue oxygenation and perfusion in unanesthetized sheep. *Am J Physiol Regul Integr Comp Physiol*. 2015;308:R832-R839.
34. Koeners MP, Ow CPC, Russell DM, et al. Telemetry-based oxygen sensor for continuous monitoring of kidney oxygenation in conscious rats. *Am J Physiol Renal Physiol*. 2013;304:F1471-F1480.
35. Koeners MP, Ow CPC, Russell DM, Evans RG, Malpas SC. Prolonged and continuous measurement of kidney oxygenation in conscious rats. *Methods Mol Biol*. 2016;1397:93-111.
36. Calzavacca P, Evans RG, Bailey M, Bellomo R, May CN. Cortical and medullary tissue perfusion and oxygenation in experimental septic acute kidney injury. *Crit Care Med*. 2015;43:e431-e439.
37. Emans TW, Janssen BJ, Pinkham MI, et al. Exogenous and endogenous angiotensin-II decrease renal cortical oxygen tension in conscious rats by limiting renal blood flow. *J Physiol*. 2016;594:6287-6300.
38. Lankadeva YR, Kosaka J, Evans RG, Bailey SR, Bellomo R, May CN. Intrarenal and urinary oxygenation during norepinephrine resuscitation in ovine septic acute kidney injury. *Kidney Int*. 2016;90:100-108.
39. Igarashi P, Somlo S. Genetics and pathogenesis of polycystic kidney disease. *J Am Soc Nephrol*. 2002;13:2384-2398.
40. Grantham JJ, Torres V, Chapman AB, et al. Volume progression in polycystic kidney disease. *N Engl J Med*. 2006;354:2122-2130.
41. Wei W, Popov V, Walocha JA, Wen J, Bello Reuss E. Evidence of angiogenesis and microvascular regression in autosomal-dominant polycystic kidney disease kidneys: a corrosion cast study. *Kidney Int*. 2006;70:1261-1268.
42. Ow CPC, Abdelkader A, Hilliard LM, Phillips JK, Evans RG. Determinants of renal tissue hypoxia in a rat model of polycystic kidney disease. *Am J Physiol Regul Integr Comp Physiol*. 2014;307:R1207-R1215.
43. Bernhardt W, Wiesener M, Weidemann A, et al. Involvement of hypoxia-inducible transcription factors in polycystic kidney disease. *Am J Pathol*. 2007;170:830-842.
44. Ding A, Kalaighanasundaram P, Ricardo SD, et al. Chronic treatment with tempol does not significantly ameliorate renal tissue hypoxia or disease progression in a rodent model of polycystic kidney disease. *Clin Exp Pharmacol Physiol*. 2012;39:917-929.
45. Lorenz G, Desai J, Anders H-J. Lupus nephritis: update on mechanisms of systemic autoimmunity and kidney immunopathology. *Curr Opin Nephrol Hypertens*. 2014;23:211-217.
46. Yung S, Tsang RCW, Leung JKH, Chan TM. Effect of human anti-DNA antibodies on proximal renal tubular epithelial cell cytokine expression: implications on tubulointerstitial inflammation in lupus nephritis. *J Am Soc Nephrol*. 2005;16:3281-3294.
47. Deng W, Ren Y, Feng X, et al. Hypoxia inducible factor-1 alpha promotes mesangial cell proliferation in lupus nephritis. *Am J Nephrol*. 2014;40:507-515.
48. Nechemia-Arbely Y, Khamaisi M, Rosenberger C, et al. In vivo evidence suggesting reciprocal renal hypoxia-inducible factor-1 upregulation and signal transducer and activator of transcription 3 activation in response to hypoxic and non-hypoxic stimuli. *Clin Exp Pharmacol Physiol*. 2013;40:262-272.
49. Rosenberger C, Khamaisi M, Abassi Z, et al. Adaptation to hypoxia in the diabetic rat kidney. *Kidney Int*. 2008;73:34-42.
50. Franzen S, Pihl L, Khan N, Gustafsson H, Palm F. Pronounced kidney hypoxia precedes albuminuria in type I diabetic mice. *Am J Physiol Renal Physiol*. 2016;310:F807-F809.
51. Palm F, Cederberg J, Hansell P, Liss P, Carlsson P-O. Reactive oxygen species cause diabetes-induced decrease in renal oxygen tension. *Diabetologia*. 2003;46:1153-1160.
52. Manotham K, Ongvilawan B, Urusopone P, et al. Angiotensin II receptor blocker partially ameliorated intrarenal hypoxia in chronic kidney disease patients: a pre/post-study. *Intern Med J*. 2012;42:e33-e37.
53. Yin W, Liu F, Li X, et al. Noninvasive evaluation of renal oxygenation in diabetic nephropathy by BOLD-MRI. *Eur J Radiol*. 2012;81:1426-1431.

54. Wang ZJ, Kumar R, Banerjee S, Hsu C-Y. Blood oxygen-level dependent (BOLD) MR imaging of diabetic nephropathy—preliminary experience. *J Magn Reson Imaging*. 2011;33:655-660.
55. Pruijm M, Hofmann L, Piskunowicz M, et al. Determinants of renal tissue oxygenation as measured with BOLD-MRI in chronic kidney disease and hypertension in humans. *PLoS ONE*. 2014;9:e95895.
56. Hostetter TH, Olson JL, Rennke HG, Venkatachalam MA, Brenner BM. Hyperfiltration in remnant nephrons: a potentially adverse response to renal ablation. *Am J Physiol Renal Physiol*. 1981;241:F85-F93.
57. Nath KA, Croatt AJ, Hostetter TH. Oxygen consumption and oxidant stress in surviving nephrons. *Am J Physiol Renal Physiol*. 1990;27:F1354-F1362.
58. Takakuta K, Fujimori A, Chikanishi T, et al. Renoprotective properties of pirfenidone in subtotaly nephrectomized rats. *Eur J Pharmacol*. 2010;629:118-124.
59. Yang B, Vohra P, Janardhanan R, Misra KD, Misra S. Expression of profibrotic genes in a murine remnant kidney model. *J Vasc Interv Radiol*. 2011;22:1765-1772.
60. Chen J-F, Liu H, Ni H-F, et al. Improved mitochondrial function underlies the protective effect of pirfenidone against tubulointerstitial fibrosis in 5/6 nephrectomized rats. *PLoS ONE*. 2013;8:e83593.
61. Lai EY, Luo Z, Onozato ML, et al. Effects of the antioxidant drug tempol on renal oxygenation in mice with reduced renal mass. *Am J Physiol Renal Physiol*. 2012;303:F64-F74.
62. Manotham K, Tanaka T, Matsumoto M, et al. Evidence of tubular hypoxia in the early phase in the remnant kidney model. *J Am Soc Nephrol*. 2004;15:1277-1288.
63. Palm F, Nangaku M, Fasching A, et al. Uremia induces abnormal oxygen consumption in tubules and aggravates chronic hypoxia of the kidney via oxidative stress. *Am J Physiol Renal Physiol*. 2010;299:F380-F386.
64. Priyadarshi A, Periyasamy S, Burke TJ, Britton SL, Malhortra D, Shapiro JI. Effects of reduction of renal mass on renal oxygen tension and erythropoietin production in the rat. *Kidney Int*. 2002;61:542-546.
65. Schoenberg SO, Bock M, Kallinowski F, Just A. Correlation of hemodynamic impact and morphologic degree of renal artery stenosis in a canine model. *J Am Soc Nephrol*. 2000;11:2190-2198.
66. Palm F, Connors SG, Mendoca M, Welch WJ, Wilcox CS. Angiotensin II type 2 receptors and nitric oxide sustain oxygenation in the clipped kidney of early goldblatt hypertensive rats. *Hypertension*. 2008;51:345-351.
67. Welch WJ, Mendoca M, Aslam S, Wilcox CS. Roles of oxidative stress and AT1 receptors in renal hemodynamics and oxygenation in the postclipped 2K, 1C kidney. *Hypertension*. 2003;41:692-696.
68. Rognant N, Guebre-Egziabher F, Bacchetta J, et al. Evolution of renal oxygen content measured by BOLD MRI downstream a chronic renal artery stenosis. *Nephrol Dial Transpl*. 2011;26:1205-1210.
69. Glociczki ML, Glockner JF, Lerman LO, et al. Preserved oxygenation despite reduced blood flow in poststenotic kidneys in human atherosclerotic renal artery stenosis. *Hypertension*. 2010;55:961-966.
70. Saad A, Crane JC, Glockner J, et al. Human renovascular disease: estimating fractional tissue hypoxia to analyze blood oxygen level-dependent MR. *Radiology*. 2013;268:770-778.
71. Saad A, Herrmann SMS, Crane J, et al. Stent revascularization restores cortical blood flow and reverses tissue hypoxia in atherosclerotic renal artery stenosis but fails to reverse inflammatory pathways or glomerular filtration rate. *Circ Cardiovasc Interv*. 2013;6:428-435.
72. Glociczki ML, Glockner J, Crane JA, et al. Blood oxygen level-dependent magnetic resonance imaging identifies cortical hypoxia in severe renovascular disease. *Hypertension*. 2011;58:1066-1072.
73. Babickova J, Klinkhammer BM, Buhl EM, et al. Regardless of etiology, progressive renal disease causes ultrastructural and functional alterations of peritubular capillaries. *Kidney Int*. 2017;91:70-85.
74. Hoste EAJ, Schurgers M. Epidemiology of acute kidney injury: how big is the problem? *Crit Care Med*. 2008;36:S146-S151.
75. Coca SG, Singanamala S, Parikh CR. Chronic kidney disease after acute kidney injury: a systematic review and meta-analysis. *Kidney Int*. 2012;81:442-448.
76. Leung KCW, Tonelli M, James MT. Chronic kidney disease following acute kidney injury—risk and outcomes. *Nat Rev Nephrol*. 2013;9:77-85.
77. Lameire N, Bagga A, Cruz D, et al. Acute kidney injury: an increasing global concern. *Lancet*. 2013;382:170-179.
78. Legrand M, Almac E, Mik EG, et al. L-NIL prevents renal microvascular hypoxia and increase of renal oxygen consumption after ischemia-reperfusion in rats. *Am J Physiol Renal Physiol*. 2009;296:F1109-F1117.
79. Bonventre JV, Yang L. Cellular pathophysiology of ischemic acute kidney injury. *J Clin Invest*. 2011;121:4210-4221.
80. Sheridan AM, Bonventre JV. Cell biology and molecular mechanisms of injury in ischemic acute renal failure. *Curr Opin Nephrol Hypertens*. 2000;9:427-434.
81. Sadowski EA, Djamali A, Wentland AL, et al. Blood oxygen level-dependent and perfusion magnetic resonance imaging: detecting differences in oxygen bioavailability and blood flow in transplanted kidney. *Magn Reson Imaging*. 2010;28:56-64.
82. Siegemund M, van Bommel J, Stegenga ME, et al. Aortic cross-clamping and reperfusion in pigs reduces microvascular oxygenation by altered systemic and regional blood flow distribution. *Anesth Analg*. 2010;111:345-353.
83. Conde E, Alegre L, Blanco-Sanchez I, et al. Hypoxia inducible factor 1-alpha (HIF-1 alpha) is induced during reperfusion after renal ischemia and is critical for proximal tubule cell survival. *PLoS ONE*. 2012;7:e33258.
84. Oostendorp M, de Vries EE, Slenter JMGM, Peutz-Koorstra CJ, Snoeijs MG, Post MJ. Ernest van Heurn LW, Backes WH: MRI of renal oxygenation and function after normothermic ischemia-reperfusion injury. *NMR Biomed*. 2011;24:194-200.
85. Pohlmann A, Hentschel J, Fechner M, et al. High temporal resolution parametric MRI monitoring of the initial ischemia/reperfusion phase in experimental acute kidney injury. *PLoS ONE*. 2013;8:e57411.
86. Lannemyr L, Bragadottir G, Krumbholz V, Redfors B, Sellgren J, Ricksten S-E. Effects of cardiopulmonary bypass on renal perfusion, filtration, and oxygenation in patients undergoing cardiac surgery. *Anesthesiology*. 2017;126:205-213.
87. Stafford-Smith M, Grocott HP. Renal medullary hypoxia during experimental cardiopulmonary bypass: a pilot study. *Perfusion*. 2005;20:53-58.

88. Darby PJ, Kim N, Hare GMT, et al. Anemia increases the risk of renal cortical and medullary hypoxia during cardiopulmonary bypass. *Perfusion*. 2013;28:504-511.
89. Sgouralis I, Evans RG, Gardiner BS, Smith JA, Fry B, Layton AT. Renal hemodynamics, function, and oxygenation during cardiac surgery performed on cardiopulmonary bypass: a modeling study. *Physiol Rep*. 2015;3:e12260.
90. Sgouralis I, Evans RG, Layton AT. Renal medullary and urinary oxygen tension during cardiopulmonary bypass in the rat. *Math Med Biol*. 2017;34:313-333.
91. Redfors B, Bragadottir G, Sellgren J, Sward K, Ricksten S. Acute renal failure is NOT an “acute renal success” - A clinical study on the renal oxygen supply/demand relationship in acute kidney injury. *Crit Care Med*. 2010;38:1695-1701.
92. Patel NN, Lin H, Toth T, et al. Reversal of anemia with allogenic RBC transfusion prevents post-cardiopulmonary bypass acute kidney injury in swine. *Am J Physiol Renal Physiol*. 2011;301:F605-F614.
93. Fahling M, Seeliger E, Patzak A, Persson PB. Understanding and preventing contrast-induced acute kidney injury. *Nat Rev Nephrol*. 2017;13:169-180.
94. Heyman SN, Brezis M, Epstein FH, Spokes K, Silva P, Rosen S. Early renal medullary hypoxic injury from radiocontrast and indomethacin. *Kidney Int*. 1991;40:632-642.
95. Liss P, Aukland K, Carlsson P-O, Palm F, Hansell P. Influence of iohalamate on renal medullary perfusion and oxygenation in the rat. *Acta Radiol*. 2005;8:823-929.
96. Liss P, Nygren A, Revsbech NP, Ulfendahl HR. Intrarenal oxygen tension measured by a modified Clark electrode at normal and low blood pressure and after injection of x-ray contrast media. *Pflügers Arch*. 1997;434:705-711.
97. Prasad PV, Priatna A, Spokes K, Epstein FH. Changes in intrarenal oxygenation as evaluated by BOLD MRI in a rat kidney model for radiocontrast nephropathy. *J Magn Reson Imaging*. 2001;13:744-747.
98. Zhang Y, Wang J, Yang X, et al. The serial effect of iodinated contrast media on renal hemodynamics and oxygenation as evaluated by ASL and BOLD MRI. *Contrast Media Mol Imaging*. 2012;7:418-425.
99. Hofmann L, Simon Zoula SC, Nowak A, et al. BOLD-MRI for the assessment of renal oxygenation in humans: acute effect of nephrotoxic xenobiotics. *Kidney Int*. 2006;70:144-150.
100. Haller C, Hizoh I. The cytotoxicity of iodinated radiocontrast agents on renal cells in vitro. *Invest Radiol*. 2004;39:149-154.
101. Uchino S, Kellum JA, Bellomo R, et al. Acute renal failure in critically ill patients: a multinational, multicenter study. *JAMA*. 2005;294:813-818.
102. Neveu H, Kleinknecht D, Brivet F, Loirat P, Landais P. Prognostic factors in acute renal failure due to sepsis: results of a prospective multicentre study. *Nephrol Dial Transpl*. 1996;11:293-299.
103. Kaukonen K-M, Bailey M, Suzuki S, Pilcher D, Bellomo R. Mortality related to severe sepsis and septic shock among critically ill patients in Australia and New Zealand, 2000-2012. *JAMA*. 2014;311:1308-1316.
104. Schrier RW, Wang W. Acute renal failure and sepsis. *N Engl J Med*. 2004;351:159-169.
105. Doi K, Leelahavanichkul A, Yuen PST, Star RA. Animal models of sepsis and sepsis-induced kidney injury. *J Clin Invest*. 2009;119:2868-2878.
106. Dyson A, Bezemer R, Legrand M, Balestra G, Singer M, Ince C. Microvascular and interstitial oxygen tension in the renal cortex and medulla studied in a 4-H rat model of LPS-induced endotoxemia. *Shock*. 2011;36:83-89.
107. James PE, Bacic G, Grinberg OY, et al. Endotoxin-induced changes in intrarenal PO₂, measured by in vivo electron paramagnetic resonance oximetry and magnetic resonance imaging. *Free Radic Biol Med*. 1996;21:25-34.
108. Legrand M, Bezemer R, Kandil A, Demirci C, Payen D, Ince C. The role of renal hypoperfusion in development of renal microcirculatory dysfunction in endotoxemic rats. *Intensive Care Med*. 2011;37:1534-1542.
109. Wang Z, Holthoff JH, Seely KA, et al. Development of oxidative stress in the peritubular capillary microenvironment mediates sepsis-induced renal microcirculatory failure and acute kidney injury. *Am J Pathol*. 2012;180:505-516.
110. Yasuda H, Yuen PST, Hu X, Zhou H, Star RA. Simvastatin improves sepsis-induced mortality and acute kidney injury via renal vascular effects. *Kidney Int*. 2006;69:1535-1542.
111. Tran M, Tam D, Bardia A, et al. PGC-1 α promotes recovery after acute kidney injury during systemic inflammation in mice. *J Clin Invest*. 2011;121:4003-4014.
112. Bouglé A, Duranteau J. Pathophysiology of sepsis-induced acute kidney injury: the role of global renal blood flow and renal vascular resistance. *Contrib Nephrol*. 2011;174:89-97.
113. Neusser MA, Lindenmeyer MT, Moll AG, et al. Human nephrosclerosis triggers a hypoxia-related glomerulopathy. *Am J Pathol*. 2010;176:594-607.
114. Rosenberger C, Pratschke J, Rudolph B, et al. Immunohistochemical detection of hypoxia-inducible factor-1 α in human renal allograft biopsies. *J Am Soc Nephrol*. 2007;18:343-351.
115. Belibi F, Zafar I, Ravichandran K, et al. Hypoxia-inducible factor-1 α (HIF-1 α) and autophagy in polycystic kidney disease (PKD). *Am J Physiol Renal Physiol*. 2011;300:F1235-F1243.
116. Rosenberger C, Madriota S, Jurgensen JS, et al. Expression of hypoxia-induced factor-1-alpha and -2alpha in hypoxic and ischemic rat kidneys. *J Am Soc Nephrol*. 2002;13:1721-1732.
117. Haase VH. Hypoxia-inducible factors in the kidney. *Am J Physiol Renal Physiol*. 2006;291:F271-F281.
118. Greer SN, Metcalf JL, Wang Y, Ohh M. The updated biology of hypoxia-inducible factor. *EMBO J*. 2012;31:2448-2460.
119. Ke Q, Costa M. Hypoxia-inducible factor-1 (HIF-1). *Mol Pharmacol*. 2006;70:1469-1480.
120. Semenza GL. Targeting HIF-1 for cancer therapy. *Nat Rev Cancer*. 2003;3:721-732.
121. Gunaratnam L, Bonventre JV. HIF in kidney disease and development. *J Am Soc Nephrol*. 2009;20:1877-1887.
122. Donnelly S. Why is erythropoietin made in the kidney? The kidney functions as a ‘critmeter’ to regulate the hematocrit. *Am J Kidney Dis*. 2001;38:415-425.
123. Lee FS, Percy MJ. The HIF pathway and erythrocytosis. *Annu Rev Pathol*. 2011;6:165-192.
124. Farsijani NM, Liu Q, Kobayashi H, et al. Renal epithelium regulates erythropoiesis via HIF-dependent suppression of erythropoietin. *J Clin Invest*. 2016;126:1425-1437.
125. Stockmann C, Fandrey J. Hypoxia-induced erythropoietin production: a paradigm for oxygen-regulated gene expression. *Clin Exp Pharmacol Physiol*. 2006;33:968-979.

126. Sharples E, Patel NN, Brown P, et al. Erythropoietin protects the kidney against the injury and dysfunction caused by ischemia-reperfusion. *J Am Soc Nephrol.* 2004;15:2115-2124.
127. Yang B, Hosgood S, Bagul A, Waller H, Nicholson M. Erythropoietin regulates apoptosis, inflammation and tissue remodelling via caspase-3 and IL- β in isolated hemoperfused kidneys. *Eur J Pharmacol.* 2011;660:420-430.
128. Hu L, Yang C, Zhao T, et al. Erythropoietin ameliorates renal ischemia and reperfusion injury via inhibiting tubulointerstitial inflammation. *J Surg Res.* 2012;176:260-266.
129. Gobe GC, Bennett NC, West M, et al. Increased progression to kidney fibrosis after erythropoietin is used as a treatment for acute kidney injury. *Am J Physiol Renal Physiol.* 2014;306:F681-F692.
130. Genovese F, Manresa AA, Leeming DJ, Karsdal MA, Boor P. The extracellular matrix in the kidney: a source of novel non-invasive biomarkers of kidney fibrosis? *Fibrogenesis Tissue Repair.* 2014;7:4.
131. Norman JT, Orphanides C, Garcia P, Fine LG. Hypoxia-induced changes in extracellular matrix metabolism in renal cells. *Exp Nephrol.* 1999;7:463-469.
132. Norman JT, Clark IM, Garcia PL. Hypoxia promotes fibrogenesis in human renal fibroblasts. *Kidney Int.* 2000;58:2351-2366.
133. Rana MK, Srivasta J, Yang M, Chen CS, Barber DL. Hypoxia increases extracellular fibronectin abundance but not the assembly of extracellular fibronectin during epithelial cell transdifferentiation. *J Cell Sci.* 2015;128:1083-1089.
134. Strutz F, Zeisberg M, Ziyadeh FN, et al. Role of basic fibroblast growth factor-2 in epithelial-mesenchymal transformation. *Kidney Int.* 2002;61:1717-1728.
135. Tan TK, Zheng G, Hsu TT, et al. Matrix metalloproteinase-9 of tubular and macrophage origin contributes to the pathogenesis of renal fibrosis via macrophage recruitment through osteopontin cleavage. *Lab Invest.* 2013;93:434-449.
136. Catania JM, Chen G, Parrish AR. Role of matrix metalloproteinases in renal pathophysiology. *Am J Physiol Renal Physiol.* 2007;292:F905-F911.
137. Orphanides C, Fine LG, Norman JT. Hypoxia stimulates proximal tubular cell matrix production via a TGF- β -independent mechanism. *Kidney Int.* 1997;52:637-647.
138. Rama I, Bruene B, Torras J, et al. Hypoxia stimulus: an adaptive immune response during dendritic cell maturation. *Kidney Int.* 2008;73:816-825.
139. Kuhlicke J, Frick JS, Morote-Garcia JC, Rosenberger P, Eltzschig HK. Hypoxia inducible factor (HIF)-1 coordinates induction of toll-like receptors TLR2 and TLR6 during hypoxia. *PLoS ONE.* 2007;2:e1364.
140. Rius J, Guma M, Schachtrup C, et al. NF- κ B links innate immunity to the hypoxic response through transcriptional regulation of HIF-1 α . *Nature.* 2008;453:807-811.
141. Walmsley SR, Print C, Farahi N, et al. Hypoxia-induced neutrophil survival is mediated by HIF-1 α -dependent NF- κ B activity. *J Exp Med.* 2005;201:105-115.
142. Murdoch C, Muthana M, Lewis CE. Hypoxia regulates macrophage functions in inflammation. *J Immunol.* 2005;175:6257-6263.
143. Baud L, Ardaillou R. Tumor necrosis factor in renal injury. *Miner Electrolyte Metab.* 1995;21:336-341.
144. Burke B, Giannoudis A, Corke KP, et al. Hypoxia-induced gene expression in human macrophages: implications for ischemic tissues and hypoxia-regulated gene therapy. *Am J Pathol.* 2003;163:1233-1243.
145. Hall AM, Molitoris BA. Dynamic multiphoton microscopy: focusing light on acute kidney injury. *Physiology.* 2014;29:334-342.
146. Small DM, Sanchez WY, Gobe GC. Intravital multiphoton imaging of the kidney: tubular structure and metabolism. *Methods Mol Biol.* 2016;1397:155-172.
147. Sharfuddin AA, Sandoval RM, Berg DT, et al. Soluble thrombomodulin protects ischemic kidneys. *J Am Soc Nephrol.* 2009;20:524-534.
148. Hall AM, Rhodes GJ, Sandoval RM, Corridon PR, Molitoris BA. In vivo multiphoton imaging of mitochondrial structure and function during acute kidney injury. *Kidney Int.* 2013;83:72-83.
149. Hato T, Winfree S, Kalakeche R, et al. The macrophage mediates the renoprotective effects of endotoxin preconditioning. *J Am Soc Nephrol.* 2014;26:1347-1362.
150. Camirand G, Li Q, Demetris AJ, et al. Multiphoton intravital microscopy of the transplanted mouse kidney. *Am J Transplant.* 2011;11:2067-2074.
151. Schuh CD, Haenni D, Craigie E, et al. Long wavelength multiphoton excitation is advantageous for intravital kidney imaging. *Kidney Int.* 2016;89:712-719.
152. Matsumoto M, Tanaka T, Yamamoto T, et al. Hypoperfusion of peritubular capillaries induces chronic hypoxia before progression of tubulointerstitial injury in a progressive model of rat glomerulonephritis. *J Am Soc Nephrol.* 2004;15:1574-1581.
153. Nakagawa T, Lan HY, Kang D-K, Schreiner GF, Johnson RJ. Differential regulation of VEGF by TGF- β and hypoxia in rat proximal tubular cells. *Am J Physiol Renal Physiol.* 2004;287:F658-F664.
154. Grone H-J, Simon MC, Grone EF. Expression of vascular endothelial growth factor in renal vascular disease and renal allografts. *J Pathol.* 1995;177:259-267.
155. Kairaitis LK, Wang Y, Gassman M, Tay Y-C, Harris CH. HIF-1 α expression follows microvascular loss in advanced murine adriamycin nephrosis. *Am J Physiol Renal Physiol.* 2005;288:F198-F206.
156. Kang D-H, Joly AH, Oh S-W, et al. Impaired angiogenesis in the remnant kidney model: I. potential role of vascular endothelial growth factor and thrombospondin-1. *J Am Soc Nephrol.* 2001;12:1434-1447.
157. Kang D-H, Hughes J, Mazzali M, Schreiner GF, Johnson RJ. Impaired angiogenesis in the remnant kidney model: II. vascular endothelial growth factor administration reduces renal fibrosis and stabilizes renal function. *J Am Soc Nephrol.* 2001;12:1448-1457.
158. Basile DP, Friedrich JL, Spahic J, et al. Impaired endothelial proliferation and mesenchymal transition contribute to vascular rarefaction following acute kidney injury. *Am J Physiol Renal Physiol.* 2011;300:F721-F733.
159. Hakrout S, Moeller MJ, Theilig F, et al. Effects of increased renal tubular vascular endothelial growth factor (VEGF) on fibrosis, cyst formation, and glomerular disease. *Am J Pathol.* 2009;175:1883-1898.
160. Bernhardt WM, Gottmann U, Doyon F, et al. Donor treatment with a PHD-inhibitor activating HIFs prevents graft injury and prolongs survival in an allogenic kidney transplant model. *Proc Natl Acad Sci.* 2009;106:21276-21281.

161. Bernhardt WM, Campean V, Kany S, et al. Preconditional activation of hypoxia-inducible factors ameliorates ischemic acute renal failure. *J Am Soc Nephrol*. 2006;17:1970-1978.
162. Wang Z, Schley G, Turkoglu G, et al. The protective effect of prolyl-hydroxylase inhibition against renal ischaemia requires application prior to ischaemia but is superior to EPO treatment. *Nephrol Dial Transpl*. 2012;27:929-936.
163. Nordquist L, Friederich-Persson M, Fasching A, et al. Activation of hypoxia-inducible factors prevents diabetic nephropathy. *J Am Soc Nephrol*. 2015;26:328-338.
164. Tanaka S, Tanaka T, Nangaku M. Hypoxia as a key player in the AKI-to-CKD transition. *Am J Physiol Renal Physiol*. 2014;307:F1187-F1195.
165. Dallatu MK, Choi M, Oyekan AO. Inhibition of prolyl hydroxylase domain-containing protein on hypertension/renal injury induced by high salt diet and nitric oxide withdrawal. *J Hypertens*. 2013;31:2043-2049.
166. Friederich-Persson M, Persson P, Fasching A, Hansell P, Nordquist L, Palm F. Increased kidney metabolism as a pathway to kidney tissue hypoxia and damage: effects of triiodothyronine and dinitrophenol in normoglycemic rats. *Adv Exp Med Biol*. 2013;789:9-14.
167. Friederich-Persson M, Thorn E, Hansell P, Nangaku M, Levin M, Palm F. Kidney hypoxia, attributable to increased oxygen consumption, induces nephropathy independently of hyperglycemia and oxidative stress. *Hypertension*. 2013;62:914-919.
168. Johannes T, Mik EG, Nohe B, Unertl KE, Ince C. Acute decrease in renal microvascular PO₂ during acute normovolemic hemodilution. *Am J Physiol Renal Physiol*. 2007;292:F796-F803.
169. Cody JD, Hodson EM. Recombinant human erythropoietin versus placebo or no treatment for the anaemia of chronic kidney disease in people not requiring dialysis. *Cochrane Database Syst Rev*. 2016:CD003266.
170. Franzen S, Friederich-Persson M, Fasching A, Hansell P, Nangaku M, Palm F. Differences in susceptibility to develop parameters of diabetic nephropathy in four mouse strains with type 1 diabetes. *Am J Physiol Renal Physiol*. 2014;306:F1171-F1178.
171. Heijnen BFI, Peutz-Koorstra CJ, Mullins JJ, Janssen BJ, Struijker-Boudier HA. Transient renin-angiotensin system stimulation in an early stage of life causes sustained hypertension in rats. *J Hypertens*. 2011;29:2369-2380.
172. Heijnen BFI, Nelissen J, van Essen H, et al. Irreversible renal damage after transient renin-angiotensin system stimulation: involvement of an AT1-receptor mediated immune response. *PLoS ONE*. 2013;8:e57815.
173. Evans RG, Ow CPC, Bie P. The chronic hypoxia hypothesis: the search for the smoking gun goes on. *Am J Physiol Renal Physiol*. 2015;308:F101-F102.
174. Jankovic B, Aquino-Parsons C, Raleigh JA, et al. Comparison between pimonidazole binding, oxygen electrode measurements, and expression of endogenous hypoxia markers in cancer of the uterine cervix. *Cytometry B Clin Cytom*. 2006;70B:45-55.
175. Varghese AJ, Gulyas S, Mohindra JK. Hypoxia-dependent reduction of 1-(2-nitro-1-imidazolyl)-3-methoxy-2-propanol by chinese hamster ovary cells and KHT tumor cells in vitro and in vivo. *Cancer Res*. 1976;36:3761-3765.
176. Rosenberger C, Rosen S, Paliege A, Heyman SN. Pimonidazole adduct immunohistochemistry in the rat kidney: detection of tissue hypoxia. *Methods Mol Biol*. 2009;466:161-174.
177. Rosenberger C, Heyman SN, Rosen S, et al. Up-regulation of HIF in experimental acute renal failure: evidence for a protective transcriptional response to hypoxia. *Kidney Int*. 2005;67:531-542.
178. Efrati S, Berman S, Aharon GB, Siman-Tov Y, Averbukh Z, Weissgarten J. Application of normobaric hyperoxia therapy for amelioration of haemorrhagic shock-induced acute renal failure. *Nephrol Dial Transpl*. 2008;23:2213-2222.
179. Edremtilioğlu M, Kiliç D, Oter S, et al. The effect of hyperbaric oxygen treatment on the renal functions in septic rats: relation to oxidative damage. *Surg Today*. 2005;35:653-661.
180. Hering D, Zdrojewski Z, Krol E, et al. Tonic chemoreflex activation contributes to the elevated muscle sympathetic nerve activity in patients with chronic renal failure. *J Hypertens*. 2007;25:157-161.
181. van der Bel R, Caliskan M, van Hulst RA, van Lieshout JJ, Stroes ESG, Krediet CTP. Blood pressure increase during oxygen supplementation in chronic kidney disease patients is mediated by vasoconstriction independent of baroreflex function. *Front Physiol*. 2017;8:186.
182. Jamieson D. Oxygen toxicity and reactive oxygen metabolites in mammals. *Free Radic Biol Med*. 1998;7:87-108.
183. Brezis M, Agmon Y, Epstein FH. Determinants of intrarenal oxygenation I. Effects of diuretics. *Am J Physiol*. 1994;36:F1059-F1062.
184. Brezis M, Rosen S, Silva P, Epstein FH. Transport activity modifies thick ascending limb damage in the isolated perfused kidney. *Kidney Int*. 1984;25:65-72.
185. Heyman SN, Brezis M, Greenfeld Z, Rosen S. Protective role of furosemide and saline in radiocontrast-induced acute renal failure in the rat. *Am J Kidney Dis*. 1989;14:377-385.
186. Fouque D, Laville M. Low protein diets for chronic kidney disease in non diabetic adults. *Cochrane Database Syst Rev*. 2009:CD001892.
187. Heyman SN, Brezis M, Epstein FH, Spokes K, Rosen S. Effect of glycine and hypertrophy on renal outer medullary hypoxic injury in ischemia reflow and contrast nephropathy. *Am J Kidney Dis*. 1992;19:578-586.
188. Rui T, Feng Q, Lei M, et al. Erythropoietin prevents the acute myocardial inflammatory response induced by ischemia/reperfusion via induction of AP-1. *Cardiovasc Res*. 2005;65:719-727.
189. Shanley PF, Rosen MD, Brezis M, Silva P, Epstein FH, Rosen S. Topography of focal proximal tubular necrosis after ischemia with reflow in the rat kidney. *Am J Pathol*. 1986;122:462-468.
190. Pugh CW, Ratcliffe PJ. Regulation of angiogenesis by hypoxia: role of the HIF system. *Nat Med*. 2003;9:677-684.
191. Reinders MEJ, Sho M, Izawa A, et al. Proinflammatory functions of vascular endothelial growth factor in alloimmunity. *J Clin Invest*. 2003;112:1655-1665.
192. Basu RK, Hubchak S, Hayashida T, Runyan CE, Schumacker PT, Schnaper HW. Interdependence of HIF-1 α and TGF- β /Smad3 signaling in normoxic and hypoxic renal epithelial cell collagen expression. *Am J Physiol Renal Physiol*. 2011;300:F898-F905.
193. Grimshaw MJ. Endothelins and hypoxia-inducible factor in cancer. *Endocr Relat Cancer*. 2007;14:233-244.
194. Morishita Y, Ookawara S, Hirahara I, Muto S, Nagata D. HIF-1 α mediates hypoxia-induced epithelial-mesenchymal transition in peritoneal mesothelial cells. *Ren Fail*. 2016;38:282-289.

195. Jing S-W, Wang Y-D, Kuroda M, et al. HIF-1 α contributes to hypoxia-induced invasion and metastasis of esophageal carcinoma via inhibiting E-cadherin and promoting MMP-2 expression. *Acta Med Okayama*. 2012;66:399-407.
196. Olson N, van der Vliet A. Interactions between nitric oxide and hypoxia-inducible factor signaling pathways in inflammatory disease. *Nitric Oxide*. 2011;25:125-137.
197. Wilkinson-Berka JL, Wraight C, Werther G. The role of growth hormone, insulin-like growth factor and somatostatin in diabetic retinopathy. *Curr Med Chem*. 2006;13:3307-3317.
198. Pricci F, Pugliese G, Romano G, et al. Insulin-like growth factors I and II stimulate extracellular matrix production in human glomerular mesangial cells. Comparison with transforming growth factor- β . *Endocrinology*. 1996;137:879-885.
199. Feld SM, Hirschberg R, Artishevsky A, Nast C, Adler SG. Insulin-like growth factor I induces mesangial proliferation and increases mRNA and secretion of collagen. *Kidney Int*. 1995;49:45-51.
200. Lee SC, Han SH, Li JJ, et al. Induction of heme oxygenase-1 protects against podocyte apoptosis under diabetic conditions. *Kidney Int*. 2009;76:838-848.
201. Bolisetty S, Traylor AM, Kim J, et al. Heme oxygenase-1 inhibits renal tubular macroautophagy in acute kidney injury. *J Am Soc Nephrol*. 2010;21:1702-1712.
202. Lee PJ, Alam J, Wiegand GW, Choi AK. Overexpression of heme oxygenase-1 in human pulmonary epithelial cells results in cell growth arrest and increased resistance to hyperoxia. *Proc Natl Acad Sci*. 1996;93:10393-10398.
203. Lum JJ, Bui T, Gruber M, et al. The transcription factor HIF-1 α plays a critical role in the growth factor-dependent regulation of both aerobic and anaerobic glycolysis. *Genes Dev*. 2013;21:1037-1049.
204. Linden KC, DeHaan CL, Zhang Y, et al. Renal expression and localization of the facilitating glucose transporters GLUT1 and GLUT12 in animal models of hypertension and diabetic nephropathy. *Am J Physiol Renal Physiol*. 2006;290:F205-F213.
205. Patel NN, Toth T, Jones C, et al. Prevention of post-cardiopulmonary bypass acute kidney injury by endothelin A receptor blockade. *Crit Care Med*. 2011;39:793-802.

How to cite this article: Ow CPC, Ngo JP, Ullah MM, Hilliard LM, Evans RG. Renal hypoxia in kidney disease: Cause or consequence?. *Acta Physiol*. 2017;e12999. <https://doi.org/10.1111/apha.12999>

APPENDIX 2

RESEARCH ARTICLE

Absence of renal hypoxia in the subacute phase of severe renal ischemia-reperfusion injury

Connie P. C. Ow,¹ Jennifer P. Ngo,¹ Md Mahbub Ullah,¹ Giannie Barsha,¹ Ruth C. Meex,² Matthew J. Watt,³ Lucinda M. Hilliard,¹ Maarten P. Koeners,^{4,5} and Roger G. Evans¹

¹Cardiovascular Disease Program, Biomedicine Discovery Institute, Department of Physiology, Monash University, Melbourne, Victoria, Australia; ²Department of Human Biology, NUTRIM School of Nutritional and Translational Research in Metabolism, Maastricht University Medical Centre, Maastricht, The Netherlands; ³Metabolism, Diabetes and Obesity Program, Biomedicine Discovery Institute, Department of Physiology, Monash University, Melbourne, Victoria, Australia; ⁴School of Physiology, Pharmacology and Neuroscience, Biomedical Sciences, University of Bristol, Bristol, United Kingdom; and ⁵Institute of Biomedical and Clinical Science, University of Exeter Medical School, Exeter, United Kingdom

Submitted 22 May 2018; accepted in final form 9 August 2018

Ow CPC, Ngo JP, Ullah MM, Barsha G, Meex RC, Watt MJ, Hilliard LM, Koeners MP, Evans RG. Absence of renal hypoxia in the subacute phase of severe renal ischemia-reperfusion injury. *Am J Physiol Renal Physiol* 315: F1358–F1369, 2018. First published August 15, 2018; doi:10.1152/ajprenal.00249.2018.—Tissue hypoxia has been proposed as an important event in renal ischemia-reperfusion injury (IRI), particularly during the period of ischemia and in the immediate hours following reperfusion. However, little is known about renal oxygenation during the subacute phase of IRI. We employed four different methods to assess the temporal and spatial changes in tissue oxygenation during the subacute phase (24 h and 5 days after reperfusion) of a severe form of renal IRI in rats. We hypothesized that the kidney is hypoxic 24 h and 5 days after an hour of bilateral renal ischemia, driven by a disturbed balance between renal oxygen delivery ($\dot{V}O_2$) and oxygen consumption ($\dot{V}O_2$). Renal $\dot{V}O_2$ was not significantly reduced in the subacute phase of IRI. In contrast, renal $\dot{V}O_2$ was 55% less 24 h after reperfusion and 49% less 5 days after reperfusion than after sham ischemia. Inner medullary tissue P_{O_2} , measured by radiotelemetry, was $25 \pm 12\%$ (mean \pm SE) greater 24 h after ischemia than after sham ischemia. By 5 days after reperfusion, tissue P_{O_2} was similar to that in rats subjected to sham ischemia. Tissue P_{O_2} measured by Clark electrode was consistently greater 24 h, but not 5 days, after ischemia than after sham ischemia. Cellular hypoxia, assessed by pimonidazole adduct immunohistochemistry, was largely absent at both time points, and tissue levels of hypoxia-inducible factors were downregulated following renal ischemia. Thus, in this model of severe IRI, tissue hypoxia does not appear to be an obligatory event during the subacute phase, likely because of the markedly reduced oxygen consumption.

acute kidney injury; hypoxia; ischemia-reperfusion; kidney; oxygen

INTRODUCTION

Acute kidney injury (AKI) is a major cause of death and disability globally and places a major acute burden on health care systems (26). It also renders patients more susceptible to later development of chronic kidney disease (CKD; 2). For example, a diagnosis of AKI was found to be associated with

an 8.8-fold excess risk of later development of CKD (8). Furthermore, the risk of later development of CKD increases with the severity of AKI (8). Tissue hypoxia has been proposed as an important driver in the pathogenesis of both AKI and CKD, although this proposition remains to be definitively tested (33).

Ischemia-reperfusion injury (IRI) sustained from medical interventions often arises from the obligatory need to restrict or completely prevent blood flow to the kidney, resulting in a period of severe hypoxia or complete anoxia (15). Cellular damage such as acute tubular necrosis and tubular apoptosis is evident during the reperfusion period and is likely driven in part by the presence of tissue hypoxia during the period of ischemia. In experimental IRI, cortical (27, 28, 41) and medullary (27, 28, 34) tissue hypoxia has also been observed during the first few hours of reperfusion after complete renal ischemia. Importantly, in the longer term (weeks to months) after renal IRI the kidney was observed to be hypoxic even with some level of, albeit incomplete, structural and functional recovery (3, 4). However, there are few available data regarding renal tissue oxygenation beyond the first few hours of reperfusion during the extension and recovery phases of IRI. This information is required if we are to understand the role of tissue hypoxia in the natural history of AKI, either as it progresses to end-stage renal disease or as renal function recovers but the risk of later CKD is increased.

The chief aim of the present study was to assess the time course of changes in, and the spatial distribution of, tissue oxygen tension (P_{O_2}) during the subacute phase of severe IRI (the first 5 days of reperfusion after 60 min of bilateral renal ischemia). We chose severe IRI in an attempt to model the clinical situation of severe AKI leading to end-stage renal disease, cognizant of the possibility that renal oxygenation in this scenario might differ considerably from that in milder forms of renal IRI. We tested the hypothesis that renal tissue is hypoxic during the subacute phase of IRI. Four approaches were used for assessment of renal tissue oxygenation, each with varying temporal and spatial resolution. Radiotelemetry was used to examine the time course of changes in inner medullary tissue P_{O_2} in freely moving rats (22, 23). Clark-type electrodes were used to characterize the spatial variations in

Address for reprint requests and other correspondence: C. P. C. Ow, Dept. of Cardiac Physiology, National Cerebral and Cardiovascular Center Research Institute, 5-7-1 Fujishirodai, Suita-Shi, Osaka 565-8565, Japan (e-mail: ow.peichenconnie73@nccvc.go.jp).

renal tissue P_{O_2} in the renal cortex and medulla of anesthetized rats at both 24 h and 5 days after reperfusion. This experiment also provided an opportunity to determine the contribution of changes in renal oxygen delivery (DO_2) and oxygen consumption ($\dot{V}O_2$) to alterations in renal tissue P_{O_2} 24 h and 5 days after reperfusion. Pimonidazole adduct immunohistochemistry was used to characterize the spatial distribution of cellular hypoxia 24 h and 5 days after reperfusion. We also measured the expression of hypoxia-inducible factors (HIF-1 α and HIF-2 α) and some of their downstream gene targets.

METHODS

Experimental Animals

Ten- to twelve-week-old male, Sprague-Dawley rats ($n = 70$) were obtained from the Animal Resources Centre (Perth, WA, Australia). They were housed in a room maintained at 21–23°C with a 12-h light-dark cycle. The rats were allowed free access to water and standard laboratory rat chow. All procedures were approved in advance by the Animal Ethics Committee of the School of Biomedical Sciences, Monash University, as being in accordance with the Australian Code of Practice for the Care and Use of Animals for Scientific Purposes.

Induction of Bilateral Renal Ischemia

Rats were anesthetized with isoflurane (IsoFlo, 05260-05; Abbott Laboratories, Abbott Park, IL), using a vaporizer, and maintained at 2.5–3.0% vol/vol. A midline incision was made to expose the left and right renal arteries. To induce bilateral renal ischemia ($n = 36$), blood flow to both kidneys was prevented by the application of microvascular clamps (no. 00398; S&T, Neuhausen am Rheinfall, Switzerland) placed on both the left and right renal arteries and veins. Complete ischemia was confirmed by observing the blanching of the kidneys. After an hour, the microvascular clamps were removed, so blood flow to both kidneys was restored. Wounds were closed in layers with sutures, and each rat was then allowed to recover from the surgery on a heated pad for an hour. A separate cohort of rats ($n = 34$) underwent the same procedure with the exception of the application of the microvascular clamps and so served as controls (sham ischemia). Rats received subcutaneous injections of an analgesic (carprofen, 1.25 mg; Pfizer) for 2 consecutive days following recovery from surgery.

Protocol 1: Temporal Changes in Renal Tissue Oxygenation Following Renal Ischemia

We employed a radiotelemetric method (22, 23) to characterize the temporal profile of changes in renal tissue P_{O_2} after renal ischemia and reperfusion. Briefly, the oxygen telemeter was implanted under isoflurane anesthesia so that the tip of the oxygen-sensing carbon paste electrode was in the inner medulla of the left kidney (5 mm below the renal capsule). One week after implantation of the telemetric probe, the rats underwent a second surgical procedure for the induction of either bilateral renal ischemia ($n = 7$, body weight = 501 ± 20 g, mean \pm SE) or sham ischemia ($n = 5$, body weight = 491 ± 21 g). Renal tissue P_{O_2} was recorded continuously for 1 day before and for 5 days after recovery from surgery. Rats received subcutaneous injections of an analgesic (carprofen, 1.25 mg; Pfizer, Australia) before laparotomy and for 2 consecutive days following recovery from surgery.

Measurements and calculations. Current measured by the telemeters was filtered with a 25-Hz low-pass filter, and artifactual measurements were removed when the first-order derivative of the measured current exceeded the threshold of 5–500 nA/s. The zero-offset current, acquired when the rat was killed at the end of the study via induction of cardiac arrest under anesthesia (22), was determined and sub-

tracted. Data are presented as a percentage of the average value on the day before surgery to induce ischemia or sham ischemia.

Protocol 2: Renal Tissue Oxygenation and Its Determinants After Renal Ischemia

Either 24 h or 5 days following recovery from renal ischemia or sham ischemia, rats were anesthetized and prepared for the assessment of regional tissue P_{O_2} using a Clark electrode (50- μ m tip, OX-50; Unisense, Aarhus, Denmark). We assessed 1) cortical tissue P_{O_2} across a range of sites on the dorsal surface of the kidney and 2) a profile of tissue P_{O_2} with depth from the cortical surface. In this set of studies, we also determined the major determinants of tissue P_{O_2} , renal DO_2 , and $\dot{V}O_2$.

Rats ($n = 6$ –11 per group) were anesthetized with sodium thiobarbital (100 mg/kg ip, Inactin; Sigma-Aldrich, St. Louis, MO). A tracheostomy was performed to facilitate artificial ventilation with 40% inspired oxygen at a ventilation rate of 90–100 breaths/min and a tidal volume of 3.5 ml (Ugo Basile, model 7025; SDR Clinical Technology, Sydney, NSW, Australia) as previously described (1). The left carotid artery was catheterized to facilitate arterial blood sampling and blood pressure measurement. The right jugular vein was catheterized to facilitate infusion of maintenance fluid (154 mM NaCl) at a rate of 6 ml/h during the period of surgical preparation. The bladder was catheterized, for collection of urine from the left kidney, for assessment of renal function using standard clearance methods. The degree of saturation of hemoglobin with oxygen was measured continuously using a sensor placed on the foot (Mouse Ox; Starr Life Sciences, Oakmont, PA).

The right renal artery and vein were ligated, and a catheter was passed from the right renal vein through the vena cava and into the left renal vein for the sampling of renal venous blood. Total renal blood flow (RBF) was measured using a transit time ultrasound flow probe (type 0.7 VB; Transonic Systems, Ithaca, NY) placed around the left renal artery. Following completion of the surgical preparations, rats received bolus doses of [3 H]inulin (10 μ Ci in 50 μ l; PerkinElmer Australia, Melbourne, VIC, Australia) and pancuronium bromide (2 mg/kg; AstraZeneca, Sydney, NSW, Australia) intravenously. A maintenance infusion of 2% wt/vol bovine serum albumin (Sigma-Aldrich) in 154 mM sodium chloride delivered 676 nCi/h [3 H]inulin and 0.1 mg \cdot kg $^{-1}$ \cdot h $^{-1}$ pancuronium bromide through the jugular vein at a rate of 2 ml/h. The infusion commenced once all surgical preparations were completed and was maintained throughout the rest of the protocol.

After a 1-h equilibration period, a 0.5-ml sample of arterial blood was taken for blood oximetry. The plasma component of the sample was later used for assessment of the concentrations of [3 H]inulin and sodium. A 0.1-ml sample of renal venous blood was also collected for blood oximetry. Renal tissue P_{O_2} was then assessed using a Clark electrode attached to a micromanipulator. Two series of measurements were taken. In the first series, the electrode was advanced 2 mm from the renal surface, into the cortex, at six randomly chosen sites across the left kidney. The second series established a profile of tissue P_{O_2} with depth below the cortical surface. The electrode was moved to the midpoint of the cortical surface of the kidney and advanced into the kidney at 1-mm increments up to a depth of 10 mm from the renal surface as previously described (32). Once all measurements were taken, a second set of blood samples, from the carotid artery and the renal vein, was taken as before. Urine made by the left kidney, during the period of measurement of tissue P_{O_2} , was collected for measurement of the concentrations of [3 H]inulin and sodium.

Measurements and calculations. Arterial pressure, heart rate (triggered by arterial pressure), RBF, core body and tissue temperature, and renal tissue P_{O_2} measured by Clark electrode were digitized as previously described (32). Urinary and plasma concentrations of sodium were determined using ion-sensitive electrodes (EasyElectrolytes; Medica, Bedford, MA). Glomerular filtration rate (GFR) was

determined by the clearance of [^3H]inulin. Blood chemistry was assessed using a point-of-care device (iSTAT, CG8+ cartridges; Abbott Laboratories). Arterial and venous blood oxygen content was calculated as previously described (1).

Protocol 3: Cellular Hypoxia and Hypoxic Signaling After Renal Ischemia

Either after 24 h or 5 days of recovery from bilateral renal ischemia or sham ischemia ($n = 6$ per group), rats were prepared for perfusion fixation of the right kidney. In this set of studies, the chief aim was to assess cellular hypoxia using pimonidazole adduct immunohistochemistry. Pimonidazole chloride (HP1-1000 kit; Hydroxyprobe) was administered, at a dose of 60 mg/kg ip 3 h before perfusion fixation of the kidney.

Three hours after the injection of pimonidazole, rats were anesthetized with sodium pentobarbital (60 mg/kg ip; Sigma-Aldrich). The left carotid artery was catheterized to facilitate arterial blood sampling. A midline incision was then made exposing both kidneys and the bladder. A urine sample was taken by puncturing the bladder wall and was frozen at -20°C for later analysis. The left renal artery and vein were isolated and freed from surrounding connective tissue and fat. Lidocaine (2% wt/vol, Xylocaine; AstraZeneca) was applied onto both vessels to prevent spasm of the renal artery. Silk ligatures (3-0 Dysilk; Dynek, Hendon, SA, Australia) were placed around the vena cava above the level of the right kidney, around the left renal artery and vein, and around the abdominal aorta. An incision was made in the abdominal aorta below the level of the left kidney, and a polyurethane catheter connected to the perfusion apparatus was advanced into the aorta, facing upstream, thereby facilitating retrograde perfusion. A 1-ml blood sample was taken from the carotid artery for later analysis. The left renal artery and vein were then ligated, and the left kidney was removed, decapsulated, and snap-frozen in liquid nitrogen for later analysis of HIF-1 α and HIF-2 α protein and gene expression of HIF-1 α , HIF-2 α , VEGF- α , and heme oxygenase 1 (HO-1). Prior to freezing, the left kidney was sectioned in the coronal plane into 4–5 slices of ~ 1 –2-mm thickness.

The ligatures surrounding the vena cava and abdominal aorta were tied off, and the right kidney was perfused with 100–150 ml of 4% wt/vol paraformaldehyde (paraformaldehyde powder, no. 158127; Sigma-Aldrich) at room temperature and a pressure of 150 mmHg. The inferior vena cava was incised to vent perfusate. The perfused kidney was removed, decapsulated, and stored in 4% paraformaldehyde for 48 h before it was processed for embedding and staining at the Monash Histology Platform.

Blood chemistry was assessed using a point-of-care device (iSTAT, CHEM8+ cartridges; Abbott Laboratories). Urinary albumin concentration was determined using direct competitive enzyme-linked immunosorbent assay (Nephrot II, NR-002; Exocell, Philadelphia, PA). Urinary creatinine concentration was determined using an assay based on Jaffe's reaction of alkaline picrate solution with creatinine (Creatinine Companion Strip Plate, no. 1012; Exocell).

Quantification of fibrosis. The right kidney was processed, embedded in paraffin, and sectioned at a thickness of 5 μm in the coronal plane. Collagen deposition was assessed by staining with 1% wt/vol picrosirius red. The cortical and outer and inner medullary region of the kidney in each section was identified using Aperio ImageScope (Leica Biosystems Imaging). The amount of collagen deposited was quantified as a percentage of the entire area in each region.

Pimonidazole adduct immunohistochemistry. Antigen retrieval was performed by incubating the sections in citrate buffer (Target Retrieval Solution; Dako) at 90°C for 30 min. Sections were then washed in Tris-buffered saline (154 mM NaCl) with Tween 20 (TBST; Dako) once they had cooled to 80°C . Excessive tissue peroxidase activity was then quenched using 0.03% vol/vol hydrogen peroxide containing sodium azide (Dako) for 10 min. Sections were then incubated in a protein block serum (Protein Block Serum-Free; Dako) for 10 min, to

remove nonspecific binding, and washed twice more in TBST. Sections were then treated with an affinity-purified polyclonal anti-pimonidazole antibody raised in the rabbit (1:200 dilution, PAb-2627AP; Hydroxyprobe) for 1 h at room temperature before incubation in goat anti-rabbit secondary antibody conjugated with horseradish peroxidase (HRP; polyclonal goat, EnVision; Dako) for 30 min at room temperature. Sections were washed twice with TBST before incubation with 3-diaminobenzidine (Dako) for 10 min and then counterstained with hematoxylin (Automation Hematoxylin; Dako) before coverslips were mounted.

Western blot analysis of HIF-1 α and HIF-2 α proteins. The snap-frozen kidney was thawed, and the cortex and outer and inner medulla inclusive of the papilla were rapidly dissected. To stop further enzymatic reactions, the tissue samples were placed in radioimmunoprecipitation assay buffer [8 $\mu\text{l}/\text{mg}$; consisting of 50 mM Tris-HCl, 150 mM NaCl, 0.1% Triton X-100, 0.5% sodium deoxycholate, 0.1% sodium dodecyl sulfate (SDS), 1 mM sodium orthovanadate, 1 mM NaF, 1:25 of 25X phosphatase inhibitor, 1:10 of 10X PhosphoSTOP, and 1:1,000 dithiothreitol]. The tissues were then homogenized at 14,000 rpm at 4°C for 20 min, and equal amounts of protein (30 μg , determined by a Bradford protein assay) were loaded into a 7.5% precast gel (7.5% Mini-Protein TGX Precast Protein Gels, 4561025; Bio-Rad Laboratories) and fractionated electrophoretically in Tris-glycine-SDS running buffer at 300 V for 20 min. The fractionated protein in the gel was then transferred onto a nitrocellulose membrane (Bio-Rad Laboratories). Nonspecific binding was blocked with 5% skim milk in TBST buffer. As the primary antibodies for HIF-1 α (NB100-479; Novus Biologicals, Littleton, CO) and HIF-2 α (NB100-122; Novus Biologicals) are similar in molecular mass (115 and 118 kDa), we performed the immunoblot analysis of each protein of interest on separate gels. The nitrocellulose membranes were incubated overnight at 4°C in the primary antibody (1:1,000, raised in rabbit) made up in a solution of 2.5% wt/vol bovine serum albumin. The membranes were then incubated with 1:4,000 secondary antibody (ECL anti-rabbit IgG, HRP-linked whole antibody; GE Healthcare) and 1:15,000 conjugate (Precision Protein StrepTactin-HRP conjugate; Bio-Rad Laboratories) for an hour at room temperature. The nitrocellulose membrane was developed using equal parts of Clarity Western Peroxide Reagent (Bio-Rad Laboratories) and Clarity Western Luminol/Enhancer Reagent (Bio-Rad Laboratories) for 3 min before imaging. The intensity of the bands observed on the membrane was quantified and corrected for variability in protein migration down the gel and for total protein content loaded into the wells. Comparisons were made between treatment groups across the two time points within each region (i.e., cortex and outer and inner medulla).

Quantitative real-time PCR. The tissue samples were homogenized, and total RNA was isolated using the RNeasy Mini Kit (no. 74104; Qiagen). Predesigned assays for primers of the 18s housekeeping gene (Rn03928990_g1) and HIF-1 α (Rn01472831_m1), HIF-2 α (Rn00576515_m1), VEGF- α (Rn01511602_m1), and HO-1 (Rn00561387_m1) genes were obtained from Thermo Fisher Scientific. Real-time PCR was performed on ABI 7900 HT (Thermo Fisher Scientific). Data were calculated by the $2^{-\Delta\Delta\text{Ct}}$ method (where Ct is threshold cycle).

Statistical Analysis

Statistical analyses were performed using the software package SYSTAT (version 13; Systat Software, San Jose, CA). Two-sided $P \leq 0.05$ was considered statistically significant. Normality was assessed using the Shapiro-Wilk test (40). Data that did not violate normality are presented as means \pm SE, whereas data that violated normality are presented as medians (25th percentile, 75th percentile). Analysis of variance (ANOVA) was used to assess the independent effects of treatment and time and their interaction. For data that violated normality, an ANOVA on ranking (9) was performed instead. Dichotomous comparisons of continuous variables were made using Student's

t-test for data that did not violate normality, and the Mann-Whitney *U*-test was performed for data that violated normality. To protect against the risk of type I error arising from multiple comparisons, *P* values were conservatively adjusted using the Dunn-Sidak procedure (30). *P* values derived from within-subjects factors in repeated-measures ANOVA were conservatively adjusted using the Greenhouse-Geisser method (31).

RESULTS

Protocol 1: Temporal Changes in Renal Tissue Oxygenation Following Renal Ischemia

On the first day after reperfusion, inner medullary tissue P_{O_2} measured by telemetry was $25 \pm 12\%$ greater than its control level (*day -1*; Fig. 1). Tissue P_{O_2} then gradually fell to be close to its control level by the fifth day after reperfusion of the kidney. After sham ischemia, inner medullary tissue P_{O_2} tended to gradually fall and so was $22 \pm 11\%$ less than its control level by *day 5* after surgery.

Protocol 2: Renal Tissue Oxygenation and Its Determinants After Renal Ischemia

Systemic parameters. Twenty-four hours after reperfusion, body weight did not differ significantly from that of rats that underwent sham ischemia. By 5 days after renal ischemia, rats had lost 39.2 ± 6.1 g of their body weight. Left kidney weight 24 h after renal ischemia was similar to that after sham ischemia. In contrast, left kidney weight was 56% greater 5 days following renal ischemia than after sham ischemia (Table 1). Mean arterial pressure was similar in the two groups of rats at both 24 h and 5 days after surgery.

Renal tissue oxygenation. Tissue P_{O_2} in the renal cortex was highly heterogeneous, both 24 h and 5 days after either ischemia or sham ischemia (Fig. 2A). Cortical P_{O_2} was, on average, 40% greater 24 h following renal ischemia than after sham ischemia.

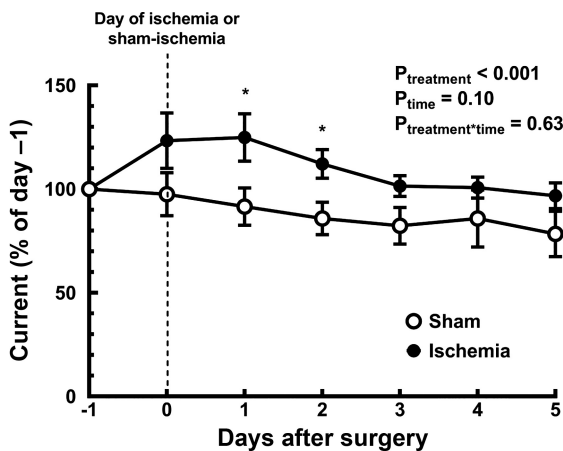


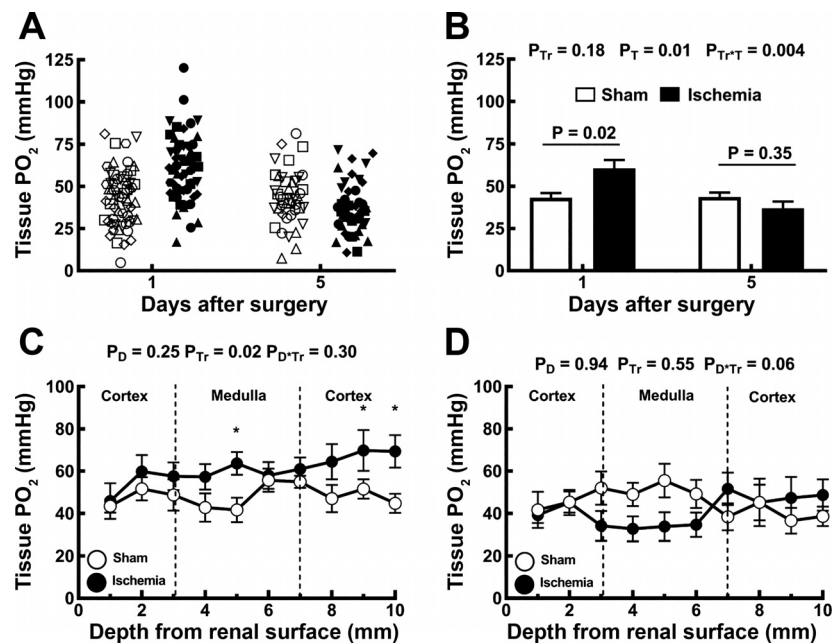
Fig. 1. Temporal changes of inner medullary tissue P_{O_2} following renal ischemia or sham ischemia. Values are means \pm SE for rats subjected to either an hour of sham (*n* = 5) or bilateral renal ischemia (*n* = 7). Tissue P_{O_2} , assessed as current through the carbon paste electrode, was recorded before (*day -1*) and after (*days 0-5*) surgery. Current was averaged over each 24-h period and is expressed as a percentage of its mean value on the day before the surgery (*day -1*). $P_{treatment}$, P_{time} , and $P_{treatment*time}$ are the outcomes of a two-way repeated-measures analysis of variance with factors treatment and time. * $P \leq 0.05$ for specific comparisons between the two treatment groups at each time point using Student's unpaired *t*-test, without correction for multiple comparisons.

Table 1. Systemic and blood oxygen parameters of rats 24 h or 5 days after ischemia or sham ischemia

Parameter	Sham (24 h)		Ischemia (24 h)		Sham (5 days)		Ischemia (5 days)		2-Way ANOVA		Dichotomous Comparison	
	Value	n	Value	n	Value	n	Value	n	P_{Tr}	P_{Tr*T}	S1 vs. II	S5 vs. I5
Systemic												
Body weight after ischemia or sham ischemia, g	397.6 \pm 23.8	10	378.2 \pm 17.6	9	469.4 \pm 14.9	7	364.5 \pm 19.7	8	0.005	0.17	0.05	0.77
Kidney weight, g	1.5 (1.3, 1.5)	10	1.5 (1.4, 1.6)	9	1.4 (1.4, 1.7)	7	2.2 (2.2, 2.8)	8	<0.001	<0.001	0.04	0.92
Kidney weight, g/kg body wt	3.6 (3.3, 4.1)	10	3.9 (3.7, 4.2)	9	3.3 (3.2, 3.5)	7	6.6 (5.4, 8.3)	8	<0.001	0.16	<0.001	0.55
Mean arterial blood pressure, mmHg	118.3 (108.4, 140.4)	10	123.9 (108.7, 134.4)	9	116.9 (102.3, 118.7)	7	116.3 (87.2, 122.3)	8	0.59	0.07	0.79	0.86
Blood oximetry												
Arterial blood P_{O_2} , mmHg	113.7 \pm 6.1	10	89.2 \pm 4.7	9	97.4 \pm 5.0	7	100.7 \pm 7.7	8	0.09	0.70	0.03	0.01
Hematocrit, %	44.8 (41.9, 45.6)	10	38.5 (35.4, 40.3)	9	43.0 (41, 44.5)	7	42.1 (41.4, 43.3)	8	0.01	0.35	0.06	0.07
Arterial blood oxygen saturation, %	98.3 (97.1, 99.0)	10	96.5 (92.3, 97.5)	9	96.5 (94, 97.5)	7	97.5 (96.6, 98.5)	8	0.36	0.80	0.003	0.02
Renal oxygen delivery, μ mol/min	30.5 \pm 2.7	10	21.7 \pm 2.4	9	29.7 \pm 5.5	7	20.8 \pm 2.9	8	0.03	0.95	0.99	0.06
Renal oxygen delivery, μ mol-min ⁻¹ ·g body wt ⁻¹	80.5 \pm 2.7	10	57.7 \pm 5.6	9	64.3 \pm 12.7	7	56.5 \pm 6.8	8	0.20	0.60	0.60	0.10
Renal oxygen consumption, μ mol/min	2.9 (1.1, 6.0)	6	1.1 (0.7, 2.7)	7	2.6 (1.8, 4.1)	7	1.4 (0.9, 2.1)	8	0.04	0.99	0.99	0.06
Renal oxygen consumption, μ mol-min ⁻¹ ·g body wt ⁻¹	8.3 \pm 2.8	6	4.1 \pm 1.1	7	6.1 \pm 1.2	7	3.8 \pm 0.6	8	0.08	0.70	0.80	0.30
Fractional extraction O_2 , %	10.1 (6.0, 17.8)	6	5.1 (3.3, 11.7)	7	7.9 (7.1, 14.4)	7	6.9 (4.7, 8.2)	8	0.11	0.95	0.70	0.44

Values of variables that did not violate normality are means \pm SE, whereas values of variables that violated normality are medians (25th percentile, 75th percentile); *n* = no. of rats. Normality of the data was assessed using the Shapiro-Wilk test. P_{Tr} , P_{Tr*T} , and P_{Tr+T} are the outcomes of 2-way analysis of variance (ANOVA) with factors treatment (Tr) and time (T) for data that did not violate normality. For data that violated normality, an ANOVA on ranking was performed instead. Dichotomous comparisons of continuous variables were made using Student's *t*-test for data that did not violate normality. For data that violated normality, a Mann-Whitney *U*-test was performed for dichotomous comparisons. *P* values for dichotomous comparisons were conservatively adjusted using the Dunn-Sidak correction with *k* = 2 to account for the fact that comparisons were made at 24 h and 5 days. I1, 24 h after ischemia and reperfusion; I5, 5 days after ischemia and reperfusion; S1, 24 h after sham ischemia; S5, 5 days after sham ischemia.

Fig. 2. Assessment of tissue PO_2 by Clark electrode. The electrode was first inserted 2 mm into the cortex at six random sites across the left kidney. **A**: multiple measurements are shown for each rat, with the various rats represented by different symbols. Closed symbols represent rats subjected to renal ischemia ($n = 9$ at 24 h and $n = 8$ at 5 days), whereas open symbols represent rats subjected to sham ischemia ($n = 10$ at 24 h and $n = 7$ at 5 days). **B**: measurements of cortical tissue PO_2 for each rat were averaged and are presented as between-rat means \pm SE. In **B**, P_{Tr} , P_{T} , and $P_{\text{Tr}\times\text{T}}$ are the outcomes of a two-way analysis of variance (ANOVA) with factors treatment (Tr) and time (T). P values above each pair of columns and error bars show the outcomes of Student's unpaired t -test conservatively adjusted using the Dunn-Sidak correction with $k = 2$ to account for the fact that comparisons were made at 24 h and 5 days. **C** and **D**: a tissue PO_2 profile with depth was established by advancing the electrode from the cortical surface at 1-mm increments, up to 10 mm into the left kidney either 24 h (**C**) or 5 days (**D**) following recovery from either ischemia or sham ischemia. Symbols and error bars are the means \pm SE for rats subjected to either an hour of sham (\circ) or bilateral renal ischemia (\bullet). In **C** and **D**, P_{D} , P_{Tr} , and $P_{\text{D}\times\text{Tr}}$ are the outcomes of two-way repeated-measures ANOVA with factors depth (D) and treatment. $*P \leq 0.05$ and is the outcome of Student's unpaired t -test without correction for multiple comparisons.



By 5 days after renal ischemia, cortical tissue PO_2 was 39% less than 24 h after ischemia and similar to that in rats subjected to sham ischemia 5 days previously (Fig. 2B). Tissue PO_2 varied little with depth from the cortical surface. At 24 h after reperfusion, tissue PO_2 tended to be greater in rats subjected to ischemia than in those subjected to sham ischemia, the difference reaching statistical significance at depths of 5 mm (inner medulla) and 9 and 10 mm (cortex; Fig. 2C). Five days after renal ischemia, tissue PO_2 did not differ significantly from its level in rats subjected to sham ischemia, at any depth below the cortical surface (Fig. 2D).

Renal hemodynamics and function. RBF was not significantly different in rats subjected to ischemia compared with rats subjected to sham ischemia, both 24 h and 5 days after surgery (Table 2). Twenty-four hours after ischemia, mean GFR (-99%), urine flow (-82%), and sodium excretion (-85%) were less than in rats subjected to ischemia than in those subjected to sham ischemia (Table 2). Fractional excretion of sodium did not differ significantly 24 h after ischemia compared with sham ischemia. By 5 days after ischemia, renal function was highly variable between rats, with some rats having recovered relatively normal GFR while others remained in apparent renal failure. Consequently, none of these variables differed significantly from their level in rats subjected to sham ischemia. We were unable to detect a significant correlation ($r^2 = 0.03$, $n = 8$), in rats subjected to ischemia, between GFR and tissue PO_2 at day 5 after surgery.

Blood oximetry and renal oxygen consumption and delivery. Arterial blood hematocrit 24 h after renal ischemia was 12% less than after sham ischemia (Table 1). We were unable to detect a significant correlation ($r^2 = 0.034$, $n = 9$), in rats subjected to ischemia, between hematocrit and tissue PO_2 24 h after reperfusion. By 5 days after renal ischemia, hematocrit was similar in the two groups of rats. Arterial blood PO_2 was 22% less, and oxygen saturation was 2.7% less, in rats 24 h after renal ischemia than after sham surgery. Renal DO_2 tended to be (29%) less 24 h after renal ischemia than after sham

ischemia, although this apparent effect was not statistically significant ($P = 0.06$). There was no significant difference in renal DO_2 5 days after surgery. When both time points were considered together (24 h and 5 days), renal $\dot{V}\text{O}_2$ was 55% less in rats subjected to ischemia than in those subjected to sham surgery. The fractional extraction of oxygen did not differ significantly between the treatments at either time point.

Protocol 3: Cellular Hypoxia and Hypoxic Signaling After Renal Ischemia

Pimonidazole adduct immunohistochemistry. No pimonidazole adducts were detected in tissues from rats that did not receive pimonidazole chloride or in sections that were not incubated with the primary antibody (data not shown). Kidney sections from sham-operated rats appeared morphologically normal (Figs. 3 and 4). Pimonidazole adducts were largely absent in the cortical region of rats 24 h following sham ischemia. However, there was diffuse staining of pimonidazole adducts in tubular elements of the outer and inner medulla following sham ischemia. Kidney sections from rats 24 h following recovery from renal ischemia showed relatively little staining for pimonidazole adducts across all regions of the kidney, but some diffuse staining was present 5 days following ischemia and reperfusion. However, luminal aspects of tubules were often stained positive for pimonidazole adducts after renal ischemia, suggestive of marked tubular obstruction. There was significant cellular sloughing and disintegration of the brush border/apical membrane of tubules after renal ischemia. In addition, there were considerable cellular debris in the luminal aspects of tubules at 24 h after renal ischemia. Tubular profiles surrounding the debris-riddled tubules were often flattened. In contrast, tubules appeared to be mostly dilated 5 days after renal ischemia. By 5 days after ischemia, tubules in the cortex and outer and inner medulla appeared to be more dilated than after sham ischemia or 24 h after renal ischemia.

Table 2. Renal hemodynamic parameters of rats 24 h or 5 days after ischemia or sham ischemia

Parameter	Sham (24 h)		Ischemia (24 h)		Sham (5 days)		Ischemia (5 days)		2-Way ANOVA			Dichotomous Comparison	
	Value	n	Value	n	Value	n	Value	n	P _{Tr}	P _T	P _{Tr+T}	S1 vs. II	S5 vs. I5
Renal blood flow, ml/min	3.5 ± 2.9	10	3.0 ± 0.4	9	3.6 ± 0.7	7	2.4 ± 0.3	8	0.13	0.83	0.68	0.55	0.29
Renal blood flow, µl·min ⁻¹ ·g body wt ⁻¹	9.09 ± 0.98	10	7.93 ± 0.79	9	7.71 ± 1.59	7	6.65 ± 0.78	8	0.30	0.21	0.96	0.60	0.81
Renal plasma flow, ml/min	1.7 (1.5, 2.1)	10	1.7 (1.4, 2.0)	9	1.6 (1.5, 3.0)	7	1.6 (0.9, 1.9)	8	0.42	0.65	0.87	0.36	0.51
Renal plasma flow, µl·min ⁻¹ ·g body wt ⁻¹	5.1 ± 0.6	10	4.9 ± 0.5	9	4.4 ± 0.9	7	3.8 ± 0.4	8	0.77	0.31	0.94	0.96	0.80
Glomerular filtration rate, ml/min	0.8 (0.7, 1.2)	10	0.001 (0, 0.008)	9	1.0 (0.5, 1.8)	7	0.07 (0.01, 0.4)	9	<0.001	0.17	0.11	<0.001	0.14
Glomerular filtration rate, nl·min ⁻¹ ·g body wt ⁻¹	2,400 (1,520, 2,960)	10	3.3 (0, 2.2)	9	2,110 (1,040, 3,470)	7	190 (27, 1,080)	8	<0.001	0.18	0.03	<0.001	0.20
Urine flow, µl/min	7.0 ± 1.0	10	1.0 ± 0.5	9	10.0 ± 4.0	7	6.0 ± 2.0	8	0.01	0.09	0.99	0.001	0.36
Urine flow, nl·min ⁻¹ ·g body wt ⁻¹	16.0 (10.0, 28.0)	10	2.2 (0, 5.5)	9	17.0 (13.0, 25.0)	7	15 (1.1, 39.0)	8	0.04	0.05	0.06	0.002	0.66
Sodium excretion, µmol/min	0.4 (0.2, 1.0)	9	0 (0, 0.18)	9	0.20 (0.2, 0.6)	7	0.20 (0.1, 0.3)	8	0.004	0.46	0.09	0.003	0.38
Sodium excretion, nmol·min ⁻¹ ·g body wt ⁻¹	1.0 (0.5, 2.1)	9	0 (0, 0.47)	9	0.5 (0.36, 1.3)	7	0.6 (0.35, 0.71)	8	0.02	0.53	0.05	0.01	0.90
Sodium reabsorption, µmol/min	111.9 (93.6, 170.2)	9	0.17 (0, 1.0)	9	138.3 (63.3, 250.4)	7	8.75 (1.5, 52.0)	8	<0.001	0.2	0.15	<0.001	0.14
Sodium reabsorption, nmol·min ⁻¹ ·g body wt ⁻¹	307.5 (204.7, 427.6)	9	0.46 (0, 2.7)	9	310 (143.6, 479.3)	7	25.7 (3.6, 153.1)	8	<0.001	0.18	0.03	<0.001	0.20
Filtration fraction, %	46.9 (34.1, 69.8)	10	0.1 (0, 0.5)	9	48.5 (29.7, 60.5)	7	7.0 (0.6, 21.7)	8	<0.001	0.13	0.02	<0.001	0.20

Values of variables that did not violate normality are means ± SE, whereas values of variables that violated normality are expressed as medians (25th percentile, 75th percentile); n = no. of rats. Normality of the data was assessed using the Shapiro-Wilk test. P_{Tr}, P_T, and P_{Tr+T} are the outcomes of two-way analysis of variance (ANOVA) with factors treatment (Tr) and time (T) for data that did not violate normality. For data that violated normality, an ANOVA on ranking was performed instead. Dichotomous comparisons of continuous variables were made using Student's *t*-test for data that did not violate normality. For data that violated normality, a Mann-Whitney *U*-test was performed for dichotomous comparisons. *P* values for dichotomous comparisons were conservatively adjusted using the Dunn-Sidak correction with *k* = 2 to account for the fact that comparisons were made at 24 h and 5 days. I1, 24 h after ischemia and reperfusion; I5, 5 days after ischemia and reperfusion; S1, 24 h after sham ischemia; S5, 5 days after sham ischemia.

HIF-1α and HIF-2α proteins. When both the 24-h and 5-day time points were considered collectively, the expression of HIF-1α protein in the cortex, outer medulla, and inner medulla was less after renal ischemia than after sham ischemia (Fig. 5, A–C). However, not all comparisons at individual time points were statistically significant. HIF-1α levels in the cortex were 88.3% less 5 days after renal ischemia than at the corresponding time-point after sham ischemia (Fig. 5A). Similarly, in the outer medulla, HIF-1α was 62.2% less 24 h after renal ischemia and 79.7% less 5 days after renal ischemia than after sham surgery (Fig. 5B). In contrast, in the inner medulla, levels of HIF-1α protein did not differ significantly, between rats subjected to ischemia and those subjected to sham ischemia, at either the 24-h or 5-day time point (Fig. 5C). When both the 24-h and 5-day time points were considered collectively, the expression of HIF-2α protein was markedly less, in rats subjected to ischemia compared with those subjected to sham ischemia, in the cortex and the outer medulla but not in the inner medulla. The level of HIF-2α in the cortex was 86.9% less 5 days after ischemia than after sham ischemia (Fig. 5D). In the outer medulla of rats subjected to renal ischemia, HIF-2α expression was 55% less 24 h and 89.2% less 5 days after ischemia than after sham ischemia (Fig. 5E). The deficits in HIF-1α and HIF-2α in rats subjected to renal ischemia did not diminish between the 24-h and 5-day time points, if anything, becoming more marked (Fig. 5).

Expression of genes for HIF-1α, HIF-2α, VEGF-α, and HO-1. There were no significant differences in the expression of mRNA for HIF-1α, HIF-2α, or VEGF-α, either 24 h or 5 days following renal ischemia compared with after sham ischemia (Fig. 6). The expression of HO-1 mRNA tended to be greater after ischemia than after sham ischemia, although this apparent effect was only statistically significant at the 5-day time point.

Collagen deposition. Twenty-four hours after renal ischemia, picrosirius red staining did not differ significantly from that seen in rats subjected to sham ischemia in either the cortex or the outer medulla. However, it was 43% less in the inner medulla (Fig. 7). By 5 days after renal ischemia, picrosirius red staining was 50% greater in the cortex of rats subjected to ischemia than in those subjected to sham ischemia. There was an apparent effect of the duration of recovery period on picrosirius red staining, which in the cortex and inner medulla was significantly greater 5 days after ischemia or sham ischemia than at the 24-h time point.

Indexes of renal dysfunction. The plasma concentrations of urea and creatinine and the urinary albumin-to-creatinine ratio were all greater in rats after ischemia than after sham ischemia (Fig. 8). These effects were statistically significant at the individual time points with the exception of the urinary albumin-to-creatinine ratio 24 h after ischemia, where sufficient urine for analysis could only be generated from two animals.

DISCUSSION

We determined the time course of changes in, and the spatial distribution of, renal tissue Po₂ during the subacute phase of severe renal IRI. Using four different methods for assessing renal tissue oxygenation, we could not detect tissue hypoxia during the extension/recovery phase of IRI. Indeed, if anything, there was relative hyperoxia up to 48 h after an hour of

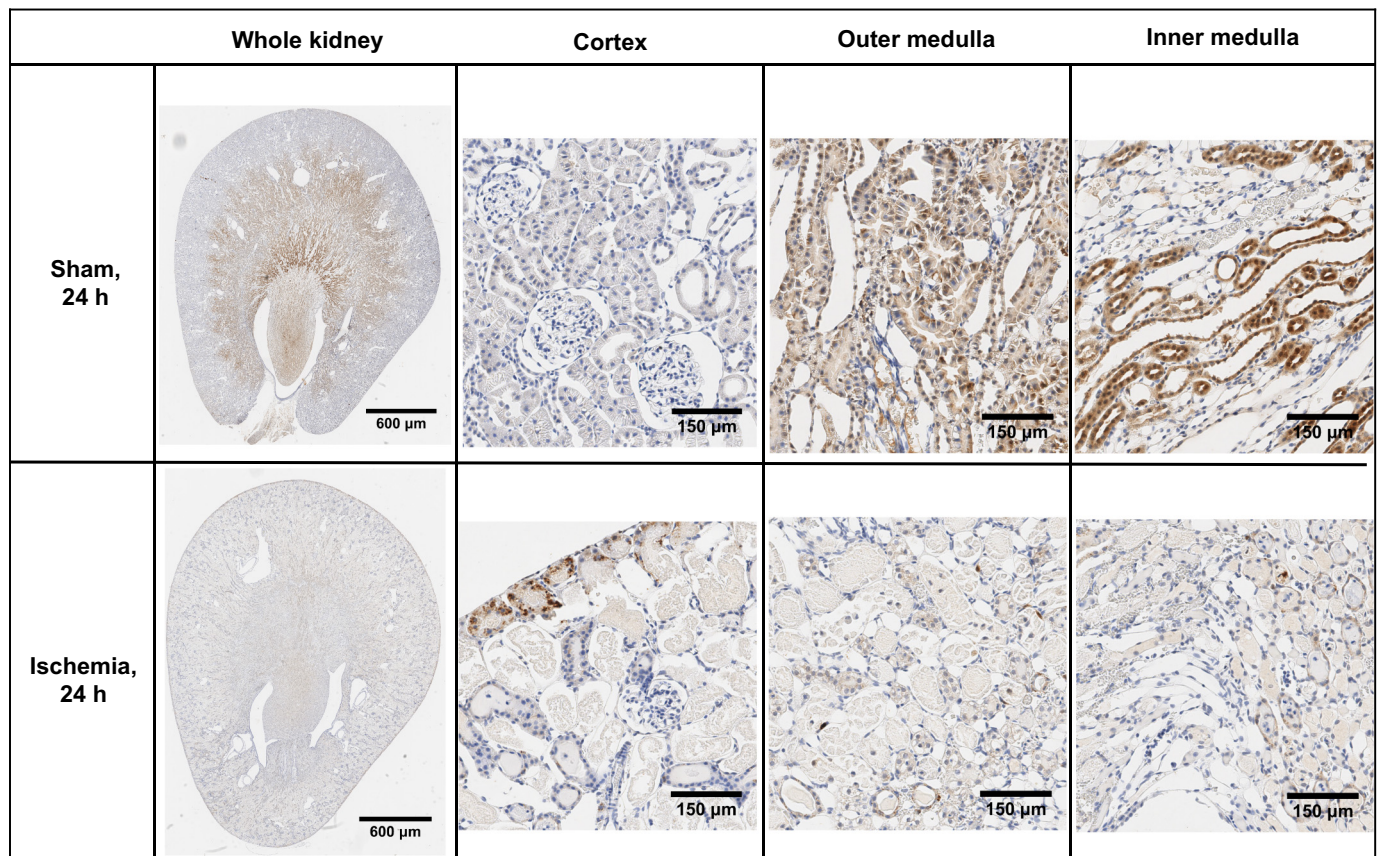


Fig. 3. Pimonidazole adduct immunohistochemistry of renal sections 24 h following recovery from bilateral renal ischemia or sham ischemia. Images are typical of the cortical and outer and inner medullary region of the six kidneys examined in each group.

bilateral renal ischemia. We also observed downregulation of the abundance of HIF-1 α and HIF-2 α protein, particularly in the cortex and outer medulla, both 24 h and 5 days after reperfusion. The apparent absence of renal hypoxia is consistent with the pattern of changes in renal $\dot{V}O_2$ and $\dot{V}O_2$ after ischemia and reperfusion. That is, RBF was relatively normal, but there was a marked reduction in sodium reabsorption, and so presumably oxygen utilization for sodium reabsorption, at both 24 h and 5 days after reperfusion. When both time points were considered together, renal $\dot{V}O_2$ was significantly less, and $\dot{V}O_2$ tended to be less, in rats subjected to ischemia than in those subjected to sham ischemia. Thus, tissue P_{O_2} appears to be well maintained during the extension/recovery phase of severe renal IRI because changes in renal $\dot{V}O_2$ and $\dot{V}O_2$ are relatively balanced.

The methods we used to assess renal oxygenation have both strengths and weaknesses (11, 33). Radiotelemetry allows continuous measurement of renal tissue P_{O_2} in the absence of confounding effects of anesthesia (22, 23). However, tissue P_{O_2} can only be expressed in relative terms and can be measured at only one site in each animal. Clark electrodes allow generation of a spatial map of tissue P_{O_2} , but only in anesthetized animals (11, 33). Furthermore, it is not possible to resolve tissue P_{O_2} to the level of specific vascular and tubular elements, except in the superficial cortex (43). In addition, as we have found previously with Clark electrodes inserted into renal tissue from the dorsal surface of the kidney (32), the steep corticomedullary gradient in tissue P_{O_2} generated in many

previous studies (6, 10, 29) is not obviously evident. We have no adequate explanation for this, although it may relate to our use of relatively large electrodes (50 μ m) or the angle of entry to the renal tissue, from the dorsal surface of the kidney, as a consequence of which the tip of the electrode does not enter the renal papilla. Pimonidazole adduct immunohistochemistry allows detection of cells with $P_{O_2} < 10$ mmHg but does not provide a quantitative measure of tissue P_{O_2} (37). Furthermore, as we found in the present study and previously (1), it is prone to artifactual staining of cellular debris and casts within damaged tubules. Quantification of the abundance of HIF-1 α and HIF-2 α protein provides information about the state of hypoxia signaling pathways. However, factors other than tissue P_{O_2} contribute to the regulation of HIF signaling (16). Thus, interpretation of our failure to detect hypoxia by any one of these methods would merit caution. However, the fact that our observations were consistent across the four methods provides compelling evidence that at least in this severe form of IRI, tissue hypoxia is not an obligatory characteristic of the period from 24 h to 5 days after severe renal ischemia and reperfusion.

The most likely explanation for the absence of hypoxia 24 h and 5 days after reperfusion, and even increased tissue P_{O_2} at 24 h, is reduced sodium reabsorption and thus renal $\dot{V}O_2$. In the rats we studied, the deficit in sodium reabsorption 24 h after ischemia and reperfusion could be attributed to the decreased filtered load of sodium. This appears to drive downregulation of Na^+K^+ -ATPase activity. For example, in response to severe renal ischemia (i.e., 60 min), the abundance (and activ-

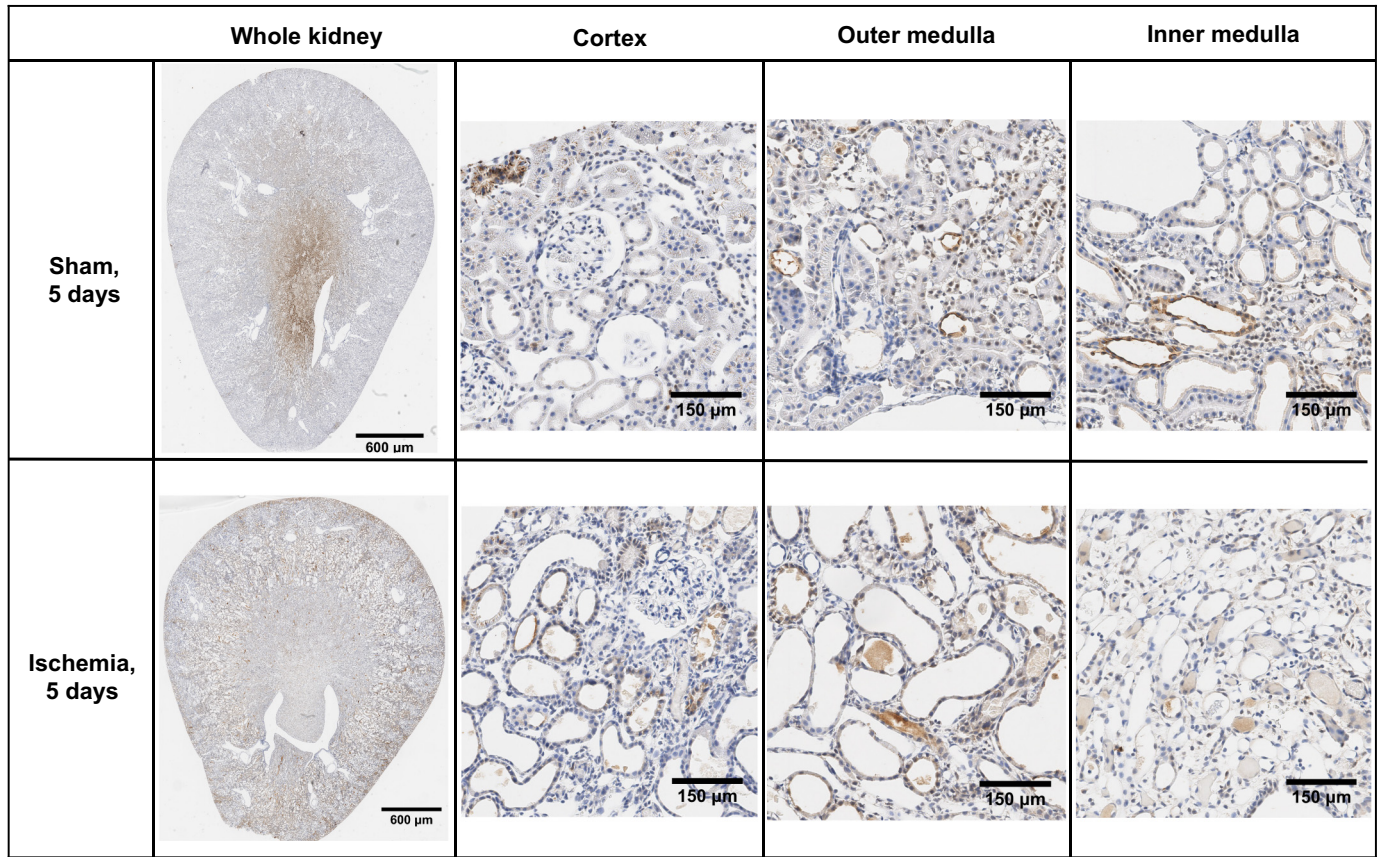


Fig. 4. Pimonidazole adduct immunohistochemistry of renal sections 5 days following recovery from bilateral renal ischemia or sham surgery. Images are typical of the cortical and outer and inner medullary region of the six kidneys examined in each group.

ity) of basolateral $\text{Na}^+\text{-K}^+\text{-ATPase}$ pumps and the apical Na-K-2Cl and thiazide-sensitive $\text{Na}^+\text{-Cl}^-$ cotransporters were shown to be greatly reduced (25). However, the magnitude of the apparent reduction in renal $\dot{V}\text{O}_2$ we observed was considerably less than the magnitude of the reduction in sodium reabsorption. For example, sodium reabsorption was $<1\%$ of rats subjected to sham ischemia, whereas $\dot{V}\text{O}_2$ was 34% that of rats subjected to sham ischemia 24 h after reperfusion. These observations are consistent with the concept that oxygen utilization for sodium reabsorption becomes less efficient in AKI. In support of this concept, Redfors et al. studied renal oxygen utilization in patients with AKI subsequent to cardiothoracic surgery (35). They found a deficit in sodium reabsorption of 59% in patients with AKI after cardiothoracic surgery compared with patients without AKI (35). In contrast, renal $\dot{V}\text{O}_2$ was similar in the two groups of patients. Furthermore, renal $\dot{V}\text{O}_2$ per unit of reabsorbed sodium was 2.4 times greater in patients with AKI than in those without AKI (35). The inefficiency of oxygen utilization for sodium reabsorption in AKI appears to be driven by multiple factors, including loss of polarity of $\text{Na}^+\text{-K}^+\text{-ATPase}$ pumps, oxidative stress, and reduced bioavailability of nitric oxide (17, 24).

Renal tissue Po_2 is determined by the balance between local Do_2 and $\dot{V}\text{O}_2$ (12). Thus, tissue Po_2 during recovery from AKI is likely to be model dependent. In a model of severe AKI such as the one used in the present study, in which the filtered load of sodium (and thus oxygen utilization for sodium reabsorption) is greatly reduced but RBF (and thus presumably local

tissue Do_2) is well preserved, the absence of tissue hypoxia, and even tissue hyperoxia, might be expected. On the other hand, tissue hypoxia might be predicted in a model of less severe renal dysfunction, and thus better preserved GFR. This concept is consistent with clinical observations in patients after renal transplantation. Using blood oxygen level-dependent magnetic resonance imaging, Sadowski et al. observed greater renal medullary oxygenation in the transplanted kidneys of patients with acute allograft rejection than in patients with normal functioning allografts, despite the former having a deficit in renal medullary perfusion (38). Similarly, Rosenberger et al. observed low HIF-1 α abundance in biopsies of patients with nonfunctional allografts but induction of HIF-1 α in biopsies from functional grafts (36). Thus, there is a strong rationale for the methods used in the present study to be applied to a less severe model of AKI, in which tissue hypoxia might be more likely to occur.

It is noteworthy that HIF-1 α and HIF-2 α protein expression was downregulated not just at 24 h after reperfusion, presumably driven in part by increased tissue oxygen availability, but also 5 days after reperfusion, when tissue Po_2 was similar in rats exposed to ischemia and sham ischemia. Inhibition of HIF-1 α and HIF-2 α abundance appears to be mediated by posttranslational processes at both 24 h and 5 days after reperfusion, since the expression of mRNA for these proteins was relatively normal at both time points. The bioavailability of HIFs is influenced by various factors, such as their phosphorylation (20) and hydroxylation of proline and asparagine

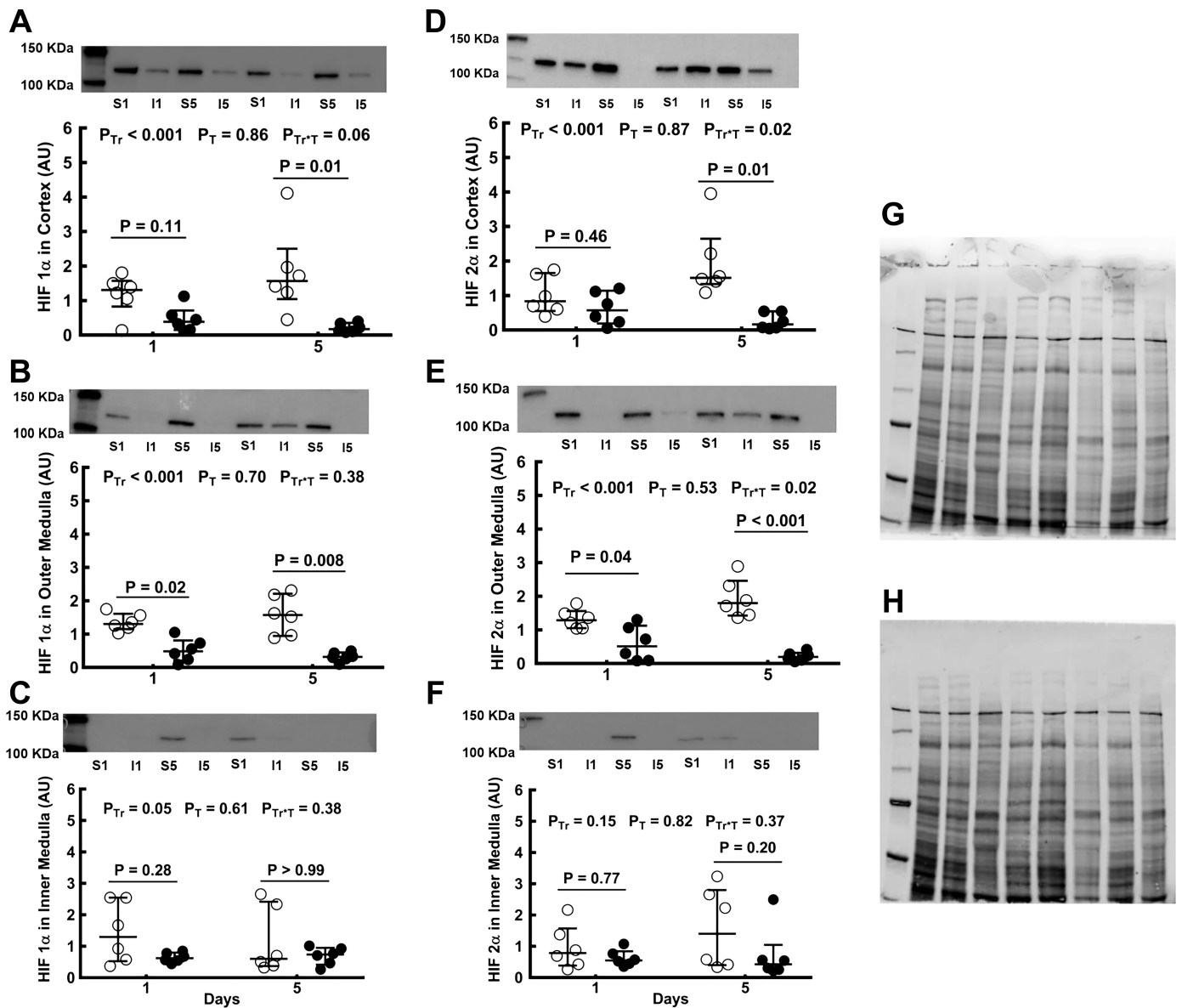


Fig. 5. Expression of hypoxia-inducible factor (HIF) proteins after bilateral renal ischemia or sham ischemia. Immunoblots for HIF-1 α (A–C) and HIF-2 α (D–F) of tissue extracts from the cortex and outer and inner medulla of the left kidneys of rats 24 h and 5 days following recovery from either sham ischemia (○) or bilateral renal ischemia (●); $n = 6$ per group. G: typical image of the gel following electrophoresis. H: typical image of the nitrocellulose membrane following transfer. Values are expressed as medians (25th percentile, 75th percentile). Paired comparisons were performed using the Mann-Whitney *U*-test. Because paired comparisons were made at two time points, *P* values were conservatively adjusted using the Dunn-Sidak method with $k = 2$. P_{Tr} , P_T , and P_{Tr+T} are the outcomes of two-way analysis of variance on ranking with the factors treatment (Tr) and time (T). AU, arbitrary unit; I1, 24 h after ischemia; I5, 5 days after ischemia; S1, 24 h after sham ischemia; S5, 5 days after sham ischemia.

residues on HIFs (44) that target these protein for ubiquitinylation. The levels of proline hydroxylases (PHDs) have been shown to be unaltered following ischemia and reperfusion of the kidney (13, 39). A caveat to that is that the posttranslational modification of HIFs by PHDs in the kidney is likely complex given that the expression patterns, and thus sensitivity, of PHDs vary in different regions of the kidney likely because of the heterogeneity of renal tissue P_{O_2} under physiological conditions (39). It is also noteworthy that mRNA for VEGF- α and HO-1, genes under the control of the HIF-1 α and HIF-2 α promoter, were not downregulated at 24 h or 5 days after reperfusion. This observation is consistent with the concept that factors other than HIFs regulate expression of these genes

in the subacute phase of severe IRI. The signaling pathway for VEGFs is complex and is critical for neovascularization. A myriad of factors apart from HIFs, such as VEGF receptor signaling complexes and neuropilin, are able to modulate the abundance and activity of VEGFs (21). Kanellis et al. showed that expression of VEGF was unaltered in response to ischemia-reperfusion of the kidney (18). Interestingly, the expression of VEGF receptor 2 was increased following ischemia, and VEGF was redistributed to the basolateral membrane, consistent with the established role of VEGF in the maintenance of an adequate blood supply, in remaining viable tissues, as evinced in the present study by relatively well-maintained RBF (19). Nevertheless, the permanent loss

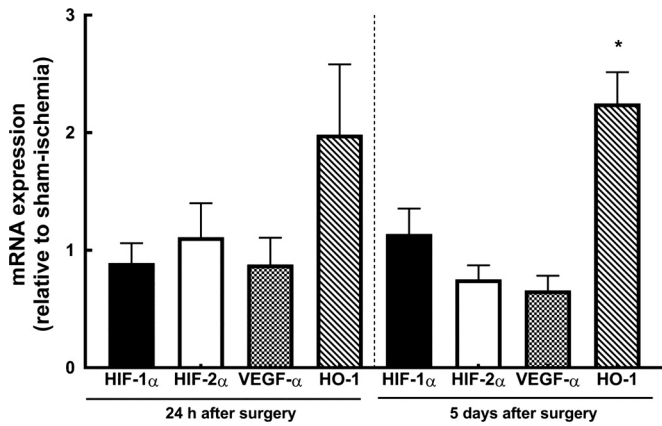


Fig. 6. mRNA expression of HIF-1α, HIF-2α, VEGF-α, and heme oxygenase 1 (HO-1). Expression of HIF-1α, HIF-2α, VEGF-α, and HO-1 mRNA is presented as relative to that of control animals. Values are expressed as means ± SE. **P* ≤ 0.05 for specific comparisons between the two treatment groups at each time point using Student's unpaired *t*-test.

of peritubular capillaries, due to inadequate vascular reparation and/or neovascularization, appears to be an important event in the progression from ischemia-induced AKI to CKD (2, 4).

Perspectives and Significance

In models of AKI induced by complete renal ischemia, hypoxia during the period of ischemia is obligatory and is likely one of the drivers of necrosis and apoptosis associated with the development of AKI after reperfusion. Furthermore, other important factors during reperfusion, such as oxidative stress (5, 7) and influx of immune-modulatory cells (14, 42), are initiated, at least partly, by the hypoxia during ischemia. In

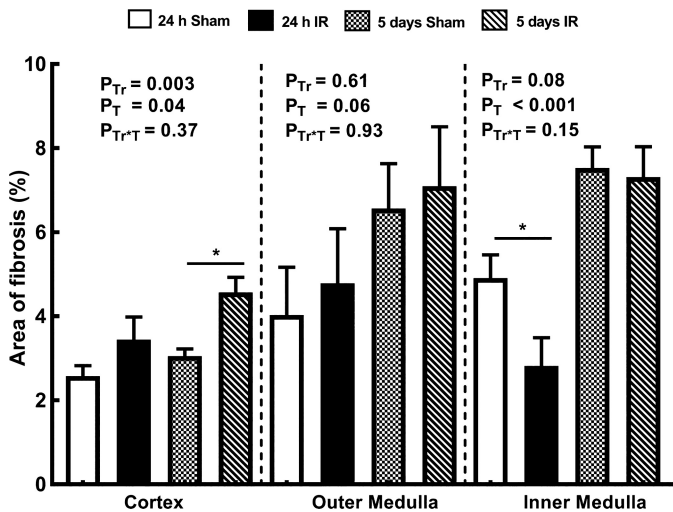


Fig. 7. Collagen deposition in kidneys of rats. The percent areas of interstitial fibrosis relative to the areas of the cortex and outer and inner medulla are shown for rats 24 h and 5 days after recovery from either sham ischemia or bilateral renal ischemia (IR); *n* = 6 per group. Values are expressed as means ± SE. Paired comparisons were performed using Student's unpaired *t*-test (**P* ≤ 0.05). Because paired comparisons were made at two time points, *P* values were conservatively adjusted using the Dunn-Sidak method with *k* = 2. *P*_{Tr}, *P*_T, and *P*_{Tr×T} are the outcomes of two-way analysis of variance with the factors treatment (Tr) and time (T).

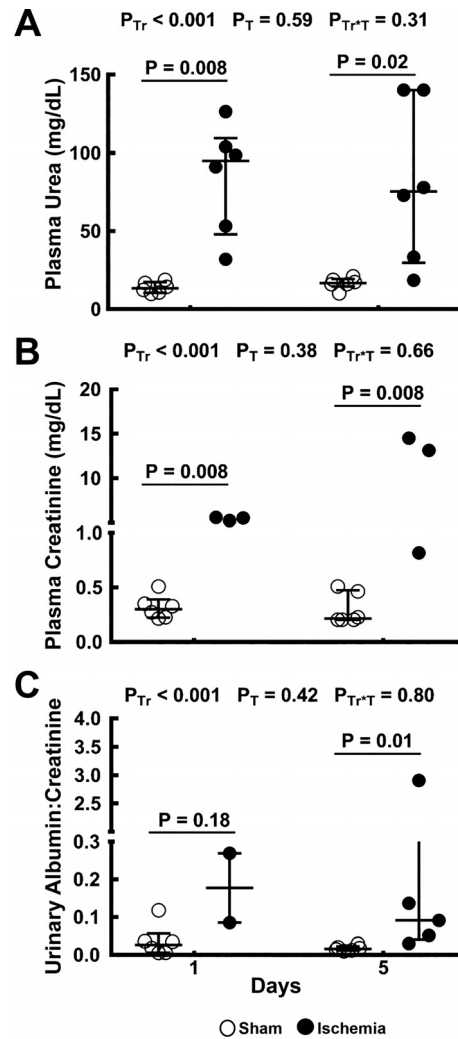


Fig. 8. Indicators of renal dysfunction. Plasma concentrations of urea (A) and creatinine (B) and the urinary albumin-to-creatinine ratio (C) are shown for rats 24 h and 5 days after sham ischemia (○) or bilateral renal ischemia (●); *n* = 6 per group. Values are expressed as medians (25th percentile, 75th percentile). Comparisons were performed using the Mann-Whitney *U*-test. Because comparisons were made at two time points, *P* values were conservatively adjusted using the Dunn-Sidak method with *k* = 2. *P*_{Tr}, *P*_T, and *P*_{Tr×T} are the outcomes of two-way analysis of variance with ranking with the factors treatment (Tr) and time (T).

the first few hours after reperfusion (acute phase), reduced renal tissue or microvascular Po₂ has been observed in some (27, 28), but not all (1), cases. To the best of our knowledge, our present report describes the first detailed investigation of tissue oxygenation during the subacute phase of renal IRI. We provide compelling evidence that at least in severe IRI modeling subacute and end-stage renal disease, renal tissue hypoxia is not present 24 h and 5 days after reperfusion. It is possible that the absence of hypoxia at these time points in this experimental model of severe IRI is a consequence of the degree of renal damage and the consequent deficit in renal oxygen consumption. Thus, future studies should focus on less severe models of AKI and follow animals for longer periods after reperfusion, to better characterize the natural history of renal oxygenation during progression from AKI to CKD.

ACKNOWLEDGMENTS

Present address of C. P. C. Ow: Dept. of Cardiac Physiology, National Cerebral and Cardiovascular Center Research Institute, 5-7-1 Fujishirodai, Suita-Shi, Osaka 565-8565, Japan (e-mail: ow.peichenconnie73@nccv.go.jp).

GRANTS

This work was supported by National Health and Medical Research Council of Australia Grants GNT606601 and GNT1024575. M. P. Koeners is supported by the British Heart Foundation (FS/14/30630) and the European Union, Seventh Framework Programme, Marie Curie Actions [Cardio Renal Paradigms Elucidated through an International Exchange Scheme (CAR-PEDIEM) Grant 612280 and International Outgoing Fellowship 282821]. M. J. Watt is supported by National Health and Medical Research Council of Australia Grant GNT1077703.

DISCLOSURES

No conflicts of interest, financial or otherwise, are declared by the authors.

AUTHOR CONTRIBUTIONS

C.P.C.O. and R.G.E. conceived and designed research; C.P.C.O., J.P.N., and G.B. performed experiments; C.P.C.O. analyzed data; C.P.C.O., J.P.N., and R.G.E. interpreted results of experiments; C.P.C.O. prepared figures; C.P.C.O. drafted manuscript; C.P.C.O., J.P.N., M.M.U., G.B., R.C.M., M.J.W., L.M.H., M.P.K., and R.G.E. edited and revised manuscript; C.P.C.O., J.P.N., M.M.U., G.B., R.C.M., M.J.W., L.M.H., M.P.K., and R.G.E. approved final version of manuscript.

REFERENCES

- Abdelkader A, Ho J, Ow CPC, Eppel GA, Rajapakse NW, Schlaich MP, Evans RG. Renal oxygenation in acute renal ischemia-reperfusion injury. *Am J Physiol Renal Physiol* 306: F1026–F1038, 2014. doi:10.1152/ajprenal.00281.2013.
- Basile DP, Bonventre JV, Mehta R, Nangaku M, Unwin R, Rosner MH, Kellum JA, Ronco C; ADQI XIII Work Group. Progression after AKI: understanding maladaptive repair processes to predict and identify therapeutic treatments. *J Am Soc Nephrol* 27: 687–697, 2016. doi:10.1681/ASN.2015030309.
- Basile DP, Donohoe DL, Roethe K, Mattson DL. Chronic renal hypoxia after acute ischemic injury: effects of L-arginine on hypoxia and secondary damage. *Am J Physiol Renal Physiol* 284: F338–F348, 2003. doi:10.1152/ajprenal.00169.2002.
- Basile DP, Donohoe D, Roethe K, Osborn JL. Renal ischemic injury results in permanent damage to peritubular capillaries and influences long-term function. *Am J Physiol Renal Physiol* 281: F887–F899, 2001. doi:10.1152/ajprenal.00050.2001.
- Basile DP, Leonard EC, Beal AG, Schleuter D, Friedrich J. Persistent oxidative stress following renal ischemia-reperfusion injury increases ANG II hemodynamic and fibrotic activity. *Am J Physiol Renal Physiol* 302: F1494–F1502, 2012. doi:10.1152/ajprenal.00691.2011.
- Baumgärtl H, Leichtweiss HP, Lübbers DW, Weiss C, Huland H. The oxygen supply of the dog kidney: measurements of intrarenal pO₂. *Microvasc Res* 4: 247–257, 1972. doi:10.1016/0026-2862(72)90036-2.
- Chatterjee PK, Cuzzocrea S, Brown PAJ, Zacharowski K, Stewart KN, Mota-Filipe H, Thiemermann C. Tempol, a membrane-permeable radical scavenger, reduces oxidant stress-mediated renal dysfunction and injury in the rat. *Kidney Int* 58: 658–673, 2000. doi:10.1046/j.1523-1755.2000.00212.x.
- Coca SG, Singanamala S, Parikh CR. Chronic kidney disease after acute kidney injury: a systematic review and meta-analysis. *Kidney Int* 81: 442–448, 2012. doi:10.1038/ki.2011.379.
- Conover WJ, Iman RL. Rank transformation as a bridge between parametric and nonparametric statistics. *Am Stat* 35: 124–129, 1981. doi:10.1080/00031305.1981.10479327.
- Epstein FH, Agmon Y, Brezis M. Physiology of renal hypoxia. *Ann N Y Acad Sci* 718: 72–82, 1994. doi:10.1111/j.1749-6632.1994.tb55706.x.
- Evans RG, Gardiner BS, Smith DW, O'Connor PM. Methods for studying the physiology of kidney oxygenation. *Clin Exp Pharmacol Physiol* 35: 1405–1412, 2008. doi:10.1111/j.1440-1681.2008.05063.x.
- Evans RG, Ince C, Joles JA, Smith DW, May CN, O'Connor PM, Gardiner BS. Haemodynamic influences on kidney oxygenation: clinical implications of integrative physiology. *Clin Exp Pharmacol Physiol* 40: 106–122, 2013. doi:10.1111/1440-1681.12031.
- Fang Y, Zhang H, Zhong Y, Ding X. Prolyl hydroxylase 2 (PHD2) inhibition protects human renal epithelial cells and mice kidney from hypoxia injury. *Oncotarget* 7: 54317–54328, 2016. doi:10.18632/oncotarget.111104.
- Friedewald JJ, Rabb H. Inflammatory cells in ischemic acute renal failure. *Kidney Int* 66: 486–491, 2004. doi:10.1111/j.1523-1755.2004.761_3.x.
- Fu Q, Colgan SP, Shelley CS. Hypoxia: the force that drives chronic kidney disease. *Clin Med Res* 14: 15–39, 2016. doi:10.3121/cmr.2015.1282.
- Haase VH. Hypoxia-inducible factors in the kidney. *Am J Physiol Renal Physiol* 291: F271–F281, 2006. doi:10.1152/ajprenal.00071.2006.
- Hansell P, Welch WJ, Blantz RC, Palm F. Determinants of kidney oxygen consumption and their relationship to tissue oxygen tension in diabetes and hypertension. *Clin Exp Pharmacol Physiol* 40: 123–137, 2013. doi:10.1111/1440-1681.12034.
- Kanellis J, Mudge SJ, Fraser S, Katerelos M, Power DA. Redistribution of cytoplasmic VEGF to the basolateral aspect of renal tubular cells in ischemia-reperfusion injury. *Kidney Int* 57: 2445–2456, 2000. doi:10.1046/j.1523-1755.2000.00103.x.
- Kanellis J, Paizis K, Cox AJ, Stacker SA, Gilbert RE, Cooper ME, Power DA. Renal ischemia-reperfusion increases endothelial VEGFR-2 without increasing VEGF or VEGFR-1 expression. *Kidney Int* 61: 1696–1706, 2002. doi:10.1046/j.1523-1755.2002.00329.x.
- Kietzmann T, Mennerich D, Dimova EY. Hypoxia-inducible factors (HIFs) and phosphorylation: impact on stability, localization, and trans-activity. *Front Cell Dev Biol* 4: 11, 2016. doi:10.3389/fcell.2016.00011.
- Koch S, Claesson-Welsh L. Signal transduction by vascular endothelial growth factor receptors. *Cold Spring Harb Perspect Med* 2: a006502, 2012. doi:10.1101/cshperspect.a006502.
- Koeners MP, Ow CP, Russell DM, Abdelkader A, Eppel GA, Ludbrook J, Malpas SC, Evans RG. Telemetry-based oxygen sensor for continuous monitoring of kidney oxygenation in conscious rats. *Am J Physiol Renal Physiol* 304: F1471–F1480, 2013. doi:10.1152/ajprenal.00662.2012.
- Koeners MP, Ow CP, Russell DM, Evans RG, Malpas SC. Prolonged and continuous measurement of kidney oxygenation in conscious rats. *Methods Mol Biol* 1397: 93–111, 2016. doi:10.1007/978-1-4939-3353-2_9.
- Kwon O, Corrigan G, Myers BD, Sibley R, Scandling JD, Dafoe D, Alfrey E, Nelson WJ. Sodium reabsorption and distribution of Na⁺/K⁺-ATPase during posts ischemic injury to the renal allograft. *Kidney Int* 55: 963–975, 1999. doi:10.1046/j.1523-1755.1999.055003963.x.
- Kwon TH, Frøkiaer J, Han JS, Knepper MA, Nielsen S. Decreased abundance of major Na⁺ transporters in kidneys of rats with ischemia-induced acute renal failure. *Am J Physiol Renal Physiol* 278: F925–F939, 2000. doi:10.1152/ajprenal.2000.278.6.F925.
- Lameire NH, Bagga A, Cruz D, De Maesseneer J, Endre Z, Kellum JA, Liu KD, Mehta RL, Pannu N, Van Biesen W, Vanholder R. Acute kidney injury: an increasing global concern. *Lancet* 382: 170–179, 2013. doi:10.1016/S0140-6736(13)60647-9.
- Legrand M, Almac E, Mik EG, Johannes T, Kandil A, Bezemer R, Payen D, Ince C. L-NIL prevents renal microvascular hypoxia and increase of renal oxygen consumption after ischemia-reperfusion in rats. *Am J Physiol Renal Physiol* 296: F1109–F1117, 2009. doi:10.1152/ajprenal.90371.2008.
- Legrand M, Kandil A, Payen D, Ince C. Effects of sepiapterin infusion on renal oxygenation and early acute renal injury after suprarenal aortic clamping in rats. *J Cardiovasc Pharmacol* 58: 192–198, 2011. doi:10.1097/FJC.0b013e31821f8ec3.
- Lübbers DW, Baumgärtl H. Heterogeneities and profiles of oxygen pressure in brain and kidney as examples of the pO₂ distribution in the living tissue. *Kidney Int* 51: 372–380, 1997. doi:10.1038/ki.1997.49.
- Ludbrook J. On making multiple comparisons in clinical and experimental pharmacology and physiology. *Clin Exp Pharmacol Physiol* 18: 379–392, 1991. doi:10.1111/j.1440-1681.1991.tb01468.x.
- Ludbrook J. Repeated measurements and multiple comparisons in cardiovascular research. *Cardiovasc Res* 28: 303–311, 1994. doi:10.1093/cvr/28.3.303.
- Ow CP, Abdelkader A, Hilliard LM, Phillips JK, Evans RG. Determinants of renal tissue hypoxia in a rat model of polycystic kidney disease. *Am J Physiol Regul Integr Comp Physiol* 307: R1207–R1215, 2014. doi:10.1152/ajpregu.00202.2014.

33. **Ow CP, Ngo JP, Ullah MM, Hilliard LM, Evans RG.** Renal hypoxia in kidney disease: cause or consequence? *Acta Physiol (Oxf)* 222: e12999, 2018. doi:10.1111/apha.12999.
34. **Pohlmann A, Hentschel J, Fechner M, Hoff U, Bubalo G, Arakelyan K, Cantow K, Seeliger E, Flemming B, Waiczies H, Waiczies S, Schunck WH, Dragun D, Niendorf T.** High temporal resolution parametric MRI monitoring of the initial ischemia/reperfusion phase in experimental acute kidney injury. *PLoS One* 8: e57411, 2013. doi:10.1371/journal.pone.0057411.
35. **Redfors B, Bragadottir G, Sellgren J, Swärd K, Ricksten SE.** Acute renal failure is NOT an “acute renal success”: a clinical study on the renal oxygen supply/demand relationship in acute kidney injury. *Crit Care Med* 38: 1695–1701, 2010. doi:10.1097/CCM.0b013e3181e61911.
36. **Rosenberger C, Pratschke J, Rudolph B, Heyman SN, Schindler R, Babel N, Eckardt KU, Frei U, Rosen S, Reinke P.** Immunohistochemical detection of hypoxia-inducible factor-1 α in human renal allograft biopsies. *J Am Soc Nephrol* 18: 343–351, 2007. doi:10.1681/ASN.2006070792.
37. **Rosenberger C, Rosen S, Paliege A, Heyman SN.** Pimonidazole adduct immunohistochemistry in the rat kidney: detection of tissue hypoxia. *Methods Mol Biol* 466: 161–174, 2009. doi:10.1007/978-1-59745-352-3_12.
38. **Sadowski EA, Djamali A, Wentland AL, Muehrer R, Becker BN, Grist TM, Fain SB.** Blood oxygen level-dependent and perfusion magnetic resonance imaging: detecting differences in oxygen bioavailability and blood flow in transplanted kidneys. *Magn Reson Imaging* 28: 56–64, 2010. doi:10.1016/j.mri.2009.05.044.
39. **Schödel J, Klanke B, Weidemann A, Buchholz B, Bernhardt W, Bertog M, Amann K, Korbmayer C, Wiesener M, Warnecke C, Kurtz A, Eckardt KU, Willam C.** HIF-prolyl hydroxylases in the rat kidney: physiologic expression patterns and regulation in acute kidney injury. *Am J Pathol* 174: 1663–1674, 2009. doi:10.2353/ajpath.2009.080687.
40. **Shapiro SS, Wilk MB.** An analysis of variance test for normality (complete samples). *Biometrika* 52: 591–611, 1965. doi:10.1093/biomet/52.3-4.591.
41. **Siegemund M, van Bommel J, Stegenga ME, Studer W, van Iterson M, Annaheim S, Mebazaa A, Ince C.** Aortic cross-clamping and reperfusion in pigs reduces microvascular oxygenation by altered systemic and regional blood flow distribution. *Anesth Analg* 111: 345–353, 2010. doi:10.1213/ANE.0b013e3181e4255f.
42. **Vinuesa E, Hotter G, Jung M, Herrero-Fresneda I, Torras J, Sola A.** Macrophage involvement in the kidney repair phase after ischaemia/reperfusion injury. *J Pathol* 214: 104–113, 2008. doi:10.1002/path.2259.
43. **Welch WJ, Baumgärtl H, Lübbers D, Wilcox CS.** Nephron pO₂ and renal oxygen usage in the hypertensive rat kidney. *Kidney Int* 59: 230–237, 2001. doi:10.1046/j.1523-1755.2001.00483.x.
44. **Zurlo G, Guo J, Takada M, Wei W, Zhang Q.** New insights into protein hydroxylation and its important role in human diseases. *Biochim Biophys Acta* 1866: 208–220, 2016. doi:10.1016/j.bbcan.2016.09.004.

